The Effects of Mechanical Properties and Physical Inputs on Stem Cells of the Central Nervous System

Philippa Elizabeth Clarkson

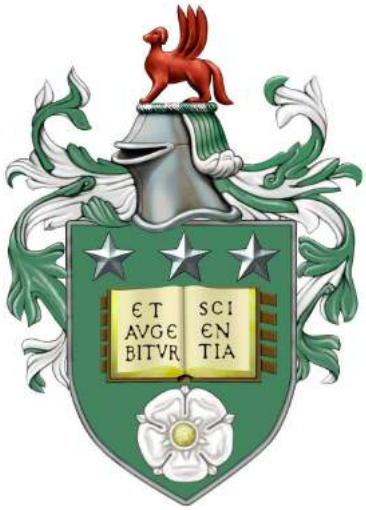

The University of Leeds

School of Mechanical Engineering

Thesis

Submitted in accordance with the requirements for the degree of Doctor of Philosophy

February 2018

The candidate confirms that the work submitted is her own and that appropriate credit has been given where reference has been made to the work of others.

About The Author

The author of this thesis obtained an integrated masters (BEng & MEng) with honours in Mechanical Engineering from the University of Leeds in 2011, which included modules in biomedical engineering. Regarding the fields of biology and chemistry, the author obtained a GCSE in double award science in 2005.

Acknowledgments

I would like to thank the Engineering and Physical Sciences Research Council (EPSRC) for providing the funding for this project and the White Rose Doctoral Training Centre in Tissue Engineering and Regenerative Medicine for giving a mechanical engineer the opportunity to undertake a biological research project. I am extremely grateful to my supervisors, particularly Richard Hall and Joanne Tipper, for their guidance and expertise for this project. I would like to thank Helen Lee, Jeni Smith and Dan Thomas for providing much of the practical training for this project, and to Carlos Grattoni for carrying out NMR logging and analysis.

I am very thankful to my fellow coursemates for all the emotional support- no one else understood the ordeal quite like them. I am indebted to my family - to my mother Hilary, who is the cleverest person I know and a constant source of inspiration; to my father Peter, who taught me that exploration is the purpose of life, love is the meaning of life and that in any situation you always have the choice to either laugh or cry; to my older brothers Rob and Tim, who made me so stubborn that when doubt is cast over my capabilities, it merely makes me more determined to succeed; and to Ed, who has been the rock in a storm and with whom I wonder at the greatest questions in life.

I would like to dedicate this thesis to the third of PhD students who suffer mental health issues during their studies.

Abstract

Injury to the central nervous system (CNS) can be extremely debilitating and the regenerative capacity of this tissue is notoriously poor. Intracranial pressure (ICP) levels after injury is known to be a predictor of patient outcome, however the reasons behind this remain unclear. It is known that neural stem cells, present in the CNS may be affected by the elastic modulus of their surrounding matrix however efforts to investigate this have also altered other physical parameters, most notably the pore size of the matrix. It was hypothesised that the activities of neural stem cells are affected by the elastic modulus of their 3D environment, altered independently of pore size; and by the hydrostatic pressure of their environment, altered within a biomimetic range of ICP after traumatic brain injury. The hypotheses were interrogated using an in vitro system, and with a hydrogel of tunable elastic modulus and a hydrostatic environment.

The effects of elastic modulus, independently of pore size, on the activities of neural stem cells was investigated using a chemically crosslinked hydrogel. Hydrogels variants were synthesised with two different crosslinker types, 1,3-phenylenediacetic acid (Ph) and tartaric acid (Ta), and shear storage modulus was found through rheometry to be significantly higher ($p<0.05$) in the Ta hydrogel, although neither hydrogel fell into the target biomimetic range. Analysis of scanning electron microscopy (SEM) images, of a trinitrobenzenesulfonic acid (TNBS) assay and of T_2 relaxation by nuclear magnetic resonance (NMR) logging found no significant differences between the two hydrogels in pore diameter, degree of crosslinking or pore volume, respectively. The porosity of Ta hydrogels was found to be highly significantly ($p<0.01$) larger by comparison of water content. The phenotype and cell spreading of the CB660 neural stem cell line was measured, finding no significant difference in protein expression, however cells cultured in the Ta hydrogel were significantly ($p<0.05$) more spread. These findings indicated that it may be pore size and not elastic modulus that affects stem cell differentiation, however further research is required to improve the power of these stem cell studies.

The effects of hydrostatic pressure on the activities of the CB660 neural stem cell line was investigated using a pressurised modular incubator. The migration of cells was evaluated using a novel layered gel assay, a significant increase was observed in

glial cell migration under increased pressure ($p<0.05$, 0-25mmHg) while it was found that neural stem cell migration may be inhibited by increased pressure, with a 61.5% reduction in migrated cell number comparing 30mmHg to 10mmHg. Cell viability was assessed using successive CyQuant and ATPlite assays, finding that ATPlite readings were significantly ($p<0.05$) lower at 50mmHg compared to 30mmHg, indicating that increased pressure may diminish cell viability. Cell phenotype and morphology was assessed in 2D, finding that increased pressure may encourage neuronal differentiation, ($p<0.01$, 10-50mmHg), however may inhibit the formation of projections ($p<0.05$ 10-50mmHg). Again however, further research is required to improve the power of these stem cell studies due to low repeat numbers.

The results of the study of elastic modulus and pore size indicated that pore size may indeed be an important parameter to consider when studying stem cell differentiation in response to mechanosensitivity as it may be pore size and not elastic modulus that stem cells respond to, and this may be an important parameter for future researchers to include. The results of the study of hydrostatic pressure indicated that pressure does have a direct effect on both glial and neural stem cells, and that the combination of characterisitics of Lundberg A waves including high pressure (>40mmHg), short wavelength (<30 minutes) and a return to normal pressure levels (5-15mmHg) between waves may all be instrumental in the cellular repair processes and improved patient outcome. However, the power of the studies using the CB660 neuronal stem cell line were limited and should therefore be regarded with caution.

Contents

List of Figures

List of Tables

Table 1: Common Nomenclature

A	Area
C	Molecular absorption coefficient
δ	Change in
ε	Strain
E	Tensile Elastic Modulus
F	Force
G'	Shear Storage Modulus
G"	Shear Loss Modulus
K	Bulk Modulus
L	Length
δL	Precentage Length Change
μ	Viscosity
N	Number of molecular groups
n	Number of repeats
ν	Poisson's Ratio
σ	Stress
τ	Shear Force
T_2	NMR Decay Time
u	Velocity
V	Volume
y	Thickness

Table 2: Abbreviations and Acronyms

2D	Two Dimensional
3D	Three Dimensional
ABI	Acquired Brain Injuries
Ad	Hydrogel with Adipic Acid
AFM	Atomic Force Microscopy
ANS	Autonomic Nervous System
ChAT	Choline Acetyltransferase
CNS	Central Nervous System
CNPase	2',3'-cyclic-nucleotide 3'-phosphodiesterase
CPP	Cerebral Perfusion Pressure
CSF	Cerebrospinal Fluid
μCT	Micro-Computer Tomography
DNA	Deoxyribonucleic Acid
DOC	Disorders of Consciousness
ECM	Extracellular Matrix
EDC	1-ethyl-3(3-dimethylaminopropyl) carbodiimide
ESWT	Extracorpreal Shockwave Treatment
GABA	γ-aminobutyric Acid
GFAP	Glial Fibrillary Acid Protein
HA	Hyaluronic Acid
H&E	Hematoxylin and Eosin
Hyl	Hydroxylysine
ICP	Intacranial Pressure
LVER	Linear Viscoelastic Region
Lys	Lysine
MAP2	microtubule-associated protein 2
MRI	Magnetic Resonance Imaging
NF-H	Neurofilament-H
NHS	N-hydroxysuccinimiide

Continued on next page.

NIBSC	National Institute for Biological Standards and Control
NMR	Nuclear Magnetic Resonance
NRP	Neural Restricted Progenitor
PCR	polymerase chain reaction
PEG	Polyethylene Glycol
Ph	Hydrogel with 1,3 Phenylenediactetic Acid
PNS	Peripheral Nervous System
RNA	Ribonucleic Acid
SEM	Scanning Electron Microscope
SCI	Spinal Cord Injury
SGZ	Subgranular Zone
Su	Hydrogel with Suberic Acid
SVZ	Subventricular Zone
Ta	Hydrogel with Tartaric Acid
TBI	Traumatic Brain Injury
TNBS	2,4,6-Trinitrobenzenesulfonic Acid
TNF-α	Tumour Necrosis Factor Alpha
UV	Ultraviolet
WP	Well Plate

1 Introduction

To date most research into the CNS has focused on its chemical influences, for example the effects of hormones, with little concern for other factors. It is clear that during physical injury, such as the sudden impact during a car crash, the CNS is exposed to sudden, large forces. As damage to the tissue is so debilitating and natural repair is poor, the effects these types of forces have on the function and repair of the CNS will be explored and other physical or mechanical factors that may affect the repair is identified. In this introduction, the literature was reviewed regarding interactions between the CNS and its physical or mechanical environment, particularly at a cellular level. After establishing the interactions between cells and their physical and mechanical environment, the scope for further review was established and a review of these areas was conducted.

1.1 Rationale for the Project

Dysfunction of the central nervous system (CNS) is caused by a wide range of diseases which can occur due to physical, chemical or biological damage to the tissue, such as traumatic events or autoimmune diseases. Due to the primary purpose of the central nervous system, which is to collect, interpret and transmit information (Diamond et al., 1985), this damage contributes to a wide range of conditions, from physical disability to Alzheimer's disease. The causes of many of these conditions are still poorly understood when compared to dysfunction of other areas of the body. The lymphatic vessels present in the CNS remained unrecorded until 2014, and it was that discovery that provided new insight into how the brain is affected by immune system dysfunction as these vessels govern the transport of immune cells in the CNS (Louveau et al., 2015). This means that categorising CNS dysfunctions is problematic as the underlying cause of many symptoms is still unknown, and any one symptom can be the result of a range of different abnormalities, for example the symptom of a headache can be caused by dehydration or hormone imbalances, but in rare cases could be caused by meningitis or a tumour (Choices, 2016). For many diseases, the link between the cause and effect has not been straightforward. For example, recent research has found that meditation can physically change the

structure of the brain (Luders et al., 2009), that social interaction can lower vulnerability to addiction (Whitaker et al., 2013) and bipolar disorder has been linked to Parkinson's disease (Cannas et al., 2002). Medically, "disease" can refer to any dysfunction of tissue where the underlying causes are known, and it has been argued that traumatic brain injury should be considered a disease rather than an event, due to the biological processes that occur days to weeks after the initial impact (Masel and DeWitt, 2010) such as oedema and ischaemia. Clearly, there are many areas regarding CNS dysfunction that remain to be understood.

Physical injury to the central nervous system occurs when a force is applied to the tissue that affects its function, and most of the injuries to the brain are collectively known as acquired brain injuries (ABI) (Headway, 2015a). ABI includes haemorrhage, infection and stroke and there are over 300,000 hospital admissions for ABI every year in the UK. In 2013-14, 47% of these were caused by head injury and 37% were stroke victims (Headway, 2015a). ABI does not include damage to the spinal cord or other physical forces that can affect the CNS, such as tumour growth. In Britain alone, around 1000 people per year sustain a spinal cord injury, with approximately 50,000 people currently living with paralysis (Spinal Research, 2011). There are also around 10,000 patients diagnosed with tumours in the CNS per year in the UK (Cancer Research UK, 2014), which also cause physical pressure to the surrounding tissue. Worldwide, it is estimated that there are over 300,000 people living with a CNS tumour (Globocan, 2012). Physical injury to the CNS can be extremely debilitating for the patient and therefore can significantly affect not only their life in terms of their independence, but also the friends and family that the patient often becomes reliant on. When considering the people both directly and indirectly affected by CNS injuries, the effects are substantial. In Europe alone, the total cost of diagnosing and treating brain disorders was approximately €798 billion in 2010, (Olesen et al., 2012) with traumatic brain injury costing around €33 billion.

The field of tissue engineering adopts a "bioactive" (i.e. promotes interaction with the tissue) approach to tissue repair, aiming to exploit the natural abilities of cells to create a biologically functional repair. The field of regenerative medicine meanwhile also adopts a bioactive approach, providing holistic treatments to target the body's

own repair mechanisms. Current treatment options for CNS injury are largely focussed on symptom relief as the tissue has a notoriously limited capacity to repair itself. By investigating how cells and tissues respond to mechanical and physical changes, new treatments may be developed. The aim of this project was to discover whether the physical environment of the CNS can affect the activities of the cells, in order to better understand the cellular responses and develop improved treatments of ABI.

1.2 General Introduction

To begin, the terms of the title will be defined: mechanical properties, physical inputs and CNS cells. The scope of these ideas with relation to the project will be described.

1.2.1 Mechanical Properties and Physical Inputs to the CNS

Mechanical Properties

Mechanical testing is used to reveal the properties of a material by application of a force and analysis of the physical change in the material. The tissue of the CNS can be mechanically classed as "soft matter" (Cheng et al., 2008) and it possesses properties of both solids and liquids, and therefore requires characterising for both sets of properties. In solids, when a force is applied the material will usually initially deform elastically, in which the deformation is linearly proportional to the force . This linear relationship is known as the Young's modulus of the object and is a consequence of the rigidity of the material it is made from and its shape (Lin, 2010). Stress-strain curves are commonly used to visualise this relationship.

Using a Cartesian co-ordinate system such as that described in Figure 1 (a), the application of forces on an object can be described. A force applied in a direction can be described by a vector with a length proportional to the magnitude of the force, and an orientation in the direction of the force, as described by the angle in the x, y and z directions from the origin. A plane can also be described by a vector, as shown in (b) where the length is proportional to the size of the area of the plane

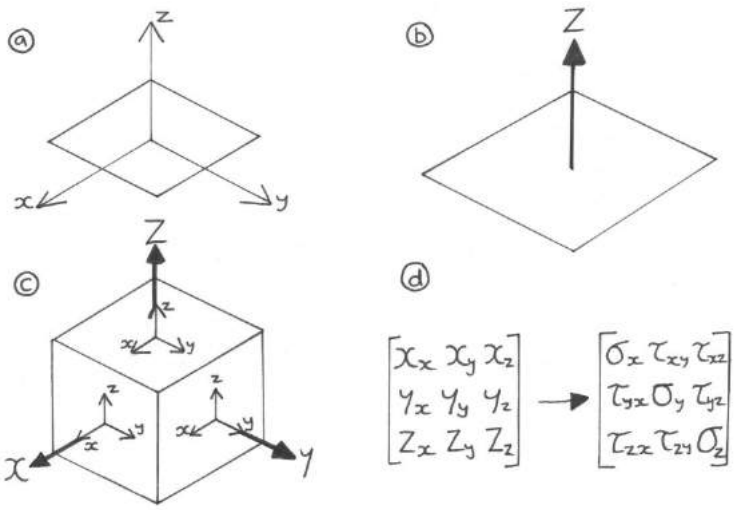

Figure 1: Deriving the various forces that can act on an object via vector notation. (a) describes the three unit vectors of forces in relation to a plane. (b) indicates the way in which a plane can be described by a vector. (c) shows how any force acting on an object can be described by a force vector and a plane vector. (d) shows how these vector couples can be described mathematically, with tension or compression forces (σ) and shear forces (τ).

and the orientation is perpendicular to the plane. Combining vectors describing a plane and the force applied to it, the overall stress applied to any object can be described, as shown in (c). Here, the force vectors have been denoted x, y and z, while the plane vectors are denoted X, Y and Z. As described in (d), it then becomes clear that a force vector acting in the same or opposite direction as a plane vector is a tensile or compressive force, respectively. This generates a stress within the material (Lin, 2010).

Tensile or compressive stress (σ) is defined as the force (F) applied to the material per unit area (A) perpendicular to the force (Equation 1), while strain (ε) describes the percentage length change (δL) of the material in the direction of the force compared to its original length (L) (Equation 2). Forces acting perpendicular to the plane vector, i.e. along the plane, are known as shear forces (Lin, 2010), denoted by τ in Figure 1.

$$\sigma = F/A \tag{1}$$

$$\varepsilon = \delta L/L \tag{2}$$

The elastic or storage modulus, E (Equation 3), describes the ability of a material

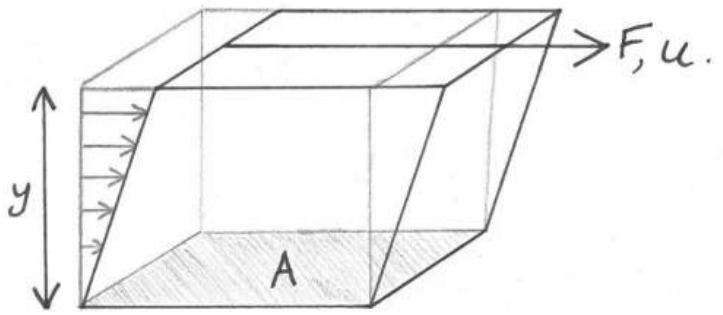

Figure 2: Shear testing is used to determine the viscosity of a liquid. The shaded region represents the area, A; while y is the thickness of the material. F is the shear force applied to the area at velocity u.

to store and return energy. The energy supplied to cause the deformation is stored in the material and when the force is released, the object will return to its original shape. When the material has reached its elastic limit, it will deform plastically and the deformation is no longer proportional to the force. The energy supplied to cause deformation is dissipated as heat as the bonds in the material break, changing the structure permanently (Lin, 2010).

$$E = \sigma/\varepsilon \tag{3}$$

Plastic deformation in solids is akin to the physical response to forces in liquids, described by viscosity. Viscosity describes a materials resistance to flow (Law and Rennie, 2015). The modulus of a viscous material (where all energy is dissipated) is typically measured using shear forces:

$$\mu = Fy/Au \tag{4}$$

Where F is the shear force applied, A is the area in which the force is applied, y is the thickness of the material (perpendicular to the force) and u is the velocity with which it is applied, as shown in Figure 2. The viscosity can be time dependent and affected by the speed of the fluid movement so the rate at which a force is applied may affect the moduli that are measured.

Viscoelastic materials such as soft tissues in the body and hydrogels respond to forces in both an elastic and viscous manner (Saunders, 2015), and are therefore

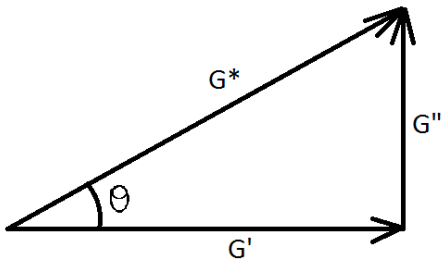

Figure 3: The relationship of complex modulus (G) and phase angle (θ) to the storage (G') and loss (G") components of a viscoelastic system.*

often both characterised by shear testing, as described by Figure 2 or by τ in Figure 1 which causes a hysteresis or lag of the stress-strain curve as the energy returned by the system is less than the energy that was applied. For viscoelastic materials, Young's modulus (i.e., the elastic component) is known as the storage modulus, while the viscous component is known as the loss modulus (G' and G" respectively, for shear tests). Combined, these can be described by the complex modulus and phase angle, where the phase angle represents the time dependence of the viscous component of the system. The relationship of these values is described in Figure 3.

Physical Inputs

Besides mechanical properties, there are other physical properties of a material that could generate an effect on cells. Physical properties are those which can be measured or observed without interacting with the material. This introduction will cover those that could incite an effect cells in the CNS. For hydrous materials this includes the microarchitecture - i.e. size of pores within the material, fibril spacing, surface roughness or patterning. It also includes the overall porosity or density or water content and the effective porosity (i.e the proportion of interconnected pores allowing fluid flow or cell migration). These properties contribute to altering the overall surface of the material. Pore size, surface roughness and micro-patterning of materials is typically measured using a scanning electron microscope (SEM) or nuclear magnetic resonance (NMR). To determine porosity, micro-computer tomography (μCT) can be used to produce a three dimensional (3D) x-ray image of the structure or dry and wet weights can be compared.

Pressure is also another important attribute. Pressure is defined as the force per area, typically measured in N/m^2 or pascals (Pa). In the CNS there are different

fluids such as cerebrospinal fluid (CSF) and blood at a macro-scale, and interstitial fluid and intracellular fluid at a micro scale, all of which have specific pressures in healthy subjects. In medicine, reported pressures are gauge pressures (Cox et al., 2014) i.e. the pressure measured is the difference between the absolute pressure and atmospheric pressure. Atmospheric pressure is measured using a barometer and is around 100kPa, while gauge pressure is measured using a manometer.

The temperature is commonly regarded as an important physical property, as cells will not survive for long when cultured at room temperature. This is measured in Kelvin or more commonly in degrees Celsius, where 273K=0°C and $\Delta K = \Delta C$. For neuronal cells, electrical conductivity of the cellular environment may also be an important factor, as research has found that electrical stimulation can help an injured spinal cord to heal (Hamid and Hayek, 2008).

1.2.2 The Central Nervous System

Anatomy and Physiology of the CNS

The CNS comprises the brain and spinal cord, and is distinguished from the peripheral nervous system (PNS) which is located in the rest of the body. The autonomic nervous system (ANS) runs alongside the PNS and innervates internal organs which operate without concious thought, such as the cardiac and digestive systems (Diamond et al., 1985). The brain and spinal cord have different structures and cellular compositions, however both contain what is known as grey matter, and white matter. Grey matter is comprised largely of neuronal and glial cell bodies, while white matter contains mainly the pale, myelinated axons of the neurons (Diamond et al., 1985).

The brain is the third largest organ in the body and is mostly enclosed by the skull. The skull includes eight cranial bones which cover the cortex and provide much of the mechanical protection for the brain (Diamond et al., 1985). The rigid and enveloping structure of the skull provides a fixed volume for its contents (Rose and Johnson, 1996), unlike most other internal organs. Internally, the contents of the skull comprise approximately 10% CSF, 10% blood and 80% cerebral parenchyma (i.e. functional tissue) (Rodriguez-Boto et al., 2015). The brain is comprised of

distinct regions, each with its own tissue type and orientation. The brain has three main areas; the forebrain, midbrain and hindbrain which contain many different sub-areas, some of which are detailed in Figure 4. All of the areas of the brain have their own structure and so, as a whole the brain has a particularly complex and inhomogeneous structure.

The forebrain is the most recently evolved and includes the cerebrum, which makes up the largest area of the surface of the brain. Different areas of the cerebrum have specific functions, however as a whole it is dedicated to processing sensory information, planning ahead and speech formation (Diamond et al., 1985). The cerebrum is split into two hemispheres, marked by the longitudinal fissure, however they are joined at the corpus callosum, which is a band of myelinated axons running between the two hemispheres. Below the corpus callosum are the basal ganglia, groups of cell bodies concerned with execution of movement, and the thalamus, hypothalamus, pineal gland and pituitary gland. The thalamus links the sensory pathways of all senses (except for smell) to the brain. The hypothalamus controls the ANS and hormonal secretions from the pituitary gland (Diamond et al., 1985).

The pineal gland is the "body clock" of the body and controls circadian rhythm and it was thought by Descartes to be the "seat of the soul". The midbrain is connected to the ventral surface of the hypothalamus and controls reflexes related to the visual and auditory systems, and movement patterns (i.e. "muscle memory"). The hindbrain is connected to the ventral surface of the midbrain and has three main structures. The cerebellum is a large structure which protrudes dorsally, inferior to the cerebrum and controls movement and balance via muscle co-ordination. The cerebellum is connected to the brainstem via the pons (Diamond et al., 1985). The medulla oblongata is the most caudal structure of the brain and is therefore connected to the spinal cord. It regulates blood pressure, heart rate and breathing (Palahniuk, 1996).

The spinal cord, shown in Figure 4, resides in the spinal canal which is formed by the vertebral foramen in the centre of each of the thirty three vertebrae of the spine. The intervertebral discs separate each vertebra and are fibrous sacs consisting of collagen layers surrounding a gel centre and serve to provide movement and cushion axial impacts (such as jumping) (Diamond et al., 1985). The most rostral vertebrae, the

atlas, is connected to the skull, while the vertebrae at the cordal end are connected to the pelvis. The spinal cord has a central area of grey matter, surrounded by white matter. There is a small central canal containing CSF that runs through the entire cord (Diamond et al., 1985).

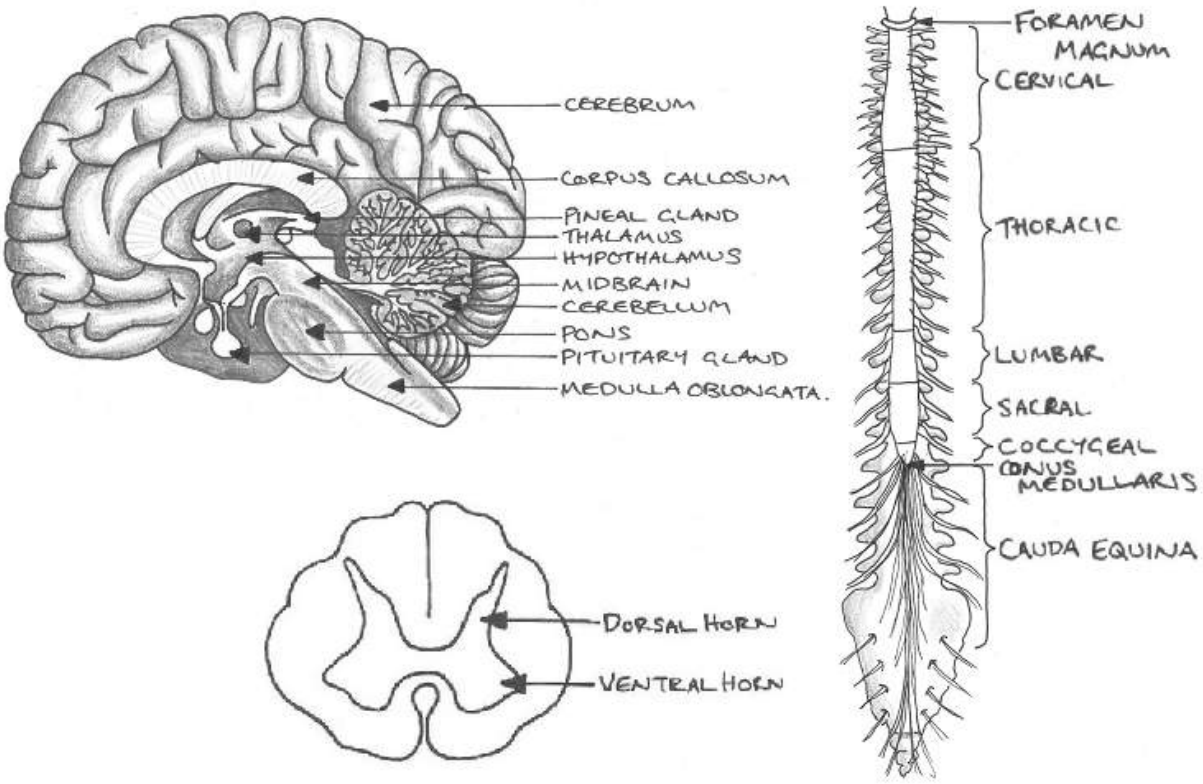

Figure 4: Top left: The anatomy of the brain in a median plane cross section. It identifies some of the complex structures of the brain, including the cerebrum, corpus callosum, cerebellum and medulla oblongata. Bottom and right: The structure of the spinal cord and its surrounding vertebrae in a coronal section (right) and transverse cross section (bottom). The opening of the skull, the foramen magnum are labelled; as is the tapered end of the cord, the conus medullaris.

The CNS Environment

The CNS is encapsulated by three meninges, from inner to outer; the pia, arachnoid and dura maters. The dura mater is comparitavely thick and fibrous and is comprised of two layers: the endosteal and meningeal. The endosteal layer directly lines the cranial bones and the various peripheral nerves and vessels sit between this and the meningeal layer (Diamond et al., 1985). The arachnoid layer sits directly next to the meningeal layer of the dura, and the pia mater is directly attached to the CNS tissue. Trabeculae span the space between the arachnoid and pia maters

both in the brain and the spinal cord which is known as the subarachnoid space and has been measured to be 3mm thick on average in humans (Maes et al., 2000). The space is markedly enlarged in certain areas, known as cisterns which can expand and contract to help maintain a constant CSF pressure.

CSF is contained within the subarachnoid space (between the pia and arachnoid mater) and in the ventricular system which penetrates the bulk brain structure, and also runs through the central canal of the spinal cord. The CSF acts to cushion and support the weight of the CNS to ensure that ventral structures and blood vessels are not compressed by its weight (Diamond et al., 1985). The CSF maintains a pressure that supports the brain and this fluid can be displaced into cisterns in the event of brain swelling, in order to maintain this pressure (Murad et al., 2012). In younger patients, the cisterns can compensate for 60-80ml fluid, while elderly patients can accommodate 100-140ml (Raboel et al., 2012). The human brain weighs around 1400g, however due to the density of the CSF it is suspended in, its net weight is around 25g (Adigun and Bhimji, 2017). The trabeculae of the brain and denticulate ligaments of the spinal cord suspend the remaining weight of the CNS so that it essentially "floats" in the fluid, not resting on any other tissue.

The CNS ECM

Cells *in vivo* reside within an extracellular matrix (ECM) which gives the tissue its structure as well as providing chemical and physical cues to the cells. Although the ECM of many tissues in the body contains a high proportion of collagen and fibronectin, the majority of the CNS ECM does not. The perineuronal nets of the CNS, for example, are comprised of hyaluronic acid (HA), tenascins and lecticans (a type of proteoglycan) (Li et al., 2012; Lau et al., 2013). Cunicular brain has been reported to contain 65μg HA/g wet tissue (Cowman et al., 2015). The cell adheres to the ECM via integrins which are proteins that span the cell membrane and attach to glycoprotein ligands present in the ECM. Many chemical signals are present in the ECM which affect cell physiology and phenotype (Hidalgo-Bastida and Cartmell, 2010), however other signals are also present.

Physical cues such as the geometry of the pores within which the cells reside and the nanotopography of the surface of the ECM is known to effect the differentiation of mesenchymal stem cells (McNamara et al., 2010). Mechanical cues such as the

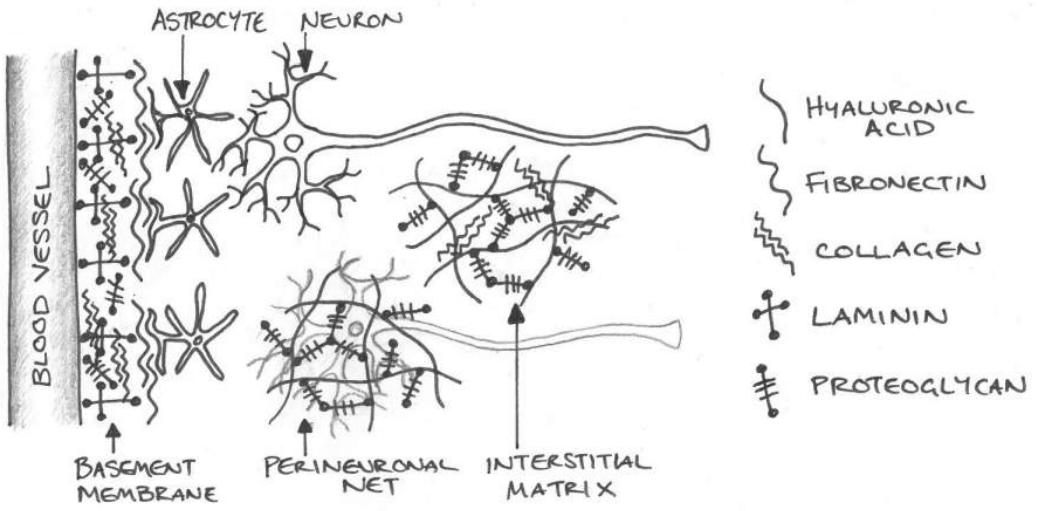

Figure 5: Showing the composition of the three subdivisions of the CNS ECM; including the basement membrane which lines the vascular network, the perineuronal net which covers the soma of the neuron and the interstitial matrix. Image adapted from Lau et al. (Lau et al., 2013) with permission.

transmission of forces to the cells and the mechanical properties of the matrix are known to also direct stem cell fate (Guilak et al., 2009). The CNS ECM has three major subdivisions which are described in detail by Ricks et al. (2014), Figure 5 provides a summary of the constituent proteins found in these subdivisions. The basement membrane that lines the vessels of the brain, the perineuronal net that surrounds the bodies of neurons and dendrites and the interstitial matrix which makes up the rest .

Physiology of the CNS

The purpose of the CNS is to retrieve and process the sensory information and produce a motor output. It does this by a network of interlinking cells which harvest information from the body and send motor signals, for example limb movement or gland secretion. In short, it controls behavior i.e. response to stimulus. The body's use of nervous tissue is an expensive procedure - a fifth of total oxygen and energy requirements are taken up by the brain (Rodriguez-Boto et al., 2015), which is a larger share than any other organ. As with any tissue in the body, the CNS requires oxygen and nutrients and expels waste and carbon dioxide. This high expenditure of energy requires a corresponding high blood flow to allow the exchange of materials such as nutrients and waste. To maintain a constant flow of oxygen and nutrients to the brain, the blood pressure must be maintained to keep

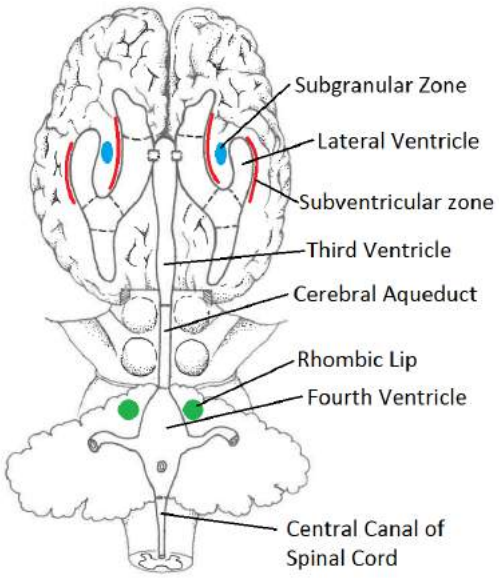

Figure 6: Schematic diagram of the posterior view of the ventricular system, including the areas in which stem cells have been located. The SVZ is in red, the SGZ is in blue and the rhombic lip is in green. Adapted with permission from Diamond et al. (1985).

the difference in pressure between the blood and the intracranial pressure (ICP) constant at 5-15mmHg (Steiner and Andrews, 2006; Fleischman and Allingham, 2013; Murad et al., 2012), thus maintaining a constant cerebral perfusion pressure (CPP) of at least 70mmHg (Harrington et al., 2007). This is achieved through what it known as cerebral autoregulation, which dilates or constricts blood vessels as necessary (Raboel et al., 2012).

Unlike other tissues however, the CNS is not in direct contact with the all the components in the vascular system due to the blood-brain barrier formed by tight junctions between the endothelial cells that line the blood vessels (Yao et al., 2013). The barrier allows selective passage of small molecules such as water, glucose and amino acids, while larger molecules such as hormones pass through circumventricular organs within the CNS. These are received in sensory organs or released into the bloodstream by secretory organs (Diamond et al., 1985).

CSF is produced by the choroid plexuses, located in the lateral, third and fourth ventricle and is used to wash metabolic waste from the CNS tissues (Diamond et al., 1985). The CNS is intersected by the ventricles (Figure 6) which allow the CSF contained within them to contact a larger surface area of the CNS. CSF works to

maintain chemical stability as it is totally replaced by the choroid plexuses approximately four times a day by fresh fluid, flushing waste from the brain and draining into the dural sinuses for resorption into the bloodstream. Lymphatic vessels line the dural sinuses, allowing drainage of immune cells and other small molecules (Louveau et al., 2015).

CNS Cells

Cells of the CNS include neurons, stem cells and glia. Neurons are excitable cells which are able to transmit signals from one location to another, which is the primary function of the nervous system. They have multiple dendrites and one axon which are long, branching structures protruding from the cell body. While the cell bodies are typically less than 1μm, the axon of motor neurons can reach over one metre in length (Diamond et al., 1985). Dendrites collect information from surrounding neurons and transmit it to the nucleus to be processed. The cell generates an output signal at the axon hillock, which is transferred down the axon, transmitting information to other cells .

Almost all the other cells found in the CNS are collectively known as glial cells. Biochemically, these are the "supporting" cells to the neurons and are responsible for maintaining homeostasis. Astrocytes are the most common cells of the nervous system, outnumbering neurons by a factor of five (Sofroniew and Vinters, 2010) and control the chemical environment of the neurons. The purpose of glia was originally thought to be to glue the neurons together or provide structural support, but given that they have a lower elastic modulus, their mechanical influence on neurons is more likely to be a cushioning effect to provide a "crumple zone" in case of mechanical damage to the tissue, to protect the neurons (Lu et al., 2006). The main purpose of glial cells is to maintain the chemical balance of the neuronal environment (Cooper, 2000). Neurotransmitters are commonly used to pass signals between neurons and are expelled into the surrounding interstitial matrix, and glia are able to absorb and recycle these. Other glial cells include oligodendrocytes which create the myelin sheath which covers and insulates the axons of neurons. Ependymal cells are arranged in a sheet and line the spinal cord and the ventricles of the brain, controlling the passage of nutrients between the CNS tissue and the cerebrospinal fluid (CSF) (Diamond et al., 1985). Microglia are the macrophages of

the nervous system, their responsibilities are to remove debris and pathogens and following trauma they are quickly drawn to the site to destroy material such as dead or damaged cells.

Stem cells are capable of replicating themselves and differentiating into other cells and are of special interest to tissue engineering applications because of this property. Stem cells were only relatively recently identified in the CNS (Richards et al., 1992), before this it was assumed that the CNS was unable to regenerate. CNS stem cells have been found in three separate areas of the brain:

- Proximal to the ependymal cells that line the ventricles of the forebrain, in what is known as the subventricular zone (SVZ) .
- The rhombic lip outer germinal layer of the cerebellum which is involved in movement.
- The subgranular zone (SGZ) of the dentate gyrus of the hippocampus which has functions in learning and memory as well as emotion (Ricks et al., 2014).

These areas are labelled in Figure 6 and are noted to be in close proximity to the ventricles. Stem cells have also been found in the lumbar and sacral spinal cord and spinal canal (Weiss et al., 1996). Neural stem cells transplanted outside of these "niches" have been observed to differentiate mostly into glial cells (Yao et al., 2013).

There have been attempts to further categorise the stem cells based on their potency or state of commital. Fawcett et al. (2002) note four different cell states: stem cell, multipotential progenitor cells, committed progenitor cells (e.g. neuroblasts and gliablasts) and differentiated cells (e.g. neurons and glia). However these terms have no concrete definition; for example committed progenitor cells are also known as precursor cells elsewhere. According to this terminology, neural stem cells may fall in the category of multipotential progenitor cells as they are already committed to the CNS. There have been calls for clearer terminology (Tajbakhsh, 2009) and although it can be frustrating, it would perhaps be more prudent to wait until the topic of stem cell differentiation is more completely understood before agreeing on definitions. Presently at least, for articles that do not fully describe what they

themselves mean by the terms they use, it must be assumed that stem, progenitor and precursor are used interchangeably.

Investigation of activities of CNS Cells *In Vitro*

The activity of cells *in vivo* is dependent on the cues that are given, be they chemical or mechanical, for example both hormones and increased physical activity can cause growth of new tissue. Similarly, *in vitro* cells can be controlled by external inputs. Measuring the cellular activity is a complicated process as there are numerous techniques to indicate a range of output signals, all with their own limitations. These techniques are known collectively as assays. Assays include any procedures that are used to observe the activity of cells, be these physical appearances or activities, or chemical secretions. Assays can be used to measure the effect of changes in environment on cell activity, be that quantitatively such as cell counts or qualitatively as in neurite outgrowth assays. The phenotype of a cell may also be determined through investigation of protein or gene expression. As cells are characterised by their expressions, using immunology or polymerase chain reaction (PCR) for cell-specific expressions, the phenotype of the cell may be inferred (Cooper, 2000).

The most basic investigation into cell activities is that of their viability and proliferation which can be assessed in several ways (Kepp et al., 2011), however popular choices include the use of trypan blue, which is an inexpensive chemical able to penetrate the membrane of dead cells and stain the cell, while cells that are alive remain unstained (Stoddart, 2011). Other assays can be used on adhered cells, such as MTT which records the metabolism of the mitochondria in cells, or ATP consumption which measures the respiration of the cells. The proliferation of cells in culture may be measured with the same assays as for viability, and measurements compared over a span of days to weeks depending on the application of the cells, as the proliferation of cells varies temporally.

The projection of neurites is a unique property of neural cells. The growth of these neurites may be observed via microscopic inspection and characterised or measured. Neurite projections are important not only as it means that the cell itself is viable and functioning correctly, but also because these projections are essential for the cells main purpose in the body, and so without these the cell would be defunct (Diamond et al., 1985).

Movement of cells in 2D occurs through the reorganisation of the actin filaments within the cytoskeleton into protrusions at the leading edge (lamellipodia) and the contraction of myosin II to generate a force and create a movement within the cell. In 3D, often the cells use an entirely different migratation mechanism. By increasing the hydrostatic pressure within the cell, the membrane detaches from the cytoskeleton and balloons outwards, forming a protrusion known as a bleb (Driscoll and Danuser, 2015). The actin cortex of the cytoskeleton can then reassemble to follow the shape of the bleb. Blebs have long been known to be involved in apoptosis but have more recently been observed in cell division and migration (Charras and Paluch, 2008). It is not known how migrating cells polarise their blebs to enable migration in a specific direction although suggestions include polariasation of the membrane-cytoskeleton attachments creating a weakened area, or heightened contractions of the mysoin causing a tear in the actin cortex at the leading edge.

Differentiation and De-differentiation

Stem cells are of particular interest in the field of tissue engineering as they have the property of cell plasticity: they can differentiate into many different cell types. The differentiation of stem cells is traditionally determined by measuring their phenotype, including its appearance and secretions. Different cell types produce different proteins and these may be detected and thereby the cell type distinguished (Sternberger, 1986). Neural restricted progenitors (NRPs) of the spinal cord express ChAT (choline acetyltransferase), while some NRPs of the brain express GABA (γ-aminobutyric acid), glutamate (Rao, 2010) or SOX2 (Her et al., 2013) other common markers for stem cells include nestin and CD-133 (Sun et al., 2008). PSA-NCAM is known to be expressed by neuonal progenitors and therefore may be used as an early indicator of neuronal differentiaion (Sun et al., 2008). β III-tubulin is a microtubule protein that is produced in neurons, while microtubule-associated protein 2 (MAP2) and neurofilament-H (NF-H) genes may also be used for neuronal marking (Her et al., 2013).

2',3'-cyclic-nucleotide 3'-phosphodiesterase (CNPase) is expressed by glial cells, as is glial fibrillary acid protein (GFAP) (which is also expressed by ependymal cells) and so can be a useful tool for looking at stem cell differentiation. GFAP is the prototypical astrocyte marker (Sofroniew and Vinters, 2010) and has been found

to be a reliable marker of astrocytes proximal to an injury site, it has also been found to be expressed by adult neural stem cells (Yao et al., 2013). Mikkola et al. (2002) demonstrated that stem cells committed to a certain lineage may be able to reprogramme and commit to a new lineage given the appropriate chemical cues, while Liao et al. (2015) similarly showed umbilical cord blood cells can be converted into neural stem cells.

Although the ability of stem cells to differentiate into many different kinds of cells is well known, research now suggests that certain mature cells are able to de-differentiate, increasing their potency and are then able to re-differentiate into another cell type. The idea that mature mammalian cells may be able to de-differentiate was first proposed by Shoshani and Zipori (2011) who reasoned that the stressful environment created by tissue damage may stimulate mature cells to reprogramme, citing studies which had observed reprogramming in simpler organisms. Researchers have been able to increase the potency of mature cells studied *in vivo*. Tata et al. (2013) used ablation to remove basal stem cell populations in murine airways. Lineage tracing showed the neighbouring luminal secretory cells de-differentiated to progenitors, able to differentiate down a different lineage and thus allowing repair of the epithelium. The study by Tata et al. (2013) also cultured the secretory cells *in vitro*, finding that when cultured without stem cells, the cells could de-differentiate; however when cultured in contact with a single basal stem cell, the secretory cell would not de-differentiate.

Mechanosensitivity

The mechanosensitivity of cells is well known; for example osteoblasts in the femur form new bone in response to increased load, through exercise or weight gain to prevent fracture from occurring (Skerry, 2008). Indeed, studies involving culturing mesenchymal stem cells under pressure have found that increased pressure was able to directly stimulate the cells to both proliferate and undergo differentiation to both osteogenic and chondrogenic lineages (Hess et al., 2010; Zhao et al., 2015). Similarly, Aung et al. (2012) studied the effects of raised fluid pressure on angiogenesis in solid tumours, finding that application of 20mmHg pressure to osteosarcoma cell lines suppressed growth factors associated with angiogenesis.

However, Engler et al. (2006) found that mesenchymal stem cells were able to not

only sense forces but to generate a contractile force themselves, pulling on their surroundings (Mohammadi et al., 2015) and discerning the deformation response to distinguish between substrates of varying stiffness and differentiate accordingly. In addition to the mechanical properties, it has also been found that stem cells may respond to the topography of their surroundings. Topography can control cell adhesion and spreading as well as changes in gene expression (Hoffman-Kim et al., 2010). For example, for a neurite to extend from the cell body, it must encounter some form of solid mechanical resistance in its environment (Willits and Skornia, 2004) such as the ECM *in vivo*. This extension can be controlled with microfabrication techniques to control topography.

Damage and Repair of the CNS

Disease, damage and degeneration are interrelated; physical damage can often (particularly in the nervous system) trigger or expedite degeneration, and similarly degeneration can render tissue susceptible to physical damage. Diseases such as breast cancer and Alzheimer's are associated with a change in tissue properties (Franze et al., 2013; Janmey et al., 2013). The term "disease" encompasses any impairment to a healthy functioning tissue, while degenerative diseases describe ones that worsen with time. Damage can be temporary, lasting only until the body has healed, however more severe damage is likely to be permanent and contribute to the degeneration of the tissue. Damage can be categorised into two aspects: chemical damage and physical damage. Although the focus of this thesis is on physical inputs, the effects of this damage can often lead to detrimental chemical imbalances, which will be discussed presently. Physical damage can broadly be considered as an application of abnormal forces within the tissue, be these rapid or progressive, leading to a physical and biochemical change in the system.

Traumatic injury is often regarded as a short-term event, however the effects of an impact to the central nervous system are much longer lasting, and can be described in two stages. The forces that cause the primary injury last less than 100ms (Greve and Zink, 2009), while secondary injury is characterised by the symptoms that progress seconds to weeks after the incident. At a cellular level, the immune response involves an influx of cells to the site of injury. Microglia are the first to migrate to the injury within a matter of minutes to clear out any debris, followed by leukocytes (white

blood cells) if the blood-brain barrier has been compromised: neutrophils within a few hours, and monocytes days later (Shoichet et al., 2008). While these cells work to remove damaged or dangerous matter, the flow of these cells to the injury site creates an area of high pressure which can compress the surrounding tissue causing pain, or in the case of the easily-compressible CNS tissue, a temporary loss of function (North and Reilly, 1990).

Primary Injury

During the primary injury the cells are damaged by physical forces which can compress, stretch, and lacerate the tissue and cells. Due to differences in the mechanical properties of the different areas of the brain, the degree of deformation across these areas is not uniform. While one area may compress significantly, an adjacent area may be more resistant (Briar and Lasserson, 2003). This can lead to the neuronal processes (i.e. dendrites and axons) that span between these different areas becoming stretched and damaged. The injury can cause rupture of the blood vessels of the brain and cause haemorrhaging.

There are three different traumatic brain injury (TBI) scenarios as identified by Headway (2015b). A closed head injury is commonly caused by sudden acceleration e.g. in a car crash and can significantly damage the brain tissue without skull penetration, due to its delicate structures. An open wound is caused by an object which penetrates the skull. A crushing injury is caused by the skull being compressed, and these types of injury often cause most damage to the brain stem (Headway, 2015b). The Glasgow Coma Scale assesses TBI outcome severity from a score of 3: no response; to 15: fully responsive. The scoring is based on eye opening, verbal response and motor response (*Glasgow Coma Score* 2014).

There also are three spinal cord injury (SCI) scenarios identified by Winter et al. (2014). Distraction is commonly caused by sudden acceleration and is characterised by the spine being hyperextended. Compression is caused by axial loading on the spine, however this results in a transverse loading to the spinal cord as the compressive force results in a burst fracture, with vertebral bone fragments or intravertebral discs encroaching into the spinal canal. Thirdly, a penetrating trauma is caused by an object that directly damages the spinal cord and often results in permeation of the meninges and laceration of axons (Lee et al., 2004). The American Spinal Injury

Association scales SCI outcomes from A to E, decreasing in severity, based on both the sensory and motor capabilities of the body caudal to the trauma site (*American Spinal Injury Association Impairment Scale* 2013).

The difference in structure between the brain and spinal cord means that there is a variance in the effects when considered at a cellular level. In the brain, cell bodies are found in the cortex, and so an open wound impact would cause damage to these cell bodies, while a closed wound would also include damage to the axons deeper in the brain. In the spinal cord the cell bodies are centrally located with axons situated in the outer regions, and given it is a thinner structure, any impact is likely to affect both the white and grey matter (Shoichet et al., 2008).

Secondary Injury

Secondary injury can develop over the following hours to weeks (Ward et al., 2014) and is generally identified by two common factors: ischaemia (lack of oxygen) and oedema (swelling) of the tissue local to the injury (Briar and Lasserson, 2003; Ricks et al., 2014).

At rest, the CNS accounts for 20% of the body's oxygen requirements, and 90% of this is used by neurons, despite glial cells making up more than half of the tissue volume (Rodriguez-Boto et al., 2015). Ischaemia is caused by a lack of blood flow to the tissue which is typically due to either a respiratory issue, or a blockage or haemorrhage in the vessel, upstream of the tissue. Disruption to the blood flow results in a shortage of oxygen to the cells of the CNS so a restriction can result in a stroke, infarction or even death of the patient (Murad et al., 2012; Lazarus et al., 2015). Haemorrhaging not only prevents blood from reaching its target, but also inflames the surrounding tissue, and along with the rush of other cells to the injury site, causes oedema.

Most strokes are caused by a blood clot blocking a vital blood vessel to the brain and causing ischaemia. Strokes can occur independently of injury, however can also occur during secondary injury from a TBI as the blood clots to close the wound. In some studies, it has been found that injuries to the spinal cord may result in cell death in the brain (Lee et al., 2004). Although these outcomes of TBI and SCI are well documented, the individual cellular responses to these injuries have

been studied in less detail, with evidence suggesting that the response may vary depending on the location of the injury (Slemmer et al., 2004), whether the white or grey matter is damaged (Ward et al., 2014) and with gender (Lazarus et al., 2015).

Swelling is considered part of the inflammatory response as it is caused by an influx of cells and plasma to the injury site (Wang et al., 2007). The effects of this swelling include inhibition of movement for any joints or breaks and compression of nerve fibres. Both of these effects prevent more damage from being created by making it difficult and painful to move, forcing the body to rest. In the CNS, there is a swelling response similar to elsewhere in the body. As the CNS is enclosed by bone, swelling here can cause a sharp rise in pressure and medical intervention to control this swelling is made more difficult than in other tissues (North and Reilly, 1990).

A severe oedema may compress vital blood vessels, which can be fatal. As the brain is largely enclosed within the hard exterior of the skull, its soft tissue can be damaged as it swells and presses against the skull. The blood flow and swelling of the tissue displaces the CSF into the intracranial compartment which can hold up to 100-150ml. However after this is filled, any additional swelling causes an increase in pressure (Murad et al., 2012). As the swelling increases, blood vessel walls that were weakened in the inital impact can become stretched and tear, further exacerbating the effects. The increase in pressure is of importance clinically as it bears relation to patient outcome, however this relationship is not linear (Rose and Johnson, 1996; Cox et al., 2014).

Non-Traumatic Physical Injury

Tumours in the spinal canal can result in pressure on the cord as they grow in size. The rate of tumour growth is not particularly well investigated in the literature as it appears to be affected by many factors, including the type, location and patient. Metastatic tumour growth in the brain has been found to occur at a rate of 11.7mm^3/day (Yoo et al., 2011a), and malignant brain tumours have been seen to double in size every 19.5 days on average (Yamashita and Kuwabara, 1983).

Evers et al (Evers et al., 2015) found that meningomas at different locations within the brain grew at different rates, averaging 90mm^3/year. Myelopathy is a narrowing of the spinal cord, largely attributable to degenerative osteoarthritis (Bernhardt et

al., 1993) and is one of the most common causes of neck pain in adults, characterised by chronic forces on the spinal cord (Long et al., 2013). Neck pain can be caused by normal aging, as the calcification of the discs of the spine causes them to compress, pushing into the spinal canal which houses the spinal cord. Herniation of a disc, and inflammation caused by rheumatoid arthritis can also put pressure on the cord. Myelopathy can also be caused by injury, as muscle or ligament tears or bone fractures can put excess pressure on the cord. Symptoms of myelopathy include loss of sensation and dexterity, pain, muscle weakness and paralysis (Choices, 2017).

Repair and Regeneration

The processes that occur in the body in the days to weeks after the initial traumatic injury are known as the secondary injury due to the effects presented by the patient (North and Reilly, 1990). However, the secondary injury is occurring at the same time as cellular processes are working to limit the damage and repair or replace damaged cells. Therefore while this period of time is known as the secondary injury, it may also be thought of as the primary repair phase.

In the event of an injury that results in laceration of an axon, a neuron will undergo degeneration, which can happen over the course of a week or more. Due to the compromised cell membrane, the influx of extracellular fluid causes the cell body to swell (Diamond et al., 1985). Proximal to the laceration, the retrograde degeneration can stretch back one or more nodes of Ranvier, where the plasma membrane will close off to limit further cellular damage. The retrograde and Wallerian (anterograde) degeneration involves the fragmentation of the myelin and axons, and the proliferation of oligodendrocytes to up to ten times their number in healthy conditions (Diamond et al., 1985).

The cellular fragments are phagocytosed by the oligodendrocytes, and these cells then form chains of cells along the same path as the degenerated axon, known as bands of Büngner (Diamond et al., 1985). The regenerating axon may find these chains and grow along them, however often a glial scar blocks the path and the neuron is unable to regenerate (McKeon et al., 1991). Glial scarring can occur in the brain or spinal cord. The scar is a feature of the ECM and is formed by an increase in chondroitin sulfate and a change in sulfatation patterns after injury (Ricks et al., 2014). Chondroitin sulfate has been found to inhibit neurogenesis (McKeon et al.,

1991), while the sulfation pattern forms a physical barrier. Atrophy can occur in the target, for example a muscle fibre or another neuron, if the regeneration does not occur.

The role of the neural stem cells in injury repair in humans is not well documented (Kornblum, 2007), however in a model for stroke in rats, neurogenesis was increased after ischaemia; peaking at 8 days after injury (Yagita et al., 2001). Similarly, Li et al. (2002) found that proliferation of neural precursor cells, measured by bromodeoxyuridine reactivity, increased after induced stroke in rats. Studies into mesenchymal stem cells has found they migrate from bone marrow to ischaemic skin within 2-3 days after injury (Hamou et al., 2009) and so their role in the replacement of lost cells is prompt after injury. Johansson et al. (1999) found that neural stem cells proliferated after injury to the spinal cord and these progenitors then migrate to the injury within one week before differentiating further into astrocytes. Fawcett et al. (2002) noted that lesions in the cortex required a substantially larger migration of cells from the SVZ, and so it is unlikely that the same process occurs throughout the CNS. Cellular studies have found that stem cells are present in many areas of the CNS, and *in vitro*, they are highly migratory (Gage, 2000).

The CNS regenerates poorly when compared with other tissues in the body. Fawcett et al. (2002) describe two separate reasons for this: the inability of neurons to regenerate their axons, and inhibitory effects of the environment. The regenerative ability of the neuron is inhibited by three main causes. Firstly its age, as adult neurons do not grow as fast as developing cells; secondly the site of the injury, as when a laceration is near to the cell body the regeneration is often much quicker than those farther away; and individual differences that arise between each cell (Fawcett et al., 2002). The inhibitory effects of the environment are noted to be caused by inhibitory molecules that are present in the damaged tissue, and most notably the glial scar. Aside from the glial scar, no other physical barriers to regeneration are identified by Fawcett et al. (2002), reflecting the limited knowledge available in this field.

1.2.3 Scope of Review

The introductory section has provided an overview of the CNS in health and disease as well as the activities and characteristics of the cells in this tissue. Two cases have been identified in which the CNS appears to interact directly with its physical environment. The current extent of the knowledge in these two areas was critically reviewed.

The first case is that cells are mechanosensitive: the physical structure of the environment can *directly* affect the activities of stem cells in two ways. Firstly, cells appear to contract and pull on their surroundings, discern the response of the material, and respond accordingly (Mohammadi et al., 2015). Secondly the local microarchitecture, such as pore size, can affect the spreading and adhesion of cells, and may also affect gene expression of stem cells (McNamara et al., 2010). These two factors may be interrelated: attaching to a material with a higher elastic modulus (where cellular contractions result in less "give") and being able to form more attachment sites (where cells are located in a matrix with smaller pores) could both result in the contraction force increasing.

The second case is that during secondary injury, oedema can cause pressure in the CNS to rise, and this pressure has been found to be related to patient outcome. While it may be that these two variables have a common underlying cause, it may be that the pressure contributes to patient outcome. Blebbing, the pressure-mediated mechanism (Driscoll and Danuser, 2015) cells use for both division and migration in 3D (Charras and Paluch, 2008), relies on internal cell pressure being greater than external pressure, so an increase in pressure in the CNS could affect this process.

1.3 Investigation of Cellular Mechanosensitivity

As stem cells have been found to be responsive to their mechanical environments, their path of differentiation can be affected by the elastic modulus of their surroundings. This ability means that they can be manipulated through changing this environment. This has implications for the development of new methods of controlling stem cell development as well as understanding their behaviour in the body,

and therefore could also contribute to optimising therapeutic interventions.

1.3.1 Mechanisms of Mechanosensitivity

Receptors on the cell surface known as focal adhesions form the physical links between the cell and its surroundings (Bershadsky et al., 2003). The cell is able to contract and pull on its surroundings with a strain rate of around 1μm/min (Mohammadi et al., 2015), and the different deformation responses of one material to another can trigger different cellular cascades (Altman et al., 2002). The actin in the cytoskeleton of the cell is bound to the integrins at the focal adhesions (Cooper, 2000) and also bound to the nucleus of the cell (Kaivosoja et al., 2012). The actin is also connected to myosin which is the same protein that allows contraction in muscles. The myosin is able to contract and pull the actin fibrils which exerts a force on its extracellular environment (through the focal adhesions), but crucially also exerts a force on the intracellular environment as it does this, creating stress fibres such as those shown in Figure 7.

The magnitude of contractile force that the cell generates is influenced by its environment. Cells within a material with a high elastic modulus have been found to generate a higher force than cells in a lower modulus environment (Lam et al., 2011). Similarly, cells that are in a material with more available sites for attachment are able to form more focal adhesions. Tan et al. (2003) found that a greater force was generated by these cells as each focal adhesion site is attached to myosins. However, Huang et al. (2000) argue that cell shape may also be an important factor in controlling cell fate, introducing the idea of self-organising structures within the cell that are affected by the microarchitecture of the cellular environment and contribute to cell fate direction.

The exact mechanism as to how the cell senses and responds to the mechanics of its environment is still under debate, although the leading hypothesis is that the forces that these actin fibrils experience propagate through the cytoskeleton and change the structure of the nuclear envelope. This membrane has pores and also contains a laminin matrix, both of which would be affected by transmission of these forces. The internal components of the nucleus are contained within this matrix

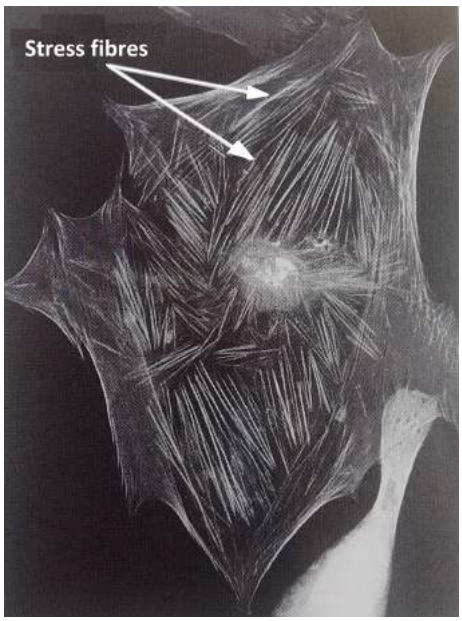

Figure 7: Fluorescently stained actin filaments highlight the stress fibres within a fibroblast. Adapted with permission from Cooper and Hausman (2013).

and therefore any change in structure could alter the organisation of its components (Foisner, 2000). This could physically change the transcription process and thereby decide the fate of a stem cell.

The sensitivity to mechanical properties appears to change depending on stem cell type; Hsiong et al. (2008) found that uncommitted stem cells were not as sensitive to substrate stiffness as preosteoblasts were. Indeed, Engler et al. (2006) found that when MSCs were exposed to a substrate of a different stiffness, they were able to remodel their actin filaments in response during the first week of culture, and the actin filaments bundled together to form stress fibres on stiffer matrices, shown in Figure 7. De Santis et al. (2011) found that this remodelling changes the range of stiffness within which the stem cells were most sensitive to match the substrate: cells with thicker stress fibres were more sensitive to changes within a higher range of stiffnesses. This remodelling both allows the cells to pull harder on their surroundings and also causes a change in the mechanics of the cell itself as thicker stress fibres have a higher stiffness than thinner ones.

A curious aspect of the mechanosensitivity of cells is that *in vivo* the cells themselves initially synthesise their surroundings, and then are directed by the chemical and physical cues of this matrix. In the rest of the body, cells have a short lifespan compared to the body as a whole; red blood cells live for about 4 months while skin

cells live for 2-3 weeks (Cooper, 2000). This means that a new cell residing in an existing matrix may harvest the chemical and mechanical cues that have been left there by their predecessors. In the nervous system, glial cells continuously divide throughout their whole lives, and have been estimated to have a half life of 600 days (Elson et al., 2004) however a large proportion of neurons live as long as the body does, meaning that any cues they take from their ECM were originally synthesised by themselves or their neighbours.

1.3.2 Natural Tissue Mechanics

The measurement of the mechanical properties of soft matter is complex as it is affected by many variables and length scales. As already discussed, the method of testing (i.e. tensile, compressive or shear) will affect the type of moduli found. Other methods for finding the mechanical properties include pressure-volume studies, ultrasound and MRI elastography (Cheng et al., 2008), although each of these focus on different aspects of tissue mechanics. These methods are certainly useful for *in vivo* imaging, however the assumptions made about the tissue can produce inaccurate measurements. Soft tissue such as that of the central nervous system often exhibits a viscoelastic response, introduced in Section 1.2.1 (Saunders, 2015). This means the rate of testing and size of force applied can also affect results. Other test set-ups such as pre-loading, maximum strain, stress relaxation and oscillatory testing can also produce different results, while tissue variables such as age, species, size and orientation can also produce significant effects (Haschek et al., 2013).

Fluid flow out of the material during the testing could also contribute to the viscoelastic response (Cheng et al., 2008). When studying the properties of the CNS, it is important to choose relevant parameters. For studying viscoelastic materials like nervous tissue, it is useful to find the linear viscoelastic region (LVER) of shear strain which, when applied produces a reliable deformation response. When looking at cellular responses, it may seem appropriate to study the material under the conditions that the cells themselves produce as they contract, however applying the same testing parameters that cells do *in vivo* may not always be practical in a laboratory setting. Cellular contractions in a three-dimensional (3D) environment will subject the ECM to tensile stress, however applying this condition to brain tissue is not

as straightforward as its low modulus means that maintaining a firm hold on the samples during testing is not always possible. Secondly, the force applied by each cell is extremely small: cardiomyoctyes derived from human pluripotent stem cells contract with a stress of $100nN/mm^2$, for example (Kosmidis et al., 2015), which is equal to 0.1Pa.

ECM Mechanics

Biological polymers like collagen often possess unusual rheological phenomena not found in synthetic materials (Wen et al., 2012), for example strain stiffening. In collagen structures, the strain stiffening exhibited can be explained by consideration of the triple helical structure of collagen fibrils. As the force is applied, these helices are able to stretch elastically, however as more and more helices become fully stretched, the stress is transferred to the crosslinks of the structure which have a stiffer structure (Wen et al., 2012). This concept has been further described in Figure 8. The elastic modulus of mammalian tendon has been reported to comprise 60-85% collagen type I (Cen et al., 2008). Whole tendons were excised from various quadruped species and immediately tested in moist conditions under cyclic low tensile strain (5-6% strain, 0.05-11Hz) by Pollock and Shadwick (1994). The study reported the tensile modulus to be 1.2GPa when measured in the linear portion of the stress-strain graph, which appeared to occur at approximately 0.05% strain although no precise strain was mentioned.

Elastin was purified from bovine ligament through repeated autoclaving by Aaron and Gosline (1981) and dried. Single elastin fibres were isolated through re-hydration of the elastin in distilled water and the tensile properties were found through a ramped extension to failure; up to 200% strain. The fibrils were found to have a Young's modulus of 1.2MPa although some damage to the fibrils may have occurred during the purification procedure. As bovine ligament has been reported to contain up to 80% elastin (Muiznieks and Keeley, 2013), testing of the fresh tissue may have been more appropriate to minimise damage. HA is an abundant protein in the CNS (Li et al., 2012; Lau et al., 2013), however only mechanical measurements of HA hydrogels were identified in the present review. The elastic modulus of crosslinked HA has been tested under compression and was found to be 2.20kPa (Collins and Birkinshaw, 2008) while under shear was been found to be 390Pa (Jha et al., 2009)

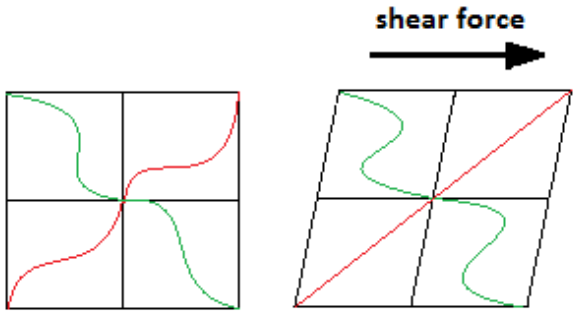

Figure 8: The mechanism of strain stiffening. As the shear force is applied, the polymer in red becomes fully stretched and the forces are transmitted to the crosslinks, as described by Wen et al. (2012).

although neither of these properties may be directly compared to those tested under tensile loads.

Biological materials also exhibit negative normal stress which is where a shear stress (for example τ_{zy} described in Figure 1) can create an internal force perpendicular to the force which creates a contraction in the tissue (negative σ_z). This is an unusual phenomenon and is created by stretched fibrils exerting a larger force on the structure than compressed ones, creating an overall negative tension in the material normal to the force (Janmey et al., 2007). Affine deformation describes a homogeneous deformation where each section of the material deforms by the same degree as any other section (i.e. that the strain is constant throughout the sample) and many soft matter characterisation techniques assume that the deformation will be affine. However, it has been found that many hydrogels exhibit non-affine behaviour due to their complex polymer structure (Wen et al., 2012).

Macro Tissue Mechanics

The properties of fresh porcine cortical grey matter have been found to be homogenous when tested at various locations (Gefen and Margulies, 2004), however the underlying white matter is inherently anisotropic as it is made up of directed fibres. The elastic moduli of brain tissue reported in the literature spans from 40Pa to 20kPa (Franze et al., 2013). As the tissue is strain stiffening, the properties were measured as 200Pa at 10% strain, to over 2kPa at 30% strain (Franze et al., 2013). However, the LVER of bovine brain tissue has been found to be under 0.1% strain when tested by an oscillatory shear strain sweep (Bilston et al., 1997) and

therefore the elastic moduli reported by Franze et al. (2013) of 200-2000Pa may not be reliable. Bilston et al. (1997) tested the white matter of the brain under cyclic shear at frequencies of 1, 5 and 20Hz. were used, finding a shear modulus (G') of 1.5kPa at 1Hz. The axial tensile modulus of fresh spinal cord under low strain rates (<0.25/sec) was found to be 1.2MPa by Bilston and Thibault (1996).

Lu et al. (2006) found the properties of cells in the hippocampus using scanning force microscopy. Neural and glial values were found to be $E'_{Neural} \approx 480Pa$ and $E'_{Glial} \approx 300Pa$ respectively at 30Hz. Bulk tissue properties were found using rheology and at 1Hz, 2% strain, $G'_{Tissue} \approx 105Pa$. To compare these two measurements, the cellular properties were converted from tensile to shear, however the article makes no indication of how this was achieved which is a significant omission as these properties are only related for isotropic materials, which the hippocampus is not (Kim et al., 2017). This conversion found tissue and cell properties $G'_{Tissue} \approx 300Pa$ and $G'_{Cell} \approx 100Pa$ for 25 and 30Hz respectively, suggesting that the ECM makes up the difference. Different areas within the cell such as the soma and cell processes contain different mechanical properties (Lu et al., 2006), for example the processes of radial glial cells have been found to have an elastic modulus of 200Pa, while the soma was 600Pa (Franze et al., 2013). The high water content of brain tissue has raised questions about how perfusion affects the mechanical properties of a living and dead brain, however studies by (Gefen and Margulies, 2004) found that there was no statistically significant difference in the measurements of shear modulus of *in situ* and *in vitro* porcine brain tissue, using tissue immediately after sacrifice for *in situ* testing.

Studies into the shear properties of brain tissue under low strain, such as those presented in Figure 9 and Table 3 by Brands et al. (1999), Shen et al. (2006), and Hrapko et al. (2006) on porcine brain tissue has found that at 1% strain, 1Hz, G' was between 200-600Pa, while G" was 20-40Pa. These data was extracted from the publications using the WebPlotDigitizer (Rohatgi, 2017). Mechanical testing of biological tissues has many complexities. Variation is introduced not only by testing methods but also through natural tissue variation, the sample type and the testing environment. Animal tissues vary between species and human tissue properties may also differ. Tissue that is tested is often frozen to -80°C before being defrosted

for testing. The freezing process can often damage tissue structures, cause cell necrosis and affect perfusion of water within the tissue, all of which can result in a change the mechanical properties (Szarko et al., 2010). Using in vitro methods, cell environments can be more reproducibly controlled for experimental investigation than *in vivo*.

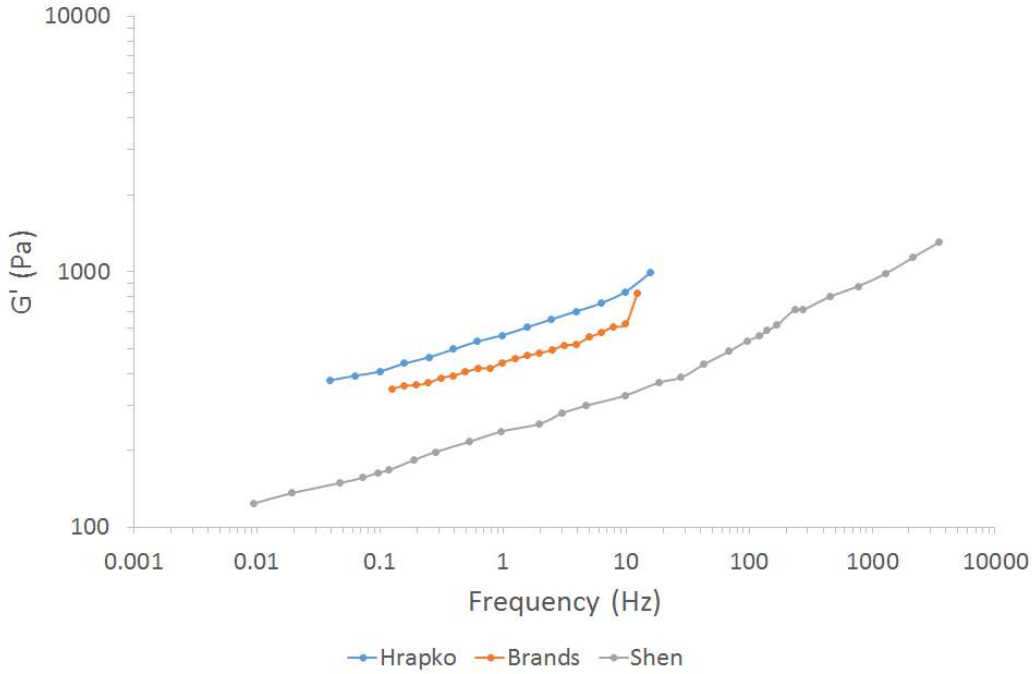

Figure 9: Average modulus response of porcine brain undergoing oscillatory shear frequency sweeps at 1% strain, adapted from studies performed by: Hrapko et al. (2006) on white matter, showing storage modulus, n=7; Brands et al. (1999) on grey and white matter, showing complex modulus, n=4; Shen et al. (2006) on grey and white matter, showing storage modulus n=3. Error bars not shown. Data presented with permission.

Table 3: Shear modulus response of porcine brain at 1% strain, and approximately 1Hz, found by Hrapko et al. (2006), Brands et al. (1999), and Shen et al. (2006).

Author	Frequency (Hz)	G' (Pa)	Standard Error
Hrapko	0.99	564	116
Brands	0.99	441	80
Shen	0.97	237	100

1.3.3 3D Tissue Models for Cell culture

The use of *in vitro* models to examine cells have both advantages and disadvantages over an *in vivo* model. The main disadvantage is the limitation of the model: a synthetic system cannot model the body in its entirety and so the response to factors may vary significantly between the two models. However, the advantages of an *in vitro* system include improved ethical outcomes as *in vivo* models typically include sacrifice of the animal. A second advantage is that the dynamics of the culture model can be more easily controlled and altered resulting in more precise monitoring of the cells and more reproducible results. By starting with a simple experiment design using a single cell type, the complexity can be increased in a controlled way and therefore the factors contributing to a change in response can be more easily identified. *In silico* models are popular for predicting the physical outcomes of mechanical damage, however are not useful when considering biological outcomes as the knowledge of cellular processes and the effects of these are incomplete.

The ECM of human tissues has been described as a hydrogel of collagen (Wen et al., 2012), not including fluids, and 3D *in vitro* models of ECM to date (excluding models of biological fluids) have largely used hydrogels. Hydrogels are three-dimensional networks of either physically or chemically crosslinked polymers and are popular for use in tissue engineering as their ability to hold a high concentration of water (often over 90%) and malleable properties make them extremely versatile for a wide range of applications. Monomers are linked together to form the polymer chain, and various synthetic strategies can be pursued to obtain polymers with defined physical and chemical features.

Classification of Hydrogels

In the field of tissue engineering, hydrogels are categorised primarily into synthetic and biological polymers. Synthetic hydrogels have the advantages of being readily available, with easily controllable properties. Synthetic hydrogels are traditionally designed to be bioinert to reduce the risk of adverse biological reactions to the hydrogel. Biological hydrogels are also popular as these can contain natural polymers that are found within the body, thereby mimicking specific features of biological tissues.

Hydrogels that use synthetic polymers such as polyethylene glycol or polyacrylamide typically exhibit classical elastic behavior, however as already discussed, biological hydrogels exhibit certain phenonema which cannot be described by basic polymer elasticity theory, and Mohammadi et al. (2015) found that cellular mechanosensitivity and remodelling are affected by the inelastic behaviour exhibited by collagen hydrogels, where the energy is dissipated from the system. The hydrogels were tested using an indenter which measured the maximum supported load of a dense and sparse collagen networks. The supported load for the two hydrogels was not statistically different which the authors claimed was a manifestation of the inelastic behaviour, however provided no further explanation as to why this was the case.

In biological applications, collagen is a popular material for the formation of biomimetic hydrogels. Collagen is a triple helical protein (i.e. is made of three polymer chains) that is present in most ECMs, and although each chain contains a wide variety of amino acids depending on the species of animal it is from, all types contain a repeating unit of glycine for every third amino acid. The hydroxylation of lysine residues allows the collagen to become glycosylated or covalently cross-linked. The lysine content of collagen varies widely between locations in the body, location on the helix and the state of health of the tissue (Kannicht, 2008). By cross-linking the collagen, a covalent network can be formed which provides mechanical strength to support the cells within it. The telopeptide domains at the end of collagen molecules have Lysine (Lys) and Hydroxylysine (Hyl) residues. *In vivo*, crosslinking occurs via a condensation reaction in which functionalisation changes the ε-amino groups of the lysine to aldehyde. The condensation reactions (in which H_2O is formed as a product) then occur between the lysines in the telopeptide domains and other lysines elsewhere in other molecules or in the same collagen fibril (Kannicht, 2008).

Design of Hydrogels

Aside from the use of collagen to prepare hydrogels, other popular natural materials include HA, agarose and chitosan (which is derived from crustaceans); while synthetic hydrogels such as polyacrylamide and polyethylene glycol are also growing in popularity (Li et al., 2012).

The design requirements of a hydrogel for neural applications are first and foremost to be able to sustain viable cells within it (Li et al., 2012). This means the hydrogel

must be non toxic to the cells, have a high water content to ensure cells that are seeded into the hydrogel can have access to nutrients that are supplied through aqueous means; and must be stable at physiological pH and temperature (7.4 and 37°C, respectively) (Ahmed, 2015). Secondly, the hydrogel must be porous, and these pores should be interconnected pores – so that nutrients and growth factors can pass through the hydrogel and cells can migrate and proliferate. Thirdly, the mechanical properties of the hydrogel should be similar to that of the natural tissue so that the cells are able to receive the correct biomimeticmechanical cues (Li et al., 2012).

1.3.4 Neural Cell Response to the Physical Environment

The mechanosensitive nature of stem cells was first reported by Engler et al. (2006). Seeding mesenchymal stem cells onto substrates of elastic moduli of 1kPa, 11kPa and 34kPa, the cells differentiated to neurogenic, myogenic and osteogenic lineages accordingly; without addition of any specific chemical cues. The cells were found to not only be able to sense forces, but exert forces on their surroundings through contraction. Cells were discovered to be able to probe the mechanical properties of their surroundings and are able to respond by directing their lineage accordingly.

Two Dimensional Mechanosensitive Models

Saha et al. (2008) were one of the first investigators to build on Engler's findings (Engler et al., 2006) specifically for neural stem cells. Cells were seeded in a monolayer on top of polyacrylamide hydrogels at varying concentrations and polyethylene glycol. The hydrogels were tested using a 0.1-10Hz oscillation frequency sweep to find the complex modulus. The elastic modulus was calculated at 1Hz from the complex modulus using $E' = 2G'(1 + \nu)$ based on the assumption that Poisson's ratio for the hydrogels was 0.5 which is a broad assumption to make as indeed a study into the mechanical properties of soft hydrogels conducted by Chippada et al. (2010) found Poisson's ratio to vary between 0.36-0.49. The justification for using values at 1Hz frequency is unclear. The study conducted by Saha et al. (2008) found that on hydrogels with a modulus of 10Pa, the stem cells displayed little activity, both in self-renewal and differentiation. At 100-500Pa neuron differentiation was prevalent, while moduli of 1-10kPa produced glial cells.

Leipzig and Shoichet (2009) used photocrosslinkable methacrylamide chitosan hydrogels, coated with 5μg/ml laminin to improve cell adhesion, and varied the elastic moduli by varying the photoinitiator concentrations. The storage and loss moduli were found using a compression test. Stress relaxation was measured at 90% strain which had been applied using a 1% per second strain rate. The moduli of the three synthesised hydrogels were found to be 0.80±0.18, 3.59±0.51 and 6.72±0.58kPa. Murine neural stem progenitor cells were isolated from the SVZ. The responses of murine neural stem cells that were seeded onto the hydrogels were investigated at days 0, 4 and 8. Proliferation of the cells was observed to be highest for cells seeded onto hydrogels with a modulus of 3.59kPa, took a neuronal lineage at <0.80kPa and and an astrocyte lineage on hydrogels with moduli between 0.80 and 3.59kPa. Oligodendrocytes were most prevalent at 6.72kPa, however they only mylinated axons at <0.8kPa where neurons were present. The change in pore size was observed using an SEM, and although no measurements of the pores were reported, the authors noted that increasing crosslinks resulted in smaller internal pores and improved laminin absorbance. These changes to the physical nature of the hydrogel could also affect neural stem cell differentiation as cells interacted with different microenvrionments (Christopherson et al., 2009).

Three Dimensional Mechanosensitive Models

The two dimensional studies show promise with regards to controlling the fate of neural stem cells by varying hydrogel stiffness, however as these studies were conducted with monolayers of cells on top of the hydrogels, i.e. in 2D, this may mean that the cellular response to these ranges of stiffness is not be the same when in a 3D *in vivo* environment (Huebsch et al., 2010). As the modulus was controlled by varying the crosslinker content the concentration of available ligands may have affected cell adhesion, and as described previously this may have also contributed to controlling the cell activities. Indeed, Kothapalli and Kamm (2013) found that the differentiation patterns of embryonic stem cells were significantly different in 2D and 3D substrates. The moduli of these scaffolds were altered by varying the concentration of various proteins in the scaffold network including HA and Matrigel (BD Biosciences, USA), and the properties were measured using atomic force microscopy. Table 4 summarises the 3D *in vitro* studies that investigated neural differentiation.

Table 4: Summary of 3D models for neural differentiation by mechanosensitivity

Author	Banerjee	Her	Bozza
Year	2009	2013	2014
Stem Cell Type	Neural	Mesenchymal	Embryonic
Hydrogel Type	Alginate	Collagen	Alginate
Altered Concn	Alginate, $CaCl_2$	EDC	Alginate
Mechanical Testing	Oscill. Rheol.	Ramped Compression	Cyclic Compression
Reading Taken	within LVER	At 10% strain	within LVER
Elastic Moduli	0.18-20kPa	1.1-9.9kPa	10-60Pa
Physical Testing	None	SEM - pore size	Water Content
Physical change	Not studied	Changed	Unchanged
Cell differentiation	0.18kPa: neuronal	1.1kPa: neuronal, 9.9kPa: glial	10Pa: neuronal, 60Pa: pluripotency

Banerjee et al. (2009) performed some of the first work in the field of 3D matrices of controlled modulus for neural stem cell differentiation in 2009. The elastic modulus of the hydrogels were varied by altering the concentrations of components of the hydrogel (the alginate from 0.25-1% (w/v) and calcium chloride from 10-100mM), which may have produced effects independently of hydrogel stiffness, however no other hydrogel properties were characterised. The cells were mixed with the sodium alginate solution during synthesis. More recently Her et al. (2013) studied the differentiation of mesenchymal stem cell towards neural lineages using 3D hydrogel constructs synthesised with collagen and HA, and crosslinked with a carbodiimide. The hydrogels were also characterised by morphology, porosity and pore size, water absorption and degree of crosslinking. The properties of the hydrogels were varied by modifying the concentration of the EDC crosslinker from 0.1-2% (w/v), however the authors found that there was a 67% reduction in the number of free ε-amino groups between lowest and highest crosslinker concentration and the size of the pores in the matrix, measured from SEM images, reduced by 36%. Bozza et al. (2014) mixed murine embryonic stem cells into an alginate solution to synthesise hydrogels and the properties were simply modified by varying concentrations of alginate. The properties were further modified with the addition of HA and fibronectin for some samples.

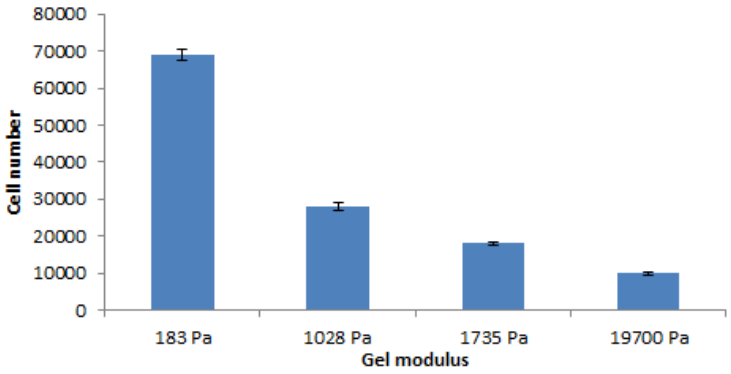

Figure 10: Oscillatory shear modulus vs neural stem cell proliferation after 7 days culture, adapted with permission from Banerjee et al. (2009). Error bars represent standard deviation.

The elastic modulus was determined by Banerjee et al. (2009) via oscillatory shear stress testing, by first performing a stress sweep at 1Hz to find the LVER, then a frequency sweep was performed within this range, approximately 0.1-10Hz. The value of stress of the LVER was not reported, nor what value was used for the subsequent frequency sweeps. Determination of elastic modulus within the LVER is important for reproducibility of results and so this is an important omission. Her et al. (2013) characterised the elastic modulus using compression tests at 0.5mm/min (17% per minute) strain rate up to 75% strain and the elastic modulus was calculated at 10% strain. The authors claimed that 10% strain was representative of the degree of strain cells can place onto their substrates, although no evidence was given for this. Wall et al. (2007) found cell strain of tenocytes to total between 37-63%. Bozza et al. (2014) tested hydrogels under cyclic compression at 1Hz, sweeping the amplitude to 10%, determining elastic modulus within the LVER.

Banerjee et al. (2009) determined that neuronal differentiation was favoured at a modulus of 183Pa as expressed by Nestin and β-tubulin III markers for neural stem and neuronal cells respectively, although this was the lowest modulus tested, the next lowest being 1028kPa, and the lowest modulus hydrogel also favoured proliferation of the neural stem cells, as shown in Figure 10. Due to this large variance in stiffness with few data points, the results show that neuronal differentiation is favoured in the 100's of Pa range rather than the kPa range, and although the authors noted that $\sim$180Pa was in the range of the elastic modulus of natural brain tissue, no further conclusions could be drawn. Assays for glial cells were not performed in this

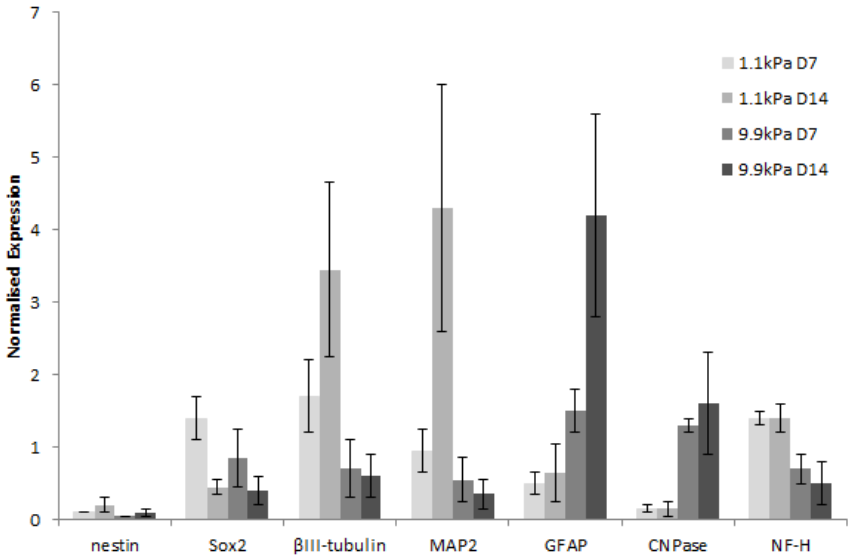

Figure 11: Differentiation of mesenchymal stem cells on hydrogels of varying compressive elastic modulus, adapted with permission from Her et al. (2013). βIII-tubulin, MAP2 and NF-H proteins are expressed during neural differentiation, while GFAP and CNPase are expressed during glial differentiation. Nestin and sox2 are markers for undifferentiated neural stem cells. D7 and D14 relate to day 7 and 14, n=3.

study, and based on previous studies in 2D, the difference in stiffness for neuronal or glial lineage specification may be in the 100-1000Pa range (Saha et al., 2008) and so this could have provided a useful insight into this lineage preference.

For Her et al. (2013), cells were seeded onto the already synthesised hydrogels, however it was observed after hematoxylin and eosin (H&E) staining that the cells were homogeneously spread throughout the scaffold from day 1. Comparing hydrogel stiffnesses of 1.1kPa with 9.9kPa, it was found that neural markers such as βIII-tubulin, MAP2 and NF-H were all most abundant at the lower stiffness, while glial markers such as GFAP and CNPase were more prolific at the higher stiffness of hydrogel, as shown in Figure 11.

Using markers for "stemness genes", ie genes transcribed by stem cells but not by differentiated cells (CD73, CD90 and CD105) Her et al. (2013) found that after 2 weeks of culture, cells on both soft and stiff substrates had differentiated, however these genes were markedly down-regulated on stiff substrates, suggesting that these cells differentiated sooner than those on softer substrates. Nestin, a marker for

neural stem cells (a less potent stem cell than that of mesenchymal stem cells) was expressed at low levels. The authors suggested that this indicated that the differentiation pathways of mesenchymal and neural stem cells was different, however it could be that all the mesenchymal cells briefly differentiated into neural stem cells before differentiating further. By modifying the concentration of crosslinker they have navigated past the effects of changing collagen concentration, however the concentration of crosslinker was reported to affect pore size and available ε-amino groups, which stem cells may well respond to. Also, as Banerjee et al. (2009) remarked, the responses of stem cells to elastic moduli may be affected by the type of stem cell used. As Her et al. (2013) use mesenchymal stem cells, this work may not be directly translated to that of neural stem cells.

Comparing the alginate-only samples, the pluripotency marker Oct 3/4 was upregulated in hydrogels with a modulus of 60Pa and neuronal differentiation markers βIII-tubulin and NCAM were upregulated in hydrogels with a modulus of 10Pa (Bozza et al., 2014). The study also tested the water content of the hydrogels, which showed no significant differences, however no other physical hydrogel properties such as pore size or free ε-amino groups were characterised.

Aside from the prevalent problem of changing hydrogel stiffness without modifying other properties, the work of Banerjee et al. (2009), Her et al. (2013), and Bozza et al. (2014) have other limitations. Although Banerjee et al. (2009) have explored a hydrogel with a stiffness <1kPa, the range of moduli is extremely large with only four values of moduli investigated. The amplitude or stress applied for the frequency sweeps in this study was not disclosed, however in a viscoelastic material this is an important factor to consider. Her et al. (2013) observed that the LVER occurred at 10% strain, which is where they take their readings from, however did not report any hydrogels with a modulus under 1kPa. Again, the range of moduli explored by Bozza et al. (2014) is insufficient, with no hydrogels above 100Pa used. Although the modulus value was taken from the LVER of the amplitude sweeps performed, there was again no disclosure as to what this amplitude was. Banerjee et al. (2009) performed an oscillatory shear stress, Her et al. (2013) described a ramped compression test while Bozza et al. (2014) used a oscillatory compression test so direct comparison of these hydrogel systems is not possible.

To date, most of the studies conducted into mechanically influenced neural stem cells have been conducted in 2D, however as discussed by Huebsch et al. (2010), the change in environment from 2D culture to 3D can significantly alter the response of stem cells to particular matrix stiffness values. The investigation into the mechanical characteristics in these studies is often somewhat incomplete. No studies were identified reporting whether it is local elastic modulus or rigidity of the macro tissue that cells respond to, and indeed it is an interesting question in the case of the mechanosensitivity of cells at tissue boundaries. A study by Mohammadi et al. (2015) produced "floating" hydrogels to examine the effects of the rigid support of tissue culture plastic upon which the hydrogels reside during cell culture. Seeding fibroblasts, they found that the cells changed their "spread" or surface area more on floating hydrogels compared to supported hydrogels. The overall properties of the bulk material incorporate that of the polymer combined with the water, however in practice the cells do not adhere to the water, only the fibre mesh that contains it.

Her et al. (2013) performed *in vitro* studies into the effect of physical environment on mesenchymal stem cells and varied the concentration of their crosslinking agent 1-ethyl-3(3-dimethylaminopropyl) carbodiimide (EDC) to produce 3D hydrogels of varied stiffness. The EDC concentrations tested were 0.1, 0.5, 1.0 and 2.0%. The degree of crosslinking was determined via the trinitrobenzine sulfonic acid (TNBS) assay and was found to increase from 37-72% crosslinking with increasing EDC concentration. Free ε-amino groups decreased three-fold over the EDC concentration range from 106-35μmoles/g.

SEM analysis revealed that although the pore size of the scaffold decreased with increasing EDC, the porosity remained above 96%. This change in EDC concentration was then related to Young's modulus via compression tests, which applied 10% strain on an Instron microtester with 10N load cell capacity. The modulus was found to increase with increasing EDC concentration from 1.1-9.9kPa, however the loss modulus of the hydrogels was not studied. Additionally, only acellular hydrogels were characterised, so the effects of cell seeding on the elastic modulus or of pore size on the cells were not investigated. As cells interact directly with each other via cell-cell interactions, an investigation into the stiffness of the seeded hydrogel could have provided further information of this relationship.

Studies have also found that differentiated cells are able to become pluripotent by being cultured in certain physical environments. Caiazzo et al. (2016) seeded murine fibroblasts onto polyethylene glycol (PEG) hydrogels. The hydrogel properties were varied by changing the polymer content and were characterised via rheology. After 16 days, cells seeded in 3D hydrogels with an elastic modulus of 300Pa were expressing pluripotency markers and were better able to maintain their pluripotency than cells cultured in 2D on tissue culture plastic, which has an elastic modulus of approximately 100MPa (Skardal et al., 2012).

Biological Polymer Variability

It is clear that the elastic modulus of biological hydrogels is tunable. However, this capability is not always able to be controlled, and this has impeded the use of hydrogels as defined 3D microenvironments (Moreno-Arotzena et al., 2015). This variation has also been identified in commercial hydrogels, for example Matrigel (Hughes et al., 2010). Indeed, Wenger et al. (2007) also commented on the causes of variation, including the state of hydration, the random differences in individual collagen fibrils and uncertainties in the test. Raub et al. (2010) found using rheology that the elastic modulus of cellularised collagen hydrogels can range from 0.5-12kPa using 3-9mg/ml collagen, while Wenger et al. (2007) found using atomic force microscopy that individual collagen fibrils range from 5-11.5GPa.

Kreger et al. (2010) used mesenchymal stem cells to determine the effects of tunable hydrogels using porcine skin collagen, found lot-to-lot variation of elastic modulus was sufficient to change the differentiation of the cells between adipogenic and osteogenic pathways. Johnson et al. (2007) noted that low variablity may be acheived when lots are quality controlled on their polymerisation potential and matrix mechanical properties. However, as argued by Abraham et al. (2008), many other properties of collagen are variable and can induce changes in cellulare response, including secondary and tertiary structure, chemical composition, hydrophobicity and surface roughness.

Topographical Models

Aside from cells responding to mechanical properties, the physical properties also have an effect. The topography of a material affects cellular adhesions to the material, cell-cell interactions and the shape of the cell and its internal components

(Griffin et al., 2015), and this topography can be the form of micro-scale or nano-scale architecture of the cellular environment (Dalby et al., 2007). While there are now many studies on the spatial sensitivity of stem cells, the cellular processes that facilitate this sensitivity remain unclear. This means that important parameters for influencing stem cells are still unknown.

McBeath et al. (2004) studied the effects of cell spreading have been examined with mesenchymal stem cells; finding cells that were allowed to spread on areas of 10,000μm^2 per cell differentiated into osteogenic lineages, while those on 1024μm^2 areas were constrained to remain rounded and were directed to adipogenic lineages. McBride and Knothe Tate (2008) varied cell density from 16,500-86,500 cells/cm^2, either seeding at the required density or seeding at a lower density and allowing proliferation to occur up to the target. Although the aim of the study was to examine cell spreading, by choosing to vary the cell density the cell-cell and cell-material interactions were inevitably also affected. The cells that proliferated to the highest density had rounded nuclei while cells that were seeded at the highest density had flattened nuclei. However, the cell group that had been proliferated to the required density was cultured for four days, while the cells that had been seeded at the required density had only been cultured for 24 hours. Many of the gene expressions were compared for the two cell groups which were at different time points in their experiments. Furthermore, the group that had been left to proliferate did not meet the target density by a significant degree. The use of cell density to investigate topographical cues is problematic as varying cell number for a given space will also affect the concentration of chemical cues secreted by neighbouring cells.

Brammer et al. (2009) identified a change in morphology of the nuclei of osteoblasts when cultured on large 70-100nm nanotubes as opposed to smaller 30nm tubes. The cells on larger tubes also upregulated alkaline phosphotase secretion, suggesting an enhanced bone-forming ability. Christopherson et al. (2009) found that neural stem cells cultured on electrospun fibre mats changed their proliferation rates and differentiation path depending on the fibre diameter. While oligodendrocyte differentiation was favoured on the thinnest fibre diameter of 283nm, the neuronal lineage was more common on 749nm fibres. The study also reported an increase in proliferation as

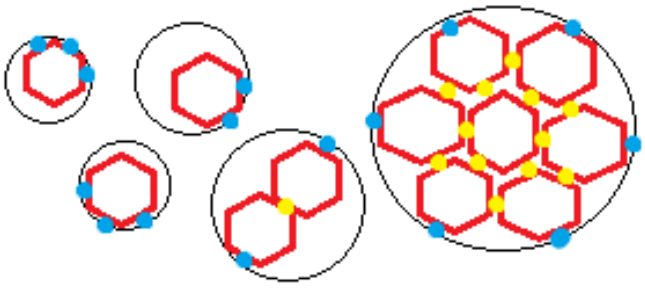

Figure 12: Potential effects of pore size on cell-cell and cell-material interactions. Pores represented by black circles, cells represented by red hexagons. Cell-cell interactions represented by blue dots, cell-material interactions represented by yellow dots.

the diameter increased. Smaller tubes would increase cell-material interactions and decrease cell-cell interactions, as explained in Figure 12.

A comparison of the importance of cell density and topography on stem cell influence was made by Beduer et al. (2012). The study used microchannels to influence human neural stem cells but found that the seeding density greatly affected the response. In a lower seeding density of less than 10 neurons per mm^2, where there were more cell/surface interactions, the neurite outgrowth aligned with the microstructure. In a higher density of more than 70 neurons per mm^2 with more cell/cell interactions, the neurites created an interconnected network amongst themselves. Again, varying seeding densities does not only change cell interactions, but also spreading other shape changes.

One of the main limitations of topographical studies that examine the effects of cell-cell and cell-substrate interactions is that the environmental set up is in 2D. While these studies prove that many physical factors influence the behaviour of cells, the clinical relevance of the findings may be limited. Secondly, it has become apparent that any attempt to study one aspect of topography, necessarily affects other parameters, making attempts to draw conclusions of one influencing factor difficult.

1.4 Investigation of the Effects of Pressure on CNS Cells

Although the effects of elastic modulus on stem cell differentiation have been widely studied, the effect of hydrostatic pressure on cellular activities currently appears to be a much smaller field of research. The ICP is the only force that is exerted onto the CNS except during injury, and so an investigation into the effects of this on CNS cells is worthwhile to understand if cell activities are directly affected by pressure. The present investigation into this area includes methods for measuring pressure both *in vitro* and *in vivo*, intra- and extra-cellular pressure, CNS pressure *in vivo* in health and disease and current progress of *in vitro* CNS cell pressure models. This investigation provides a view into the extent of current knowledge of this area, and areas of knowledge that are missing can be determined.

1.4.1 Pressure Measurements

In meteorological and engineering applications, a barometer is used for measuring atmospheric pressure while a manometer is used for measuring pressure differences, i.e. gauge pressure. Both instruments use the same principles; by measuring the displacement of a liquid in a tube (such as water or mercury) and using the cross-sectional area of the tube and the force required to move the liquid, the pressure can be calculated. For measuring gauge pressures, it may be important to also measure the atmospheric pressure, as the absolute pressure may also influence results. In practice, medical journals do not seem to record atmospheric pressure, despite studies showing that atmospheric pressure can change blood pressure, for example (Jehn et al., 2002).

In vivo, while blood pressure can be easily measured non-invasively by compression of a vessel, measurement of ICP can be more difficult. It is known that ICP can be a predictor of outcome so there is much interest in monitoring it (Rose and Johnson, 1996), however the current gold standard ICP measurement is invasive, requiring a catheter to be inserted into the cranium via Kocher's point (Raboel et al., 2012). This limits patient mobility and risks hemorrhage and infection (Kawoos et al., 2015). Non-invasive methods are therefore being developed to negate the risk of adverse consequences arising as a result of measurement. Non-invasive methods

include Transcranial Doppler Ultrasonography which uses ultrasound to measure blood flow velocity and find the pulsatility index (Raboel et al., 2012), which is known to correlate well with ICP measured invasively (Bellner et al., 2004) with a mean error of ±4.2mmHg, however only at pressures below 30mmHg, after which it increases. Tympanic Membrane Displacement measures the deflection of the stapes and the membrane covering the oval window in the ear, caused by changes in the fluid pressure in the cochlea (Raboel et al., 2012). While this technique is more difficult to apply in patients over 40 due to physical changes, it can distinguish between normal ICP and hypertension (Raboel et al., 2012). The idea of using MRI to predict ICP has been explored (Alperin et al., 2000), using a motion-sensitive MRI to measure flow of fluids in the intracranial space. The success of the technique was mixed, however offers a useful screening tool, as well as providing diagnostic capabilities to evaluate chronic disorders (Raboel et al., 2012). Finally, the observation and grading of optic disc swelling has been found to have good specificity and sensitivity, both >88% (Frisen, 1982), however is noted to be time consuming and therefore cannot be used in emergency situations (Raboel et al., 2012).

1.4.2 Hydrostatic Tissue Pressure

Intracellular pressure has been measured for a wide range of cells, using a variety of techniques (Petrie and Koo, 2014). The cytosol which is contained within the membrane is around 70% (v/v) water. Water is essential for cell viability as the self-assembly of the membranes and protein filaments depend on an aqueous environment. Physically, the cytosol provides a hydrostatic pressure to enable the cell to maintain its shape, much like the CSF does for the brain, and has been found to be at 20-100Pa (0.15-0.75mmHg) normally (Charras and Paluch, 2008), or 45-300Pa (0.33-2.3mmHg) during division (Charras et al., 2008) and 2200Pa (16.5mmHg) during 3D migration (Petrie et al., 2014). Shimada et al. (1993) noted that disruption of the cell wall occurs before 500MPa (3.75×10^6mmHg).

There is little literature on extracellular fluid pressure, however some work has been done into inflamed dental pulp pressure (Heyeraas and Berggreen, 1999). The findings for healthy tissue from these studies are mixed, ranging from 0 to 60 mmHg, although most studies did not find pressures beyond 15 mmHg. Katz (1978) mea-

sured the interstitial fluid hydrostatic pressure in canines, finding it to vary by location in the body, mean pressure in muscle was found to be 6.4mmHg, while subcutaneous readings were at 1.5mmHg. More recently, Kang et al. (2013) found subcutaneous porcine interstitial fluid hydrostatic pressure to be 7.50mmHg.

Li et al. (Li et al., 2012) claimed that the CNS is not load bearing, however this assessment does not take into account ICP. The level of ICP in the CNS is critical as it ensures constant perfusion of essential nutrients and oxygen from the blood to the brain. The body autoregulates the arterial pressure so that it is always a consistent degree higher than ICP, thus maintaining a constant perfusion pressure, ensuring a steady perfusion rate (Raboel et al., 2012). ICP itself is a product of the volume of the CNS cavity relative to the volume of its contents as well as the compliance of the tissue in this zone (Ross and Eynon, 2005). A change in ICP can therefore indicate a change in blood pressure, a change in the CNS cavity size or a change in the volume of its contents. For example, hydrocephalus is caused by a blockage or disruption to the drainage of the CSF, so when new fluid is created, this causes an increase in ICP i.e. hypertension, while a CSF leak into another cavity causes a reduction in ICP, i.e. hypotension. In healthy subjects ICP is around 5-15mmHg (0.6-2kPa) (Steiner and Andrews, 2006; Fleischman and Allingham, 2013; Murad et al., 2012) however can change in pathology. Low ICP has been found to be a risk factor for glaucoma (Fleischman and Allingham, 2013) while patients who incur a TBI have an elevated ICP of typically 20-30mmHg (2.7-5.3kPa) (Murad et al., 2012) which is sustained for several weeks and can reach peaks of 85mmHg (11.3kPa) (Stocchetti et al., 2007).

After injury, ICP rises and falls in waves as the swelling is counteracted by the bodies autoregulatory system. The waves are categorised as A, B or C Lundberg waves (Lundberg, 1960) which are differentiated by their time period and detailed in Table 5. "A" waves are also known as plateau waves and feature a sudden rise in pressure to over 40mmHg and maintenance of this pressure for five minutes or longer (North and Reilly, 1990; Cox et al., 2014). This occurrence indicates that the "overfill" cisterns introduced in Section 1.2.2 are full and the system can no longer compensate for any extra fluid. Raboel et al. (2012) asserted that the "A" waves can be a sign of loss of cerebral autoregulation, hwoever Rosner and Becker (1984)

argued that the wave demonstrates an intact autoregulation system. However, while plateau waves that last longer than 30 minutes are associated with a worse outcome due to ischaemia, patients with shorter plateau waves actually have a better survival rate than those without any at all (Cox et al., 2014).

"B" and "C" waves are deemed less clinically significant as their occurance has not been found to be a pedictor of patient outcome. 'B' waves last 1-2 minutes, and involve an increase in pressure of 20-30mmHg which is not sustained and immediately begins to fall again. 'B' waves are thought to correspond to the patients vascular condition and cerebral blood volume (North and Reilly, 1990). 'C' waves occur at a frequency of 4-8 per minute and give a rise in pressure of 10-20mmHg. 'C' waves correspond directly with breathing cycles (North and Reilly, 1990).

Table 5: Lundberg Wave Categories

Name	Time period	Pressure change	Cause
A	5 minutes+	30mmHg+	Full cisterns, loss of autoregulation
B	1-2 minutes	20-30mmHg	Cerebral blood volume
C	7-15 seconds	10-20mmHg	Breathing

1.4.3 Neural Cell Responses to External Forces

Studies involving the response of cells to force aim to replicate injury scenarios. *In vivo* models have major ethical issues and the cellular response can be difficult to monitor in isolation, however the test has the potential for few limitations as a representative model of traumatic injury. *In vitro* models utilising tissue samples or cell cultures have fewer ethical issues and the cellular response can be more easily monitored and controlled. However, the limitations of the test are greater. At a cellular level, the chemical composition of the external environment changes after injury (Cooper, 2000), while at a macro scale, the fluid pressures and blood flow may also not easily be included to models.

Primary Injury Models

Two main types of *in vivo* primary injury models exist, the majority of which have been carried out on rats and can involve damage to the brain or spinal cord:

contusion injuries model traumatic incidents and involve application of a force for a short time, or compression injuries involve static loads and are used to model the forces involved in chronic injuries or the secondary injury. There are three popular contusion injuries performed for TBI or SCI; weight drop, fluid percussion and controlled cortical injury. Lazarus et al. (2015) created a unilateral controlled cortical impact model in rats by performing a craniotomy and impacting the exposed tissue with a 3mm impactor to a depth of 2mm, at a rate of 5m/s, Liu et al. (1999) created a contusion directly on the spinal cord of rats by dropping a 5g weight from a height of 15cm, Del Mar et al. (2015) delivered an air-blast of 70psi and limited the area to a 3x5.5mm spine section in mice. Popular methods of compression injuries have include application of static loads or use of aneurysm clips for specific time periods. A static load was created by Ward et al. (2014) by a 50g weight applied for 5 minutes to rats investigate the secondary response to traumatic impacts, while Long et al. (2013) inserted expanding polyurethane sheets in the epidural space between rat vertebrae.

In vitro CNS damage models that exist in the literature include that of Weightman et al. (2014), which modeled a spinal cord laceration injury. A scalpel was used to create a basic lesion model, used to screen regenerative materials. Slemmer et al. (2004) and Weber et al. (1999) induced a stretch trauma to flexible collagen-coated cell culture plates to model the effects of mild, moderate and severe trauma to CNS, which was first introduced by Ellis et al. (1995). The test produced a stretch of 31-54% using a 50ms pulse of compressed gas (Weber et al., 1999). The model has been demonstrated to produce a similar response in neural cells to a trauma *in vivo* such as damage to the cytoskeleton and mitochondria, increased membrane permeability, phospholipase activation (Slemmer et al., 2004) and calcium influx (Weber et al., 1999), however none of these *in vitro* models account for secondary injury effects such as compressive forces or ischaemia.

Common cytokines found to be involved in the response to traumatic injury include interleukins 1 and 6, tumour necrosis factor alpha (TNF-α) and the complement cascade, which are all involved with the inflammatory response (Helmy et al., 2011). TNF-α also has effects in both in degeneration and protection of the tissue following SCI (Garraway et al., 2014) as it has been found to promote myelination

and stem cell survival (Wang et al., 2014). The biological responses to TBI outlined above cause oxidative stress which leads to carbonylation of specific proteins, as well as astrocytes and ependymal cells, which can affect protein function and further contribute to the injury and Lazarus et al. (2015) found that protein expression most affected by TBI included GFAP, dihydropyramidase-related protein 2, fructose-biphosphate adolase C and A. Fee et al. (2003) have shown that CD4+ T cells can further the damage caused by a traumatic injury. The concentration of hydrogen peroxide has been found to significantly increase following contusion of the spinal cord and Liu et al. found that this was a contributing factor to the cause of protein oxidation and cell death (Liu and Bao, 2015). Secondary effects found by Ward et al. (Ward et al., 2014) included a loss of the axonal and dendritic proteins, a loss of myelin and a rise in β-amyloid precursor protein which is a marker of axonal dysfunction.

Secondary Injury Models

A model to study the effects of the rate of chronic compression forces *in vivo* was performed by Long et al. (2013), inserting polyurethane sheets into the epidural space which expanded at different rates, monitoring the response over a period of 1 week. The sheeting was cut to $3mm^3$ and expanded to a maximum volume of seven times its original size over three separate time periods: instant, 2 hour and 24 hour.

Lei et al. (2011) created four different test set ups to study the effect of pressure and oxygen tension *in vitro* on optic nerve astrocytes. These were used to model the effects of glaucoma, a condition associated with a build up of pressure within the eye. Lei et al. (2011) investigated cell viability and migration using a 2D cell culture which aimed to change the pressure and oxygen tension independently from one another, noting that the interrelation between these two factors is often ignored. To increase the pressure, a height difference was used between the medium reservoir and the culture chamber, whereby the medium fell through a drop of 100mm to reach the cells. In a high pressure, low oxygen set up, the cells were cultured at a depth of 100mm under media while for low pressure, low oxygen, the cells were cultured on their side at the end of a 100mm "tunnel" of media. Assuming the medium to have the same density as water, 100mm depth corresponds to 7.4mmHg which is within the normal range of ICP.

The assessment of the study by Long et al. (2013) included MRI imaging, "BBB" scoring (Basso, Beattie and Bresnahan, which is a measure of functional recovery following spinal cord injury) and H&E staining to measure the quantity of motor neurons. The results showed that hemorrhaging occurred in specimens in the "instant" group, with a severe loss of function, and the BBB score at 24 hours post treatment was significantly lower compared to the slower time periods. Comparing the gradually expanding polymer sheet groups, the results suggested that the response to a gradual increasing force is not significantly different for loads applied over two and 24 hours.

Lei et al. (2011) found that the cells cultured at low oxygen tension (100mm media depth or tunnel) were hypoxic at day 1 and using an exclusion zone assay, that higher pressure did not increase cell migration. Salvador-Silva et al. (2004) also used a 100mm media depth to create a high pressure environment, using optic nerve astrocytes cultured in 2D and an exclusion zone assay and found increasing pressure significantly increased migration from day 3. The cells were prevented from proliferation by used of an anti-mitotic drug, and at day 5 the cells under high pressure had migrated 38% more than the control group under 15mm media (1.1mmHg).

Another method is the pressure chamber model first described for cells by Sumpio et al. (1994). It involved piping pressurised air with 5% CO_2 into a sealed air tight vessel capable of withstanding the required pressures and able to fit into a standard incubator. It included a stopcock to control the air flow and a transducer to measure the pressure of the vessel. Sumpio et al. (1994) used the equipment for the culture of bovine endothelial cells and pressures of up to 120mmHg, finding the pressure stimulated proliferation of the cells. Yu et al. (2011) also measured the pH, carbon dioxide pressure (PCO_2) and oxygen pressure (PO_2) while using this set up and found there was no significant difference between this and the control which was at atmospheric pressure. The main finding of the study by Yu et al. (2011) was that the expression of glutamine synthase in rat retinal glia was significantly increased at 40mmHg and 60mmHg compared to 0mmHg. The expression of glutamine synthase is a key function of the retinal glial cells, so this study suggests that their functionality is increased at these pressures.

1.4.4 Pressure for Regenerative Therapy

Increasing evidence points to pressure inducing a regenerative effect and therapies have been developed for clinical use. Both Extracorporeal Shockwave Treatment and Ultrasonic Thalamic Stimulation utilise an increase in pressure, while so-called Negative Pressure Wound Therapy utilises a pressure lower than atmospheric pressure.

Extracorporeal Shock Wave Treatment

Pressure waves known as extracorporeal shock wave treatment (ESWT) have been found to aid the regeneration of peripheral nerves (Hausner et al., 2012). ESWT is a high amplitude longitudinal accoustic pressure wave (Zhao et al., 2013) that is applied from outside the body, directed at a particular area within the body with the aim of transmitting the pressure wave to produce an effect in the local tissue. High energy ESWT has been used in the treatment of kidney stones since the 1980s (Chaussy et al., 1982) as a method of breaking up the solid aggregates that form. Low energy ESWT is now recognised to be a valuable method for tissue regeneration such as for chronic wound healing (Mittermayr et al., 2012). The ESWT pressure wave for regenerative therapy typically includes a peak of above 100MPa for less than 10ns, followed by a trough of around -10MPa, with the whole wave lasting less than 10μs (Ventura, 2013). More recently, ESWT has been found to improve the rate of axon regeneration in the peripheral nervous system *in vitro* (Hausner et al., 2012). Using a rat model, an 8mm section of the sciatic nerve was removed, rotated 180°and replaced before ESWT was administered. The group which received ESWT showed a faster improvement in movement of the affected limb, while electrophysiology showed a significant improvement after 3 weeks. ESWT has also been found to upregulate mesenchymal markers in adipose-derived stem cells *in vitro* and also increase their differentiation capacity, with ESWT treated cells able to express schwann cell marker S100β (Schuh et al., 2014).

Ultrasonic Thalamic Stimulation

Recently, Monti et al. (2016) have found that delivering a targeted stimulation of the thalamus using low intensity focused ultrasound pulsation could have a regenerative effect on patients with disorders of consciousness (DOC) after TBI. Due to the novelty of this research, at present the treatment has only been delivered to one

patient, however the results were remarkable. The recovery was recorded using the Coma Recovery Scale - Revised which grades functionality of patients with DOC from 0 (no function) to 23. It is not uncommon for DOC to last indefinitely.

An ultrasound transducer delivered a pulse of wavelength 0.5ms at 100Hz. Each sonication lasted 30 seconds, with a 30 second pause between each one, with 10 sonications performed in total. The patient improved dramatically after treatment as shown in Table 6. By 5 days after treatment the patient attempted to walk. This finding correlates with similar studies, finding ultrasonic thalamic stimulation can reduce recovery time of anesthetised rats (Yoo et al., 2011b)

Table 6: Coma Recovery Scale - Revised score for patient with DOC who has undergone ultrasonic thalamic stimulation.

Day	Coma Recovery Scale Score
Day prior	15
Day of (before)	14
Day of (after)	13
Day after	17

Negative Pressure Wound Therapy (NPWT)

NPWT is used to treat non-healing, chronic wounds and involves the application of a vacuum to the affected area. A vacuum pump is attached to the the wound using an air-tight wound dressing that is adhered to the skin surrounding the affected area. Morykwas et al. (1997) reported the use of NPWT with a pig model. Circular defects 2.5cm in diameter were created through the skin to a depth of the connective tissue covering the spinal muscles. The NPWT was applied in 25mmHg reductions below air pressure, down to 400mmHg below. Peak blood flow was found using a needle probe to have increased four fold while at 125mmHg below air pressure. The vacuum therapy aids a number of healing processes at once. While the low pressure promotes blood flow to the area, it also helps to drain exudate, physically draw the wound closed and assist cell migration to the area, promoting tissue growth. These factors increase the speed of healing and is particularly effective for treating diabetic ulcers (Xie et al., 2010).

1.5 Discussion

During the initial exploration of the CNS in health and disease, two cases were identified in which the physical environment of the CNS may be of importance in the repair of the tissue after damage. Firstly, cells are mechanosensitive, and in the case of stem cells, the mechanics of their surroundings can cause them to change their lineage of differentiation (Engler et al., 2006). Secondly, the intracranial pressure measured in the CNS after traumatic injury has been found to be related to patient outcome (Cox et al., 2014). It is known that cells use pressure-mediated activities to undergo apoptosis, division and migration (Charras and Paluch, 2008) so the possibility of pressure external to the cell having a direct effect on cells was considered plausible.

1.5.1 Mechanosensitivity

Much of the research on stem cell mechanosensitivity has been conducted in 2D rather than 3D, due to complexities in cell encapsulation and imaging. However, Huebsch et al. (2010) determined that stem cells cultured on materials in 2D respond differently than in 3D, so the results of the 2D investigations are useful but have significant limitations. By encapsulating neural cells in a 3D hydrogel, more relevant findings can be gathered towards this field of research, allowing for a more accurate model of the *in vivo* cell niche.

Efforts to change solely the elastic modulus of hydrogels without affecting the other physical or chemical properties have not been successful. The majority of modifications to elastic modulus have been made by varying crosslinker concentration (Her et al., 2013) or polymer concentration (Banerjee et al., 2009; Bozza et al., 2014; Huebsch et al., 2010). The pore size and proportion of available ε-amino groups have been found to be affected by these methods (Her et al., 2013), both of which affect the microarchitecture of the hydrogels and therefore the local topography that the cells encounter (Her et al., 2013). While it has been reported that changing the polymer concentration has no effect on water content (i.e. porosity) of hydrogels (Bozza et al., 2014), this measurement alone is inadequate for characterising the physical nature of the hydrogels. Any study into the effects of modulus on stem

cells should also pay careful attention to the microarchitecture of the model used, in particular the pore size as this affects the amount of surface area, and therefore free ε-amino groups that a cell may adhere to.

Although the ECM of the CNS does not have the quantities of collagen that ECMs elsewhere in the body do (Li et al., 2012; Lau et al., 2013), the use of collagen to make hydrogels for this project is appealing as it is a biopolymer, meaning that it exhibits the strain stiffening phenonemon which is not reproduced by synthetic polymers (Wen et al., 2012); and it is widely available and inexpensive. As the focus of the project is on the mechanical effects of the cellular environment, the fact that collagen is not a primary constituent of the CNS ECM is of little concern.

1.5.2 Secondary Injury Raised ICP

After trauma, the natural response of inflammation in the CNS creates a substantial increase in pressure due to the finite volume governed by the skull and vertebrae (Rose and Johnson, 1996). The outcome of head trauma patients presenting Lundberg A waves, characterised by high intracranial pressures (>40mmHg), is improved over those with lower pressures (Cox et al., 2014) although the reason behind this correlation is not clear. It is unknown if the pressure could cause a direct effect on the patient outcome by having a direct effect on the cells in the system. However, it is noted that the finite volume of the CNS, and the notoriously slow repair of the tissue (Fawcett et al., 2002) are distinctive properties of the CNS, and therefore they may be linked.

ECMs in other tissue types have higher elastic moduli, while in the CNS the modulus is significantly lower (Engler et al., 2006). This means that pressure changes in the cerebrospinal fluid, such as those seen after injury, may substantially deform the CNS ECM, and therefore the force of the pressure is exerted onto the cells. The SVZ and SGZ, where the largest populations of stem cells reside in the CNS (Ricks et al., 2014), are both in close proximity to the ventricles, which means that the intracranial hypertension measured in the cerebrospinal fluid is likely to exert this force directly onto the stem cell populations located here.

Cellular studies involving pressure, while not at pressures seen in post-traumatic

hypertension, have shown that astrocytes are affected by pressure, their migration was significantly increased by 38% under 7.5mmHg hydrostatic pressure compared to a control group at 1.1mmHg (Salvador-Silva et al., 2004). Meanwhile blebbing has been found to be an important part of the process of many important cell activities such as migration and division (Charras and Paluch, 2008), and relies on the generation of an internal cellular pressure which is higher than that of the external environment.

The activities of cells after trauma are paramount to the success of the repair. The differentiation, migration and proliferation activities of stem and progenitor cells are essential to replace damaged cells. The scar formed by glial cells is a barrier to regeneration (Ricks et al., 2014), while the outgrowth of the proximal damaged axon is paramount to reconnect to the areas distal to the area of injury. An investigation into the activity of neural stem cells under pressure could provide further information how intracranial hypertension affects regeneration.

1.6 Aims and Objectives of the Project

1.6.1 Hypothesis

This project hypothesised that the activities of neural stem cells are affected by the elastic modulus of their 3D environment, altered independently of pore size; and by the hydrostatic pressure of their environment, altered within a biomimetic range for post-TBI ICP.

1.6.2 Aims

This project aimed to further understand the sensitivity of neural stem cells to the elastic modulus and pore size of their environment, and pressure of their environment. This aim included the development of an *in vitro* 3D model to allow for investigation of the activities of cells in a 3D environment; an investigation of the effects of modifying the elastic modulus of the hydrogel while maintaining a constant architecture on the activities of neural stem cells; and an investigation of the effects of raised hydrostatic pressure on the activities of neural stem cells.

1.6.3 Specific Objectives

1. To develop a 3D *in vitro* cell model appropriate for cell culture with an elastic modulus that is comparable to the natural tissue, through investigation of cell viability within the model and mechanical characteristics of the model.

2. To determine the effects of varying the elastic modulus of the *in vitro* model on the differentiation of neural stem cells, through investigation of the mechanical (shear moduli) and physical (pore diameter, pore volume, degree of crosslinking and water content) properties of model variants and the expression of neural stem (CD133) and neuronal (PSA-NCAM) markers.

3. Determine the effects of raising hydrostatic pressure on the proliferation, differentiation and 3D migration of neural stem cells, through investigation of cell viability (CyQuant and ATPlite assays), the expression of neural stem (CD133) and neuronal

markers (PSA-NCAM) and a 3D migration assay.

These objectives and their associated tasks, including the optimisation and development of methods, are presented in Figure 13.

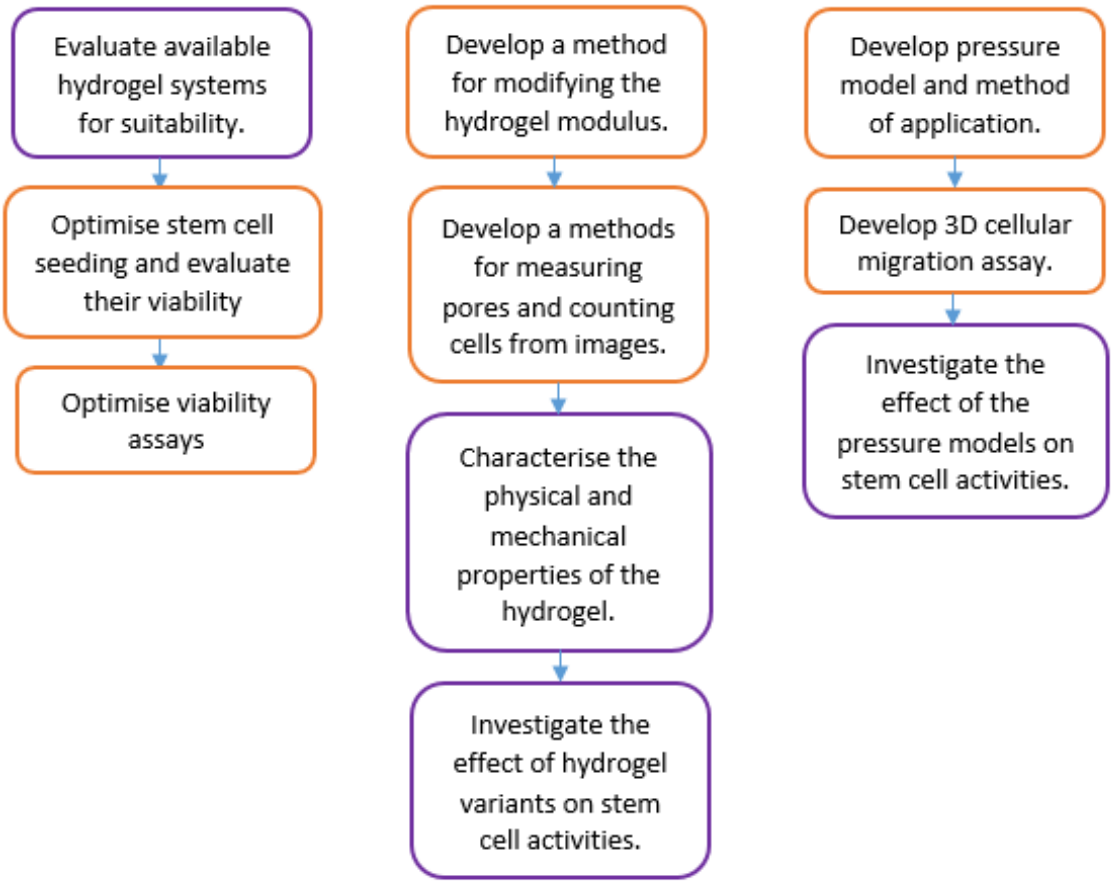

Figure 13: Overview of objectives and tasks contained within these. Tasks in orange boxes are optimisation and development that was required in order to complete the objectives, and the tasks in purple boxes are experiments that were required to interrogate the hypothesis.

2 General Methodology

The following materials and methods are those which were established and routinely used in laboratories. A description of the general protocols is included which have been used to generate a hydrogel suitable for neural cell culture and the analysis methods that have been used to determine its suitability for an *in vitro* model. The purpose of each step has been described.

2.1 Materials

The equipment used in the project are detailed in Table 7. The chemicals used in this project are detailed in Table 8. The consumables used in the project are detailed in Table 9.

Table 7: Equipment used in this project

Equipment	Model	Supplier
-20°C Freezer		Jencons Plc. East Grinstead, UK.
4°C Refrigerator		Labcold Ltd. Basingstoke, UK.
-80°C Freezer	Ultra Low	Sanyo Ltd. Osaka, Japan.
Automatic Pippette	Fastpette V2	Labnet International. Oakham, UK.
Balance	ABS-N/ABJ-NM	Kern & Sohn. Balingen, Germany.
BoneJ Plugin	Version 1.4.2	Doube et al. (2010)
Bright Field Microscope	CK-40-SLP	Olympus Optical Co. Ltd. London, UK.
Centrifuge	Avanti J-26XP	Beckman Coulter Inc. High Wycombe, UK.

Continued on next page.

Equipment	Model	Supplier
Centrifuge, Tabletop.	Harrier 15/80	Sanyo. Watford, UK.
Class II Safety Cabinet	Herasafe	Heraseus. Germany.
Confocal Microscope	LSM700	Zeiss. Oberkochen, Germany.
Excel Software	2013	Microsoft Corporation, USA.
Fluorescent Microscope	Axio Imager	Zeiss. Germany.
Freeze Dryer	Christ Alpha 2-4 LD	SciQuip Ltd. Shropshire, UK.
Fume Cupboard		Whiteley Fume Extraction Solutions Ltd. Bradford, UK.
Haemocytometer	22mmx47mm	VWR International. Poole, UK.
Ice maker	Scotsman AFE424A	Cole-Parmer. London, UK.
ImageJ	Version 1.51r	NIH. Maryland, USA.
Incubator	inCu safe	Sanyo biomedical. Leicester, UK.
Inverted Microscope	IX71	Olympus Optical Co Ltd., London, UK.
Isopropanol chamber	5100-0036	Thermo Scientific. Loughborough, UK.
Liquid Nitrogen Dewar	BIO65	Jencons Plc. East Grinstead, UK.
Magnetic Stirrer	GyroStir 280H	SciQuip Ltd. Shropshire, UK.
Magnetic Stirrer Bars	Various	Scientific Laboratory Supplies Ltd. Nottingham, UK.
Modular Incubator		Billups-Rothenberg. Del Mar, USA.

Continued on next page.

Equipment	Model	Supplier
NeuronJ	Version 1.4.3	Image Science. Rotterdam, The Netherlands.
Orbital Shaker	PSU-10i	Grant-bio. Cambridge, UK.
Oven		Genlab Ltd. Cheshire, UK.
pH meter	Jenway 3510	VWR International. Poole, UK.
Plate Shaker	SSM5	Stuart Equipment. Staffordshire, UK.
Plate Reader	Plate Chameleon	Hidex. Turku, Finland.
Rheometer	Kinexus Pro	Malvern Instruments. Worcestershire, UK.
Scanning Electron Microscope	3400-N VP	Hitachi. Krefeld, Germany.
Scalpel Handle		Swann-Morton. Sheffield, UK.
Scissors	HWB003-11	Karl Hammacher. Solingen, Germany.
Spatula	231-1059	VWR. Lutterworth, UK.
Spectrophotometer	6305	Jenway. Staffordshire, UK.
SPSS	Version 23	IBM Corp. Armonk, USA.
Tweezers	T147	TAAB. Berkshire, UK.
UV lightbox	CM-24A	Spectroline. Long Island, USA.
Water Bath	JBA5	Grant Instruments Ltd. Cambridge, UK.
Water Purifier	75L Reservoir	ELGA LabWater. High Wycombe, UK.

Table 8: Chemicals used in this project

Chemical	Storage	Supplier
1-(3-Dimethylaminopropyl)-3-ethylecarbodiimide hydrochloride (EDC)	-20°C	Alfa Aesar. Heysham, UK.
2,4,6-Trinitrobenzene Sulfonic Acid (TNBS)	4°C	Sigma-Aldrich. Poole, UK.
2-Hydroxy-4'-(2-hydroxyethoxy)-2-methylpropiophenone (photoinitiator)	20°C	Sigma-Aldrich. Poole, UK.
4-Vinylbenzyl Chloride (4-VBC)	4°C	Sigma-Aldrich. Poole, UK.
Accutase	Sterile, -20°C	Cambridge Bioscience. Cambridge, UK.
Adipic Acid (Ad)	20°C	VWR International. Leicestershire, UK.
Acetone	20°C	Sigma-Aldrich. Poole, UK.
Acetic Acid 0.1N	20°C	Sigma-Aldrich. Missouri, USA.
Alexafluor 594 Goat Anti-Mouse IgG Secondary Antibody	Sterile, 4°C	Thermofisher. Leicestershire, UK.
B27 supplement	Sterile, -20°C	Thermofisher. Leicestershire, UK.
β-mercaptoethanol	20°C	Sigma-Aldrich. Poole, UK.
CD133 IgG rabbit primary antibody	4°C	Novusbio. Poole, UK.
DAPI (4',6-diamidino-2-phenylindole)	-20°C	Sigma-Aldrich. Poole, UK.
Dimethyl Sulfoxide (DMSO)	Sterile, 20°C	Thermofisher. Leicestershire, UK.

Continued on next page.

Chemical	Storage	Supplier
Disodium Hydrogen Phosphate (Na_2HPO_4)	20°C	Thermofisher. Leicestershire, UK.
DMEM/F-12	Sterile, 20°C	Thermofisher. Leicestershire, UK.
Dulbecco's Modified Eagle Medium with phenol red	Sterile, 4°C	Thermofisher. Leicestershire, UK.
Dylight 488 Donkey Anti-Rabbit IgG Secondary Antibody	-20°C	Thermofisher. Leicestershire, UK.
Epidermal Growth Factor (EGF)	Sterile, -20°C	Millipore. Watford, UK.
Euromed Neurobasal Medium	Sterile, 4°C	Thermofisher. Leicestershire, UK.
Ethanol	20°C	Sigma-Aldrich. Poole, UK.
Fibroblast Growth Factor Beta (FGFβ)	Sterile, -20°C	Millipore. Watford, UK.
Foetal bovine serum (FBS)	Sterile, -20°C	Thermofisher. Leicestershire, UK.
Glycidyl Methacrylate (GMA)	4°C	Sigma-Aldrich. Poole, UK.
Hydrochloric Acid 37% (HCl)	20°C	Sigma-Aldrich. Poole, UK.
L-Glutamine	Sterile, -20°C	Thermofisher. Leicestershire, UK.
Laminin from Engelbreth-Holm-Swarm murine sarcoma (L2020)	Sterile, -20°C	Sigma-Aldrich. Poole, UK.
Marvel original dried skimmed milk	20°C	Premier Foods. Hertfordshire, UK.
Methanol	20°C	Sigma-Aldrich. Poole, UK.

Continued on next page.

Chemical	Storage	Supplier
Monosodium Phosphate monobasic monohydrate($NaH_2PO_4.H_2O$)	20°C	Alfa Aesar. Lancashire, UK.
Mouse IgG2a Isotype	4°C	Sigma-Aldrich. Poole, UK.
N2-plus supplement	Sterile, -20°C	Thermofisher. Leicestershire, UK.
N-Hydroxy-Succinimide (NHS)	-20°C	Merck Schuchardt. Hohenbrunn, Germany.
NeuroCult -XF Basal Medium	Sterile, 4°C	StemCell Technologies, Canada.
NeuroCult -XF Proliferation Supplement	Sterile, -20°C	Stemcell Technologies, Canada.
Paraformaldehyde	20°C	Sigma-Aldrich. Poole, UK.
Penicillin Streptomycin	Sterile, -20°C	Sigma-Aldrich. Poole, UK.
Phosphate Buffered Saline (PBS)	Sterile, 20°C	Sigma-Aldrich. Poole, UK.
p-Phenylenediacetic Acid (Ph)	20°C	Sigma-Aldrich. Poole, UK.
PSA-NCAM IgG2a mouse primary antibody	4°C	Thermofisher. Leicestershire, UK.
Rabbit IgG Isotype	4°C	Novusbio. Colarado, USA.
ReNCell Maintenance Medium	Sterile, 4°C	Sigma-Aldrich. Poole, UK.
RHB-A Medium	Sterile, 4°C	Clontech. Mountain View, USA.

Continued on next page.

Chemical	Storage	Supplier
Sodium Bicarbonate ($NaHCO_3$)	20°C	Sigma-Aldrich. Poole, UK.
Sodium Chloride (NaCl)	20°C	VWR International. Leicestershire, UK.
Sodium Hydroxide (NaOH)	20°C	Sigma-Aldrich. Poole, UK.
Suberic Acid (Su)	20°C	Thermofisher. Leicestershire, UK.
Tartaric Acid (Ta)	20°C	Sigma-Aldrich. Poole, UK.
Triethylamine (TEA)	20°C	Sigma-Aldrich. Poole, UK.
Trigene	20°C	MediChem Manufacturing Ltd. Gueenborough, UK.
Triton X-100	20°C	Sigma-Aldrich. Poole, UK.
Tris base	20°C	Sigma-Aldrich. Poole, UK.
Trypan Blue Solution	20°C	Sigma-Aldrich. Poole, UK.
Trypsin	Sterile, -20°C	Sigma-Aldrich. Poole, UK.
Tween 20	20°C	Sigma-Aldrich. Poole, UK.

Table 9: Consumables used in this project

Item	Product Number	Supplier
ATPlite kit	6016947	PerkinElmer. Massachusetts, USA.
Bijous	129A	Bibby Sterilin. Staffordshire, UK.
Culture Chamber Slides	354118	Thermofisher. Leicestershire, UK.
Corning 24 well cell culture plate	CLS3524	Sigma-Aldrich. Poole, UK.
Corning 96 well cell culture plate	CLS3596	Sigma-Aldrich. Poole, UK.
Coverslips	48376-049	VWR International. Leicester, UK.
Cryovial	1.5ml	Nange Nunc Int. corp. New York, USA.
Curvette	67.742	Sarstedt. Nümbrecht, Germany.
Culture Slides, 8 well	354118	Scientific Laboratory Suppliers Ltd. Nottingham, UK
CyQuant kit	C35011	Thermofisher, Leicestershire, UK.
Duran Bottle	Various	Thermofisher, Leicestershire, UK.
Falcon Tubes	50ml	Thermofisher, Leicestershire, UK.
Filter Pippette tips	E4860-1011	Starlab. Helsinki, Finland.
Glass Cover Slips	22mmx47mm	Scientific Laboratory Suppliers Ltd. Nottingham, UK
Live/Dead Kit	L-3224	Thermofisher. Leicestershire, UK.

Continued on next page.

Item	Product Number	Supplier
Optiplate	6005290	Perkin-Elmer. Cambridge, UK.
Microplate Adhesive Sealing Film		PerkinElmer. Windsor, UK.
Multitest slide 8-Well	6040805	MP Biomedicals. Santa Ana, USA.
Nitrile Gloves	62 5122	Sheild Scientific. Galvanistraat, The Netherlands.
Parafilm	PM996	Bemis. Neenah, USA.
Pipette tips	20μl, 200μl, 1000μl	Starlab. Ahrensburg, Germany.
ReNcell CX Kit	SCC009	Millipore. Watford, UK.
Round bottom flask	241703702	Thermofisher. Leicestershire, UK.
Scalpel blades	Various	Swann-Morton, UK.
Serological Pipettes	5ml, 10ml, 25ml	Sigma-Aldrich. Poole, UK.
Sterile Pot	60ml, 150ml, 250ml	Scientific Laboratory Supplies Ltd. Nottingham, UK.
Syringe filter	17597	Sartorius Stedim Biotech. Goettingen, Germany.
Syringe	SS-20ES2	Terumo. Lueven, Belgium.
Tissue culture flasks	10364131	Thermofisher. Leicestershire, UK.
Universal Containers	128A/P	Bibby Sterilin. Staffordshire, UK.

2.2 General Methods

2.2.1 Sterilisation

Hydrogels for *in vitro* cell studies were synthesised in house using collagen from rat tails. These were prepared on the benchtop, i.e. not under aseptic conditions. The hydrogels were sterilised by soaking in 70% (v/v) ethanol overnight, followed by washing three times with sterile PBS, and incubating with media (depending on the cell type to be used) equalling half the volume of the hydrogel.

Equipment used within the Class II safety cabinet was sterilised by spraying with 70% (v/v) ethanol, except for:

- Utensils such as spatulas were soaked in 70% (v/v) ethanol for approximately 30 minutes.
- Multitest slides were sprayed with 70% (v/v) ethanol, wrapped in foil and sterilised at 190°C for 4 hours by dry heat in an oven. The foil was sprayed with ethanol before use within the cabinet.
- Modular incubators were soaked in 1% Trigene for approximately 30 minutes. The incubators were then sprayed with 70% (v/v) ethanol before use within the cabinet.

2.2.2 Calibration of pH meter

The pH meter was calibrated before each use at 20°C using calibration solutions of pH 4 and 7.

2.2.3 Microscopy

Bright field

A bright field microscope was used for monitoring cell cultures, cell counting and development of a migration assay.

Fluorescent

A fluorescent microscope was used to image cell cultures in 2D and 3D, stained with fluorescent dyes such as in live/dead assays and immunostaining. The filters used are detailed in Table 10.

Table 10: Filters used in the fluorescent microscope

Name	Excitation/Bandwidth	Emission/Bandwidth
38GFP	470/40	525/50
20 Rhodamine	546/12	600/80
49 DAPI	365/40	445/50

Confocal

A fluorescent confocal microscope was used to image cell cultures in 3D, stained with fluorescent dyes such as in live/dead assays and immunostaining. Lasers used were: Laser diode 405:405 nm, Argon:488 nm, HeNe1:543 nm.

2.2.4 Solutions

Soultions used for the synthesis of hydrogels were not prepared in sterile conditions. Their preparations are described in Table 11.

Table 11: Solutions used in this project

Solution	Method	Details
70% ethanol	70ml ethanol, 30ml filtered water	stored at 20°C
17.4mM Acetic Acid	1ml 100%Acetic acid (17.4M), 999ml filtered water	Stored at 20°C
Sodium phosphate buffer	3.1g monosodium phosphate monobasic monohydrate, 10.9g disodium hydrogen phosphate, 1 litre filtered water	pH 7.4, stored at 20°C
10mM hydrochloric acid (HCl)	821μl 37% HCl (12.18M), 999.119ml filtered water	Stored at 20°C
100mM sodium hydroxide (NaOH)	4g NaOH, 1 litre filtered water	Stored at 20°C

2.3 Hydrogel Synthesis

Two collagen hydrogel types were synthesised: one type was chemically crosslinked, with the bonds formed by two solutions mixing together, described Tronci et al. (2013b); while another type was crosslinked under ultraviolet (UV) light, described by Tronci et al. (2013a).

2.3.1 Harvesting Collagen

Type I collagen was extracted from rat tails obtained from Central Biomedical Services, University of Leeds. The tails were frozen at -20°C and stored for up to 1 month from collection. The frozen rat tails were thawed in 70% (v/v) ethanol at room temperature for 15 minutes. A scalpel was used to score the skin of the tail along the length, and the skin was then removed with tweezers. The tails were dried for 1-2 hours at room temperature within a class II safety cabinet to allow easier tendon extraction. Tweezers were used to remove the tendons from the tail. The stages of tendon extraction are shown in Figure 14.

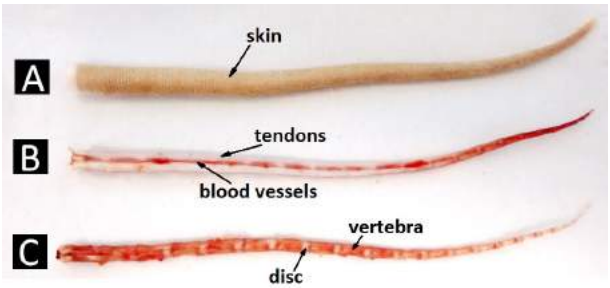

Figure 14: Three rat tails. A: whole, B: with skin removed and C: with tendons removed.

Tendons were dissolved for 48 hours by stirring in 50ml (per tail) of 17.4mM acetic acid (prepared as described in Table 11) at 4°C. The resulting mixture was centrifuged for 1 hour at 15,000g at 4°C. The supernatant containing collagen type I and acetic acid was transferred to a round-bottomed flask to allow maximum surface area exposure during freeze drying. Approximately 200-250ml was frozen at -20°C overnight and then transferred to -80°C overnight to prevent damage to glassware. The frozen solution was freeze dried to achieve sublimation and removal of the acetic

acid, as shown in Figure 15. For solutions of 200ml, for example, the freeze drying process took up to one week. The dry collagen was stored in an airtight container at 4°C. In total, three batches of dry collagen were synthesised. The first batch was used in the very early stages of the project for training and development work and the results of which are not included. The second batch was used for all development and optimisation in this thesis, while a final batch was made for the experiments that used neural stem cells.

Figure 15: The collagen-acetic acid mixture was sublimated in the freeze drier to remove the acetic acid.

2.3.2 Synthesis of UV Crosslinked Hydrogels

Vinyl monomers can be used to link collagen molecules together by the functionalisation of amino acids that recur frequently in the collagen backbone. The method described here is as described by Tronci et al. (2013a). The monomers glycidyl methacrylate (GMA) and 4-vinylbenzyl chloride (4-VBC) that were used in the synthesis of these hydrogels have functional groups which react with the amino groups that are present in lysine residues of the collagen. A photoinitiator can then be used to link the monomer molecules together, crosslinking the collagen molecules and forming a hydrogel. This method is summarised in Figure 16 and described in more detail presently.

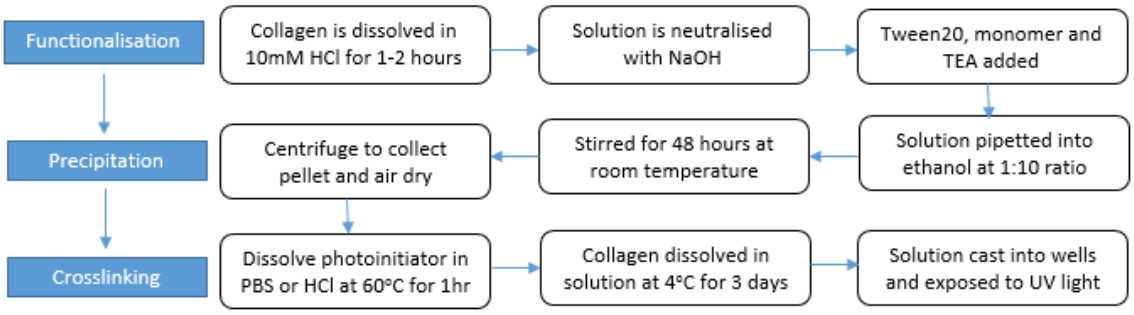

Figure 16: Flowchart summarising the synthesis steps of the UV crosslinked hydrogels

Functionalisation

To create a hydrogel, the collagen was functionalised (i.e. given functional groups that later may be crosslinked). Dry collagen was weighed and dissolved at a concentration of 0.25% (w/v) collagen in 10mM hydrochloric acid (HCl, prepared as described in Table 11) for 1-2 hours at room temperature. The collagen solution was neutralised using 100mM sodium hydroxide (NaOH, prepared as described in Table 11) dropwise, whilst monitored using a pH meter. Tween20 was added for a concentration of 1.2% (v/v) to act as a surfactant to ensure that the monomer was miscible with the collagen solution. The chosen monomer was added, either GMA or 4-VBC (both Sigma-Aldrich), at the concentration described in Equation 5. Triethylamine (TEA) was added in an equimolar ratio to the monomer.

$$V_{mono} = \frac{W_c \times Lys_c \times excess \times M_{mono}}{\rho_{mono}} \tag{5}$$

V_{mono} was the volume of monomer in ml, W_c was the weight of collagen that was used in g, Lys_c was the lysine content of collagen (3.24×10^{-4}mol/g for rat tails) (Tronci et al., 2013a). The monomer was added at a 25x excess to maximise the functionalisation. M_{mono} was the molecular mass of the monomer in g/mol and ρ_{mono} was the density of the monomer in g/cm^3, values for which can be found in Table 12.

Table 12: Molecular masses and densities of chemicals for the functionalisation of collagen

Chemical	Molecular Mass (g/mol)	Density (g/cm^3)
GMA	142.15	1.042
4-VBC	152.62	1.083
TEA	101.9	0.726

Precipitation

The functionalised collagen solution was pippetted into 100% ethanol at a 1:10 ratio of solution to ethanol and stirred for 48 hours at room temperature. The ethanol dissolved any unreacted monomer and caused the functionalised collagen to precipitate out of solution. The mixture was centrifuged at 15,000G for 1 hour at room temperature to collect the precipitant into a pellet. The pellet was air dried overnight at room temperature inside a fume cupboard.

Crosslinking

A concentration of 1% (w/v) 2-Hydroxy-4'-(2-hydroxyethoxy)-2-methylpropiophenone (photoinitiator) was dissolved in phosphate buffered saline (PBS) for GMA, or 10mM HCl for 4-VBC at 60°C for 1 hour until the solution was clear. The solution was wrapped in foil to protect from light damage and left at room temperature to cool. Functionalised collagen was added at 1.2% (w/v) concentration and the mixture was stirred at 4°C for 2-3 days until it was fully dissolved. The solution was pippetted into well plates (WP) and was crosslinked with 365nm UV light. Hydrogels were washed in distilled water overnight, replacing the water once.

2.3.3 Synthesis of Chemically Crosslinked Hydrogels

The method described here is as described by Tronci et al. (2013b). The collagen was crosslinked via a diacid (a molecule with two carboxyl groups - one on each end), in this case p-phenylenediacetic acid (Ph), which must first be activated to allow the crosslinking to occur. Freeze-dried collagen was dissolved in 17.4mM acetic acid at a concentration of 1.2% (w/v). The concentration of Ph used was determined so that the number of free carboxyl groups was equal to the number of lysine in

the collagen. The Ph crosslinker was added to sodium phosphate buffer (SPB, prepared as described in Table 11) and stirred for 1 hour at 0 °C until dissolved. N-hydroxy-succinimide (NHS) and N-(3-Dimethylaminopropyl)-N'-ethylcarbodiimide hydrochloride (EDC) were added at six times the molar content of the Ph carboxylic groups. β-mercaptoethanol was used at an equimolar ratio to the NHS to quench the EDC/NHS and stop the activation reaction. The collagen solution and activated Ph were mixed at a ratio of 2:1 and cast into WPs or vials as required. The mixture was placed in a fume cupboard overnight to allow hydrogel formation. The synthesis process is summarised in Figure 17.

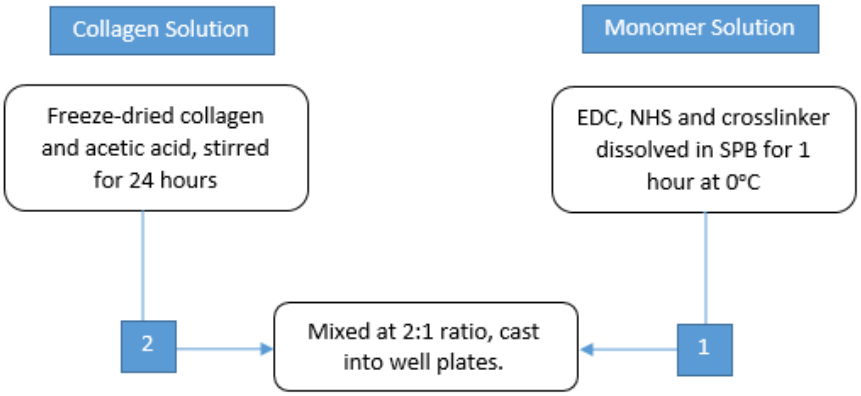

Figure 17: Schmatic diagram describing the synthesis process of the chemically crosslinked hydrogels.

2.4 Culture of CNS Cells

Several cell types were used in the developmental and investigatory work for this project. Developmental work used the glial C6 and neuronal PC12 cell lines as they were robust in terms of their resilience and performance and were readily available in the laboratory. Investigatory work used the neuronal stem cell lines CB660 and CX. The CB660 cell line has been well characterised by Sun et al. (2008) in terms of protein expression during differentiation, expressing CD133 and nestin initially, followed by PSA-NCAM and β-tubulin III after neuronal differentiation. The CX cell line has also been well characterised by Donato et al. (2007), shown to initially express nestin, and β-tubulin III and GFAP after neuronal and glial differentiation, respectively. The culture methods such as resurrection, passaging

and cryopreservation are largely similar while the specific culture requirements of the neural stem cell lines have been described in more detail afterwards.

Media for use in cell culture was prepared in aseptic conditions, the constituents of which are presented in Table 13.

Table 13: Reagents used for cell culture

Reagent	Method	Application and Storage
Penstrep	Penicillin Streptomycin containing 100 units/ml penicillin, 100μg/ml streptomycin,	All cells, -20°C
DMEM/F-12	44% (v/v) Dulbecco's modified eagle medium (DMEM), 44% (v/v) Ham's F12 media, 10% (v/v) foetal bovine serum (FBS), 2mM L-glutamine, 1% (v/v) penstrep	C6 cells, 4°C
RPMI medium	Roswell Park Memorial Institute (RPMI) medium with 10% (v/v) horse serum (HS), 2mM L-glutamine, 1% (v/v) penstrep	PC12 cells, 4°C
Cryopreservation medium	Base medium type (i.e. without additional reagents) with 2% (v/v) FBS, 1% (v/v) Dimethyl Sulfoxide (DMSO)	C6 and PC12 cells
Laminin	PBS with 20μg/ml Laminin L2020	CB660 and CX cells, -20°C
RHB-A Medium	RHB-A media with 10ng/ml EGF, 10ng/ml FGFβ, 1% (v/v) N2 supplement , 2% (v/v) B27 supplement, 1% (v/v) penicilin streptomycin	CB660 cells, 4°C
ReNCell Medium	99%ReNCell maintenance media, 20ng/ml EGF, 20ng/ml FGFβ, 1% v/v) penstrep	CX cells, 4°C
Neurocult Proliferation Medium	Neurocult Basal Medium with 10% (v/v) proliferation supplement, 10ng/ml EGF , 10ng/ml FGFβ, 1% (v/v) penicilin streptomycin	CB660 cells, 4°C
Neurocult Differentiation Medium	Neurocult Basal Medium with 1% (v/v) penicilin streptomycin	CB660 cells, 4°C

The culture of cells, including the resurrection, passaging and cryopreservation, is summarised in Figure 18 and described in more detail presently.

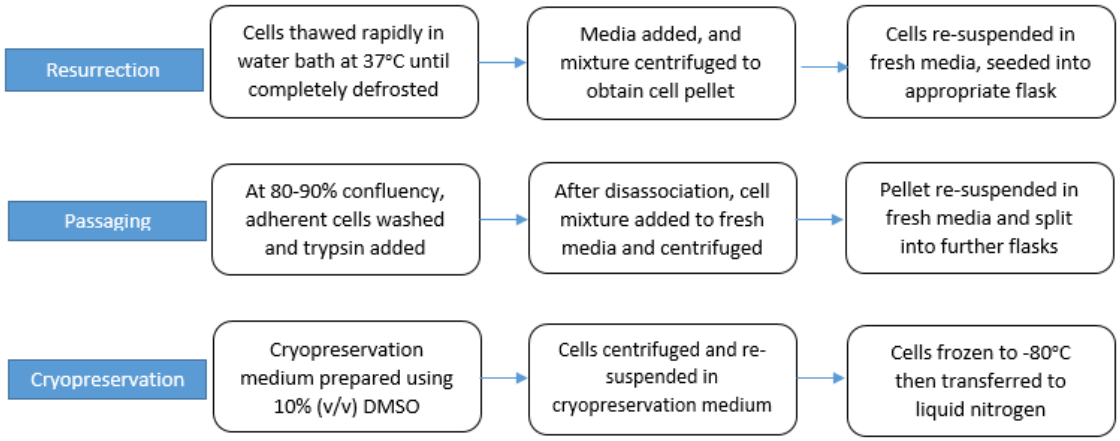

Figure 18: Normal culture of cells, including resurrection from frozen, passaging and cryopreservation procedures.

2.4.1 Resurrection of Cells from Liquid Nitrogen

Cells were stored in liquid nitrogen to preserve them and must be defrosted quickly to prevent damage by ice crystals. The cryovial containing frozen cells was removed from liquid nitrogen, placed in a pot for protection and incubated in a waterbath at 37 °C for approximately 2 minutes to defrost. A volume of 8mls of media (prepared as described, depending on the cell type, in Table 13) was pippetted into a universal. When the cells had defrosted, the 1ml contents were added to the universal. A further 1ml media was used to wash the cryovial and added to the universal. The universal was centrifuged at 200g for 10 minutes at room temperature to form a pellet. The supernatant was discarded to remove the freezing medium and the pellet was resuspended in media. The cells and extra media were added to T75 flask in a total of 13ml and incubated at 37 °C in air with 5%(v/v) carbon dioxide (CO_2). If the cells failed to form a pellet, 3mls media was added to the 10ml cell suspension and incubated overnight in a T75 flask and the media was changed the following day.

2.4.2 Passaging Cells

As the cells replicate, they become too crowded and must be split for a healthy cell population to be maintained. This should ideally occur at approximately 80-90% confluency, determined using a bright field microscope. For adherant cells, media was removed from flasks and the cells were washed with PBS to remove all traces of foetal bovine serum, as this inhibits trypsin. A volume of 5ml trypsin was added to cleave the peptide chains formed by the cells to adhere to the culture flask. The flasks were incubated for 5-10 minutes at 37 °C in air with 5%(v/v) CO_2. A volume of 10ml media was added to a universal and the trypsin cell suspension was added, as the foetal bovine serum within the media inactivated the tryspin. The universal was centifuged at 200G for 10 minutes and the supernatant was discarded. The pellet was resuspended typically in 1-2ml media depending on the size of the pellet, estimated by observation. For suspension cells, the trypsin step was not required and the cells were directly centrifuged.

To seed cells into new flasks at an appropriate cell density, a cell count was performed. A volume of 7μl of cell suspension was added to 7μl trypan blue and loaded into a haemocytometer to perform a live cell count under a bright field microscope. Trypan blue solution permeates the membrane of dead cells, leaving live cells with a white "halo". The cell count was performed in the central 5x5 grid of the haemocytometer, until at least 100 cells were counted, to ensure an accurate estimate was calculated. A counting method was applied that included cells crossing the top and left borders of the grid but not bottom and right borders as described in Figure 19, to ensure a consistent counting method was employed.

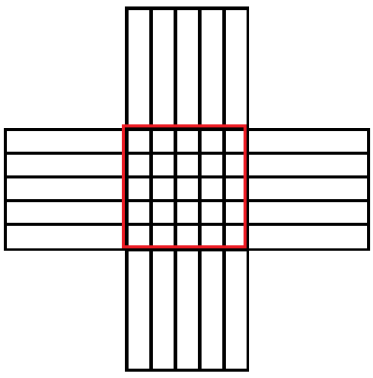

Figure 19: Diagram of the etched grid of a haemocytometer. The cell count procedure is indicated by the red box.

The number of cells was calculated as described in Equation 6. Media was added to the required number of T75 flasks and cell suspension was added so that there was an appropriate number of cells per flask, in the case of C6 and PC12 cells, this was 1 million cells per flask.

$$N_{cells} = count \times 2 \times V \times 10^4 \tag{6}$$

Where N_{cells} was the total number of cells per ml obtained from the passage, *count* is the number of live cells counted within the central 5x5 grid of the haemocytometer, the number was multiplied by 2 due to the 50% dilution in trypan blue. V was the total volume of that the pellet was resuspended in. The number was multiplied again by 10^4 to obtain a cell count per ml as the volume of media observed within the 5x5 grid is 1μl.

2.4.3 Freezing Cells

To store cells in liquid nitrogen, they must be preserved using a cryoprotective agent, e.g. Dimethyl Sulfoxide (DMSO) allow a slower cooling rate, reducing the risk of ice crystal formation which can cause cell death. A cell count was performed as outlined above. the cell suspension was centrifuged at 150g for 10 minutes to reform the pellet. A freezing medium was prepared as described in 13. The supernatant was discarded and the pellet was resuspended with appropriate volume of filter-sterilised freezing media to create 1x10^6 cells/ml. The suspension was aliquotted into cryovials at 1ml per vial. An isopropanol chamber was used to freeze cells to -80°C overnight. Cells were then transferred to liquid nitrogen.

2.4.4 Culture requirements of Stem Cells

Culture of CB660 cells

CB660 cells are a neural stem cell line from human foetal forebrain, obtained from the National Institute for Biological Standards and Control (NIBSC) and were chosen as they were inexpensive and have been well characterised by Sun et al. (2008) in terms of their protein expression during differentiation. A T25 flask was coated by

soaking with laminin L2020 (prepared as described in Table 13) for four hours prior to thawing CB660 cells. Initially, RHB-A medium was made up as described by Sun et al. (2008) and summarised in Table 13. Later, the cells were cultured using Neurocult proliferation medium as described in Table 13. The cells were thawed in a water bath at 37°C, and transferred into a universal tube containing 5ml media warmed to 37°C. The tube was centrifuged at 200G for 3.5 minutes to form a pellet. The supernatant was removed, the cells were resuspended in 5ml proliferation media and transferred to the T25, incubated at 37°C, in air with 7% CO_2. The media was changed every other day. A brightfield image of the cells was taken at day one and is presented in Image 20.

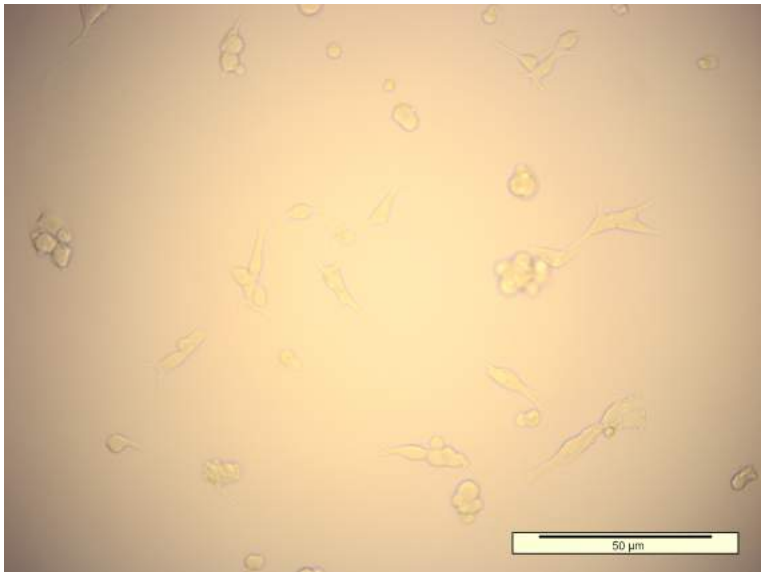

Figure 20: Brightfield microscope image at 10x magnification of CB660 cells at day 1 of culture

Culture of CX cells

CX cells are a research grade neural progenitor cell line from human foetal cortex, obtained from Merck Millipore and were chosen due to their improved culture abilities compared to the CB660 cells. A T75 flask was coated with laminin L2020 (thermofisher) for four hours prior to thawing CX cells. Proliferation media was made up using ReNCell maintenance media supplemented with epithelial growth factor (EGF) 20ng/ml, fibroblast growth factor beta (FGFb) 20ng/ml and penicillin streptomycin 1% (v/v). Before thawing, the flask was rinsed once with PBS, and 10ml proliferation media was added. The flask was incubated at 37°C, in air with 5% CO_2 (v/v) to allow the media to warm. The vial of frozen cells was thawed

in a water bath at 37°C before transferring to a universal tube and adding 9ml pre-warmed media dropwise. The tube was centrifuged at 200G for 2 minutes at 20°C to form a cell pellet. The supernatant was removed and the cells were resuspended in 5ml proliferation media, warmed to 37°C, and then added to the T75 flask. The cells were incubated at 37°C, in air with 5% CO_2 (v/v), the media was changed the next day and then every other day until confluency. Cells were passaged using accutase and seeded at $1x10^5$ cells/ml. Cells were cryopreserved in ReNCell freezing medium at $4x10^6$ cells/ml. A brightfield image of the cells was taken at day one and is presented in Figure 21.

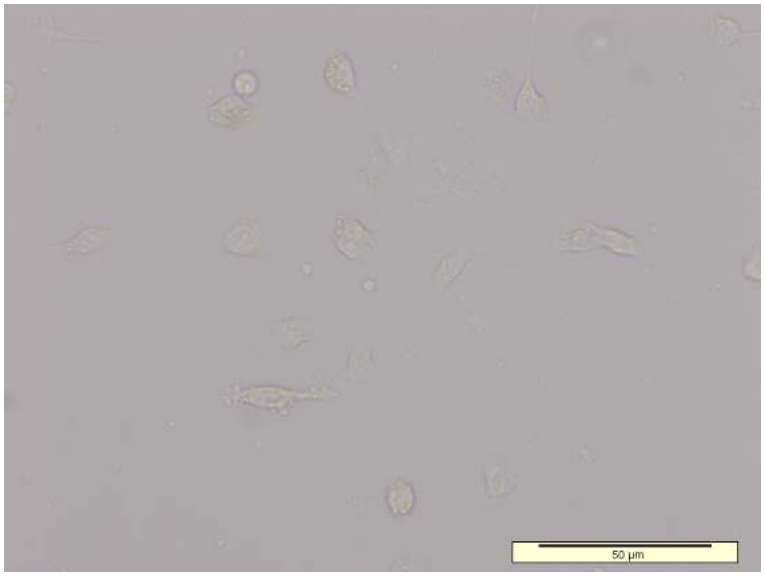

Figure 21: Brightfield microscope image at 10x maginfication of CXcells at day 1 of culture

2.5 Biological Assays

Biological assays are used to interrogate the activities of the cells. All of the assays used in this project were based on staining specific aspects of the cells using light to produce a reading: either imaging the cells under fluorescent light or using a plate reader to determine the level of luminescence or fluorescence being emitted from the cells. Quantitative assays such as ATPlite and CyQuant are used to determine the number of viable cells in a population. By comparing results on successive days, a quantitative representation of the cellular viability can be achieved. Qualitative assays such as live/dead staining provide descriptive evidence of the appearance a

sample of the cell population - both whether the cells are alive or dead as well as their morphology. This is useful to gain an impression of cellular activity, and can be converted into semi-quantitative data such as though cell counts or measurement of projections.

Table 14: Assays used in this project

Cell viability	Live/dead	Stains live and dead cells
	ATPlite	Measures actively growing cells
	CyQuant	Stains nucleus of live cells
Phenotyping	Immunostaining	Highlights expressed proteins

Table 15: Reagents used for biological assays

Reagent	Method	Environment
Live/dead stain	Calcein-AM at 25μM/ml and ethidium homodimer-1 at 7.5μM/ml in PBS and mixed	Room temp, aseptic
ATPlite substrate solution	25ml buffer to lyophilised substrate solution and agitated gently	Room temp, aseptic
CyQuant stain	48μl DNA stain, 240 μl of the background suppressor, 11.7ml media and mixed	Room temp, aseptic
TBS (10x)	0.5M Tris base, 1.55M Sodium Chloride (NaCl), filtered water	Room temp, pH 7.6
TBS	10% (v/v) TBS (10x), 90% (v/v) filtered water	Room temp
TBS-T	0.05% (v/v) Tween20, 99.95% (v/v) TBS	Room temp
4% Paraformaldehyde (PFA)	4% (w/v) PFA, 96% (w/v) filtered water	Room temp
Triton	0.1% (v/v) X-100, 99.9% (v/v) filtered water	Room temp
Blocking Solution	10% (w/v) Marvel original dried skimmed milk, 90% (w/v) TBS	Room temp

2.5.1 Determination of Cell Viability and Morphology using Live/Dead Staining

As indicated in Table 14, live/dead staining is a qualitative method of phenotyping cells. This stain can be used in 2D and 3D culture models, by changing the volumes of reagents added. For 2D cultures, for 24WPs 300μl of all reagents were used per well, whereas 100μl per well for 96WPs was sufficient. For 3D cultures, the volumes used were greater than or equal to the volume of the hydrogel. Calcein-AM fluoresces green and indicates intracellular esterase activity (live cells) while the ethidium homodimer-1 stain is red and binds to exposed DNA, indicating loss of membrane integrity (dead cells). The media was removed from each well and 100μl PBS was used to wash the cells. Two washes of PBS were performed and the plate was shaken for 5 minutes with each PBS wash. The stains were diluted in PBS as described in Table 15. The PBS was removed from each well and the stains were added at the required volumes as outlined above. The plate was shaken for one hour at 150rpm in an incubator at 37 °C, in air with 5% CO_2 (v/v). The wells were washed 3 times with PBS, while shaking for 5 minutes with each wash. While shaking, the plates were wrapped in foil to protect from light damage. The hydrogels were then transferred to glass slides for imaging using a fluorescence microscope.

Fluorescence microscopy is achieved by illuminating the sample at specific wavelengths. Cells are stained or tagged with fluorescent markers which are excitable at these specific wavelengths. Electrons that receive the incoming light are moved to an excited state, and when they release this energy they revert back to the original ground state, emitting the energy in the form of light of another wavelength. Calcein AM is excited by light at a wavelength of 495nm and emits wavelength 516nm. Ethidium homodimer-1 is excited by and emits light at wavelengths of 528nm and 617nm, respectively. By viewing the cells under a microscope and exciting each of the stains individually, the cells were viewed with more clarity, and the images may then be combined.

2.5.2 Determination of Cell Viability using the ATPlite Assay

The ATPlite assay measures free adesine triphosphate which is the energy cells use to respire. The assay was performed on cells in both 2D and 3D culture models. For the latter, the volume of chemicals was increased to match the volume of the 3D construct and shaking times were doubled. ATPlite substrate solution was prepared as described in Table 15. This may then be separated into aliquots and stored at -20°C. A volume of 200μl media was removed from each well of the 96WP and 100μl fresh media was added to each well. A volume of 50μl mammalian cell lysis was added to each well. The plate was shaken for 5 minutes at room temperature at 150rpm (or for 10 minutes for 3D cultures). A volume of 50μl substrate solution was added to each well. The plate was covered with foil to protect from light damage and shaken for 5 minutes at room temperature at 150rpm (or 10 minutes for 3D). A volume of 100μl of solution was transferred from each well into a white opti plate, and sealed using a transparent coverslip. The new WP was covered in foil to protect from the photobleaching effects of light until readings were taken the plate reader. Once in the plate reader, the plate was dark-adapted for 10 minutes to ensure accuracy of luminescence readings. The plate reader read luminescence in counts per minute for each well.

2.5.3 Determination of Cell Viability using the CyQuant Assay

CyQuant was an alternative to ATPlite as it used a DNA-binding dye in combination with a suppression dye which was impermeable to the live cell membranes. While ATP production measures the activity of cells which may be altered by stressful conditions, DNA content of cells remains stable and so can be more accurate in adverse cell environments. The stain for the CyQuant direct cell assay was prepared as described in Table 15. The reagent was added to cells in culture at the same volume as the media already present in the well. The plate was covered with foil to protect from the photobleaching effects of light and incubated for 60 minutes at 37°C in air with 5% (v/v) CO_2. Once in the plate reader, the plate was dark-adapted for 10 minutes to ensure accuracy of fluorescence readings. The plate reader used excitation wavelength 480nm and read emission wavelength 520nm in counts per minute for each well.

2.5.4 Determination of Cell Phenotype using Immunostaining

Immunofluorescence staining involves the tagging of primary antibodies onto specific antigens carried by proteins that cells may be expressing. Targetted proteins are those that are expressed by very few, or ideally only one cell type, and therefore can be used to identify the phenotype of the cell. The primary antibody has a binding site for secondary antibodies of the same host animal and antibody type. Secondary antibodies are synthesised with a fluorescent tag attached so that the cells may be phenotyped under a fluorescent microscope. Depending on the protein of interest, the fluorescent antibodies could be attached to the nucleus, the soma or dendritic projections.

For staining in 2D cultures, the cells on glass spot slides were fixed using a 1:1 acetone:methanol mixture for one minute, and allowed to air dry at room temperature for five minutes. The slides were then washed in tap water for approximately 10 minutes. Tris buffered saline (TBS, prepared as described in Table 15) was used to wash the slides for 5 minutes on an orbital shaker. Then the slides were incubated in TBS-T (prepared as described in Table 15) for 15 minutes. Slides were washed for 5 minutes with TBS three times. The hydrogels were incubated in blocking solution (prepared as described in Table 15) for 15 minutes before being washed with TBS three times for five minutes.

The primary antibodies were prepared at the required concentrations, described in 16 in blocking solution and spun at 10000G to form a non-specific binding pellet which was discarded. After adding 50μl primary antibodies to each spot of the slide, the slides were incubated in a moist environment for 1 hour by wrapping the slide plate with dampened tissue. The slides were then washed twice with TBS-T for five minutes, and twice with TBS for 5 minutes. The secondary antibody was prepared, added, incubated and washed in the same process as the primary antibody, however this was done in the dark to protect the fluorophores from photobleaching. DAPI is often added to the secondary antibody to stain the cell DNA blue. Isotypes were used as negative controls to check for non-specific binding while use of the secondary antibody only without the primary to ensure only the protein of interest was being fluorescently tagged.

Table 16: Antibodies and concentrations used for stem cell staining

Type	Antibody	Details	Conc.
Primary	PSA-NCAM anti-mouse IgG2a	Neuronal progenitor	1:200
Secondary	Alexa Fluor 594 Goat anti-mouse IgG	Red	1:200
Isotype	Mouse IgG2a		1:200
Primary	CD133 anti-rabbit IgG	Neural stem	1:50
Secondary	Dylight 488 donkey anti-rabbit	Green	1:50
Isotype	Rabbit IgG		1:50
DAPI		DNA	1:1000

Cells in 3D cultures were stained in the same way, however the hydrogels were fixed using 4% paraformaldehyde (PFA, prepared as described in Table 15) for 45 minutes before incubation with Triton (prepared as described in Table 15) for 15 minutes and washed with TBS for 5 minutes three times. Subsequently blocking solution, stains and washes were applied as described above. The staining process for two antibodies is described in Figure 22.

2.6 Mechanical Analysis

The method used to measure the properties of materials, environments or cells can often drastically affect the outcome of the test and should always be considered when analysing or comparing findings. The natural ECM has been described as a hydrogel of collagen (Wen et al., 2012) and so when considering appropriate testing for human tissue, it is useful to consider popular hydrogel characterisation techniques also.

Most mechanical properties, such as elastic modulus, strength and degree of viscoelasticity can be determined using physical tests that probe the response of a material to external forces. Tensile or compressive tests find properties denoted E, while bulk and shear tests find properties defined K and G respectively. These properties are interrelated for isotropic materials, where ν is Poisson's ratio, as described in Equation 7.

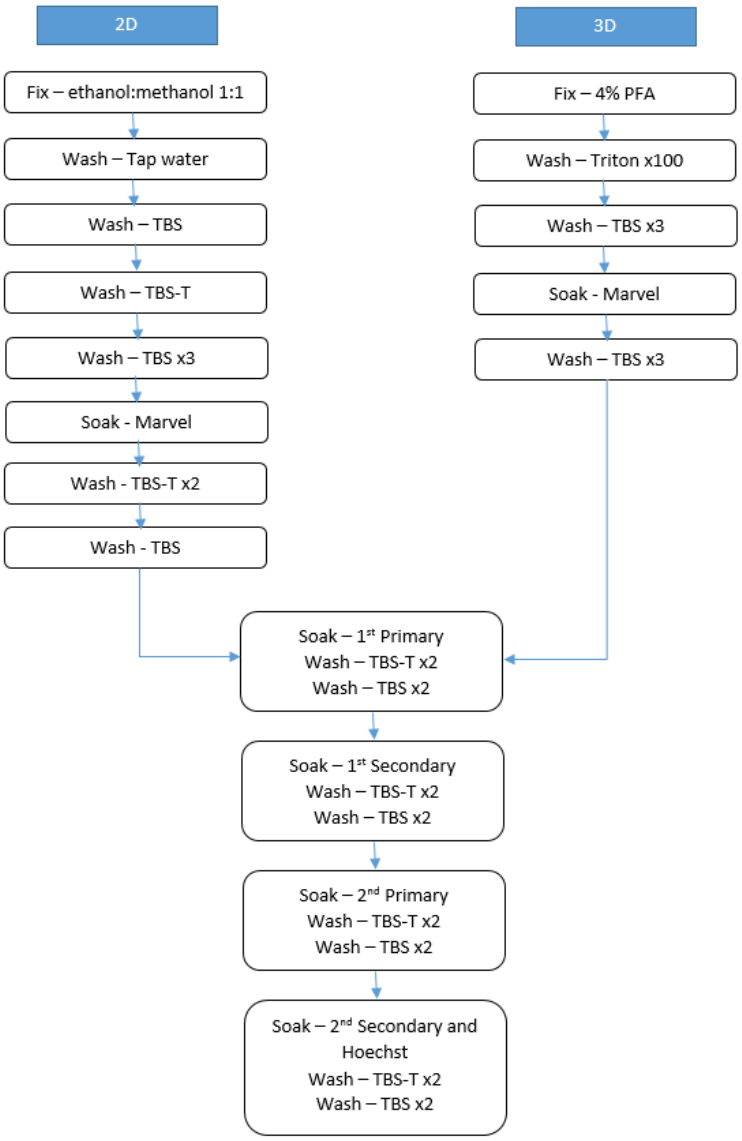

Figure 22: Schematic diagram of the sequential immunostaining process for two antibodies.

$$E = 2G(1 + \nu) = 3K(1 - 2\nu) \tag{7}$$

The outcome of tests can also be affected by environmental conditions such as temperature, pH levels, and the activity of any seeded cells (Wilson et al., 2014).

Wilson et al. (2014) claim that tensile tests are popular for hydrogel characterisation, however tensile testing may be less appropriate for hydrogels used in neural applications as the low stiffness and high viscoelastic nature of the material may make both the experimental set up and analysis of readings difficult to implement. Shear testing is often used for characterising soft matter, and indeed is popular for

brain tissue (Cheng et al., 2008), while compression tests have also been used in *in vitro* models, for example research by Her et al. (2013) and Bozza et al. (2014) who tested hydrogels for studies into neural stem cell mechanosensitivity. For the purposes of testing hydrogels with properties biomimetic to that of brain tissue, shear testing using a rheometer is considered most appropriate and is popular for investigating brain tissue (Cheng et al., 2008). This is due to the low elastic modulus and viscoelastic properties that the tissue is known to have which makes handling of the samples practically difficult.

The mechanical properties were investigated using rheology to enable the properties found to be able to be directly compared to that of natural brain tissue identified in the literature in Section 1.3.2. The microarchitecture was the focus of the physical characterisation of the hydrogel and was investigated in a number of ways. SEM imaging and NMR analysis was used to find the size of the pores in the hydrogel, TNBS analysis was used to find the degree of crosslinking that the hydrogels had developed and water content was used to measure the overall porosity of the hydrogels.

2.6.1 Measurement of Elastic Modulus using Rheology

A rheometer was used to perform the mechanical analysis of the hydrogels. The rheometer has two components which interact with the sample, which are detailed in Figure 23. The plate is a wide flat surface onto which the sample is placed. The cone is adjusted to contact the top surface of the sample. The cone is typically angled, so that there is a smaller volume of sample material in the centre as opposed to the edge. This is to enable the shear rate to be constant in a radial manner. However, for hydrogels that possess a 3D architecture, compressing the centre more than the edges would alter the local mechanical properties. For this reason the cone used for hydrogels is more commonly a flat (or parallel) plate. The inconstant shear rates created by not using a cone can be limited by using oscillatory testing at small deformations, within the linear viscoelastic region (LVER) of amplitude (Mezger, 2014).

A 20mm diameter parallel plate was used in an oscillatory testing mode. The hy-

drogel was placed in the centre of the base plate. An appropriate hydrogel height was selected that ensured the cone contacted the hydrogel, filling the space between the cone and plate without overly compressing the hydrogel and risking damage to the 3D matrix. In Figure 24, the top cone, bottom plate and hydrogel are depicted. The tests were performed with the base plate heated to 37°C. Initially, amplitude sweeps were performed to find the shear strain range of the LVER. The amplitude sweep was performed from 0.1-20% shear strain, at a frequency of 1Hz. The LVER was determined by plotting the amplitude (i.e. shear strain) vs the elastic modulus and observing the portion of the line where the gradient was closest to zero, where the modulus was constant. This is ensures that that the material is being tested within its elastic (and not plastic) region, so that the findings are reproducible.

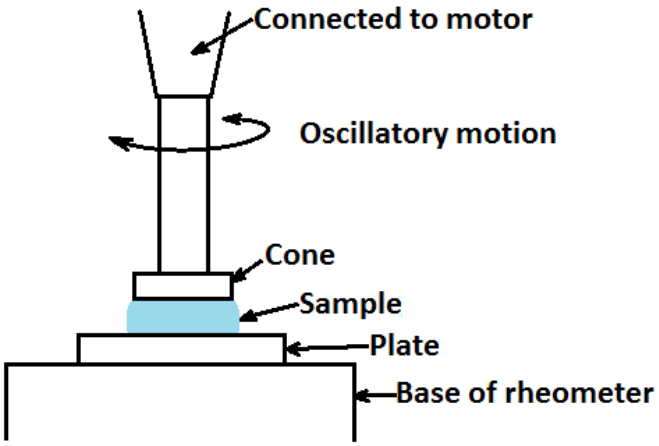

Figure 23: Schematic diagram of the rheometer when used in oscillatory testing.

A frequency sweep was performed at a shear strain that was in the LVER. The frequency of the oscillations was ramped from 0.5Hz to 5Hz. Values such as complex modulus and phase angle were recorded by the software, at a rate of 10 per decade (of frequency). The phase angle is found as described in Figure 25. The storage (G') and loss (G") moduli may then be calculated by considering Figure 3, and equations 8 and 9.

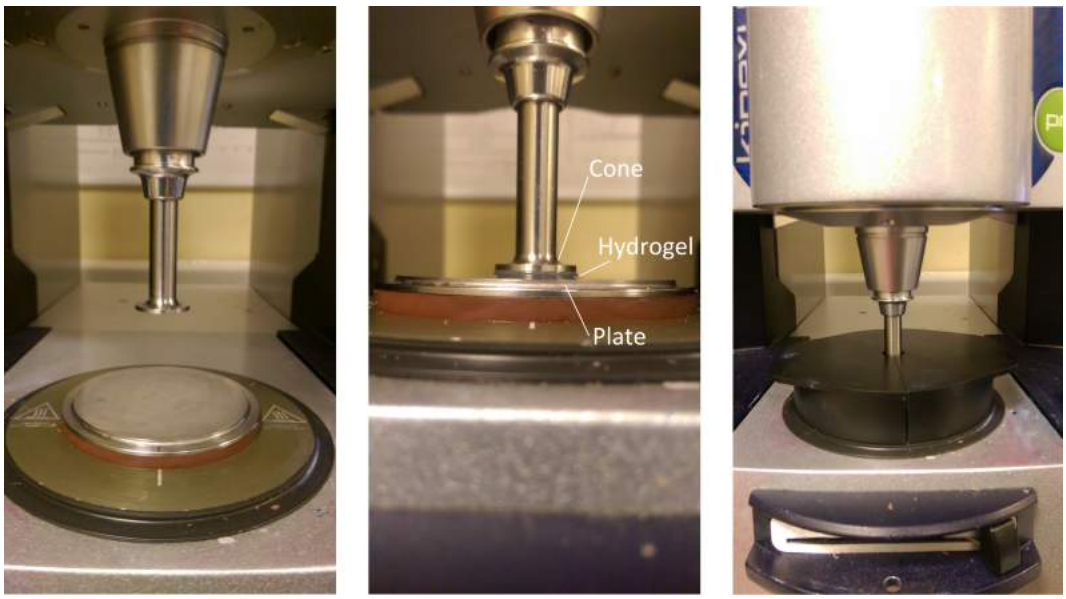

Figure 24: The hydrogels were tested under shear stress provided by the cone, rotating at varying amplitude to find the linear viscoelastic region; or at varying frequency, to find the elastic modulus.

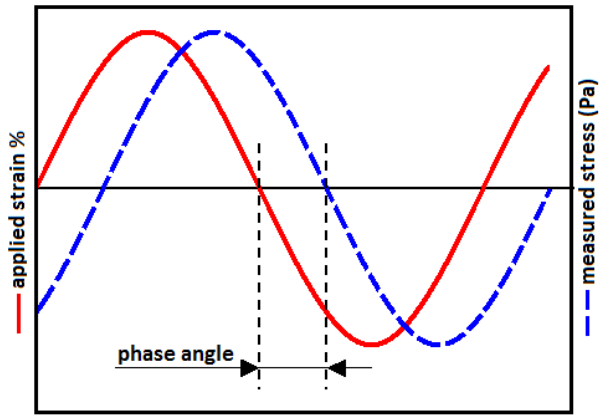

Figure 25: The applied strain and measured stress response for a material. One full sine wave represents one cycle of the oscillating cone. The phase angle was found by measuring the lag between the input and output.

$$G' = G^* sin\theta \tag{8}$$

$$G'' = G^* cos\theta \tag{9}$$

Where G' is the storage modulus, G" is the loss modulus, G* is the complex modulus and θ is the phase angle. Typical response shapes of amplitude and frequency sweeps are presented in Figure 26.

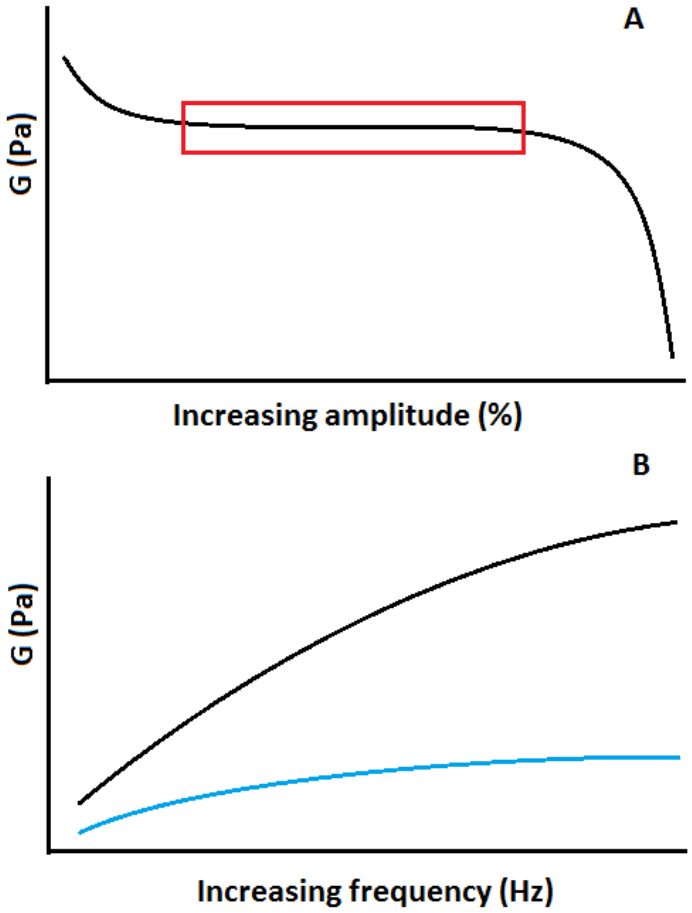

Figure 26: Schematic diagram showing typical response shapes of the amplitude sweep (A) to find the linear viscoelastic region (red boxed portion of graph) of the amplitude and the frequency sweep (B) to find the storage (black line) and loss (blue line) moduli.

2.7 Physical Analysis

The use of electron microscopy is popular for imaging the microarchitecture of hydrogels, although the analysis techniques used to perform measurements are not always reported (Bodenberger et al., 2016) or are estimated theoretically (Isobe et al., 2018). NMR is popularly used for porosity measurements in the field of petrophysics, but has also been applied to the field of hydrogels (Preparation and NMR characterisation of superporous Hydrogels (SPH) and SPH composites). Other techniques that have been used to study hydrogels include thermoporometry (Varghese et al., 2014).

2.7.1 Determination of Hydrogel Microarchitecture Using Electron Microscopy

Scanning electron microscopy (SEM) is an important tool for studying the topography of materials as it can be used to examine the architecture of a surface at the sub-micrometre scale. It fires electrons at the surface in a raster scan pattern. The electrons interact with atoms at or near the surface. These interactions result in either the electrons being repelled, absorbed (producing x-rays) or giving energy to secondary electrons which are emitted from the sample. Secondary electrons are positioned in the outer shells of the atom and emitted when they are given enough energy by the electron beam to break free of the atom. These secondary electrons are collected by a detector to form an image of the surface.

A vacuum is required to make the image as clear as possible and ensure there are no artefacts between the microscope and the sample. Unfortunately, this poses a problem for biological samples which inherently contain water, and therefore other approaches must be taken to produce a clear image of the sample. Environmental or ambient SEM allows wet samples to be used by creating a graduated vacuum. When electrons collide with gas molecules, they produce positive ions. Due to the number of electrons that are fired at the sample, the sample often becomes negatively charged. The positive ions created in an environmental SEM are attracted to the sample and neutralise it.

Using SEM to characterise the microarchitecture of the hydrogels was useful as it has a sub-micron resolution. Using a cooled stage to reduce the temperature of the hydrogel sample as the pressure was reduced, the water in the sample was prevented from boiling and disrupting the architecture of the sample. The sample was positioned on the temperature-controlled stage, excess water was removed from the surface of the sample using a pipette and the chamber was closed. Variable pressure was selected, with the target pressure set to 70Pa. As the chamber was evacuated, the temperature of the stage was gradually reduced to -20°C. By imaging the samples at a magnification of 1000x, the pores of the sample may be analysed.

2.7.2 Determination of Hydrogel Pore Volumes using NMR Logging

NMR logging uses a static magnetic field and a secondary oscillating field to interrogate porous materials. The static field exerts a torque on the hydrogen nuclei present in the water in the pores of the material. The axis of the spin of the nuclei aligns with the magnetic field. The axis of the spin of the nucleus can then be "tipped" by delivering a magnetic pulse perpendicular to the original field. The wavelength of the pulse can be adjusted so that the axis is tipped by 90°. This tipping process also phases the spins of the nuclei.

Whilst the nuclei are in phase their sum, the bulk magnetisation, can be observed by a receiver. As soon as the pulse finishes, the nuclei begin to spin away at different speeds and loses phase coherency and the bulk magnetisation signal decays. After period of time when the decay has finished, a second perpendicular magnetic pulse is applied. By doubling the wavelength of this pulse, the nuclei are tipped by 180°. By doing this, the bulk magnetisation begins to gain phase coherency as the spin path of each nucleus has been effectively reversed. After the same period of time as between the original pulse and the second pulse, this phase coherency can be observed as an "echo" which, after the time period has passed, again decays.

By repeating this second pulse after the same period of time, the echo can be repeated multiple times. The amplitude can be observed to decay with each successive echo, and this decay is known as T_2 relaxation. This raw data is then converted into a T_2 distribution graph using a mathematical inversion process known as "echo-fit" or mapping. An example of the processed data, the T_2 distribution, is presented in Figure 27.

The decay is due to an irreversible loss of phase coherence of the nuclei and happens due to three sources of relaxation: bulk, diffusion and surface relaxation. Bulk relaxation is an intrinsic property of a fluid and is controlled by its physical properties while diffusion relaxation is produced by molecules moving around within the field. Surface relaxation a product of fluid-solid interfaces, i.e. pores within the material. As the surface-to-volume ratio of 3D volumes changes with size, surface relaxation changes depending on pore size.

Using a short time period between pulses allows surface relaxation to become the

dominant factor of this decay, as opposed to bulk or diffusion relaxation. Using a short time period means that the T_2 decay time becomes approximately proportional to pore size, where larger pores with a lower surface-to-volume ratio have a longer T_2 than smaller pores (Coates et al., 1999).

NMR testing and subsequent analysis was performed by Carlos Grattoni of the School of Earth and Environment at the University of Leeds.

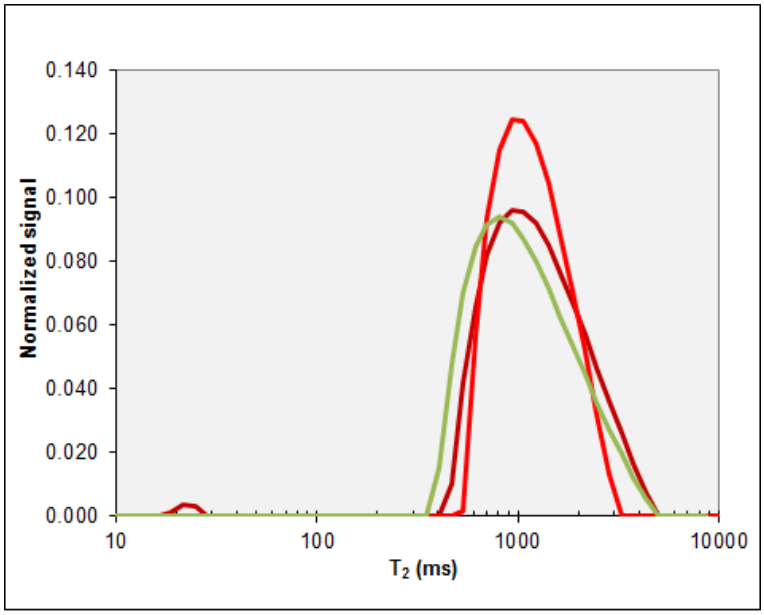

Figure 27: Example of a normalised signal of T_2 relaxation of three hydrogel samples. The small peak at low T_2 is an artifact of the experiment which occurs due to small sample volumes and can be ignored.

2.7.3 Determination of the Water Content of Hydrogels

The water content of the hydrogels was estimated by comparing the fully hydrated weight of hydrogel samples with their dehydrated, dry weight. Freshly made samples were soaked in PBS for 30 minutes, measured on a balance, before being dried over 24 hours. Samples were then weighed again once dried. The percentage of water content was calculated assuming a density of 1g/ml, using Equation 10. W was the weight of the hydrogel, wet or dry as denoted.

$$Content = \frac{W_{wet} - W_{dry}}{W_{wet}} \times 100 \tag{10}$$

2.7.4 Determining the Degree of Functionalisation of Hydrogels

Table 17: Reagents used for TNBS assay

Reagent	Method	Environment
4% $NaHCO_3$	4% (w/v) sodium bicarbonate ($NaHCO_3$), 96% (v/v) filtered water	20°C
0.5% TNBS	0.5% (v/v) 2,4,6-trinitrobenzene sulfonic acid, 99.5% (v/v) filtered water	20°C
6N HCl	33% (v/v) hydrochloric acid (HCl) (12.18M), 67% (v/v)filtered water	20°C

To determine the degree of functionalisation of the collagen, trinitrobenzine sulfonic acid (TNBS) was used as it reacted with free lysine residues in the collagen that had not been functionalised. TNBS absorbs UV light at a wavelength of 346nm and so this can be used to determine the concentration of functional groups that were unreacted by comparison with the known lysine content of unfunctionalised collagen. For rat tail collagen type I, the lysine content is 3.24×10^{-4}mol/g (Tronci et al., 2013a). For the test sample, 0.011g functionalised collagen was added to 1ml 4% $NaHCO_3$ and 1ml 0.5% TNBS (both prepared as described in Table 17) . For a blank sample, 0.11g functionalised collagen was added to 1ml 4% $NaHCO_3$, 3ml 6N HCl (prepared as described in Table 17) and 1ml 0.5% TNBS. The HCl hydrolysed the collagen, preventing the TNBS from binding.

Both samples were wrapped in foil to prevent UV exposure and shaken at 200-250rpm in an incubator at 40°C for 4 hours. For the test sample, 3ml 6N HCl was added. Both samples were incubated the oven at 60°C for 1.5 hours. A volume of 5ml of water was added to each sample. Each sample was then washed with 20 ml diethyl ether, three times for 30 seconds. Unreacted TNBS dissolved in the ether, while the reactants remained in the aqueous phase and were separated out using a separation funnel. A volume of 5 ml of each sample was diluted with 15ml of water. A volume of 2ml of each sample was dispensed into cuvettes. The wavelength on the spectrophotometer was set to 346nm and the blank sample was used as calibration. Each vial was inserted and the results were read from the display. The number of

free groups can be found using Equation 11. The degree of functionalisation can be found using equation 12.

$$Groups_{free} = \frac{N \times Abs_{346nm} \times V}{C \times L \times M_{sample}} = \frac{2 \times Abs_{346nm} \times 0.020}{1.46 \times 10^4 \times M_{sample}} \tag{11}$$

$$Functionalisation = \frac{Lys_c - Groups_{free}}{Lys_c} \times 100 \tag{12}$$

$Groups_{free}$ was the number of free groups remaining per gram of collagen, Abs_{346nm} was the absorbance value at 346nm wavelength, the path length (L) was 1cm and M_{sample} was the mass of the sample. The number of groups on each molecule (N) was two, the volume of liquid (V) used was 0.02l and the molecular absorption coefficient (C) for TNBS was 1.46x10^4 L/mol.cm-1. Lys_c is the lysine content of unfunctionalised collagen, for rat tail collagen this is 3.24x10^{-4}mol/g (Tronci et al., 2013a).

2.8 Analysis of Data

Excel was used to prepare graphical representations of the data and to find standard error. Statistics was used to compare data between sample groups, find trends, identify outliers and draw conclusions as to whether there are meaningful differences between the data.

2.8.1 Determining the Variation of Data Using Standard Error

The error bars displayed on the data presented were of standard error which was used to provide a visual guide as to the variation in the data set. Standard error was calculated by first determining the standard deviation, using Equation 13, then the standard error may be calculated using Equation 14. σ is the standard deviation, x_i is the ith datum, $\overline{x}$ is the mean and n is the sample size. $\sigma_{\overline{x}}$ is the standard error.

$$\sigma = \sqrt{\frac{\sum(x_i - \overline{x})^2}{n-1}} \tag{13}$$

$$\sigma_{\overline{x}} = \frac{\sigma}{\sqrt{n}} \tag{14}$$

2.8.2 Determining the Method of Statistical Analysis

To determine the probability that observed differences in samples occurred by chance, statistical analysis was performed. The method of statistical analysis was chosen using the flow diagram presented in Figure 28, adapted from Waning and Montagne (2001). All ordinal data was assessed using the non-parametric route in the diagram. All statistical tests were performed in SPSS, however the calculations used are presented here.

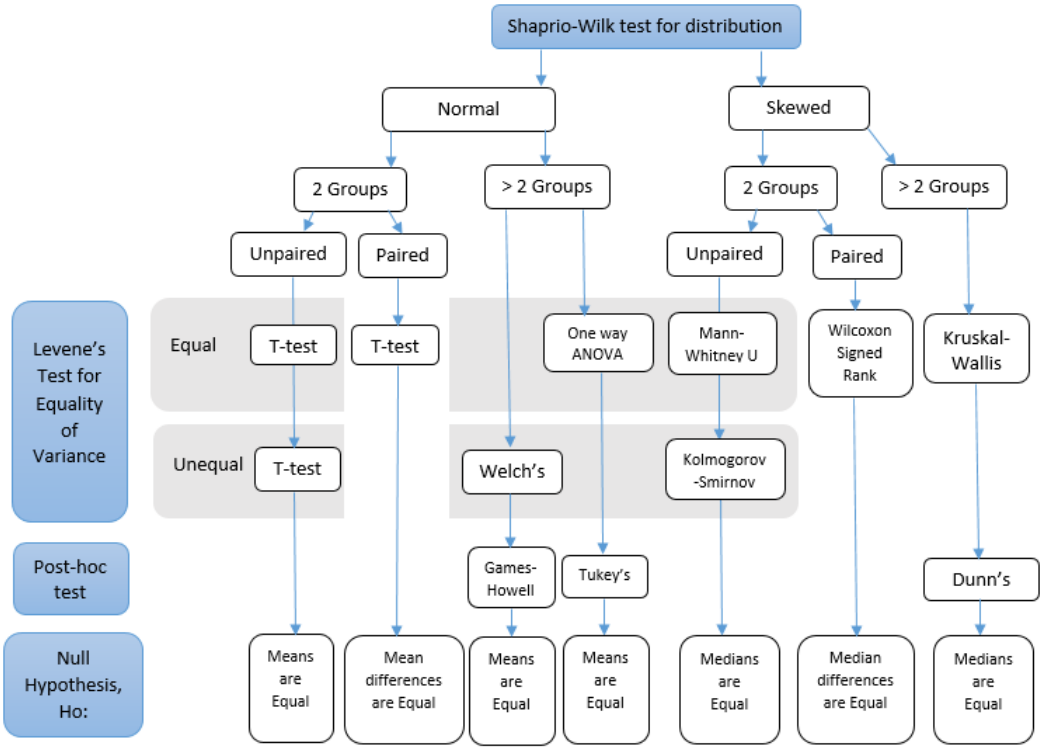

Figure 28: Decision tree used to select statistical tests for continuous data analysis, adapted from Waning and Montagne (2001).

As the figure shows, the null hypotheses used were; for parametric (normally distributed) data, that the means or mean differences were equal, while for non-parametric (skewed) data, that the medians or median differences were equal. The statistical tests calculate a p-value, which is the probability of obtaining a result as or more extreme than the values actually obtained in the experiment. The null hy-

pothesis was rejected in the cases where the p-value calculated by the statistical test was lower than the significance level, α. α is the probability of incorrectly rejecting the null hypothesis and the significance levels used in this study are presented in Table 18.

Table 18: Statistical Significance and Notation in Figures

α value	Probability of incorrect rejection	Significance	Notation
0.05	5%	Significant	*
0.01	1%	Highly Significant	**

2.8.3 Shapiro-Wilk Test for Determining Normality of Data

The Shapiro-Wilk test was used to check for normal distribution of continuous data as the number of samples was low. The null hypothesis was that the sample comes from a normally distributed population, which was failed to be rejected if the significance of the Shapiro-Wilk test found W to be greater than the confidence level, α, i.e. W>0.05. The test is only applicable for tests with 3 or more data points and orders the data from smallest (where i=1) to largest (where i=n) and uses Equation 15 to find W.

$$W = \frac{(\sum a_i x_i)^2}{\sum_{i=1}^{n}(x_i - \overline{x})^2} \tag{15}$$

Where W is the probability that the data came from a normally ditributed population, a_i is the Shapiro-Wilk constant (which changes for each datum and depends on the sample size), x_i is the i^{th} smallest datum, and $\overline{x}$ is the mean of the samples.

2.8.4 Levene's test for Determining the Equality of Variances

Levene's test was used to determine whether groups had approximately homogeneous variance, where the null hypothesis was that the variance was equal. For parametric data, Levene's test was based on the mean, while for non-parametric data, Levene's test was based on the median and with adjusted degrees of freedom. The null hypothesis was not rejected and groups were assumed to have equal vari-

ance where the significance of Levene's test was greater than the confidence level, i.e. p>0.05. The test performed an analysis of variance on the deviation of data from the mean (i.e. $x_i - \overline{x}$) or median (i.e. $x_i - \widetilde{x}$), and found the p-value from the mean deviation.

2.8.5 Determining the Probability of Differences Occurring by Chance Using Analysis of Variance of Data

An analysis of variance was performed for the Levene's test, for T-tests, ANOVA and Welch's. The null hypothesis was that there was no difference in means between samples while the alternate hypothesis was that at least one mean differs from the others. Similarly to Levene's test, to perform a paired t-test instead of analysing the means, the difference between each of the paired samples is calculated, and the analysis is performed on the mean of the differences.

The test for analysis of variance finds the F-value, which is calculated from the following sample equations. Equation 16 was used to determine the variance of each sample.

$$s^2 = \sum \frac{(x_i - \overline{x})^2}{n-1} \tag{16}$$

Where s^2 is the variance, x_i is the i^{th} smallest datum, $\overline{x}$ is the mean and n is the sample size.

Equations 17 and 18 were used to find the variance between and within groups.

$$S_B^2 = \frac{\sum n(\overline{x} - \overline{x}_M)^2}{k-1} \tag{17}$$

$$S_W^2 = \frac{\sum (n-1)s^2}{\sum (n-1)} \tag{18}$$

Where S_B^2 is the variance between groups compared to the overall mean, $\overline{x}_M$ is the overall mean of all samples in all groups, k is the number of groups. S_W^2 is the variance within groups compared to the overall mean and s^2 is the sample variance.

Finally, the F-value was calculated using Equation 19.

$$F = \frac{S_B^2}{S_W^2} \tag{19}$$

Where F is the critical value. When F falls below α, the null hypothesis may be rejected.

For Welch's test, where homogeneity of variance is not assumed, the variance between groups is determined by using the data "unpooled", i.e. calculating the variance for each group individually before summation.

For tests with 3 or more samples, if the null hypothesis was rejected, a post hoc test was used to distinguish which samples were significantly different.

2.8.6 Non-Parametric Tests for Determining Analysis of Variance of Ranks

Non-parametric tests were used for skewed continuous data or ordinal data and involved assignment of ranks to the data values. Although the plate reader used for the ATPlite and CyQuant assays gives luminescence or fluorescence counts per minute (i.e. ordinal data), due to the fact that the numbers were often over $1x10^5$, this data was treated as continuous. Non-parametric or ordinal data were ordered from smallest to largest, and ranks assigned based on their orders. Where values were the same, the rank numbers were averaged so that all with the same value had the same rank. Non-parametric tests also analysis for variance, of the assigned ranks rather than the original data.

2.8.7 Post Hoc Tests for Determining P-Values for More than 3 Groups of Data

For normally distributed data, the Tukey post-hoc test was used to establish which groups were statistically significant from each other after significance had been found when analysis was performed using an ANOVA or Welch's. The Tukey post hoc test, for example, was performed using Equation 20. For non-normally distributed data, the Dunn post-hoc test was used.

$$SD = q\sqrt{\frac{MS_{within}}{n}} \tag{20}$$

SD was the minimum difference between means required for significant difference, q was obtained from a Tukey q-value look-up table, MS_{within} was the mean square within groups, and n was the sample size.

3 Development of an *In Vitro* Cell Model for Investigation of Stem Cell Activities in 3D

3.1 Introduction

Physical and mechanical factors affecting cells of the central nervous system (CNS) are not completely understood (Li et al., 2012). Expanding the knowledge in this field may contribute to improved care for patients of CNS disease as greater understanding may lead to improved treatments. Studying the physical environment of cells has been more successful using *in vitro* models, as the chemical environment can be more easily controlled and the cellular activities can be more easily monitored. A suitable *in vitro* system was required to study the activities of neural stem cells in a three dimensional (3D) environment for the investigation of cellular mechanosensitivity.

The behaviour of cells has been found to differ when situated in a 3D environment rather than a two dimensional (2D) one (Huebsch et al., 2010; Kothapalli and Kamm, 2013), which means that it is important that studies into the effects of mechanical and physical extracellular matrix (ECM) properties such as elastic modulus and pore size should take place in 3D. Hydrogels have become popular as an *in vitro* biomimetic model for 3D studies. To answer the research questions formed in this project, a 3D environment was essential to study both the response of cells to different engineered environments, and the 3D migration of cells in a raised pressure environment.

In this chapter, two available hydrogel technologies were assessed for their suitability to interrogate the hypotheses posed in Section 1.6; that the activities of neural stem cells are affected by changes in the elastic modulus independently of pore size, and by changes in pressure. The hydrogel was required to support the homeostasis of cells whilst leaving them accessible for fluorescent labelling, and visible for imaging. Two hydrogel systems were identified which had the theoretical potential for their modulus to be modified. An initial study into the ability of the hydrogel to support viable stem cells in the hydrogel was also undertaken using live/dead staining, to ensure the hydrogel could be used for future work.

3.2 Aims and Objectives

The aim of this chapter was to develop a 3D system suitable for the culture of neural stem cells and to optimise methods for cellular investigations. The hydrogel was optimised to provide a suitable *in vitro* model to interrogate the hypotheses posed. An overview of the tasks and the specific objectives they relate to is detailed in Figure 29.

3.2.1 Specific Objectives

1. **To construct a design specification for the ideal hydrogel.** The specification should include factors relating to the synthesis of the hydrogels, their effect on cells and their mechanical properties.

2. **To characterise the properties of the hydrogels.** Both mechanical and physical characterisation as well as C6 glial cell viability must be investigated so that the hydrogels may each be compared.

3. **To evaluate potential hydrogel systems and select the most appropriate for further study.** The requirements of the specification must be evaluated using a decision matrix, which weights the requirements by importance and assigns potential outcomes scores. A decision matrix allows the hydrogels to be quantitatively compared.

4. **To perform an initial feasibility study of maintaining a culture of stem cells in the most appropriate hydrogel system.** Confirmation of the viability of the stem cells was required to allow subsequent investigations to take place.

5. **To optimise methods for cellular investigations** Including use of the CyQuant assay in 3D and successive use of the CyQuant and ATPlite assays.

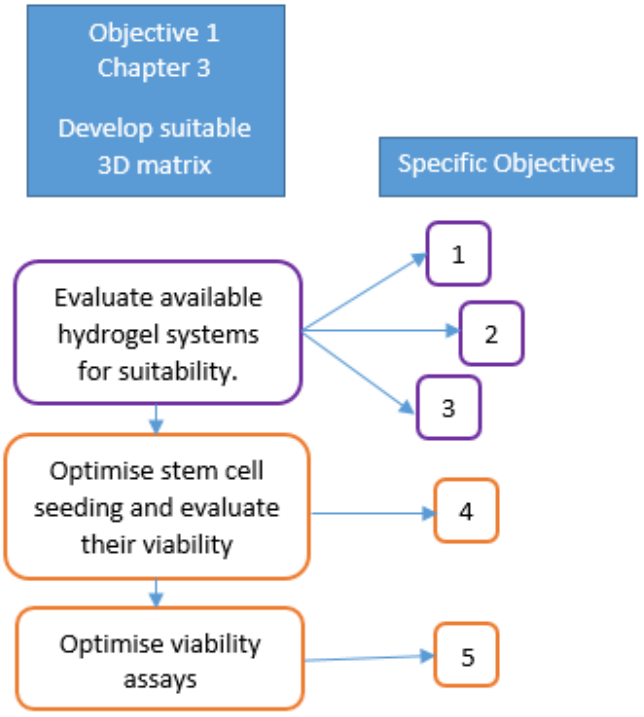

Figure 29: Overview of the tasks of chapter 3 and the specific objectives these relate to.

3.2.2 Hydrogel Design Specification

The specification included important factors relating to the synthesis of the hydrogel, the cell response and the mechanical properties. The specification is detailed in Table 19.

Table 19: Hydrogel specification

Property	Ideal outcome	How measured
Maintain viable cell culture	C6 glial cell viability increased at day 2	ATPlite assay
Suitable elastic modulus	Elastic modulus between 100-600Pa within Linear viscoelastic region (LVER) at 1Hz	Rheology
Minimum synthesis time	1 day	Count
Simple synthesis	1 step	Count
Transparency	Transparent	Visual assessment

The ability to maintain a viable cell culture was essential to perform future studies using the hydrogel. Although viability was required for longer time periods (up to ten days) in later studies, the viability was measured after 2 days initially to give an indication of viability. The hydrogel was required to have an elastic modulus within the biomimetic range to ensure results are relevant to the *in vivo* environment. As many batches will be required to be synthesised during hydrogel development, it was important that the synthesis time was relatively short. A simple synthesis process was required to limit variability between batches. The hydrogel was required to have some degree of transparency to ensure the activities and morphologies of cells could be monitored within the hydrogel using microscopy techniques.

3.3 Methods

3.3.1 Hydrogel Preparation

Hydrogel Synthesis

Two in-house hydrogel synthesis methods were identified that were able to support viable cells and were therefore evaluated for suitability for interrogating the hypotheses. Collagen Type I was harvested from rat tails as described in Section 2.3.1. Hydrogels were synthesised from dry weight collagen in two ways: UV crosslinking or chmical crosslinking. The UV crosslinked hydrogels were functionalised with either glycidyl methacrylate (GMA) or 4-vinylbenzyl chloride (4-VBC) monomers and then crosslinked under UV light as described in section 2.3.2. The chemically crosslinked hydrogels were synthesised by activation of the 1,3-phenylenediacetic acid (Ph) crosslinker and mixed with the collagen as described in section 2.3.3. Two versions of the Ph hydrogel were synthesised, Ph1 used the original method described, while Ph2 used the activated crosslinker solution diluted to 75% (v/v) its original concentration with 25% (v/v) filtered water. The four hydrogel variants are described in Table 20.

Table 20: The four different collagen hydrogels that were tested and details of their composition. The names given relate to the monomer or crosslinker used in each.

Gel Name	Composition
Ph1	Collagen was chemically crosslinked using p-Phenylenediacetic Acid (Ph) for the crosslinker (as described in Section 2.3.3). Proportions of collagen solution to activated Ph solution was 2:1.
Ph2	Collagen was chemically crosslinked using Ph for the crosslinker (as described in Section 2.3.3). Extra PBS was added so that the proportions of collagen solution to activated Ph to extra PBS was 8:3:1.
GMA	UV-crosslinked hydrogel (made as described in Section 2.3.2) using glycidyl methacrylate (GMA) for the crosslinking monomer.
4-VBC	UV-crosslinked hydrogel (made as described in Section 2.3.2), using 4-vinylbenzyl chloride (4-VBC) for the monomer.

3.3.2 Cell Culture

The C6 glial cell line was used for initial evaluation of the ability of the hydrogels variants to support viable cells as it was a neural cell line readily available in the laboratory and was inexpensive to culture. The cells were cultured as outlined in Section 2.4. For determination of the viability of stem cells on the hydrogels, the neural stem CB660 and CX cell lines were cultured as described in Section 2.4.4.

3.3.3 Cell Seeding of Hydrogels

Hydrogels were prepared for cell culture as described in Section 2.2.1. A cell suspension was prepared, and a cell count was taken as described in Section 2.4.2. To achieve the required overall seeding density per ml of hydrogel, by pippetting a cell suspension of twice the required cell concentration in media at half the volume of the hydrogel, to maximise cell attachment to the hydrogel. For example, for 100μl hydrogels requiring a cell density of 1x10^5 cells/ml, a cell suspension of 2x10^5 cells/ml in 50μl media was used for each hydrogel. The seeded hydrogels were immediately

incubated at 37°C, in air with 5% (v/v) carbon dioxide (CO_2). The media was changed the following day and then every other day, the volume of which was equal to the volume of each hydrogel sample.

The mechanical characterisation was performed on seeded and unseeded hydrogels. For this investigation, 1.5ml hydrogels were seeded at a density of 5×10^5 cells/ml hydrogel. This density was chosen as this was used by Her et al. (2013). All hydrogels were incubated at 37°C, in air with 5% CO_2 for three days and the media was changed on day 1.

3.3.4 Determination of Viability of Cells Seeded Within Hydrogels

An ATPlite assay was performed to determine the viability of the C6 glial cell line in the hydrogels, as described in Section 2.5.2. For determining the viability of the stem cell lines in the hydrogels, the ATPlite, live/dead and Cyquant Direct assays were performed, described in Sections 2.5.1 and 2.5.3.

3.3.5 Physical Characterisation

Mechanical Characterisation

The hydrogels were mechanically characterised by their storage and loss moduli on day 3 using a rheometer to determine if the elastic modulus was in a range that mimicked that of natural tissue. As described in Section 2.6.1, an amplitude sweep was performed to determine a strain level within the LVER, followed by a frequency sweep at this strain. As this was an initial experiment to determine a hydrogel for use in future expriments, the amplitude sweep had one repeat while the frequency sweep had two repeats to conserve materials.

Mechanical characterisation was performed using a rheometer as described in Section 2.6.1. Oscillatory amplitude sweeps were performed between 0.1-100% strain and at 1 and 20Hz. Oscillatory frequency sweeps between 1 and 10Hz and at a strain within the LVER were performed on cell seeded and non cell seeded hydrogels with cells after 3 days of culture. These were destructive tests.

Determination of Transparency of the Hydrogels

A method for determination of the transparency of the hydrogels was developed through qualitative means by placing a high contrast black and white image underneath the hydrogel and visually assessing the clarity of the image through the hydrogel. A scoring system was devised to enable the transparency of each hydrogel to be assessed in a way with limited bias and three hydrogels per type were scored. A score was assigned to each hydrogel based on the visual assessment of the distinction between black and white areas, and the blurriness of the edges of each shape. A representation of transparency for the Ph hydrogel is presented in Figure 30. The scoring system is presented in Table 21.

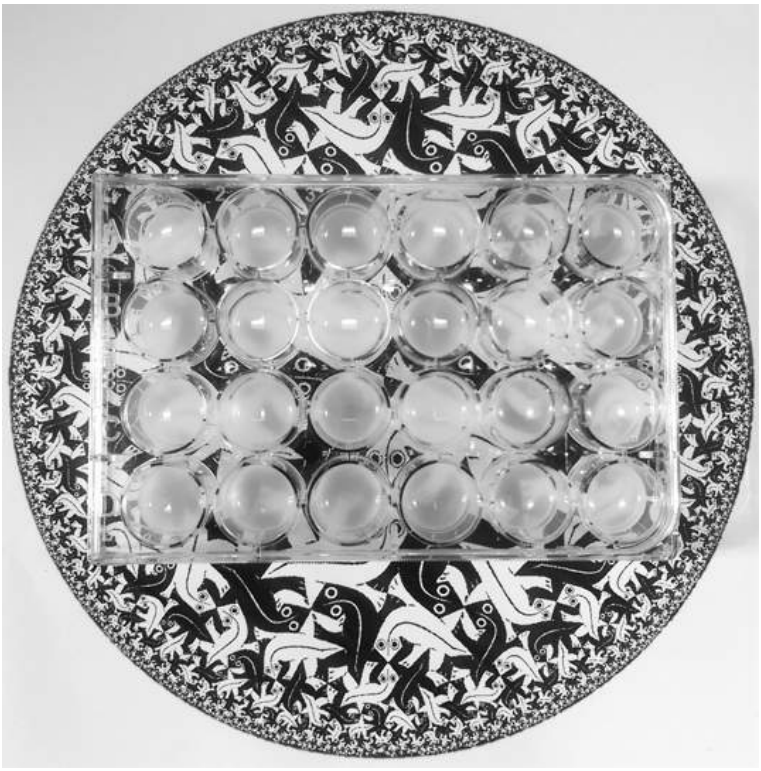

Figure 30: Transparency of Ph1 hydrogel, using a high contrast background (Escher, 1960)

Table 21: The scoring system to assess the transparency of the hydrogel

Score	Gel Description
0	Completely Opaque, no image can be seen through the hydrogel.
2	Slight distinction can be made between black and white areas.
4	Some distinction between black and white areas, edges are indistinct.
6	Distinction between black and white areas, edges are blurred.
8	Good distinction between black and white areas, edges are slightly blurred.
10	Completely transparent, the image can be seen with perfect clarity.

3.3.6 Significance Testing using Statistics

Statistical analysis was performed when required to inform decisions and assess the meaning of results, using the method described in Section 2.8.

3.3.7 Evaluation Using a Decision Matrix

The hydrogels were evaluated using a decision matrix. Parameters for assessing the hydrogels were taken from the design specification and each was given a weight depending on how important that parameter was to the project. Before assessing the hydrogels, the range of possible values for each parameter were assigned a score, with 1 being an undesirable score and 10 being a desirable score. Where possible, the matrix was structured to be able to be quantitatively assessed rather than qualitatively, to remove bias from the scoring. After the decision matrix was constructed, the values for each hydrogel were compiled, one parameter at a time, so any qualitative assessment was directly compared. These assessments were translated into scores and the scores were multiplied by the weighting value to deliver a final value. These values were then totalled for each hydrogel type to deliver an overall score which could be directly compared with the other hydrogel types.

3.4 Results

An overview of the experiments that were performed for this chapter is detailed in Table 22, including the volume of hydrogels used and the well plate (WP) format used, which was decided based on the application.

Table 22: Details of the Experiments for Evaluation of the Hydrogels

Finding	Hydrogel Volume	Test	Variables	Rep.
C6 Cell Viability	150μl in 96WP	ATPlite Assay	Hydrogel type	3
Storage and Loss Moduli	1.5ml in 24WP	Rheology	Hydrogel type	2
Transparency	500μl in 24WP	Visual Assessment	Hydrogel type	3
Stem Cell Viability	500μl in 24WP	Live/Dead stain	Stem cell type	2
3D CyQuant Assay Development	100μl in 96WP	CyQuant Assay	Seeding density	4
Stem Cell Viability Comparison	100μl in 96WP	ATPlite Assay	Stem cell type, seeding density	4
Low Seeding Density Study	100μl in 96WP		ATPlite and CyQuant Assays	4
Optimisation of Successive Cell Viability Assays	100μl in 96WP		ATPlite and CyQuant Assays	4

3.4.1 Viability of Cells Encapsulated within the Hydroels

The four hydrogel types, GMA, 4-VBC, Ph1 and Ph2 were synthesised and cast into 96WPs at a volume of 150μl, as described in Table 22. For each hydrogel type, C6 glial cells were seeded at 3.3×10^5 cells/ml of hydrogel with four repeats, described in Table 23. Cells were seeded into wells with no hydrogel as a positive control at $5x10^4$ cells/well. As a negative control was prepared at 3.3×10^5 cells/ml of hydrogel, however 75μl dimethyl sulfoxide (DMSO) was added one hour later,

with the expectation of causing cell lysis. Additionally, hydrogels were cultured in media with no cells added. As there were three control types implemented in this experiment, only two repeats for each were used to conserve materials.

Table 23: Experimental set up to determine the viability of C6 cells encapsulated within the hydrogels

Name	Description
cells+gels	Hydrogels seeded with cells, cultured normally. n=4
cells (no gel)	Cells seeded into wells without hydrogels, cultured normally. n=2
cells+gels+DMSO	Hydrogels seeded with cells, cultured with DMSO. n=2
gels (no cells)	Hydrogels not seeded with cells, incubated with media. n=2

Cell viability was determined using the ATPlite assay on day 0 (four hours after seeding), at day 1 and day 2. The ATPlite assay was performed as described in Section 2.5.2. The measurements made from the ATPlite assay for the chemically crosslinked hydrogels are presented in Figure 31 while the results for the ultraviolet (UV)-crosslinked hydrogels are presented in Figure 32. For all test scenarios, wells containing cells (no gel) increased in number from day zero to one, and then decreased from day 1 to 2. When C6 cells were seeded onto the chemically crosslinked hydrogels a similar pattern was observed, with cell viability increasing from day 0 to day 1 and then decreasing at day 2. Cell numbers were higher in Ph1 compared to Ph2, indicating this variant of hydrogel may be more biocompatible. In the UV crosslinked hydrogels, the GMA material appeared better able to support the growth of C6 cells up to day 1, however marked reductions in cell viability were seen at the day 2 time point. The cells were not viable when seeded on the 4-VBC hydrogel with very low readings observed at all time points, indicating that this hydrogel type does not support viable cells. ATPlite readings for the cells cultured with DMSO were expected to act as a negative control, however showed high readings in the Ph1 and Ph2 hydrogels, indicating that the DMSO did not acheive this. This may be an indication that the DMSO was unable to permeate the hydrogels effectively or that it was unable to lyse the cells effectively.

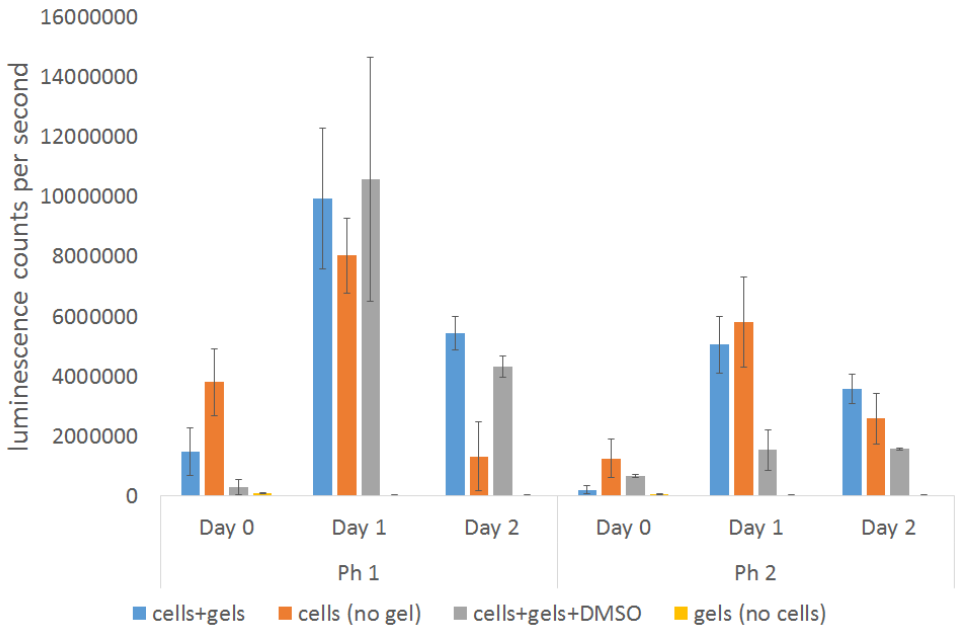

Figure 31: Viability of C6 astrocytic cells after seeding onto the two variants (Ph1 and Ph2) of the chemically crosslinked hydrogels, Ph1 and Ph2, using ATPlite assay. Cells were seeded at 3.3×10^5 *cells/ml. Error bars show standard error, n=4 for hydrogels containing cells, for other variables n=2.*

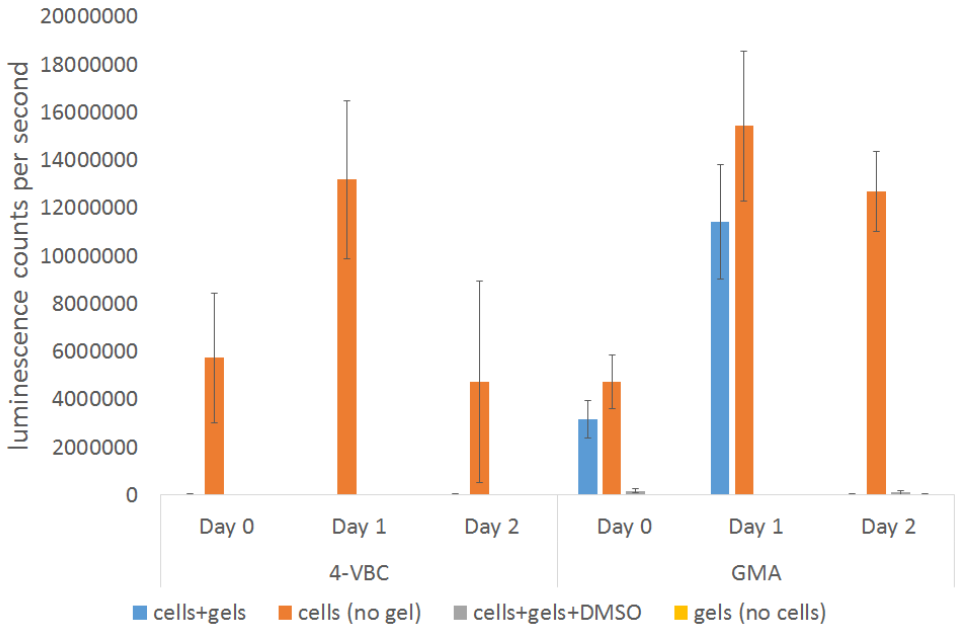

Figure 32: Viability of C6 astrocytic cells after seeding onto the two variants of the UV-crosslinked hydrogels, GMA and 4-VBC, using ATPlite assay. Cells were seeded at 3.3×10^5 *cells/ml. Error bars show standard error, n=4 for hydrogels containing cells, for other variables n=2.*

3.4.2 Mechanical Characterisation of Hydrogels

During the incubation stage before mechanical characterisation was performed, the 4-VBC hydrogels contracted significantly, as shown in Figure 33. The small size of these hydrogels observed at day 3 meant that it was not possible to perform mechanical characterisation. This was because diameter of the contracted hydrogels was significantly smaller than the rheometer cone, meaning that the rheometer would be underfilled, significantly affecting measurements taken.

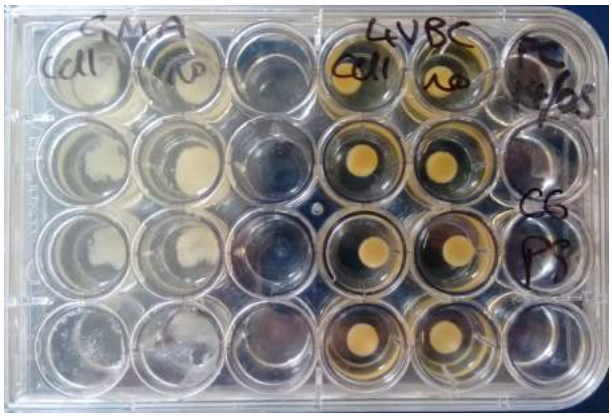

Figure 33: Well plate containing GMA hydrogels (left) and contracted 4-VBC hydrogels (right).

Figures 34 and 35 present the mechanical response of the amplitude sweeps performed by the rheometer, which were used to determine the LVER of the hydrogels. G' was found to be lower at 1Hz compared to 20Hz and further reduces at high strain, while for 20Hz G' is observed to increase at high strain. In general, the gradient of the curves is close to zero when the strain is lower than 5%.

The LVER was determined to coincide for all hydrogels and for both frequencies at 1% strain and so this amplitude was used for the subsequent frequency sweeps. The frequency sweeps for each hydrogel type from 1-10Hz are shown in Figures 36, 37 and 38. The mean storage and loss moduli for each hydrogel type at 1Hz are presented in Table 24. The moduli of all hydrogels reduced when cultured with C6 cells. The most extreme reduction was seen in the storage modulus of GMA hydrogels which reduced to 29% of its original value.

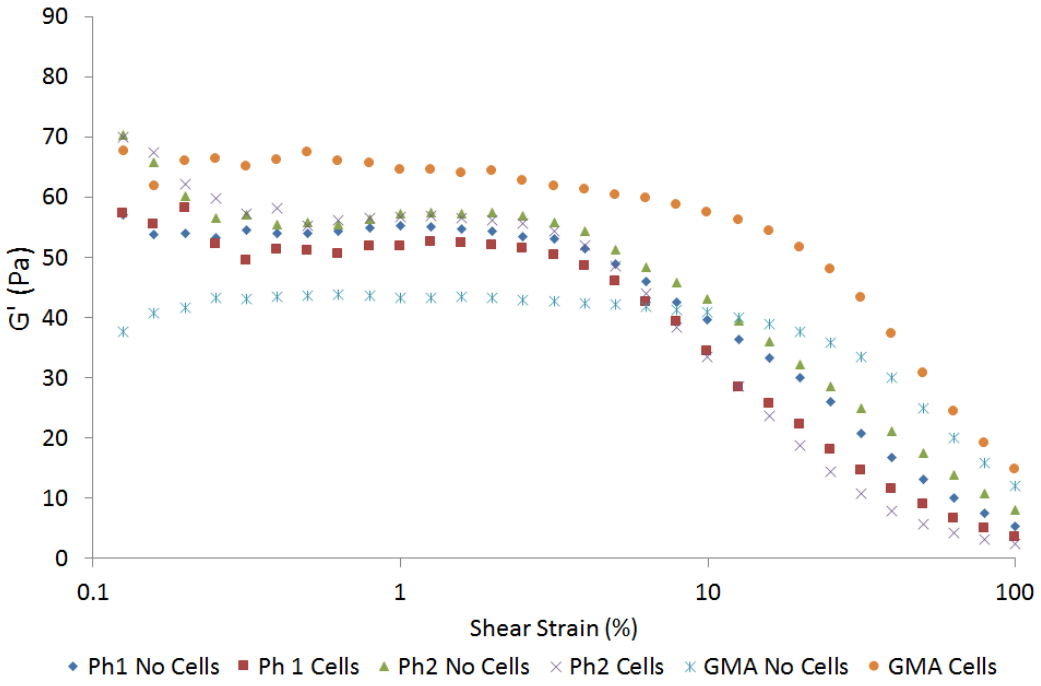

Figure 34: Elastic modulus (G') of unseeded and C6 astrocytic cell seeded Ph1, Ph2 and GMA hydrogels at day 3 over an amplitude sweep of 0.1-100% shear strain, at 1Hz.

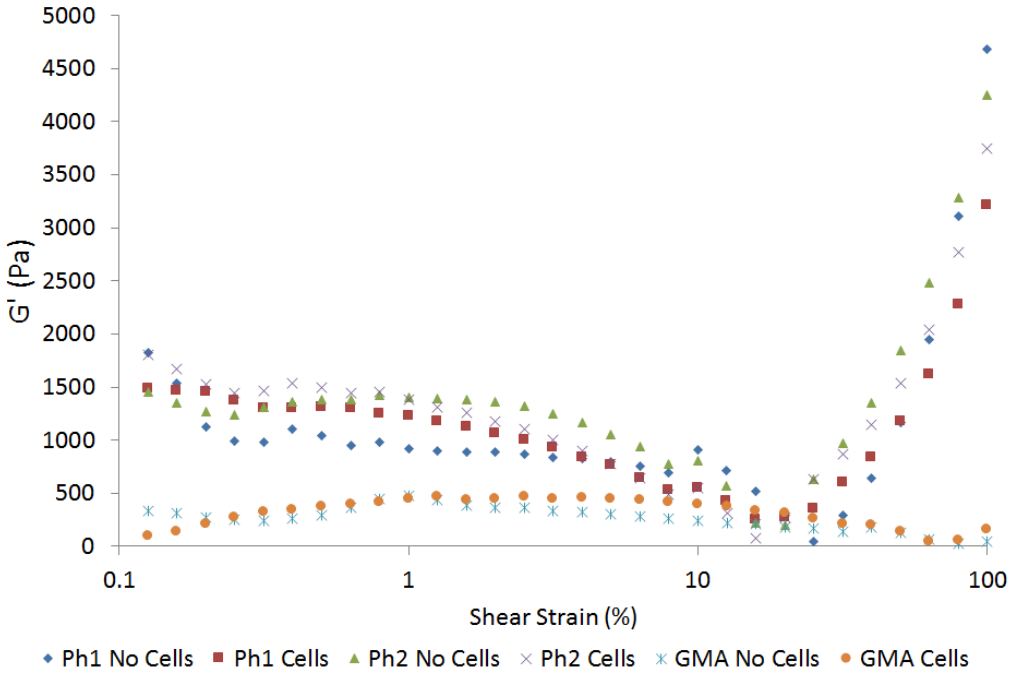

Figure 35: Elastic modulus (G') of unseeded and C6 astrocytic cell seeded Ph1, Ph2 and GMA hydrogels at day 3 over an amplitude sweep of 0.1-100% shear strain, at 20Hz.

Table 24: Storage and Loss Moduli (G' and G") for unseeded and C6 astrocytic cell seeded Ph1, Ph2 and GMA collagen hydrogels at 1Hz, 1% strain. Values in brackets represent standard error (n=2)

Hydrogel type	Storage Modulus (Pa)	Loss Modulus (Pa)
Ph1 No Cells	107.73 (±38.77)	14.83 (±5.10)
Ph1 Cells	82.41 (±11.32)	12.98 (±0.25)
Ph2 No Cells	97.09 (±10.72)	12.73 (±1.24)
Ph2 Cells	66.94 (±18.72)	79.68 (±2.65)
GMA No Cells	102.73 (±38.47)	19.91 (±7.44)
GMA Cells	29.75 (±0.97)	5.75 (±0.47)

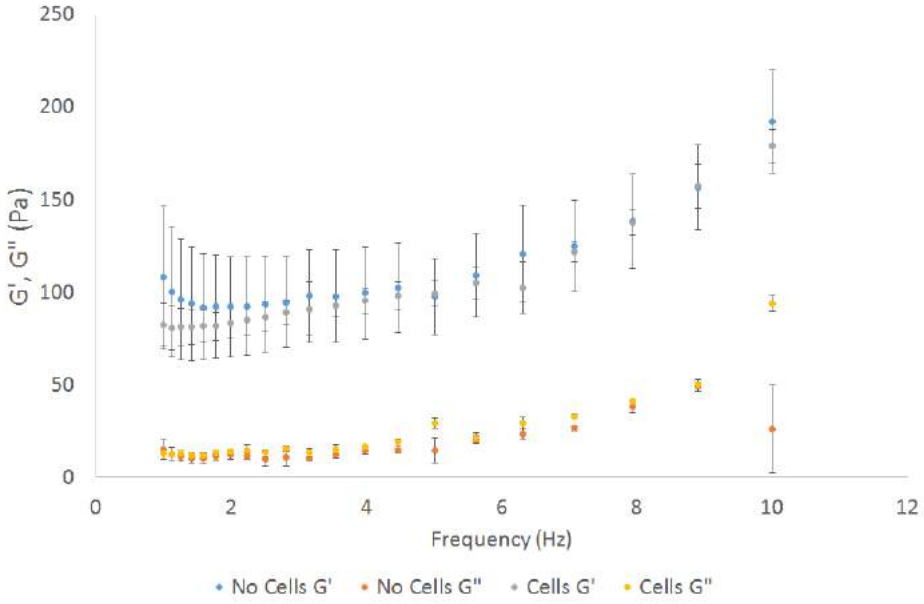

Figure 36: Storage (G') and loss (G") moduli for unseeded and C6 astrocyte seeded Ph1 collagen hydrogels at day 3 over a frequency sweep of 1-10Hz. Error bars represent standard error, n=2.

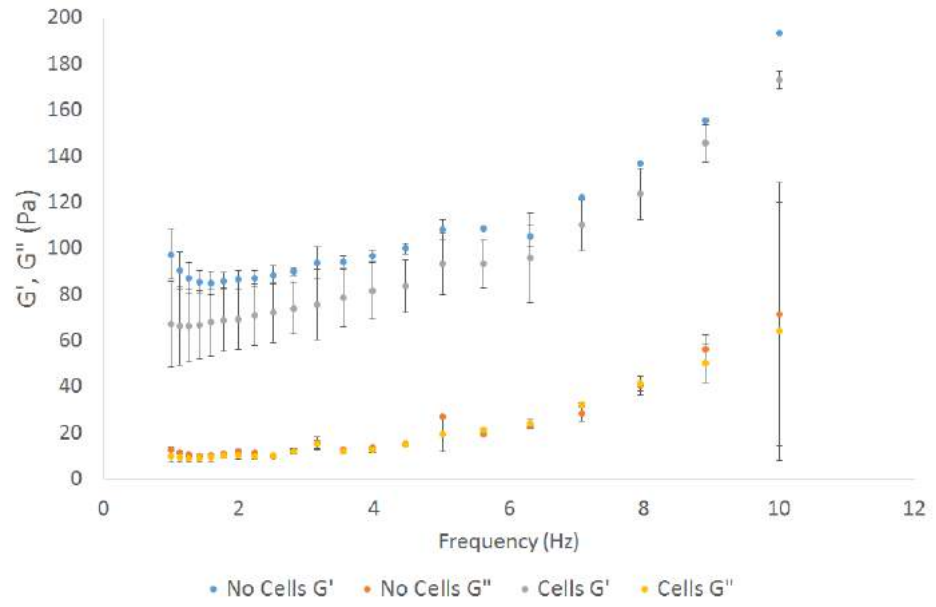

Figure 37: Storage (G') and loss (G") moduli for unseeded and C6 astrocyte seeded Ph2 collagen hydrogels at day 3 over a frequency sweep of 1-10Hz. Error bars represent standard error, n=2.

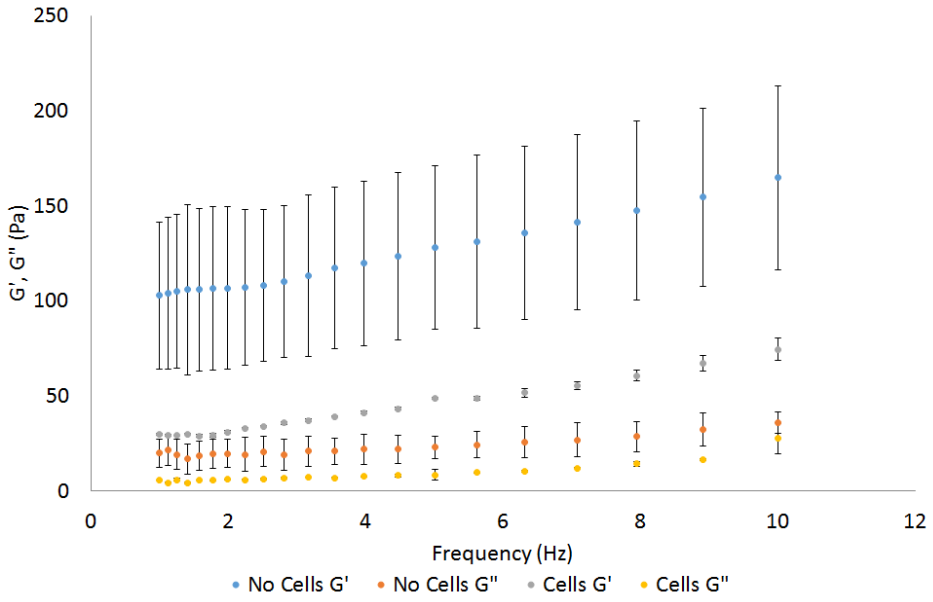

Figure 38: Storage (G') and loss (G") moduli for GMA at day 3 over a frequency sweep of 1-10Hz. Error bars represent standard error, n=2.

3.4.3 Determination of Transparency

The transparency was assessed visually for each hydrogel using 500μl hydrogel samples in a 24WP. Scores were assigned to each hydrogel based on the scoring system

outlined in 21. The mean scores are presented in Table 25. No difference in transparency was observed between the three repeats for each hydrogel.

Table 25: Scores for transparency given for each hydrogel variant

Hydrogel	Score	Reasoning
Ph1	5	Some distinction between black and white areas, edges are blurred
Ph2	6	Distinction between black and white areas, edges are blurred
GMA	9	Excellent distinction between black and white areas, edges are slightly blurred
4-VBC	6	Distinction between black and white areas, edges are blurred

3.4.4 Selection of Hydrogel for further Experimentation

A decision matrix, Table 26, was constructed to assess the suitability of the hydrogels. The final scores are recorded in Table 27.

Cell viability was deemed the most important parameter and although the hydrogels were seeded with the C6 cell line which may not correspond to stem cell viability, it was deemed to serve as a good indicator. The cell viability for each hydrogel was based on the peak value measured in the ATPlite cell viability assays. Elastic modulus was determined for cell seeded hydrogels at day 8 for chemically crosslinked hydrogels and day 3 for UV crosslinked hydrogels, at a frequency of 1Hz, and at 1% strain. Based on Banerjee et al. (2009), an elastic modulus of under 100Pa was deemed as "optimal", however as all the hydrogels tested were under this limit anyway, this parameter became irrelevant. Synthesis time was considered as manufacturing the GMA and 4-VBC cells was time consuming and held back the progress of the project, while the number of steps was also included - as each step carries with it further potential for variability and error. Finally, transparency of the hydrogels was also considered, as clear hydrogels are easier to image than opaque ones. This parameter was the only one that was scored qualitatively.

The decision matix found the Ph1 hydrogel was the best option for this research, with GMA and Ph2 scoring similarly. The 4-VBC hydrogels scored poorly as their ATPlite cell viability assay outcome was poor and it was not possible to mechanically

test these due to shrinkage of the hydrogel. The GMA hydrogel lost most points due to the length of time and number of steps required to create the hydrogel, however scored better than the Ph1 hydrogel on cell viability and transparency.

Table 26: Decision matrix used for comparing the hydrogels.

Gel Attribute	Synthesis time	Ease	Transparency	Cell viability	Elastic Modulus
Weighting	**0.2**	**0.05**	**0.1**	**0.4**	**0.25**
Units	Days	Number of steps	Observational (qualitative)	Peak ATP counts per second	Pascals
Range	1-10	1-10	Opaque-Transparent	0-16million	0-1000
Score 10	1	1	Transparent (10)	16million	<600, >100
Score 0	10	10	Opaque (0)	0	<20, >1000
Values					
Ph1	1	4	5	10 million	107.73
Ph2	1	4	6	5 million	97.09
GMA	8	7	9	11 million	102.73
4-VBC	8	7	6	0 million	not tested
Scores					
Ph1	10	6	5	6	10
Ph2	10	6	6	3	9
GMA	2	3	9	7	10
4-VBC	2	3	6	0	0
Score x weight					
Ph1	2	0.3	0.5	2.4	2.5
Ph2	2	0.3	0.6	1.2	2.25
GMA	0.4	0.15	0.9	2.8	2.5
4-VBC	0.4	0.15	0.6	0	0

Table 27: Total scores of each hydrogel as calculated via the decision matrix, Table 26.

Gel type	Ph1	Ph2	GMA	4-VBC
Total	7.7	6.35	6.75	1.15

3.5 Optimisation of Methods for Cellular Investigations

3.5.1 Optimisation of Stem Cell Culture and Seeding Protocols

Before the viability of the stem cells seeded in the hydrogels were compared quantitatively using ATPlite and Cyquant, live/dead assays were performed to confirm that the hydrogels were suitable for the two neural stem cell lines, and that the cells were able to migrate into the hydrogel so that they are situated within the 3D matrix.

CB660 Cell Line

Initially, CB660 stem cells were obtained from the UK Stem Cell Bank (NIBSC) due to their accessibility as an inexpensive source of cells (*NIBSC*). Cells were cultured as detailed in Section 2.4.4.

Although the initial thaw and first passage was successful, the proliferation of the cells stagnated soon after. The culture was attempted twice more with new batches of cells, with the same result. After three unsuccessful attempts to expand the culture over the timespan of four months, the expansion was attempted by the UK Stem Cell Bank (NIBSC). The same pattern of proliferation was observed, and the problem remained unresolved for another six months while the bank attempted to rectify the problem.

Before the proliferation deteriorated, enough CB660 cells were generated to allow them to be seeded into the chemically crosslinked hydrogel. Four 500μl hydrogels were synthesised in a 24WP at 2.5x10^5 cells/ml and cultured for 6 days. Live dead staining was performed on CB660 cells cultured in the hydrogel at day 6 is presented in Figure 39. Many of the living cells have migrated and extended processes into the hydrogel, and are therefore in a 3D environment. This evidence suggests the

cells are not stressed and that the hydrogels provide an environment suitable for maintaining viable cells. The images also show cells and processes that are outside of the field of focus, suggesting that the hydrogels are amenable for cell migration into the hydrogel matrix.

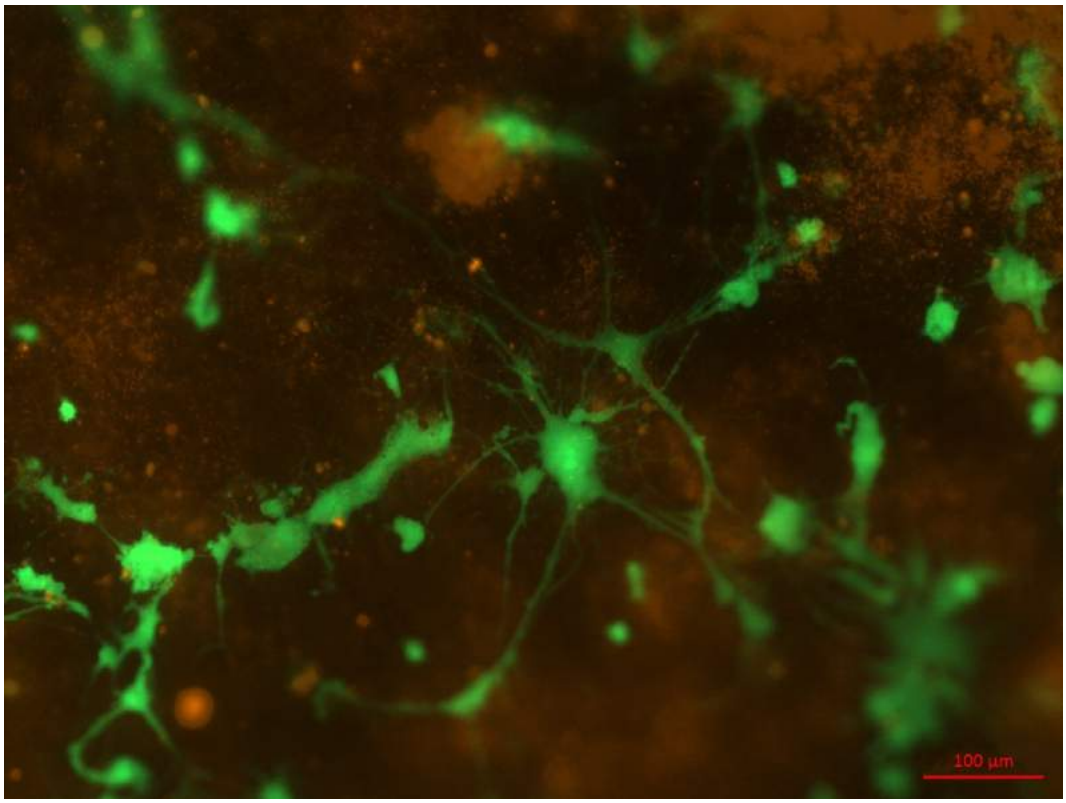

Figure 39: Representative image of CB660 stem cell viability at day 6 when seeded onto the pheneylenediacetic acid hydrogel. Live cells were labelled with Calcein AM (green) and dead cells were labelled with Ethidium Homodimer (red).

CX Cell Line

Due to the issues regarding proliferation of the CB660 culture, an alternative source of stem cells was sought. CX cells were obtained from Merck Millipore due to supervisory experience of working with the clinical grade of cells, CTX. Cells were cultured as detailed in Section 2.4.4. The initial cells that were received were found to be non-viable upon thawing, however a subsequent batch was viable. Batches were cryopreserved to form a stock of viable cells.

Four 500μl hydrogels were synthesised in a 24WP. Cells were seeded at 5x10^5 cells/ml and cultured for 3 days. Initial results of live/dead showed no cells in the hydrogel, and it was apparent that the cells were not attaching to the hydrogel, being washed

away during media changes. To remedy this, the hydrogels were re-sterilised and soaked over night with 100μl laminin at 10μg/ml each, washed once with PBS, and soaked overnight with ReNCell media. This allowed the cells to attach to the hydrogel, however no migration into the hydrogel was observed. Finally, laminin was incorporated into the hydrogel at synthesis by mixing it with the collagen solution, for a final concentration 100ng/ml (w/v) in the hydrogel, as described by Lee et al. (2011). Cells wee seeded at 5x10^5 cells/ml and cultured for 3 days.

Figure 40 shows the CX cells at day 3. The image indicates that the cells migrated into the laminin hydrogel, however the cells did not produce any dendritic projections. The small rounded projections that were visible appear to be blebs, as can be seen in more detail the inset image, indicating that the cells were possibly undergoing apoptosis.

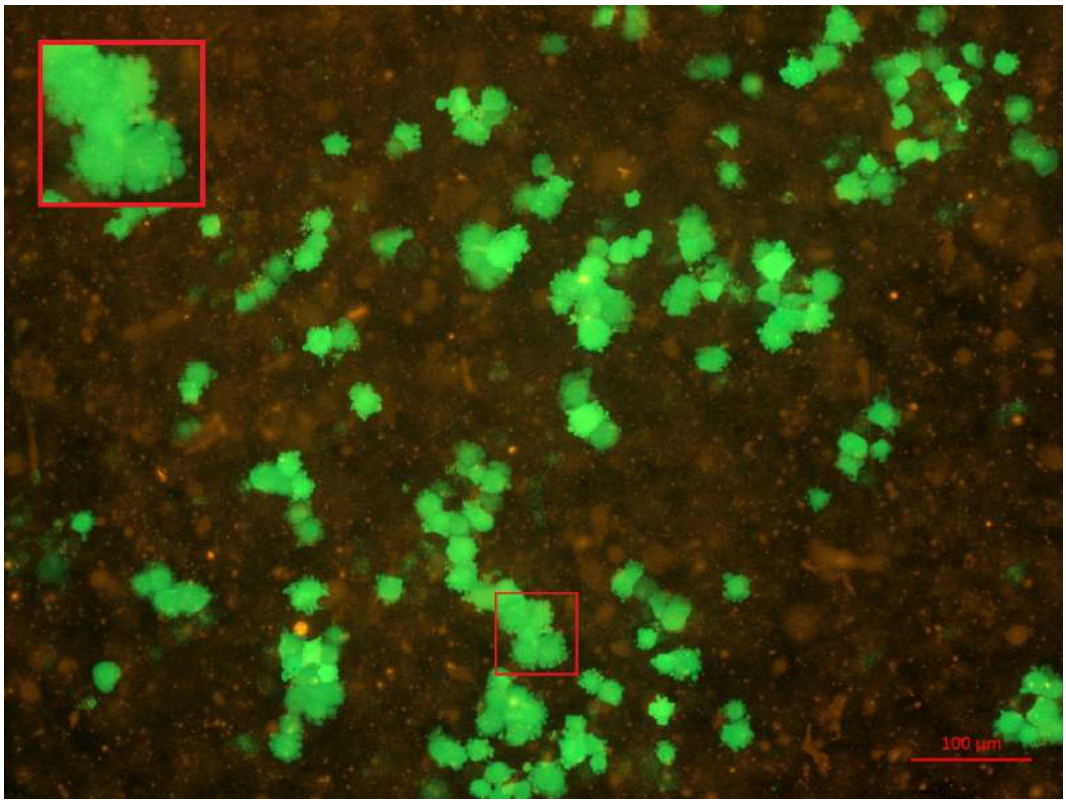

Figure 40: Cell viability of CX cells seeded in the Ph hydrogel at day 3. Live cells were labelled with Calcein AM (green) and dead cells were labelled with Ethidium Homodimer (red). Inset image shows sample of image taken from where the red square indicates, digitally magnified 400%, highlighting the formation of blebs on the surface of the cells.

The NIBSC reported the CB660 proliferation problem could be solved by using NeuroCult-XF Basal Medium and culturing at 5% CO_2 rather than 7%. However, growing the cells in this medium did not produce the improved proliferation reported by the NIBSC. Finally, the depositors of the stem cells were contacted, and it became apparent that the cells experienced senescence at passage 35; while the cell batches had been consistently supplied for this project at passage 33. Two months later, using a batch supplied at passage 28 and with NeuroCult medium slow but continued proliferation was observed, allowing the cells to reach the numbers required for further study.

The CB660 cells were chosen for the future studies because the processes that were observed to extend into the hydrogel indicated that these cells had better viability in the hydrogels than the CX cells. However, the 12 months of development work that this conclusion required meant that the resources of the project were depleted.

3.5.2 Development of a 3D CyQuant Assay

The CyQuant assay protocol was supplied by the manufacturers for use in 2D cell cultures. It has been shown to have a dynamic range of up to $2x10^4$ cells in a 384 well plate (Invitrogen, 2009). The protocol instructions require fluorescence measurements to be taken from the bottom of the plate. For use in 3D, as the cells were seeded on top of the hydrogel, the measurement was taken from above. An experiment was performed to measure efficacy of the standard protocol on cells seeded onto hydrogels. 100μl hydrogels were synthesised in a 96WP and CB660 and CX cells were seeded at $1x10^4$, $2x10^4$ and $5x10^4$ cells/ml. A positive control of cells without a hydrogel (cell only) were seeded into laminin coated wells. Each experiment had four repeats, and the CyQuant assay was performed at day 1.

The readings from the plate reader for this original protocol are presented in Figure 41. The null hypothesis that there was no difference in Cyquant readings between seeding densities was evaluated using the Kruskal-Wallis test. The test was used to compare the fluorescence readings between the seeding densities, with the null hypothesis that the medians are equal. The p-values calculated by this method are presented in Table 41 in Appendix 1, Section 7.1 and indicated that there was no

significant difference in fluorescence readings.

As there was no significant difference, the stain was removed and 100μl of PBS was added to each well. The wells were shaken at 150rpm for 10 minutes, and then the PBS was removed and replaced with the same volume. The plate was then read again, and the readings are presented in Figure 41. Statistical analysis was performed using either an ANOVA or Kruskal-Wallis test and is presented again in Table 41 , finding that fluorescence readings for both cell types were statistically different. For the CB660 Rinse results, the Tukey post hoc test indicated that $5x10^4$ was highly significantly different from both $1x10^4$ and $2x10^4$ ($p<0.01$). For the CX Rinse results, the Dunn post hoc test gave $1x10^4$ was highly significantly different from $5x10^4$ ($p<0.01$). These post hoc tests are summarised in Table 42, Section 7.1.

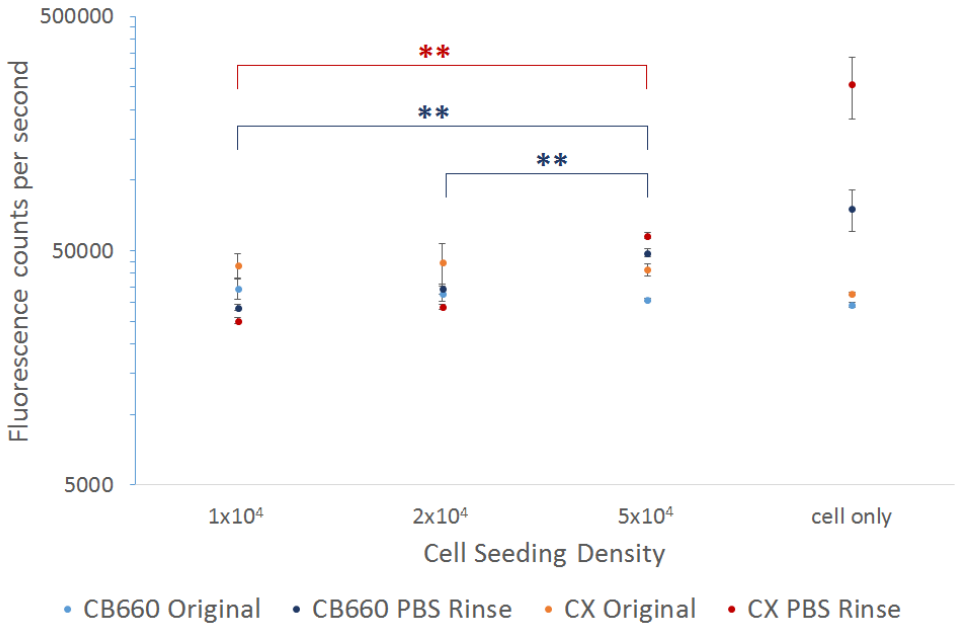

*Figure 41: Cell viability of CB660 and CX cells at Day 1 measured using the CyQuant Assay. Wells were measured following the standard CyQuant protocol where the measurement is taken with the stain left in the wells (labelled "Original") and with the stain removed and PBS applied. Error bars represent standard error, n=4. ** indicates highly significantly different medians ($p<0.01$).*

The method involving rinsing the hydrogels with PBS produced significantly different fluorescence readings for many of the samples and so this method was adopted for future use.

3.5.3 Comparison of Stem Cell Viability Seeded within the Hydrogel

An experiment was performed to directly compare the viability of the two cell types, CB660 and CX in the same batch of Ph hydrogel. 100 μl hydrogels were synthesised as described in 2.3.3, however laminin was added at 100ng/ml (w/v) final concentration to half of the hydrogels. Cells were seeded at 1x10^5, 2x10^5 and 5x10^5 cells/ml, and cultured for 5 days, with the media changed every other day.

Controls were also set up as follows: 2x10^5 cells/ml were cultured without the hydrogel in laminin coated wells for a positive control, and 2x10^5 cells/ml seeded on hydrogels were cultured with the addition of DMSO at day 1 for a negative control. This experiment set up is outlined in Table 28. Each set up had 4 repeats and the assays were performed on days 1, 3, and 5.

Table 28: Experimental set up to compare stem cell viability in the Ph hydrogel.

Name	Description
1x10^5	1x10^5 cells/ml seeded on 100μl hydrogel
2x10^5	2x10^5 cells/ml seeded on 100μl hydrogel
5x10^5	5x10^5 cells/ml seeded on 100μl hydrogel
Cell Only	2x10^5 cells/ml seeded on laminin coated well
DMSO	2x10^5 cells/ml seeded on 100μl hydrogel, cultured with DMSO

The full results are presented in Figures 42, 43, 44 and 45 for ATPlite and CyQuant assays of the CB660 and CX cells. The readings of the two cell types at day 5 are presented in Figure 46 and were compared using a Kolmogorov-Smirnov or t-test test, the results are presented in 41 in Appendix 1, Section 7.1. Significance testing indicated that the ATP luminescence counts of the CB660 cells was significantly ($p<0.05$) or highly significantly ($p<0.01$) higher, while the CyQuant fluorescence counts were not significantly different. Again, the cells cultured with DMSO were expected to act as a negative control, however showed high readings in both the ATPlite and CyQuant assays. This indicates that the DMSO was not able to permeate the hydrogels effectively, was unable to lyse the cells, or potentially directly interfered with the assay luminesnce or fluroescence readings.

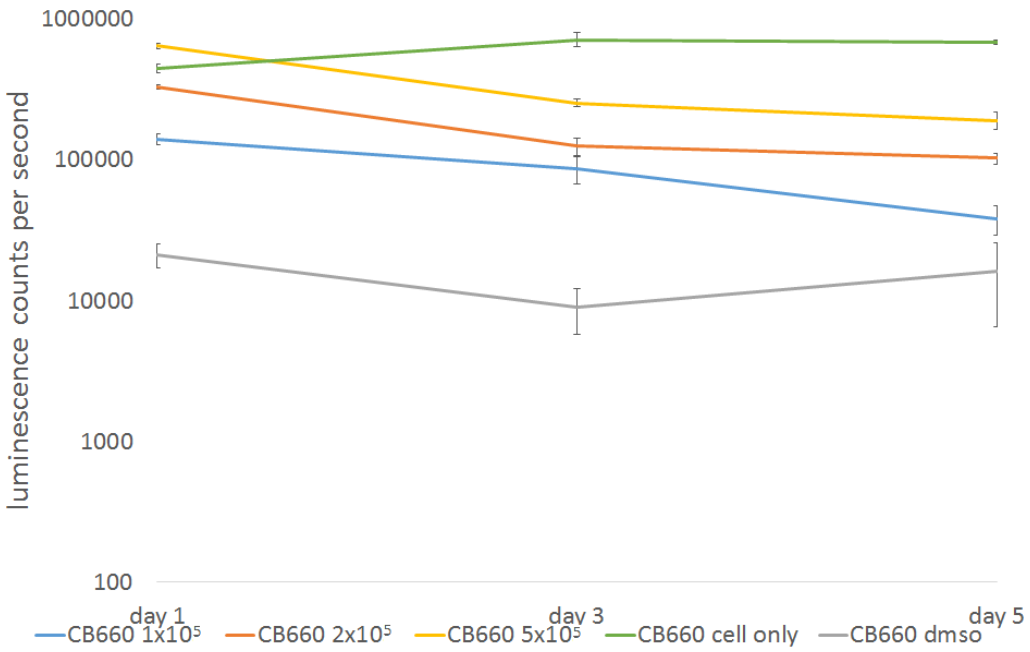

Figure 42: Cell viability of CB660 cells seeded onto hydrogels measured by ATPlite assay. Error bars represent standard error, n=4.

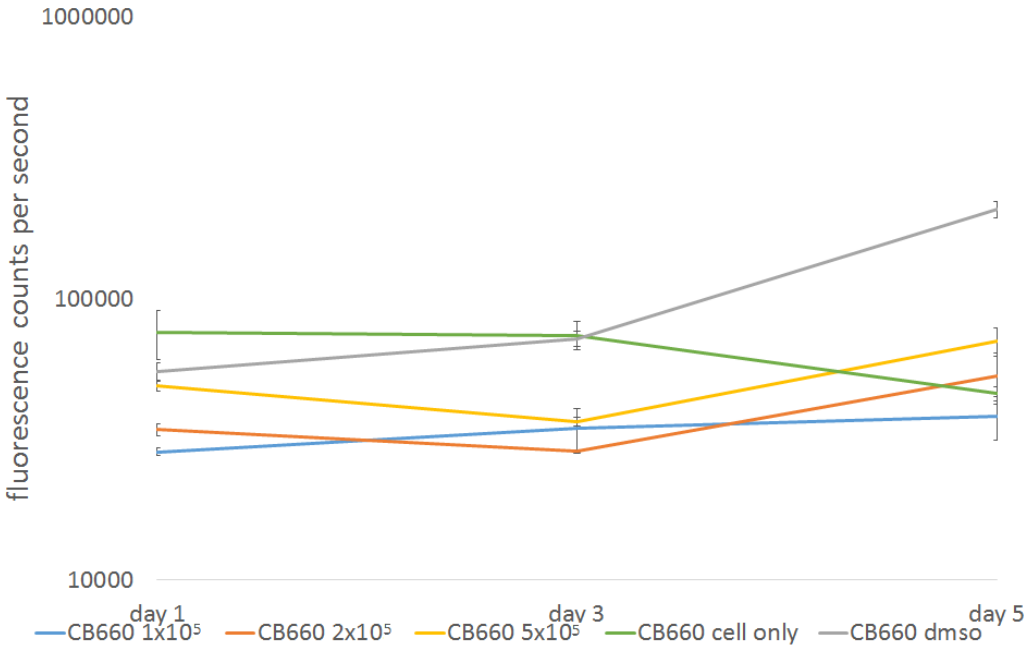

Figure 43: Cell viability of CB660 cells seeded onto hydrogels measured by CyQuant assay. Error bars represent standard error, n=4.

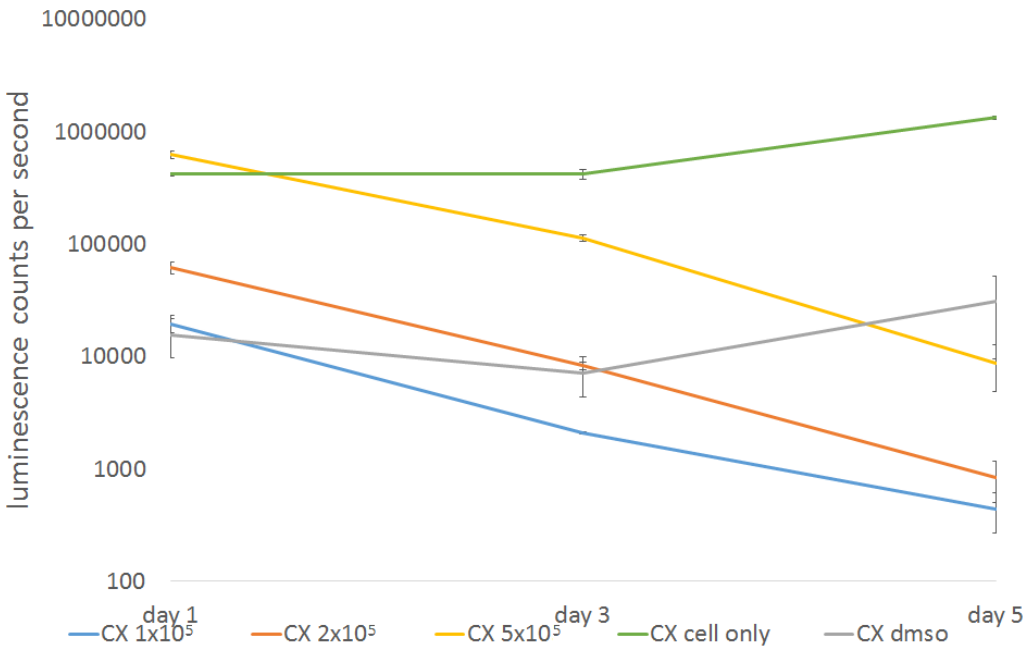

Figure 44: Cell viability of CX cells seeded onto hydrogels measured by ATPlite assay. Error bars represent standard error, n=4.

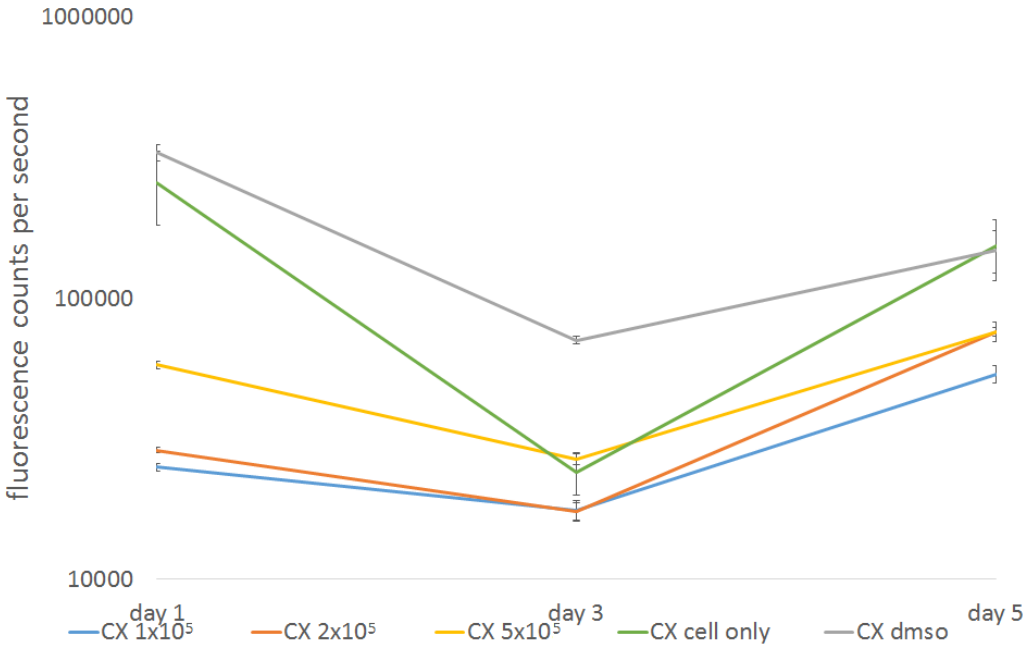

Figure 45: Cell viability of CX cells seeded onto hydrogels measured by CyQuant assay. Error bars represent standard error, n=4.

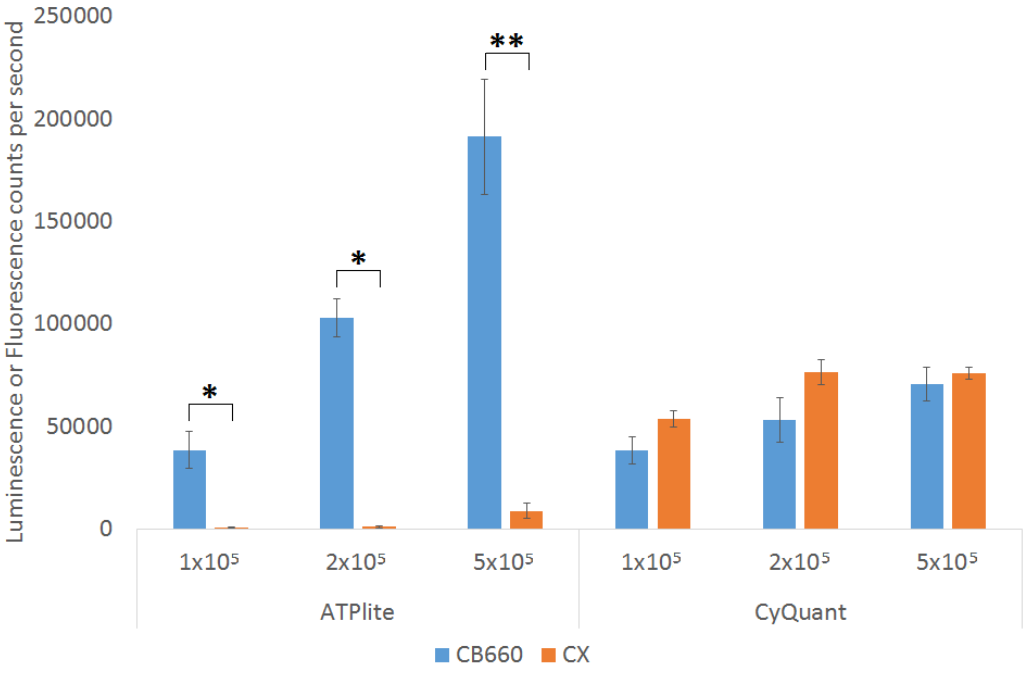

*Figure 46: Cell viability at day 5 of CB660 and CX cells seeded onto hydrogels measured by ATPlite CyQuant assay. Error bars represent standard error, n=4. * indicates a significant difference in medians ($p<0.05$) between cell types and ** indicates a highly significant difference in medians ($p<0.01$).*

CB660 cell readings were significantly higher when measured by ATPlite, while no other significant differences were calculated. Considering this result and the live/dead images that were taken of the cells seeded in hydrogels presented in Section 3.5.1 with this study, the CB660 cell line was chosen to be used in further experiments.

3.5.4 Seeding Density Study

Although the CB660 proliferation issue had been resolved, the rate of proliferation of these cells remained slow. Due to a shortage of time and resources, an experiment was performed to assess the viability of the cells and the resolution of the cell viability assays when the cells were seeded at low numbers.

100μl hydrogels were synthesised in 96WPs, and cells were seeded at densities of 5x10^3 cells/ml, 1x10^4 cells/ml and 5x10^4 cells/ml. Cells were also seeded at a density of 1x10^4 cells/ml into wells without a hydrogel, which had been coated with laminin

24 hours previously. The media was changed on days 1, 3, 5 and 7, before the assays were performed. A CyQuant assay was performed on one set of cells, and an ATPlite assay was performed on a separate set of cells. Each set up had 4 repeats and the time points were day 1, 3 and 7. The luminescence and fluorescence readings are presented in Figure 47.

The results of both the ATPlite and CyQuant assays were compared using a Mann-Whitney U test, presented in Table 41 in Appendix 1, Section 7.1, and indicated that the viability of cells seeded onto hydrogels as measured by the ATPlite assay significantly reduced after day 3 at all of the low seeding densities tested. The ATPlite assay indicated a reduced viability in the cell only experiment, however the CyQuant assay indicated an increase in viability.

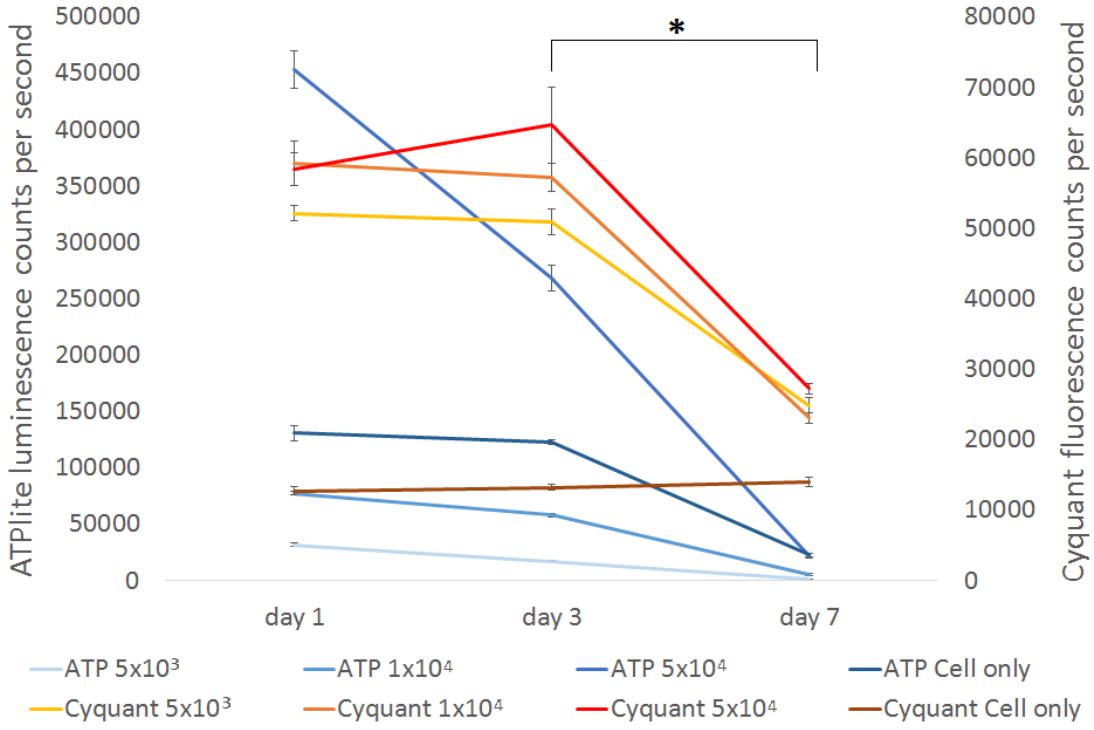

*Figure 47: Viability of cells seeded at low densities on hydrogels, except "cell only" which represents cell numbers for cells seeded onto laminin-coated wells. Error bars represent standard error, n=4. * signifies a significant difference in medians ($p<0.05$) between day 3 and 7 for samples seeded onto hydrogels.*

The viability of cells was compared between day 3 to day 7 using a Mann-Whitney U test. The cell viability was found to significantly decrease for all three cell densities seeded onto hydrogels for both CyQuant and ATPlite assays ($p<0.05$). These results

indicated that either the low seeding densities were not suitable for supporting a cell culture over 7 days, or that the cells had stopped proliferating. As the difference in readings between day 3 and 7 was significant in all cases, a seeding density of $1x10^5$ was used in future studies of significant length in time, as this seeding density whe comparing the two stem cell lines had not caused a significant drop in ATPlite readings.

3.5.5 Optimisation of Successive Cell Viability Assays

As the CyQuant Direct assay does not lyse cells, there is an opportunity to use the ATPlite assay successively, on the same cells. An experiment was performed to determine the effect of using the CyQuant assay on the ATPlite assay.

100μl hydrogels were synthesised in 96WPs and seeded with $2x10^4$ cells/ml. CB660 cells were seeded, and half were subjected to a CyQuant assay just before the time point while half were not. Each set up was also seeded into wells without hydrogels, coated with laminin 24 hours before. The test set up is summarised in Table 29.

Table 29: Experimental set up to assess the effects of the CyQuant assay on the ATPlite assay.

Seeded into	Pre-treatment	Name
Hydrogel	CyQuant	CB660 gel CyQuant
	None	CB660 gel no CyQuant
Well	CyQuant	CB660 Cell Only CyQuant
	None	CB660 Cell Only no CyQuant
Hydrogel	CyQuant	CX gel CyQuant
	None	CX gel no CyQuant
Well	CyQuant	CX Cell Only CyQuant
	None	CX Cell Only no CyQuant

Each set up had four repeats, ATPlite was performed on days 1, 3 and 5. The luminescence counts are presented in Figure 48.

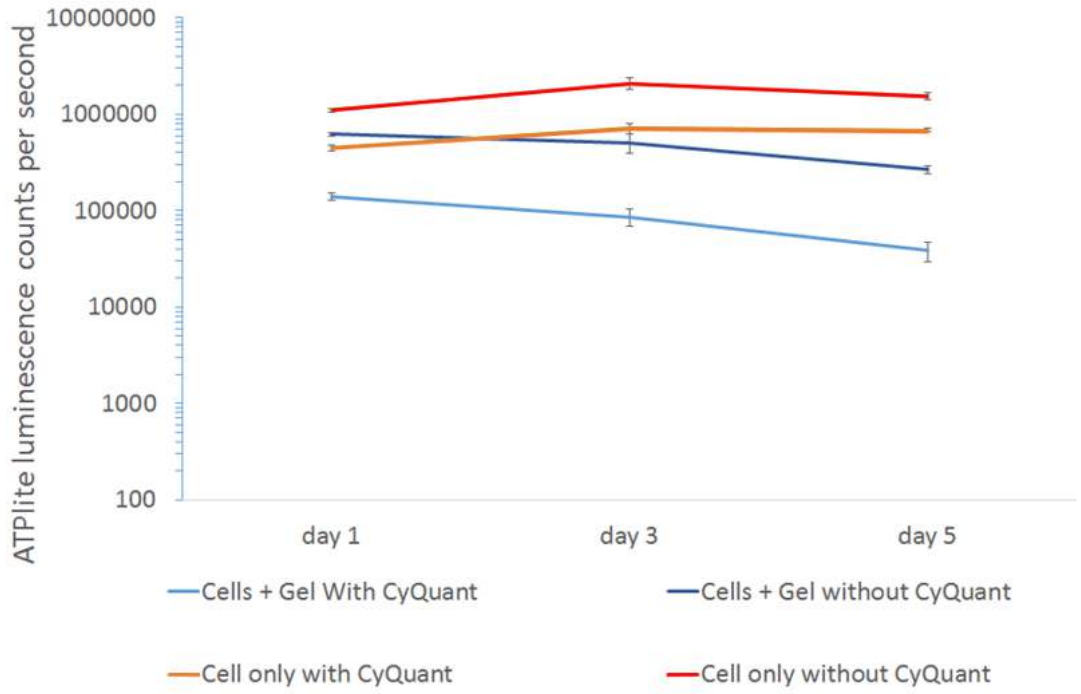

Figure 48: The effect of the CyQuant assay on ATPlite luminescence counts for CB660 cell line, seeded both onto hydrogels and directly into wells without hydrogels. Error bars represent standard error, n=4.

Using the samples with cells seeded onto a hydrogel, the readings for day 1 were averaged, and the percentage change between the day 1 average and all readings for each subsequent time point was calculated. The results are presented in Figure 49. A independent samples two-tailed t-test was used to check for statistical difference between percent change in ATPlite assay readings for cells with and without a preceeding CyQyuant assay, and the results are presented in Table 41 in Appendix 1, Section 7.1.

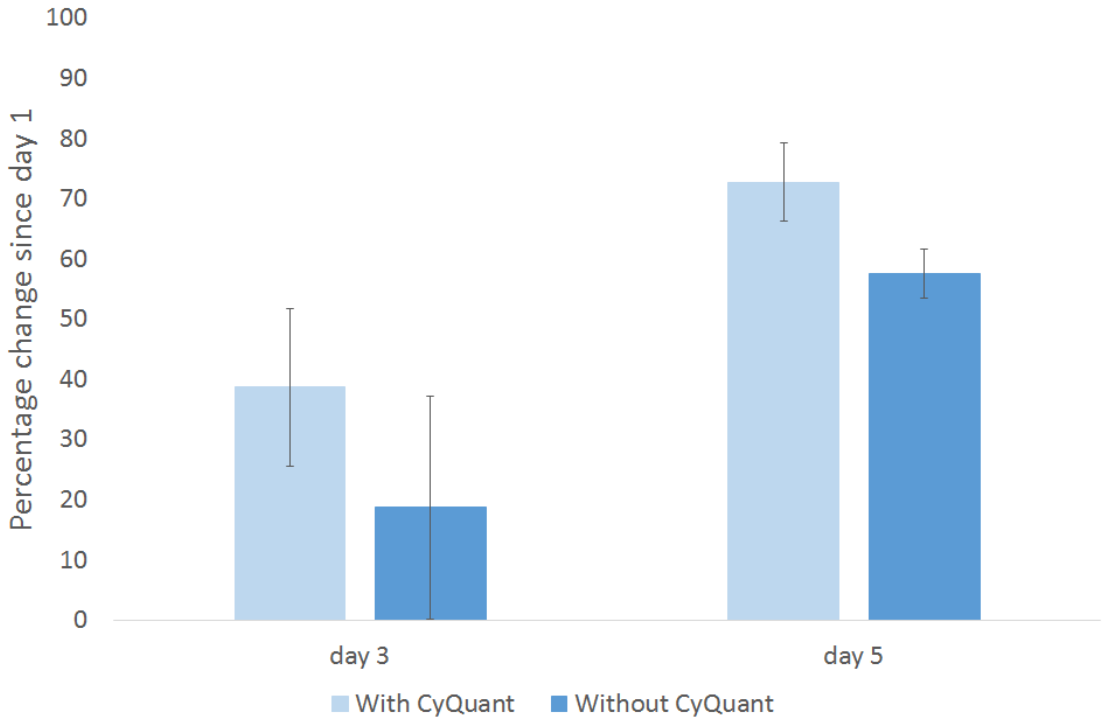

Figure 49: The percent change of ATPlite luminescence counts from an average (n=4) reading at day 1 for CB660 cells seeded onto hydrogels, with and without a preceeding CyQuant assay. Error bars represent standard error, n=4.

The statistical tests indicated that the difference in percentage change between the two methods was not significantly different on either day. This informed the decision to perform successive CyQuant and ATPlite assays on the same set of cells, allowing cell populations to be exploited further.

3.6 Discussion

The aim of this chapter was to develop a 3D system suitable for the culture of neural stem cells and to optimise methods for cellular investigations.

3.6.1 Hydrogel Selection

Hydrogels were identified as a useful tool to create a biomimetic 3D environment for *in vitro* cell studies (Wen et al., 2012). Two available hydrogel systems were identified as appropriate environments for cells and were evaluated by their synthesis time, ease of synthesis, transparency, cell viability and shear elastic modulus. The chemically crosslinked Ph hydrogel described by Tronci et al. (2013b) was identified as having properties closest to the initial design specification. This was because it had an elastic modulus at 1Hz closer to that of natural CNS than the other hydrogels (Brands et al., 1999; Shen et al., 2006; Hrapko et al., 2006) and a quicker and simpler synthesis than the UV-crosslinked hydrogels. The hydrogels were found to be simple to sterilise; soaking in ethanol followed by washing with PBS was deemed successful as no contamination was detected through visual assessment. As no discernible variability was measured in the transparency of repeated hydrogel samples, this suggests that the visualisation method used to assess the hydrogels may have lacked sensitivity. A more sensitive, quantitative method may have been more appropriate for this assessment, for example using a spectrophotometer. However, as the importance of transparency was ranked comparatively low in the decision matrix, the visualisation method was deemed sufficient in this case. This hydrogel system was taken forward for future studies, including use with neural stem cell lines.

3.6.2 Optimisation of Methods for Cellular Investigations

The CB660 stem cell line was acquired and showed great promise in terms of viability when seeded within the Ph hydrogel as projections were expressed by day 5, as seen by live/dead staining, however ongoing cell culture issues meant that another cell source was sought. The CX cell line was acquired and displayed improved viability in

2D culture compared to the CB660 line, and the addition of laminin to the hydrogel synthesis allowed cell adhesion. However as observed by use of live/dead staining, the cells were rounded with what appeared to be blebs on the outer surfaces, and no projections.The proliferation issue with the CB660 cell line was eventually rectified by the NIBSC 12 months after the original batch was cultured. A secondary outcome of these development studies was that the cells were observed to migrate into the hydrogel without further intervention.

The CyQuant assay was optimised for use with cells seeded onto hydrogels by rinsing the hydrogels with PBS before measuring the fluorescence. The two cell lines were compared using CyQuant and ATPlite assays. The CyQuant assay indicated that the viability of the two cell lines was not significantly different at day 5, while the ATPlite assay found at significantly improved viability at day 5 ($p<0.05$) of the CB660 cells when seeded at $1x10^5$ and $2x10^5$ cells/ml and high significance ($p<0.01$) at $5x10^5$ cells/ml. This information, combined with the earlier live/dead images informed the choice to use the CB660 cells in further studies.

Although the CB660 proliferation problem was rectified, the cells remained extremely slow growing and so a low seeding study was performed to investigate the affect on the cells. Viability at low cell seeding densities was assessed with ATPlite and CyQuant assays, finding that cell numbers significantly decreased ($p<0.05$) from days 3 to 7 and so a seeding density of $1x10^5$ was chosen for further studies.

Finally, an assay was developed that used the CyQuant and ATPlite assays successively on the same cell samples, exploiting the non-lysing feature of the CyQuant assay. The ATPlite assay appeared to be more sensitive than the CyQuant assay, and was already developed for use with hydrogels, however the production of ATP was noted to be increased while cells were stressed. The CyQuant assay provided a means to measure the DNA content within the hydrogel and so infer the number of cells, irrespective of their metabolism. Previous use of CyQuant to measure proliferation of cells in 3D has included the use of Proteinase K to digest the hydrogel prior to use of the assay (Bott et al., 2010). The use of the assays in succession was validated by comparing the results of ATPlite readings of cells that had been "pretreated" with the CyQuant assay with those that had not. No difference was detected at day 3 or 5 between the two variables and so the successive assay method

was deemed appropriate for use for further studies due to its advantages in requiring half the cell numbers compared to performing both assays on separate populations.

The differences between the two assays may be due to their respective sensitivity, or as a product of their use in 3D. The seeding density of $1x10^5$ was chosen due to the significant decrease in ATPlite and CyQuant readings during a 7 day culture. While the decrease may have been due to the fact that the cells had stopped proliferating and begun to differentiate, the change was not observed during previous cultures at higher seeding densities. Additionally, as the DMSO control did not create a negative control for the CyQuant assay, a different method was required for future viability assays.

3.6.3 Conclusion

The chemically crosslinked hydrogel was selected for further studies, as the elastic modulus was found to be closest to the target biomimetic range that was identified by comparing research by Hrapko et al. (2006), Brands et al. (1999), and Shen et al. (2006), and was with a comparable range to the studies of neural differentiation conducted by Bozza et al. (2014) (10-60Pa) and the hydrogel with the lowest modulus (183Pa) synthesised by Banerjee et al. (2009); while the reduced synthesis time was also advantageous. Cells were found to be viable in the hydrogels, although this assessment was limited by the use of the C6 cell line rather than stem cells, however this was to conserve the expense of the materials. Upon seeding of the stem cells it became apparent that while the CB660 cells were viable in the hydrogels, even with the addition of laminin to the hydrogel the CX cells maintained a rounded shape with bleb formation on the outer surfaces, indicating that the hydrogels were incompatible for these cells. This was unfortunate as the CX cells had improved culture capabilities. With extra resources of time and materials, it may have been more appropriate to revisit the GMA UV crosslinked hydrogels and examine whether these hydrogels produced improved viability for the CX cells.

4 Investigation into the Effects of Matrix Elastic Modulus on Neural Stem Cell Differentiation

4.1 Introduction

Since the discovery of the mechanosensitivity of stem cells (Engler et al., 2006) there has been further research conducted into different stem cells types for more specialised applications. Of the tests carried out on stem cells directed towards a neural lineage, only three studies have been performed in three dimensions (3D) (Banerjee et al., 2009; Her et al., 2013; Bozza et al., 2014). These studies used neural, mesenchymal or embryonic stem cells and alginate or collagen hydrogels, however the alterations made to the elastic modulus of the hydrogel were made by changing the concentration of hydrogel components. As (Her et al., 2013) identified, this alteration affected the size of the pores and furthermore, the elastic moduli of the hydrogels that were synthesised were not within the biomimetic range for that of natural central nervous system (CNS) tissue. It is essential for research of this nature to be performed in 3D as cells interact with the mechanical properties of their surroundings by attaching themselves to the material, contracting themselves and putting tensile stress on the material (Mohammadi et al., 2015), and then discerning the response of the material. In two dimensions (2D), with the cells seeded on top of the material in question, the contractile forces applied are different than they would be in a 3D environment, and indeed the response to these materials has been found to differ when the cells are cultured in 2D and 3D (Kothapalli and Kamm, 2013).

In the studies into the hydrogel systems for neural differentiation (Banerjee et al., 2009; Her et al., 2013; Bozza et al., 2014), the concentration of reagents within the hydrogels was altered in order to change their elastic modulus. Changing the modulus in this way also changes the microarchitecture of the hydrogels, most notably the pore size which decreases when the hydrogel is altered to increase the elastic modulus (Her et al., 2013). This is problematic as it is known that stem cells can also be manipulated based on the microarchitecture of their surroundings (Solanki et al., 2010) and so it means that the responses observed in these studies were not necessarily in response to the change in modulus, but could in fact be a response to

an increase in binding sites available to the cell, due to the smaller pores. If it is possible to change only the elastic modulus and no other major physical or chemical properties, the effect of the change in modulus may be studied independently of other factors. This is important as many studies currently compare the elastic modulus of the material to the cellular response, however if it is not this that they are responding to, then the interpretation of these studies are incorrect. The hypothesis of the present study was that the activities of neural stem cells are affected by the elastic modulus of their 3D environment, altered within the biomimetic range of CNS tissue, and independently of pore size. The null hypothesis was that stem cells are not affected by the elastic modulus.

In this chapter, a method for altering the modulus of a hydrogel independently of pore size was proposed, and a feasibility study was conducted. Variants of the hydrogel were synthesised and characterised mechanically using rheometry. The structure and pore size of the hydrogels were analysed using scanning electron microscopy (SEM), the degree of functionalisation of each hydrogel was determined using a trinitrobenzenesulfonic acid (TNBS) assay and the porosity of each hydrogel was analysed using nuclear magnetic resonance (NMR). The hydrogel variants were then seeded with stem cells and the reagents in the media were changed to promote differentiation and to maintain pluripotency. Using immunostaining, the phenotypes of the cells were compared between the two hydrogel types.

4.1.1 Assessment of Opportunities for Hydrogel Modification

The literature on the effect of hydrogel stiffness on neural differentiation reported that modifications to elastic modulus were made by changing the ratio of their constituents, which has been found to have significant implications on the microarchitecture and surface area of the hydrogel in the report that studied these physical characteristics of the hydrogel (Her et al., 2013). Changes in microarchitecture have also been shown to also affect stem cell behaviour such as proliferation and differentiation paths (McBeath et al., 2004; Christopherson et al., 2009) and so cannot be discounted.

The basic synthesis of the collagen hydrogel was examined to identify opportunities

for modification of the elastic modulus. Four opportunities were identified:

1. Collagen type

   The structure of collagen varies between different locations in the body, with different protein sequences and structures. These changes to the molecular make up of the collagen could potentially alter the tensile properties of the collagen. Indeed, Wenger et al. (2007) found a variation of 7.8GPa in the Young's modulus between type I collagen fibril samples using nanoindentation, although experimental error could have also been a factor. As the collagen makes up a significant proportion of a hydrogels constituents (after water), use of another collagen could produce significant effects on the mechanical properties. The drawback of changing collagen types is that the available ligands for cell attachment could vary widely between different collagen types, and therefore could affect the cellular response significantly.

2. Collagen concentration

   Collagen concentration in the hydrogel can also affect the mechanical properties as the collagen provides the bulk of the stiffness, and this is currently the most commonly used method for studies involving cell response to stiffness, as it can increase stiffness 100-fold (Banerjee et al., 2009). Unfortunately, increasing the collagen concentration increases the density of the material which decreases porosity. A more dense material will also mean a decrease in fibril spacing which will decrease pore size. These factors change the microenvironment of the cells, while an increase in density will also increase binding sites for the cells. All of these differences may cause the cells to change their habits and responses, all independently of stiffness change.

3. Crosslinker type

   Similar to different collagen types, different crosslinkers that are used to crosslink the collagen may have various molecular weights and structures, leading to potentially varied mechanical properties. When used to crosslink collagen molecules, the properties of these crosslinker links affect the properties of the whole structure. As cells adhere to ligands on the collagen and not the crosslinker, from a biological point of view, changing the crosslinker type could have negligible side effects on cell-material interactions, provided that

the chemical effects were suitably similar. The concentration of crosslinker used compared to that of collagen is typically extremely small, and so it could be that changing this might have only a negligible effect on the hydrogel's properties.

4. Crosslinking Conditions

   Using lower concentrations of crosslinker or allowing less time for the crosslinking reaction would result in fewer crosslinks and hence would lower the modulus (Her et al., 2013), similar to the effects of changing functionalisation. Again, changing this parameter could affect the microarchitecture of the hydrogel, having adverse consequences for the cells. Additionally, the diacids used to crosslink the collagen are highly reactive and so any unreacted crosslinker may produce a toxic effect in cells.

Of these options for modification, it is apparent that changing collagen type could have significant consequences for cell adhesion; while changing collagen concentration or degree of crosslinking could affect pore size or porosity significantly. It is appealing to explore the effect that changing the crosslinker type may have on the physical properties of the hydrogel. While it could have little to no effect due to the small proportion of crosslinker contained within the hydrogels, if it does have an effect, these hydrogel systems could be used to explore the effect of stiffness alone. If similar crosslinkers have different structures, crosslinking the collagen with these crosslinkers could produce hydrogels of different stiffness, without substantially affecting the porosity, pore size or the availability of ligands for cell attachment.

A chemically crosslinked hydrogel had the potential to be created using variations of crosslinker type as the specification for the crosslinker was only that it was a diacid (or dicarboxylic acid), i.e. contained two carboxyl (CO_2H) functional groups. The diacid group has many variants, including two amino acids of the human body (aspartic and glutamic acid). The initial crosslinker used was 1,3-phenylenediacetic acid (Ph) which is an aromatic molecule containing a benzene ring.

4.1.2 Aims and Objectives

The aims of this chapter were to investigate both the feasibility of changing the elastic modulus of the hydrogel without altering the microarchitecture and investigate the effect that this change had on neural stem cell differentiation. An overview of the tasks and the specific objectives they relate to is detailed in Figure 50.

Specific Objectives

1. **To develop a method for modifying hydrogel elastic modulus**
   To evaluate the feasibility of changing the elastic modulus by changing the crosslinker type. Using rheology and the TNBS assay, the elastic modulus of the hydrogels and their degree of crosslinking was determined. To assess the repeatability of this experiment, the study was repeated.

2. **To develop image analysis methods**
   To adapt established, validated methods within ImageJ software for measuring pore size from SEM images of the hydrogels, and for counting cell numbers.

3. **To investigate the effect of the change in elastic modulus of the hydrogel variants on stem cell activities**
   To determine the mechanical and physical properties of the hydrogels by characterisation using rheology, SEM, NMR and TNBS and to investigate the effect of the hydrogels on the differentiation of stem cells using immunostaining and confocal microscopy to determine the phenotypic cellular responses.

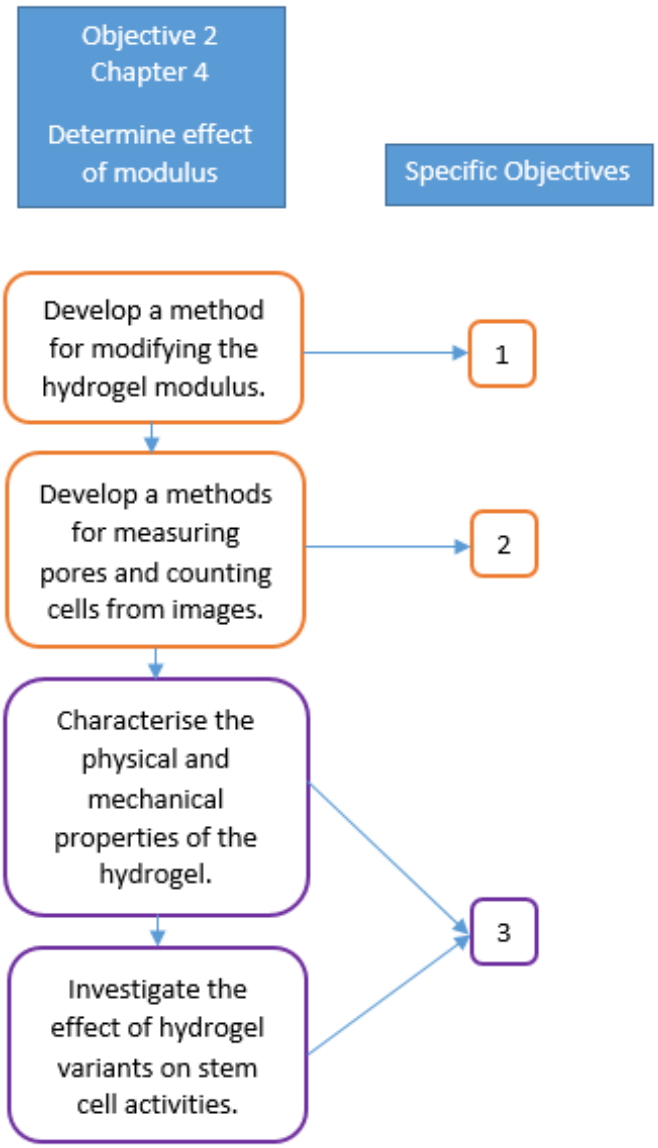

Figure 50: Overview of the tasks of chapter 3 and the specific objectives these relate to.

4.2 Methods

For the initial development of the hydrogels, mechanical and physical characterisation was performed using rheometry and the TNBS assay. Later, when the effects of the hydrogels on neural stem cells were studied, further physical characterisation methods were used. Descriptions of the amount of hydrogel and container used are presented in Table 30. The volumes varied depending on the size of the hydrogel required, which was decided upon based on the amount of manipulation required, or the application.

Table 30: Hydrogel samples created for studying stem cell response to elastic modulus.

Analysis	Volume of Hydrogel	Container
Rheology	500μl	24WP
SEM	200μl	48WP
NMR	2ml	glass vial
TNBS	500μl	24WP
Water Content	500μl	24WP
Immunostaining	200μl	chamber slides

4.2.1 Hydrogel Preparation

The collagen for the hydrogels was harvested from rat tails as described in Section 2.3.1. The hydrogels were synthesised as described in Section 2.3.3. To alter the hydrogels, different crosslinker types were used. To explore whether other crosslinker types were suitable to crosslink the collagen fibrils, three other aliphatic dicarboxylic acids were investigated, detailed in Table 31 with their chemical formulae. To modify the hydrogels, the Ph crosslinker was replaced, keeping the number of moles of the crosslinker consistent with the number of free lysine groups in the collagen, as shown in Equation 21, where $W_{crosslinker}$ is the required mass of the crosslinker, $Mols_{lys}$ is the number of free lysine groups in the collagen and $M_{crosslinker}$ is the molar mass of the crosslinker.

$$W_{crosslinker} = Mols_{lys} \times M_{crosslinker} \tag{21}$$

Table 31: Monomer variations attempted and their chemical formula.

Name	Crosslinker	Formula	Molar Mass (kg/mol)
Ph	Phenylenediacetic Acid	$C_6H_4(CH_2CO_2H)_2$	194.18
Su	Suberic Acid	$HO_2C(CH_2)_6CO_2H$	174.19
Ad	Adipic Acid	$HO_2C(CH_2)_4CO_2H$	146.14
Ta	Tartaric Acid	$HO_2CCH(OH)CH(OH)CO_2H$	150.09

4.2.2 Mechanical Characterisation

Mechanical characterisation was performed for both the initial feasibility study and the final study that involved the investigation of the stem cell response. Using 500μl hydrogels synthesised in a 24 well plate, rheological analysis was performed using a rheometer, as described in Section 2.6.1. Amplitude sweeps were performed at least between 0.05 and 5% strain, to find the linear viscoelastic region (LVER) for the hydrogels. The frequency sweeps were performed between 0.05-5Hz, at an amplitude chosen using the results of the amplitude sweep to be within the LVER, typically between 0.1-0.4%.

4.2.3 Physical Characterisation

Assessment of Degree of Crosslinking of the Hydrogels

A TNBS assay was performed for both the initial feasibility study and the final study that involved the investigation of the stem cell response. Samples of 1ml volume were created to test for the degree of functionalisation using the TNBS assay described in Section 2.7.4.

Determination of Microarchitecture of the Hydrogels

For the final study, investigation into the microarchitecture of the hydrogels was performed by SEM, as described in Section 2.7.1. Images were taken of the hydrogel at a magnification of 1000x and 100x, and a method for the measurement of pore diameter was developed, as will be described.

Determination of the Water Content of the Hydrogels

For the final study, the porosity of the hydrogels was investigated. Hydrogel samples of 1ml volume were weighed in both wet and dry states to calculate the water content of the hydrogels, as described in Section 2.7.3.

Determination of Pore Volume of the Hydrogels

For the final study, the volume of the pores of the hydrogels was investigated by NMR as described in Section 2.7.2, performed by Carlos Grattoni of the School of Earth and Environment at the University of Leeds. The T2 relaxation values for three hydrogel repeats per type were recorded, indicating the volume of the pores.

4.2.4 Determination of the Cellular Phenotypic Response

Cell Culture

To investigate the response of cells to the hydrogels, CB660 cells were cultured as described in Section 2.4.4.

Cell Seeding

Ph and Ta hydrogel variants (200μl) were synthesised in multiwell chamber slides and were sterilised and washed as described in Section 3.3.1. CB660 cells (*NIBSC*) were seeded onto the hydrogels at a concentration of 1x10^{5}cells/ml, based on the findings presented in Section 3.5.4 which investigated an optimum seeding density for the hydrogels. Cells were seeded at day 0 onto Ph hydrogels for day 1 analysis and negative controls, and Ph and Ta hydrogels for day 10 analysis. Due to low cell numbers, two repeats per hydrogel type and time point were conducted. Media was changed from Neurocult proliferation media to Neurocult differentiation media at day 1, both media types are described in Table 13, Section 2.4.

Determination of Phenotypic Response of Neural Stem Cells to the Hydrogels

To investigate the phenotypic response of cells to the hydrogels, cells were fixed and immunostained as outlined in Section 2.5.4. Cells were fixed at day 1 and day 10 and phenotypic proteins CD133 and PSA-NCAM were targeted in the cells, indicators for neural stem (i.e. remaining as a stem cell) and neuronal progenitors (i.e. differentiating towards a neuron), respectively. The expressions of these proteins were described by Sun et al. (2008) to be early indicators of differentiation (<2 weeks), who found that 66 $\pm$ 5.8% of the cells that were stained positive for PSA-NCAM at week two were positive at week four for βIII-tubulin, a marker for neurons. Additionally, no PSA-NCAM negative cells at week two became positive for βIII-tubulin and approximately 82% of the PSA-NCAM negative cells became positive for GFAP, an astrocytic marker, at week four. The details of the antibodies used in the present study are described in Table 32. DAPI was used to counterstain the nuclei blue.

Table 32: Primary antibodies used to assess the phenotype of the cells, the cell type that the antibody marks labels (as described by Sun et al. (2008)) and the secondary antibody used

Primary Antibody	Marker for	Secondary Antibody
CD133	Neural Stem Cells	Green Alexafluor 594 Goat Anti-Mouse IgG
PSA-NCAM	Neuronal Progenitors	Red Dylight 488 Donkey Anti-Rabbit IgG

Two negative controls were used. Cells were stained with either an isotype primary antibody or no primary antibody and then the secondary antibody was applied as normal. DAPI DNA stain was used as a positive control. Images of the cells were captured using a fluorescent confocal microscope, at a depth half way between the top and bottom of each hydrogel. Hydrogel thickness was measured by recording the Z position of the microscope when the signal from the cells became low. Each experiment had two repeats, and each repeat had three images taken. The x and y positions of the hydrogel were measured using the confocal microscope and images were taken in the centre, left and right areas of the hydrogel. A summary of this experiment set up is detailed in Table 33, and a schematic diagram of the imaging strategy and fields of view is presented in Figure 51.

Table 33: Experimental set up to measure the phenotypic response.

Experiment	Hydrogel Seeding	Fixing date	Staining
Day 1	Ph	Day 1	Normal
Day 10 Ph	Ph	Day 10	Normal
Day 10 Ta	Ta	Day 10	Normal
Isotype	Ph	Day 10	Isotype primary, normal secondary
No Primary	Ph	Day 10	No primary, normal secondary

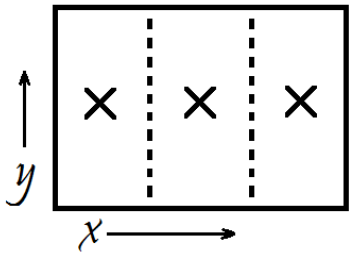

Figure 51: Plan view of imaging strategy with three fields of view for each hydrogel sample. Each image was taken at a depth half way between the top and bottom of the hydrogel, as determined by the Z position of the microscope when the signal from the cells became low. The x and y positioning of the hydrogel was determined and images were taken in the centre, left and right areas of the hydrogel, as shown.

4.2.5 Statistical Analysis

Statistical tests was chosen based on the flow diagram presented in Figure 28 in Section 2.8 and was performed to compare between the two hydrogel types (Ph and Ta). For experiments with only two repeats, the variance of the data was assumed to be equal.

4.3 Results

4.3.1 Development of Method to Alter Hydrogel Elastic Modulus

Degree of Crosslinking

One sample per hydrogel type was analysed using the TNBS assay to assess the degree of crosslinking to preserve materials. The results of the TNBS analysis are shown in Table 34 and show all four hydrogel types to have a similar degree of functionalisation.

Table 34: Degree of functionalisation of each hydrogel with various crosslinkers as determined by TNBS

Crosslinker	Spectrophotometer Reading	Degree of Crosslinking
Phenylenediacetic Acid	0.556	56.7%
Tartaric Acid	0.557	56.6%
Suberic Acid	0.575	55.2%
Adipic Acid	0.505	60.69%

Mechanical Characterisation

Three samples per hydrogel type were synthesised for mechanical characterisation. The amplitude sweep presented in Figure 52 showed a common point of the LVER was 0.1% strain, and the subsequent frequency sweep was performed at this strain. The rheological characterisation of the hydrogels, presented in Figure 53, showed that at 1Hz, the phenylenediacetic acid and suberic acid hydrogels had an elastic modulus of 314Pa (±36.7) and 330Pa (±26.1) respectively, while the modulus of the tartaric acid hydrogel was approximately 218Pa (±19.1), and adipic acid produced a hydrogel of lower stiffness still, at 156Pa(±65.8).

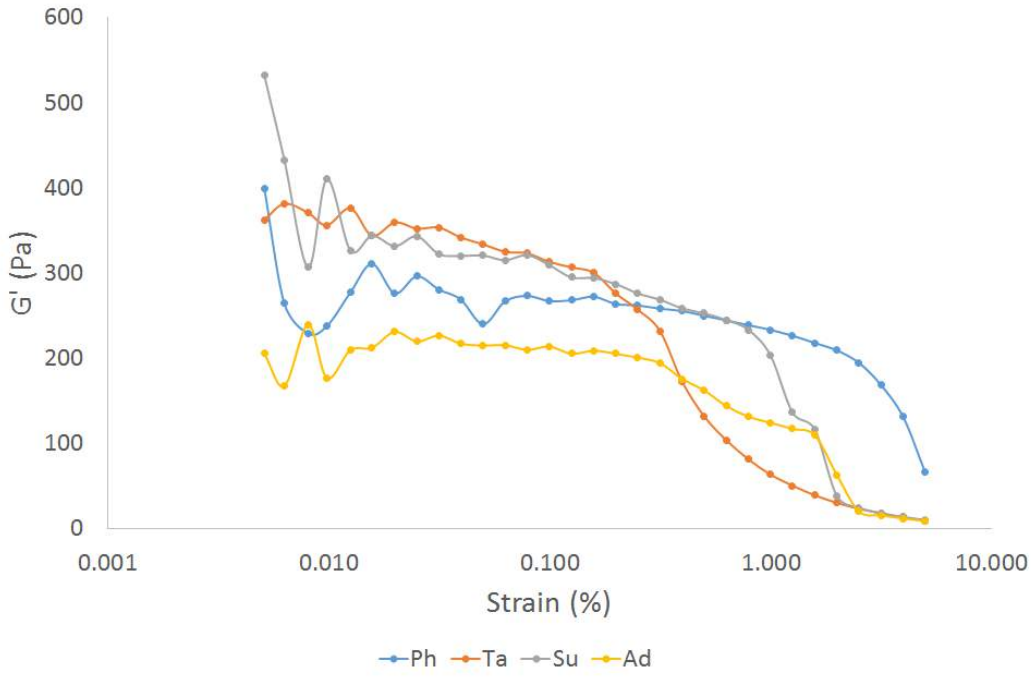

Figure 52: Rheological characterisation of hydrogels to find a common LVER with various crosslinker types; 1,3-Phenylenediacetic acid (Ph) Tartaric acid (Ta), Suberic acid (Su) and Adipic acid (Ad) over an amplitude sweep at 1Hz. n=1

A one-way ANOVA found that while there was a difference in these moduli was not statistically significant, as presented in Table 43, in Appendix 1 7.1. A Tukey post-hoc, presented in Table 44 found that the Ad hydrogel was most different from the Ph and Su hydrogel, but this was also not significant. As the degree of crosslinking of all hydrogels was similar, the results indicated that changing the crosslinker to change the stiffness without affecting the pore size was plausible, and therefore this method was adopted for future studies examining the effect of these hydrogel variants on stem cells.

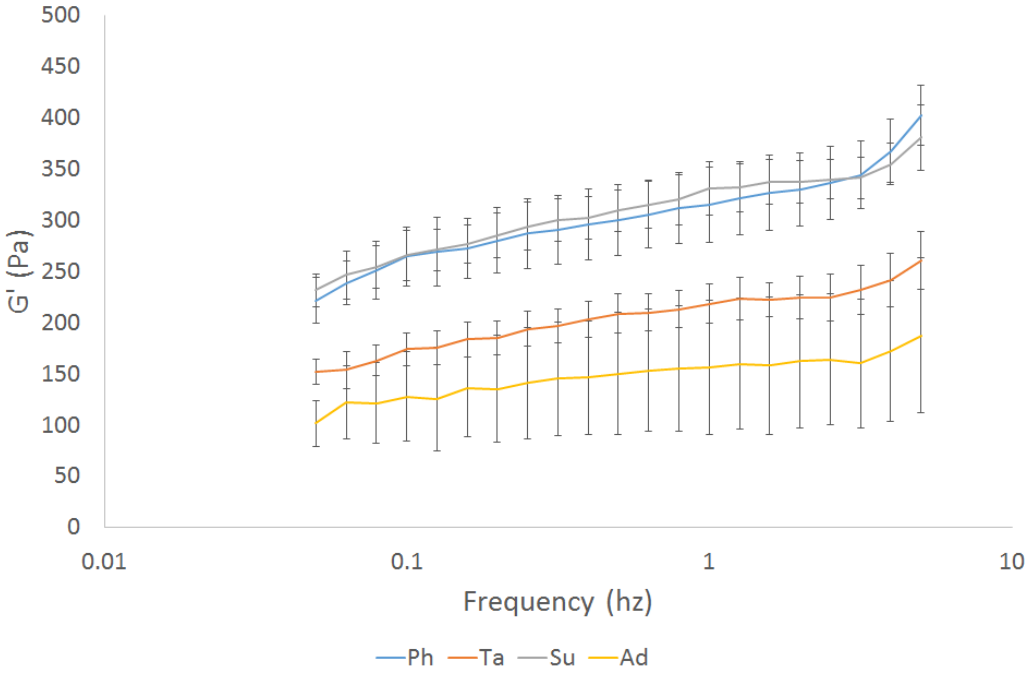

Figure 53: Rheological characterisation of the hydrogels with various crosslinker types; 1,3-Phenylenediacetic acid (Ph) Tartaric acid (Ta), Suberic acid (Su) and Adipic acid (Ad) over a frequency sweep at 0.1% strain. Error bars represent standard error, n=3

To conserve resources, two hydrogels were chosen from the four for future studies. As the phenylenediacetic acid crosslinker was originally used to crosslink the hydrogels, as described by Tronci et al. (2013b), this was preferentially chosen over the suberic acid crosslinker for future work. Although the adipic acid hydrogel showed greater difference than the tartaric acid hydrogel, as presented in Table 44, the tartaric acid hydrogel was chosen for future experiments as the elastic modulus had a lower variation than adipic acid and the degree of crosslinking was found to be more similar to the Ph hydrogel.

4.3.2 Assessment of Batch Variability

After the first feasibility experiment, mechanical characterisation was repeated on further batches of hydrogel to test the repeatability of results. However, it became apparent that the elastic modulus of the hydrogels was not repeatable, as shown in Figure 54.

During the course of these repeats, many variables of the test were examined and controlled:

- The temperature during the reaction of EDC, NHS and the crosslinker was monitored.
- Separate crosslinker solutions were made on the same day (labelled A and B in Figure 54), using the same collagen solution.
- The pH of the sodium phosphate buffer was monitored.
- The pH of the collagen solution was monitored.

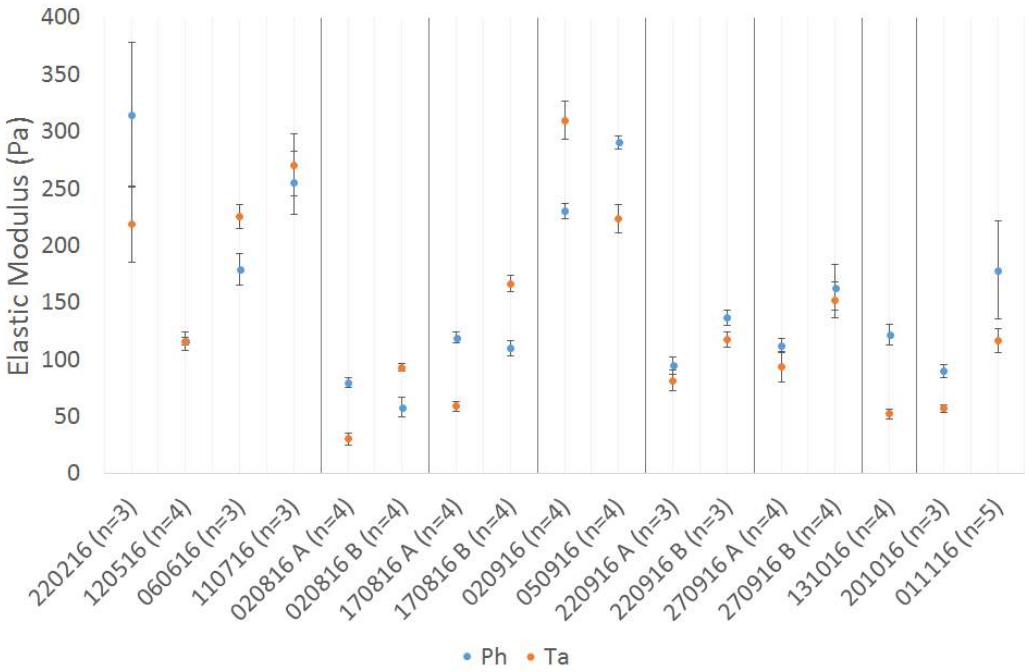

Figure 54: Elastic modulus of 1,3-Phenylenediacetic acid (Ph) and Tartaric acid (Ta) hydrogels at 1Hz, 0.1% strain. The labels show the date of hydrogel synthesis and the number of repeats used for standard error bars, n=3, 4 or 5, as shown in the axis label.

Table 35: Variable controlled for each test. Each controlled group is separated by horizontal lines. P values indicate the statisitcal significance of variation of elastic modulus between each controlled group. Statistical analysis was performed to compare the hydrogel variants separately from eachother and between each controlled group.

Name	Controlled variable	Comparison	p(Ph)	p(Ta)
220216	Original experiment			
120516	None			
060616	None			
110716	None	Between group	<0.01	<0.01
020816	Same collagen solution	A and B	>0.06	<0.01
170816	Same collagen solution	A and B	>0.06	<0.01
020916	Temp during functionalisation			
050916	Temp during functionalisation	Between group	<0.01	<0.05
220916	Same collagen solution	A and B	<0.05	<0.05
270916	Same collagen solution	A and B	<0.06	<0.05
131016	Collagen pH 4.3	With original experiment	<0.05	<0.01
201016	SPB pH 7.4			
011116	SPB pH 7.4	Between group	>0.06	<0.05

Statistical analysis was performed on each variable group using either a t-test or ANOVA, depending on the number of groups compared (t-test for two groups, ANOVA for >2). Groups are separated in the table by the horizontal lines. The significance is indicated in Table 35, showing that the Ta hydrogel at least always produced significantly different results, while the Ph hydrogel was often significantly different as well. Additionally, the relationship between the two hydrogels was also observed to change between batches. This indicated that none of these attempts to control the elastic modulus was successful. The full details of the statistics used is detailed in Table 43, Appendix 1, Section 7.1.

4.3.3 Development of Methods for Image Analysis

SEM Image Analysis

A method for analysing the SEM images of the hydrogel was developed for this

project to provide a quantitative measurement of the pore structure. The SEM images were analysed using ImageJ software (Schneider et al., 2012), as shown in Figure 55. Measurements of 2D images such as those taken using SEM have been shown to have a correlation with 3D measurments (Boutroy et al., 2011). After importing the image, the scale and units were set by drawing a line across the scale bar on the image and changing the length of the line to that stated by the scale bar on the image so that the measurements taken of the pores would be correct. The scale bar was then removed so that the analysis software would not include this in the analysis, the "smooth" tool was applied to reduce noise and the image was converted to binary, which is the required format for the analysis software. The Background Correction plugin (Wu, 2008) was used to process the image. The BoneJ plugin (Doube et al., 2010) version 1.4.2, which was developed for analysing bone structure, was used for the analysis. The thickness measurement tool was selected. This generated the mean, standard deviation and maximum values of both the collagen fibril thickness and spacing in the matrix.

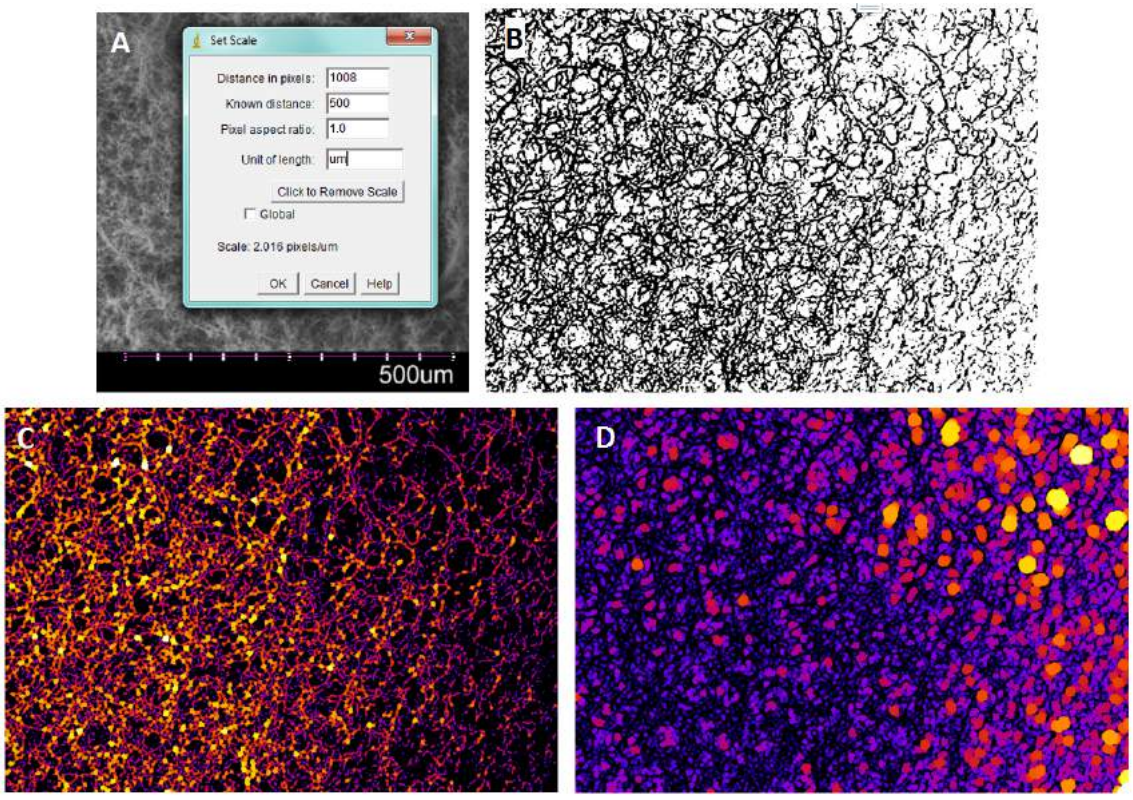

Figure 55: Processing steps to analyse scanning electron microscope images using ImageJ. A: Setting the scale. B: Binary image. C: Generate BoneJ matrix thickness image. D: Generated BoneJ matrix spacing image.

Although the BoneJ software has been validated by its authors, Doube et al. (2010), as the application in this study was collagen hydrogels and not cortical bone, the method developed here for analysis of the pore size was validated against a manual method of measurement. The scale was set in the same way as before, and a grid of 5000um^2 squares was overlaid, as shown in Figure 56. For each of the 20 squares outlined, the pore with the most apparent edges was identified and measured using the line tool. Use of the grid ensured that a broad sample size was collected. The length of each line was measured and the 20 measurements were averaged. This process was repeated for three Ph and three Ta hydrogels. The results of this study are presented in Table 36.

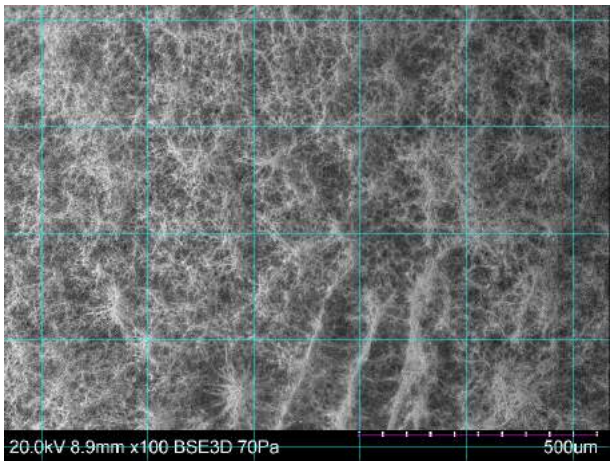

Figure 56: A 5000um^2 grid was overlaid onto the original scanning electron microscope image so that manual pore measurements could be made.

Table 36: Average pore sizes, as calculated by the BoneJ software and by manual measurements.

Hydrogel Name	BoneJ	Manual
Ph 1	22.118	21.442
Ph 2	17.734	16.076
Ph 3	23.106	23.623
Ta 1	21.172	24.188
Ta 2	20.631	19.929
Ta 3	19.262	20.356

As presented in Table 43 in Appendix 1, Section 7.1, using a two-tailed paired t-test,

the calculated p values was p>0.1, indicating that the methods produced the same results. This provided the confidence to use the BoneJ method for further analysis.

Analysis of Fluorescent Images

The ImageJ (Schneider et al., 2012) "analyse particles" tool was identified as a useful tool for counting cells, however this required a binary image input. To create a binary image the "auto local threshold" tool was used. To create a suitable image for threshold analysis, the "smooth" tool was used to reduce noise, and the image was converted into 8-bit. A flow diagram of the process is presented in Figure 57. Using this process for each separate colour, the number of cells expressing each phenotype could be recorded.

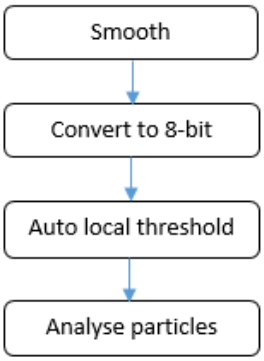

Figure 57: Flow diagram of the cell analysis process in ImageJ (Schneider et al., 2012).

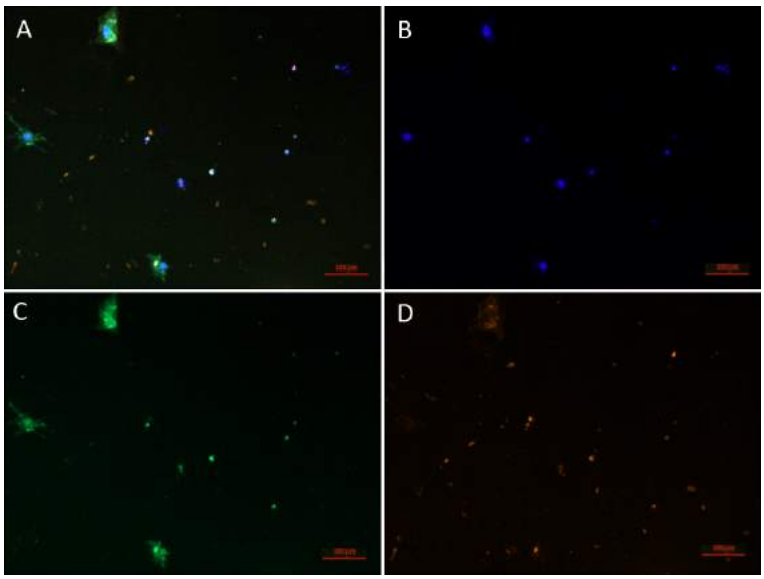

Figure 58: Example image of immuno stained cells taken using a confocal microscope, including a combined image (A), the nuclei of the cells in blue (B), CD133 (stem) expression in green (C) and PSA-NCAM (neuronal progenitor) expression in red (D). Microscope wavelengths used were 595nm (red) 518nm (green) and 421nm (blue).

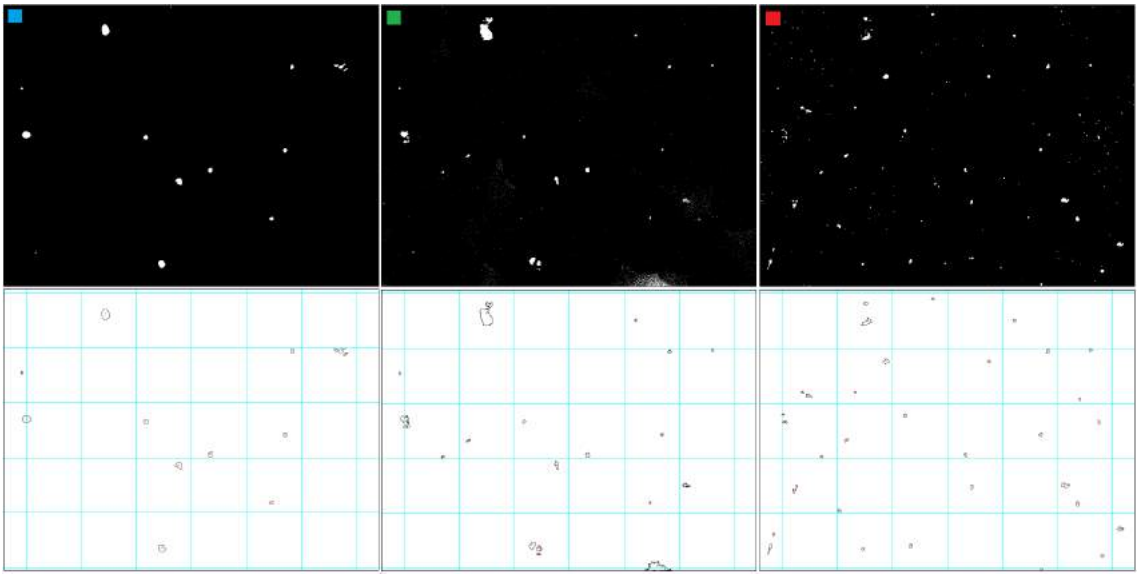

Figure 59: Binary images and particle analysis results using ImageJ (Schneider et al., 2012) using the same images as in Figure 58. Coloured square indicates the blue, green and red image used. Scale bars were removed to avoid the inclusion of these in the analysis.

Although the particle analysis tool automatically counted the cells, the cells were counted manually from the images generated by the tool, shown in Figure 58. Live

cells were identified by the blue nuclei, and the colour of the cells surrounding the nuclei were recorded. Coloured cells that were not in the same place as the nuclei were assumed to be dead and were not included in the analysis.

4.3.4 Response of CNS Stem Cells to the Hydrogel Variants

Mechanical Characterisation

To assess the storage and loss moduli of the hydrogels, rheological characterisation was performed. The amplitude sweep was performed between 0.05-5% strain at a constant frequency of 1Hz. Four repeats of each hydrogel type were tested in an amplitude sweep to find the LVER for both hydrogel types. The average elastic modulus responses are presented in Figure 60.

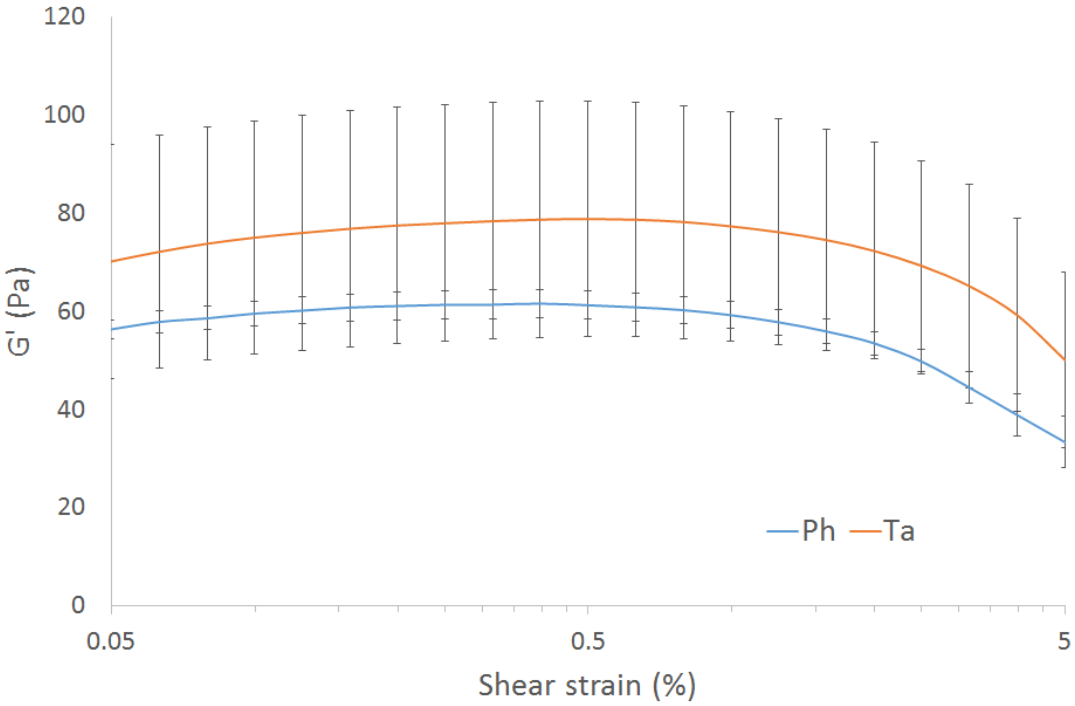

Figure 60: Elastic modulus (G') response of hydrogels tested through an amplitude sweep between 0.05-5% strain and at 1Hz frequency. Error bars represent standard error, n=4.

The percentage shear strain used for the frequency sweeps was calculated by first determining the range of strain for each sample in which the elastic modulus varied by less than 1% between readings. The median value for each range was calculated, and then averaged between all eight samples, and rounded to the nearest 0.1 value.

The data from this calculation is presented in Table 37 and shows that the average median value was 0.4.

Table 37: Range of shear strain for hydrogel samples where the elastic modulus response changed by less than 1% between readings. Median value of this range was calculated and averaged across all samples to give an appropriate shear strain for frequency sweep tests.

Hydrogel Sample	Shear strain range(%)	Median Value (%)
Ph1	0.08-0.5	0.29
Ph2	0.06-0.8	0.43
Ph3	0.15-0.6	0.375
Ph4	0.1-0.6	0.35
Ta1	0.15-0.8	0.375
Ta2	0.1-0.8	0.45
Ta3	0.15-0.8	0.475
Ta4	0.2-0.8	0.5
Average		0.4±0.026 S.E.

The amplitude of strain selected for use in the frequency sweeps was 0.4%. Four repeats of each hydrogel type were tested in the frequency sweep between 0.5-5Hz. The average storage and loss moduli responses are presented in Figure 61. The mechanical properties of each hydrogel were compared at 1Hz as presented in Figure 62. Statistical significance was performed using a Wilcoxon or t-test to compare the mechanical properties at 1Hz, the results are presented in Table 43 in Appendix 1, Section 7.1. The results indicated that at 1Hz, the difference in storage modulus of the two hydrogels was statistically significant ($p<0.05$) while the difference in loss moduli was highly significant ($p<0.01$). In both cases, the Ta hydrogel had higher moduli than the Ph hydrogel.

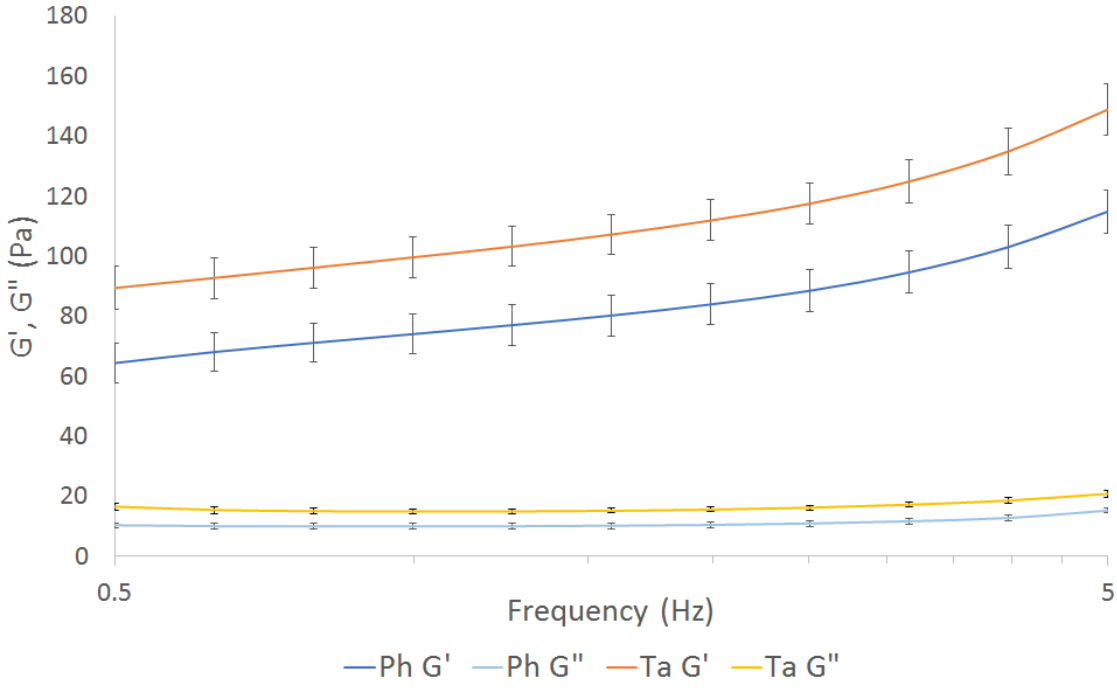

Figure 61: Average storage (G') and loss (G") moduli response of hydrogels tested through a frequency sweep between 0.5-5Hz and at 0.4% strain. Error bars represent standard error, n=4.

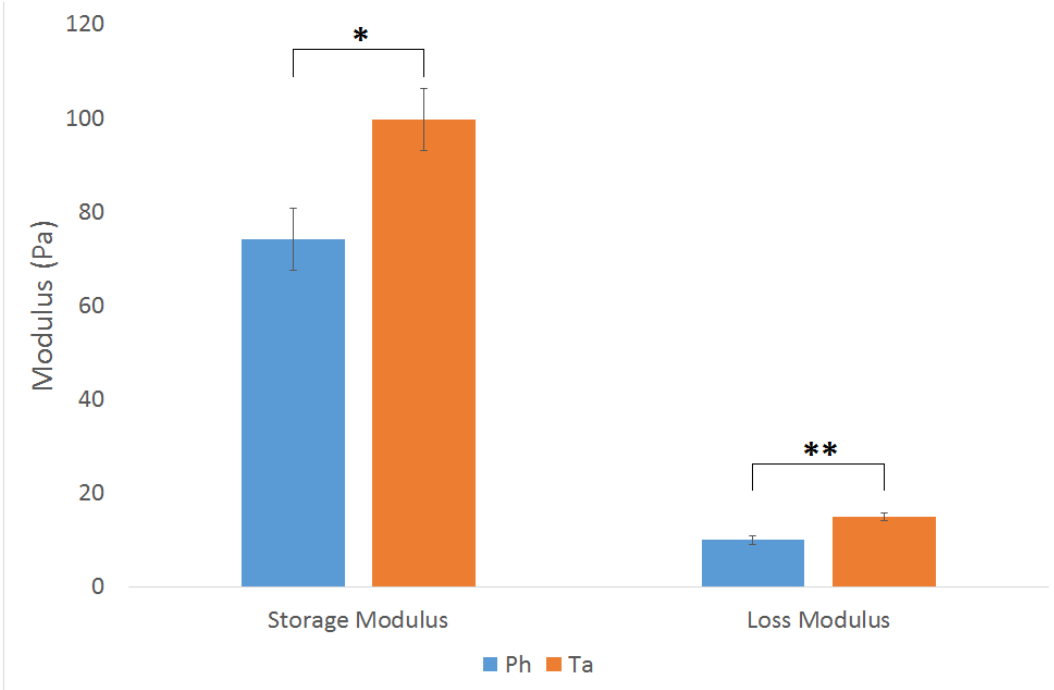

*Figure 62: Average storage (G') and loss (G") moduli response of hydrogels at 1Hz frequency and at 0.4% strain. Error bars represent standard error, n=4. * signifies a significant difference in means ($p<0.05$), while ** signifies a highly significant difference in means ($p<0.01$)*

Determination of Physical Characteristics

The physical characterisation of the hydrogels was obtained through the SEM image analysis which measured the sizes of pores in 2D, the NMR T2 analysis which measured the approximate volume of pores, the water content study which measured the overall weight of water in the hydrogel and the TNBS assay which measured the degree of crosslinking.

Pore Diameter using SEM and BoneJ

To assess the pore diameters, four samples per hydrogel variant were synthesised for SEM analysis. For each sample, three images were taken on the surface. The images were taken at locations where the pore size was homogeneous throughout the view. A representation of an SEM image obtained for the a hydrogel and the resulting image analysis output from BoneJ plugin are presented in Figure 63.

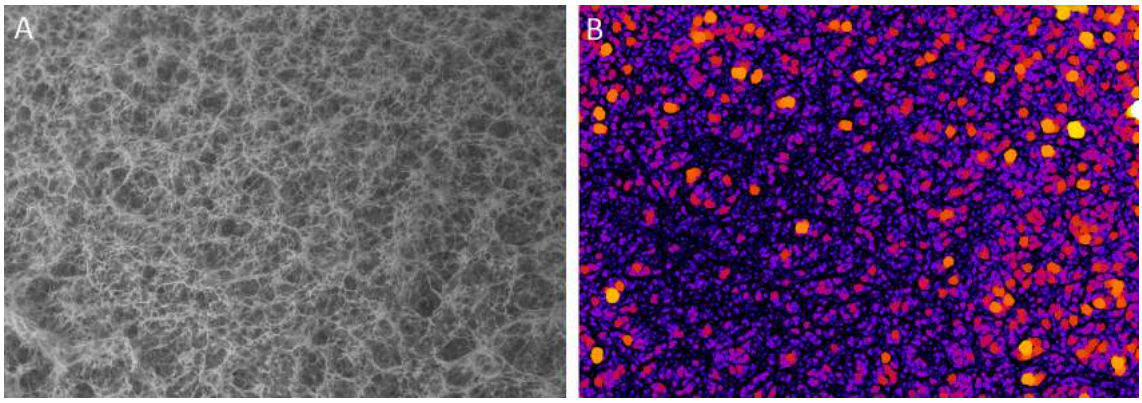

Figure 63: Image on the left of original scanning electron microscope image (A), image on the right of the graphical output of the BoneJ spacing analysis (B). Scale bars were removed to avoid the inclusion of these in the analysis.

The average size of the pores as calculated by the BoneJ plugin (Doube et al., 2010) within ImageJ software (Schneider et al., 2012) are presented in Figure 64. The measurements from the 12 images were averaged to find the mean pore size. Testing for statistical significance between the two hydrogels was performed using a two-tailed T-test, the results are presented in Table 43 in Appendix 1, Section 7.1. The statistical analysis indicated that the difference in pore diameter of the two hydrogels as calculated by the BoneJ plugin on the SEM images was not significant.

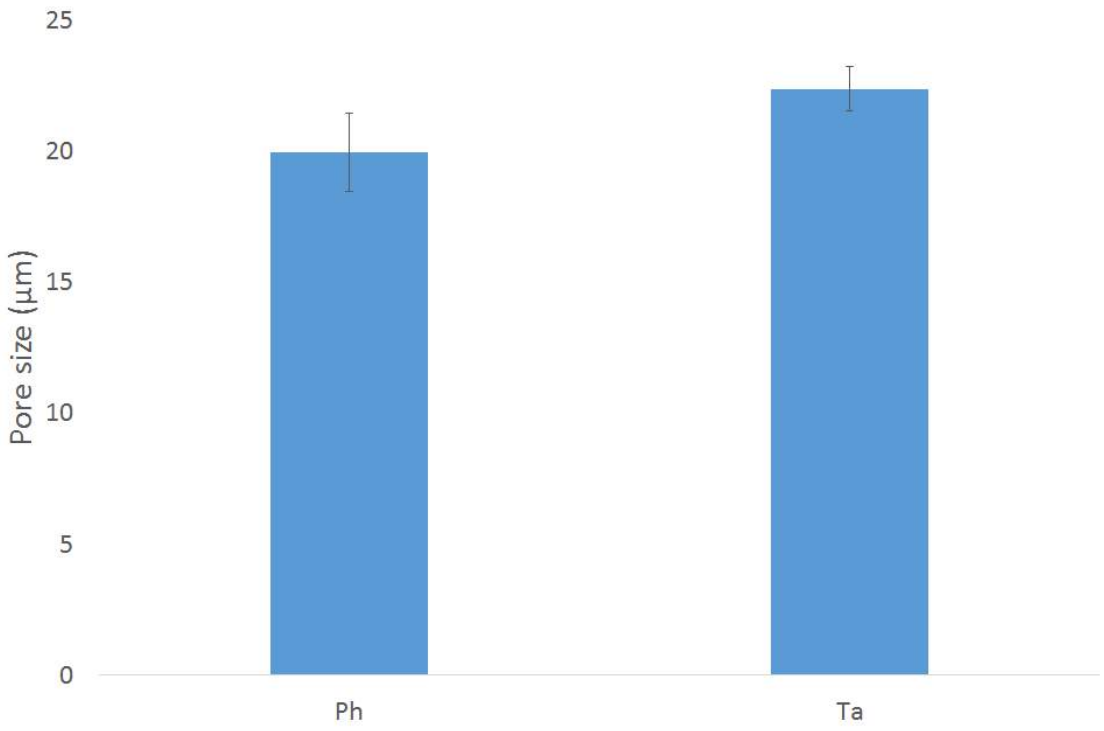

Figure 64: Average measurements of pore size as calculated by the BoneJ plugin (Wu, 2008). Error bars represent standard error, n=4.

Pore Volume using NMR

To assess the pore volumes, three samples per hydrogel variant were analysed using NMR and the mean signals were calculated by Carlos Grattoni at the School of Earth and Environment. A T_2 logging test was performed as described in Section 2.7.2. The T_2 distribution curves are presented in Figure 65 with the artefacts of the test, such as those presented in Figure 27 removed. These artefacts are small peaks at short T_2 time frames, and were caused as the number of scans taken was 5 times higher (1000 scans) than a normal test. This was to improve the signal to noise ratio, however meant that these artefacts were amplified. The distribution curves were averaged for the Ph and Ta samples.

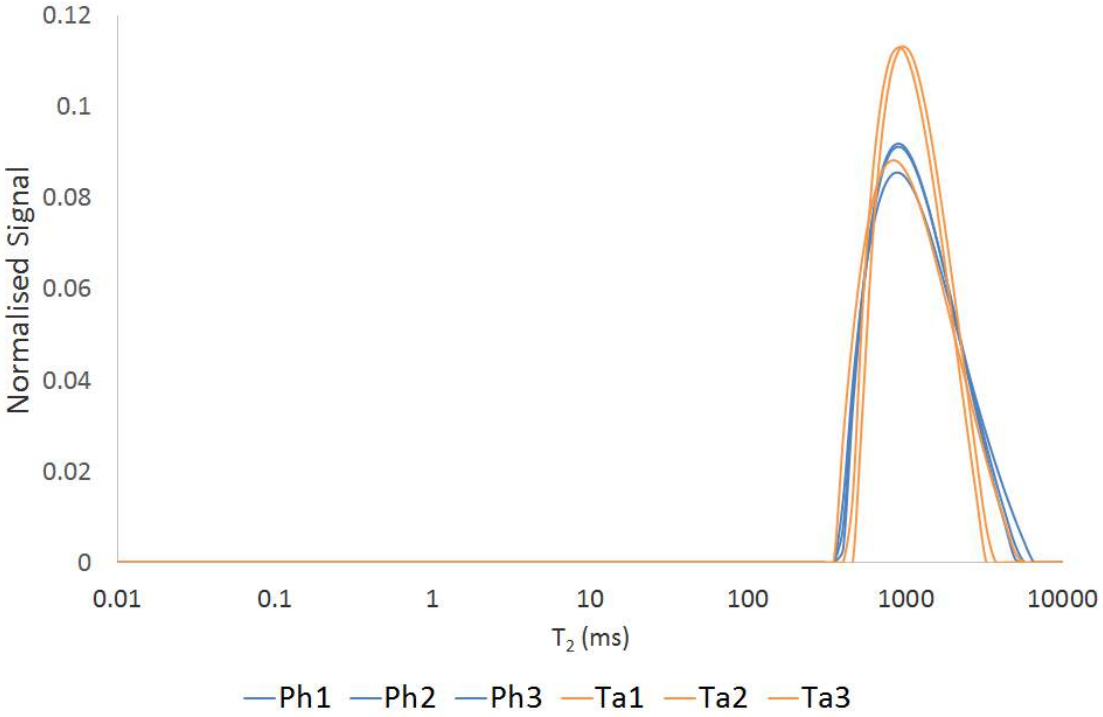

Figure 65: T_2 distribution curves, with artefacts of the experiment removed. The value of T_2 in which the signal peaks are proportional to the volume of the pores within the hydrogel.

Data from the curves was compared in three ways: the mean T_2 value, the T_2 signal range, and the maximum signal value. These comparisons are presented in Figure 66. A summary of the statistical analyses performed on the data is presented in Table 43 in Appendix 1, Section 7.1. The results indicate that there was no significant differences pore volume as calculated by NMR T_2.

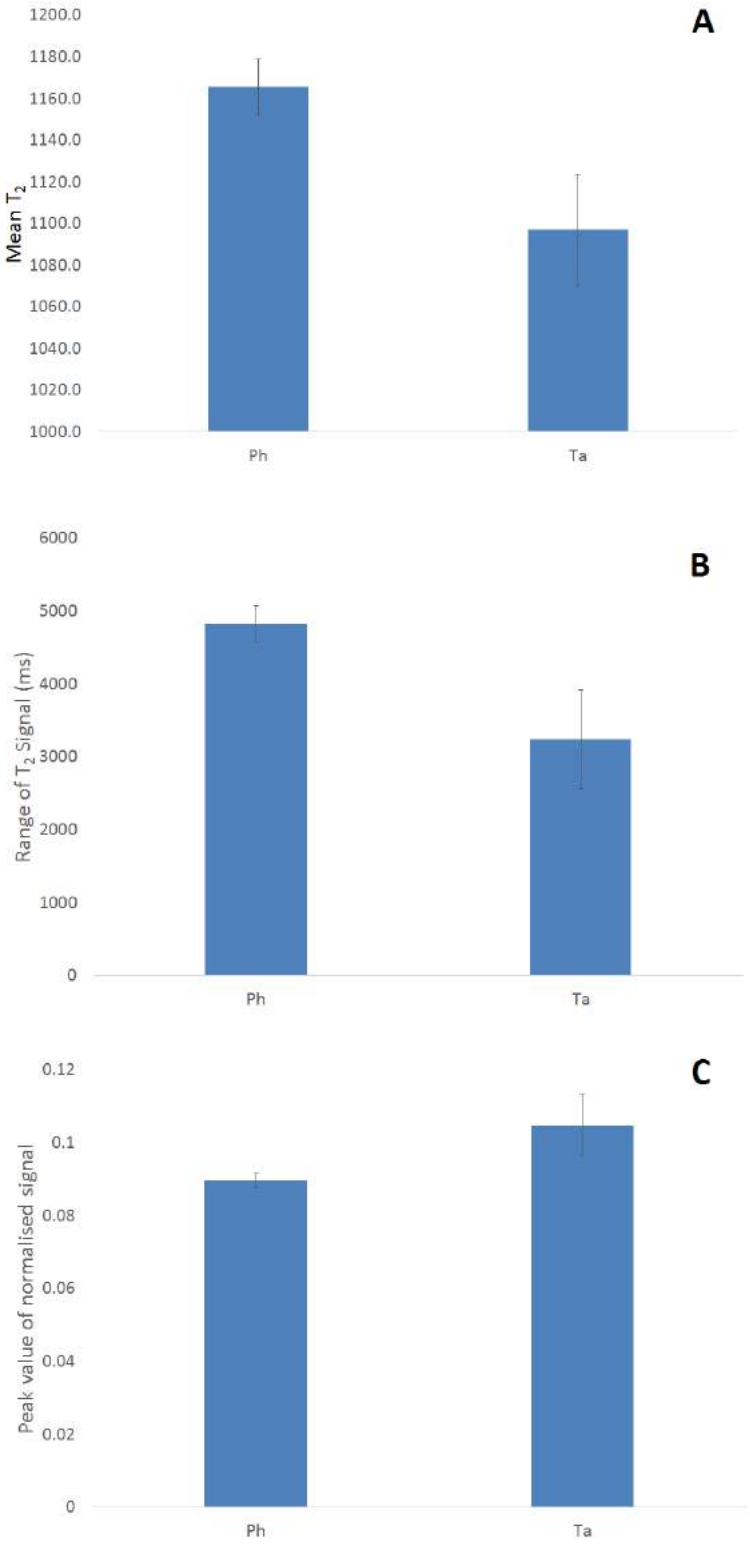

Figure 66: Analysis of the T_2 distribution curves. A: Mean T_2, B: T_2 signal range and C: Peak T_2 signal. All error bars represent standard error, n=3.

Degree of Crosslinking using the TNBS assay

To assess the degree of crosslinking, three samples per hydrogel variant were synthesised for TNBS analysis. The readings of the spectrophotometer are presented in Figure 67, while the statistical analysis was performed by an independent two-tailed t-test, the results of which are presented in Table 43 in Appendix 1, Section 7.1. The results indicated that there was no significant difference in degree of crosslinking between the two hydrogel variants as measured by TNBS analysis.

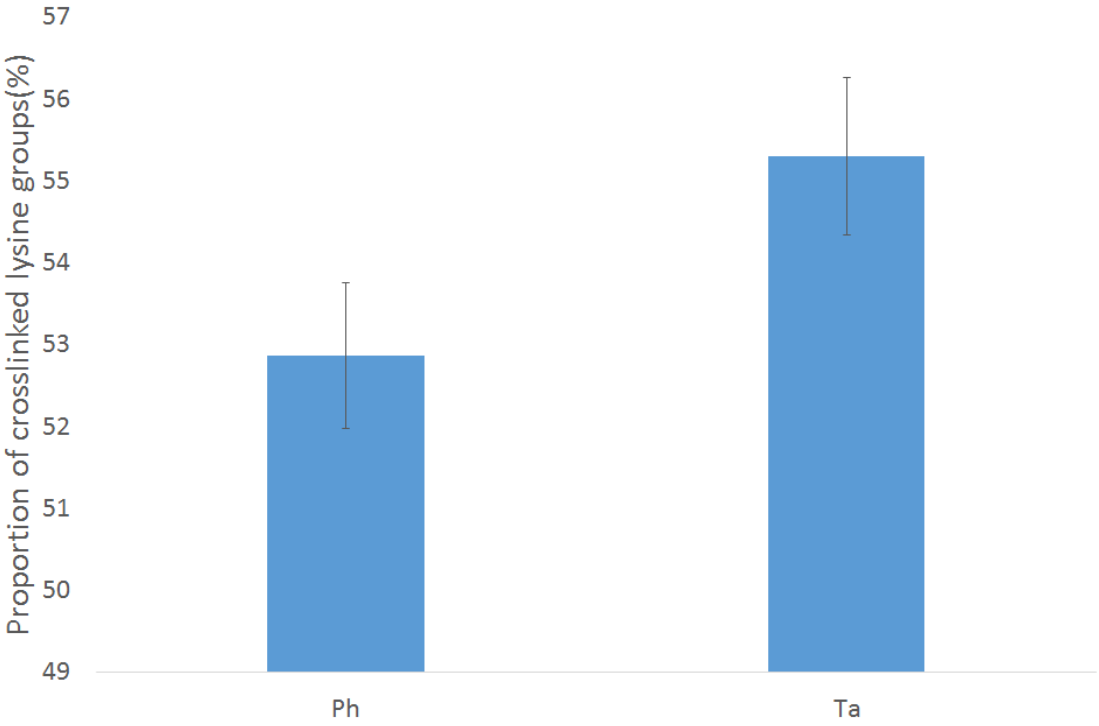

Figure 67: Comparison of average 2,4,6-Trinitrobenzenesulfonic acid (TNBS) readings of the hydrogel variants.

Water Composition

To assess the overall porosity of the hydrogels, three samples per hydrogel variant were synthesised for assessment of water content. The results of this analysis are presented in Figure 68. A two tailed t-test was performed to assess the significance of the difference between the two hydrogels, the results are presented in Table 43 in Appendix 1, Section 7.1. The p value was calculated to be $p<0.01$, therefore the increase in water content of Ta hydrogel was considered to be highly significantly different to that of the Ph hydrogel.

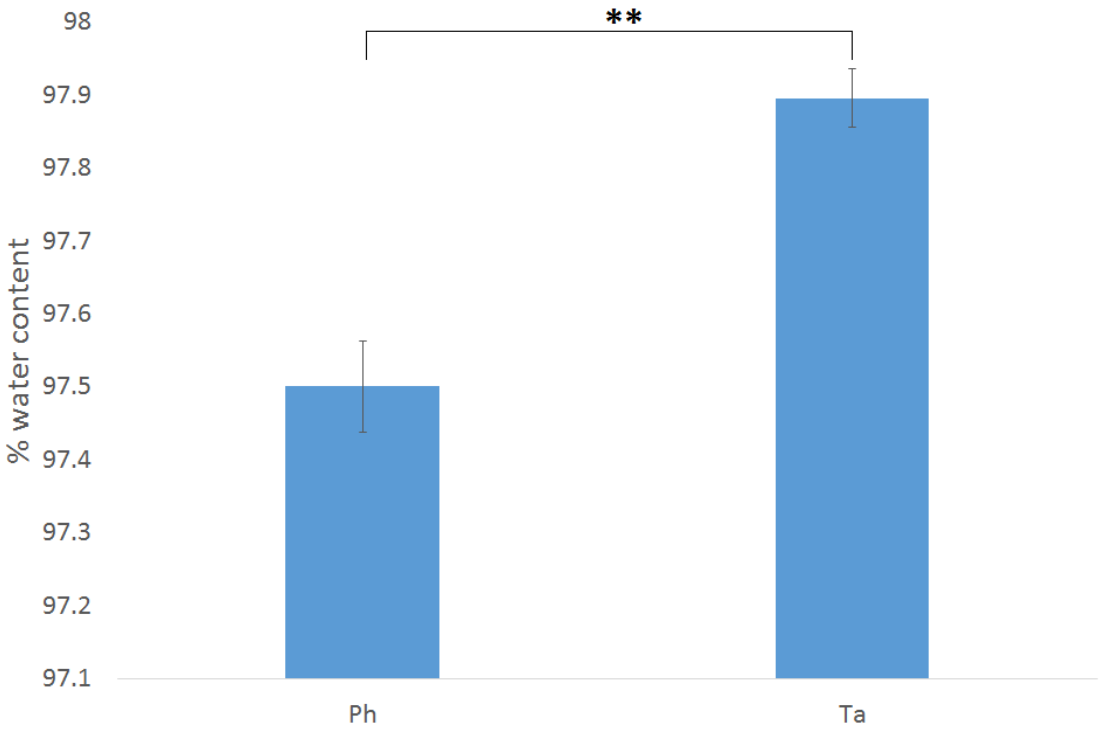

*Figure 68: The calculated percentage water content of the hydrogel variables, 1,3-Phenylenediacetic acid (Ph) and Tartaric acid (Ta). Error bars represent standard error, n=4. ** signifies a highly significant difference in means (p<0.01).*

Determination of Cellular Response

To assess the cellular phenotype and morphology, two hydrogels per hydrogel type were seeded with cells and three images per hydrogel were captured. The images were processed into binary images using ImageJ (Schneider et al., 2012) and the method developed in Section 4.3.3. For each image, the number of cells were identified by each nuclei stained blue with DAPI. For each nuclei, the phenotypic expression of the surrounding cell body was recorded as either green, red or none. The average area per cell was calculated using ImageJ (Schneider et al., 2012) and the region of interest (ROI) manager. Example images of the cells at day 10 are presented in Figure 69.

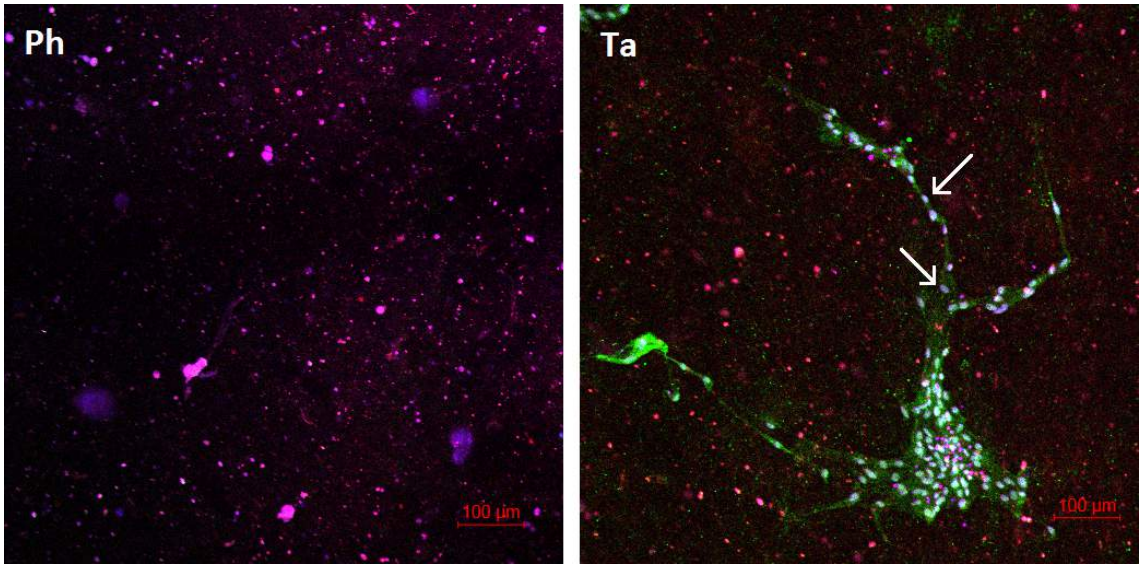

Figure 69: Examples of images taken using the confocal of immunofluorescent CB660 cells at day 10 cultured in the 1,3-Phenylenediacetic acid (Ph) and Tartaric acid (Ta) hydrogels, as indicated. Blue stain indicated nuclei, red indicated neuronal progenitors (PSA-NCAM) and green indicated neural stem cells (CD133). Arrows indicate position of nuclei.

Cell Phenotype

Cells with green staining were recorded as stem cells, cells with red staining were recorded as neuronal progenitors and cells with no staining were assumed to be glial progenitors, due to the findings of Sun et al. (2008). The cell counts from the three images were averaged, then the mean of the average cell counts was calculated. The proportions of each cell type are presented as percentages in Figure 70. Statistical analysis was performed using a independent samples t-test, the results of which are presented in Table 43 in Appendix 1, Section 7.1. The results indicated that although a greater number of neuronal progenitors were observed in the Ph hydrogel, there was no significant difference of cell proportions between the two hydrogel variants.

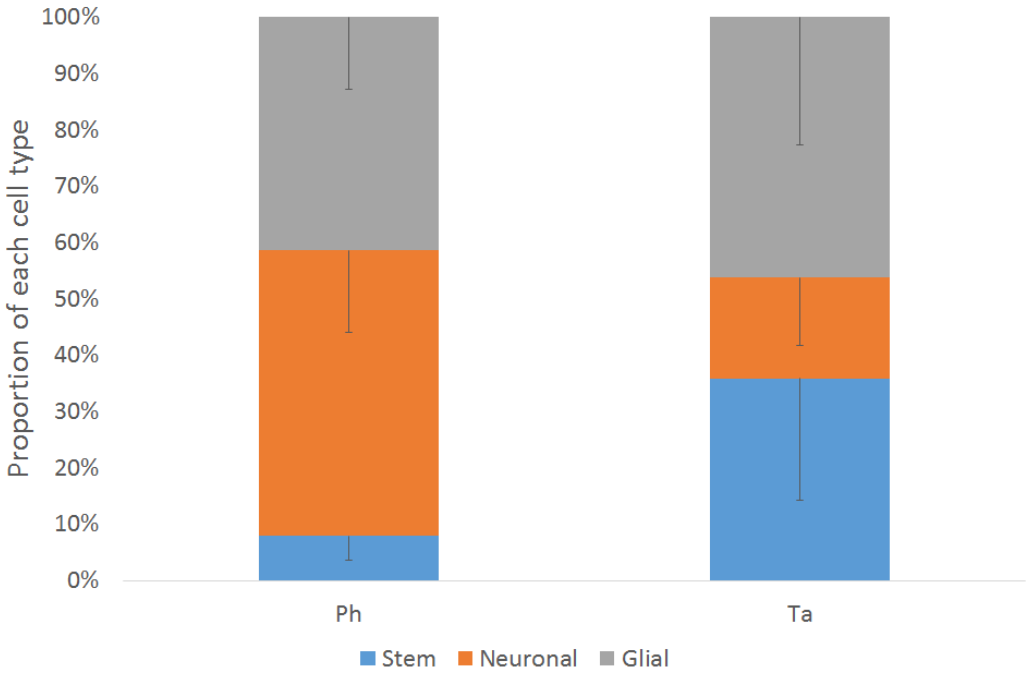

Figure 70: Average proportions of cells cultured within 1,3-Phenylenediacetic acid (Ph) and Tartaric acid (Ta) hydrogels. Error bars represent standard error (only negative error displayed for clarity), n=2.

Cell Spreading

All cells seeded onto the Ta hydrogel were observed to express processes extending into the hydrogel, while no cells in the Ph hydrogel were observed to have processes, remaining rounded. For this reason, analyses of the processes were not made, and instead, the area observed to be occupied by each cell, or the "cell spreading" was measured.

The ImageJ (Schneider et al., 2012) ROI manager was used to measure the cell area of thresholded images, the total area was divided by the cell number to find the average area per cell, the results are presented in Figure 71. An independent two-tailed t-test was performed to assess for statistical difference in the data, the results are presented in Table 43 in Appendix 1, Section 7.1. The statistical analysis indicated that the difference between cell spreading was statistically significantly increased in the Ta hydrogels ($p<0.05$).

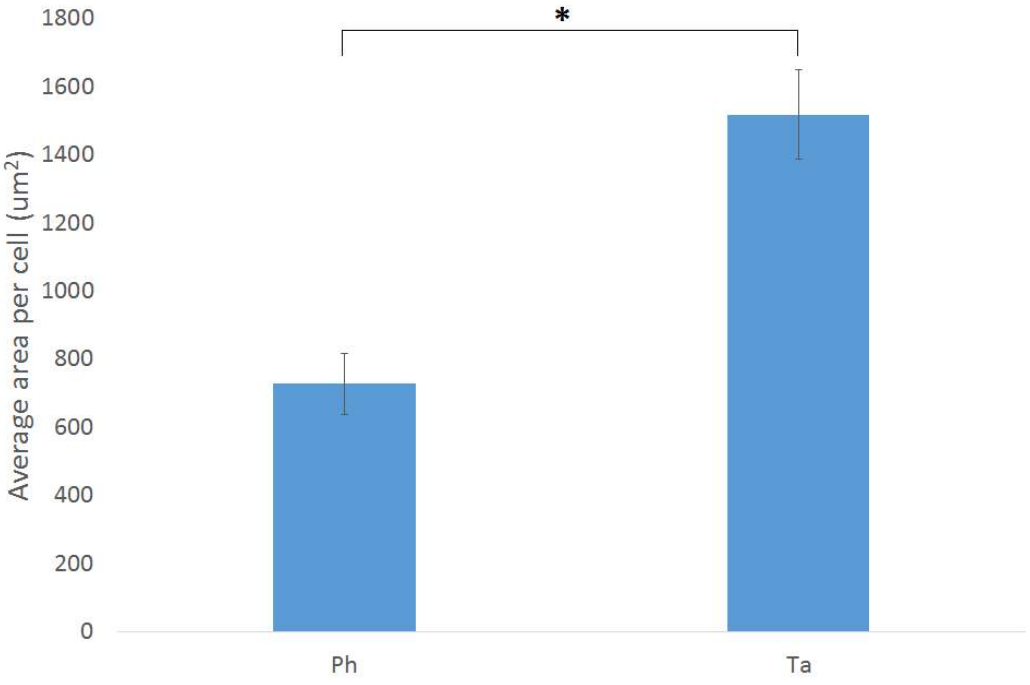

*Figure 71: Average area of cells cultured within 1,3-Phenylenediacetic acid (Ph) and Tartaric acid (Ta) hydrogels. Error bars represent standard error, n=2. * signifies a significant difference in means ($p<0.05$).*

4.4 Discussion

4.4.1 Hydrogel Development

Initially, the method of replacing the crosslinker type was found to produce a difference hydrogel moduli, while the degree of crosslinking remained similar. As this was only a study into the feasibility, only one sample per hydogel type was used to assess the degree of crosslinking, however this limited the validity of the study. Indeed, as it was later discovered, the mechanical properties of the hydrogels were highly variable and so more repeats could have provided valuable insight into the variability of the crosslinking.

Unfortunately the issue with repeatability remained unresolved, and could be due to a multitude of factors. Similar issues were not reported in the literature on hydrogels for neural applications (Banerjee et al., 2009; Her et al., 2013; Bozza et al., 2014). However, variation has been noted by many other authors (Wenger et al., 2007; Johnson et al., 2007; Kreger et al., 2010), including for commercial hydrogels (Hughes et al., 2010). Changes in the rheometry test set up, for example variations in the hydrogel thickness, compression, hydration or temperature could all lead to a change in the shear response (Wenger et al., 2007). Another cause could be the variable quality of the rat tail collagen that was extracted in-house, for example its purity or structure. For the synthesis of hydrogels with higher elastic moduli such as for muscle tissue in the range of 10kPa (Engler et al., 2006), it is unlikely that 100Pa variation between batches would be considered significant, so for other applications this variation is of little consequence.

For the purposes of studying the effect of elastic modulus (independent of changes in microarchitecture) on the activities of stem cells, a single large batch of hydrogel was synthesised so that it could be used for both characterisation and cellular experiments, with the assumption that there was no significant variability within the batch of hydrogel. This assumption was not verified and was a significant limitation of the study, and future work would benefit from locating a collagen source with lower variability. However, the standard errors of the elastic moduli of the final samples tested by rheometry were under 9% and 7% for the Ph and Ta hydrogels, respectively, which indicates a level of similarity.

The mechanical characterisation of the final batch of hydrogels showed a significant difference in storage moduli ($p<0.05$), and a high significant difference in loss moduli ($p<0.01$), with the Ta hydrogel producing a higher reading in both cases. In terms of physical characterisation, the results were mixed. The pore diameter analysis, degree of crosslinking analysis and pore volume analysis produced results that were not significantly different. However, the difference in water composition of the hydrogels was found to be highly significant, with the Ta hydrogel having a higher water content than the Ph hydrogels.

The elastic modulus of the hydrogels was observed to be 74.01 ± 6.63Pa and 99.57±6.65Pa for the Ph and Ta hydrogels, respectively (± standard error, n=3). These were not within the biomimetic target of 200-600Pa, however was comparable to another synthesis of chemically crosslinked collagen hydrogels with Ph, who found an elastic modulus of approximately 100Pa (using shear testing at 0.01Hz) (Head et al., 2016).

4.4.2 Method Development

The BoneJ plugin (Doube et al., 2010) for ImageJ (Schneider et al., 2012) was originally designed for the characterisation of cancellous bone, however was successfully adapted for the measurement of pore diameter of hydrogels. The particle analysis tool was also optimised for use in this chapter, allowing for unbiased measurement of the number of cells present in each image. Using a paired t-test, the accuracy of the BoneJ plugin was evaluated by comparison to manual pore measurements. The reported p value was 0.712, suggesting that the the variance of the two measurement methods was comparable.

It was assumed that the higher resolution 1000x magnification SEM images would provide better data for measuring pore size than the 100x magnification images. However, this proved not to be the case, as indicated in Figure 72. Firstly, the Background Correlation plugin (Wu, 2008) often included the centre of thicker fibres as part of the background (an example is contained within the orange circle in the figure) so that when analysed with the BoneJ plugin (Doube et al., 2010), these were included as pores. Secondly, the BoneJ analysis often did not include larger

pores, recognising only the smaller pores within them (an example is contained within the blue circle in the figure). Therefore the measurement of the pores in images at this magnification was deemed unsatisfactory, however images taken at 100x magnification did not appear to have this problem. Use of the 100x images meant that the resolution of pores and therefore the accuracy of measurement of these was inevitably 10 fold lower compared to the 1000x images, however due to the measurement errors made on the images of a higher magnification, use of the 100x images was deemed more appropriate.

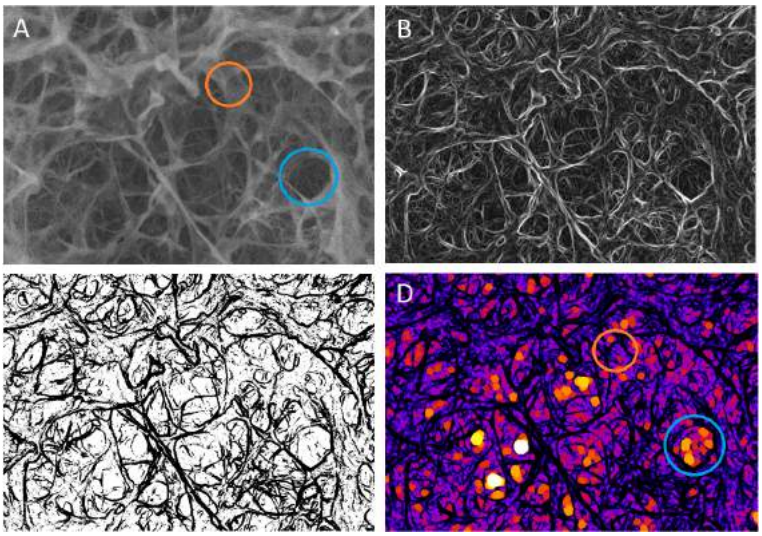

Figure 72: Image indicating the limitations of the Background Correction plugin and BoneJ analysis plugin using the x1000 magnification scanning electron microscope (SEM) images. The orange circle indicated a region in which a thick fibre seen in the original SEM image (A), has been identified as pores as seen in the image produced by the BoneJ plugin (Doube et al., 2010) (D). The blue circle indicates a region where a large pore, seen in the original image (A), has been identified as many smaller pores in (D). The results of the background correlation plugin (Wu, 2008) (B) and the binary image (C) are also included. Scale bar removed to avoid inclusion in the analysis.

4.4.3 Cellular Response

The differentiation of the CB660 stem cells when seeded onto the hydrogels was measured using antibody labelling, and found no significant difference between cell response at day 10 despite the difference in elastic moduli between the hydrogels.

The CD133 antibody was used to identify neural stem cells, while the PSA-NCAM identified for neuronal progenitors. The phenotype of cells was measured at day 10 as Sun et al. (2008) had noted that the expression of these markers changed between weeks one and two for differentiating CB660 cells. The cell numbers were calculated by counting the DAPI stained nuclei, and found that the hydrogel variants had no significant effect on the number of cells. Images of the cells were taken using a fluorescent confocal microscope, and analysis was performed using cell counting (each type of cell) and cell spread (area per cell). The differentiation of the cells was not significantly different between the two hydrogel variants. This findings indicated that pore size may produce an effect on stem cell differentiation, independent of elastic modulus. The main limitation of this method was that a glial differentiation marker was not used, and it was assumed that blue nuclei with no further colouring were progressing down a glial lineage. Another limitation was that Sun et al. (2008) reported that only approximately 66% of CB660 cells positive for PSA-NCAM at week 2 were positive for βIII-tubulin at week 4, and so over a third of these cells may not have been neuronal progenitors. With more resources such as time and materials, polymerase chain reaction (PCR) would have been used to compare with the findings of the immunostaining.

Using the ROI manager, the area of the cells was measured and divided by the total cell number. The results of this analysis indicated that cells seeded onto the Ta hydrogel were found to be significantly more spread, and all had processes extended, as opposed to the cells on the Ph hydrogel which remained rounded with no processes. The Ta hydrogel was observed to have a significantly higher storage modulus compared to the Ph hydrogel, and this difference may have enabled the cells within this hydrogel to form processes and become more spread in the Ta hydrogel compared to in the Ph hydrogel. As observed by Willits and Skornia (2004), neurite extension was increased in hydrogels with a complex elastic modulus of 2.9Pa compared to 2.2Pa (shear testing at 1Hz), although decreased in hydrogels with higher moduli (up to 20Pa). Additionally, Koser et al. (2016) found mechanical resistance is critical to axonal growth, and furthermore that axons grow preferentially towards softer substrates, becoming branched in substrates of 100Pa (shear testing, using AFM).

4.4.4 Conclusion

The mechanical characterisation of the hydrogels using rheology indicated that the elastic moduli of the Ta hydrogel was significantly higher than the Ph hydrogel, although these measurements were made on unseeded hydrogels, and the addition of cells may have changed the properties of the hydrogels. The physical characterisation methods of SEM image analysis, TNBS and NMR T_2 analysis indicated that pore size was similar in both hydrogels, as no significant differences between the two hydrogels were observed in the measurements. Meanwhile porosity of the hydrogel was assessed by measuring the water content, and the Ta hydrogel was observed to have a higher porosity that was highly significantly different ($p<0.01$). Analysis of the cellular response to the hydrogel variants found that there was no significant difference in cell number or protein expression, while a significant difference ($p<0.05$) was found in cell spreading, as cells in the Ta hydrogel were observed to be more spread than those in the Ph hydrogel.

The results indicate that although elastic modulus may affect cell spreading, it may not have any effect on other cellular activities such as differentiation and proliferation. This indicates that it could indeed be the pore size and not the elastic modulus that neural stem cells respond to. The pore size may be an important parameter that future research should include in the analysis. It is unlikely that the cells would respond to porosity as this is a macro-property, however the fact that this was highly significantly different may indicate that the fibres of the matrix of the Ph hydrogel were thicker, creating hydrogels with similar pore sizes but lower porosity compared to the Ta hydrogel. The spreading and formation of projections of the cells may also be inhibited by these thicker fibres.

A limitation of the cell studies was the low sample size. This was due to the slow proliferation of the stem cells and means that the power of the study was limited and therefore the results of the study should be regarded with caution. Another limitation was the use of different container sizes and shapes and hydrogel volumes used. While the elastic modulus of the hydrogel may have been assumed to be consistent throughout the final study, the stiffness of the hydrogels is a product of its dimensions and shape. Indeed, the properties of the container itself may have affected the property that the cells were sensing, or changed the shape of the cells.

5 Investigation of the Effects of Raised ICP on Neural Stem Cell Response

5.1 Introduction

Traumatic central nervous system (CNS) injury has been characterised by two stages: the primary injury which occurs at the time of the damage, and the secondary injury which covers the next minutes to weeks after the injury. Although secondary injury is characterised by the further deterioration of the patient's symptoms, this is also the same period of time in which many of the cellular processes of repair are occurring (Shoichet et al., 2008). Due in part to the relatively recent isolation of CNS stem cells (Temple, 1989), the role that CNS stem cells play in the repair of the CNS after a traumatic injury has not been studied in depth.

After a closed head injury, though there are a number of chemical changes during secondary injury, there is only one known change in physical stimuli - a rise in intracranial pressure (ICP). During the secondary injury phase, ICP is often recorded as it is recognised that the occurrence of certain waveforms and pressures can be used to predict patient outcomes. For example, the appearance of Lundberg A waves, where the pressure reaches above 40mmHg for 5-30 minutes before returning to normal levels of 5-15mmHg are known to predict patient survival (Cox et al., 2014). The underlying biological process that links ICP to patient outcome remains unknown.

The fixed volume of the cavity formed by the skull and vertabrae (Rose and Johnson, 1996) was identified as a unique property of the CNS, which is the property that causes the extreme rise in pressure measured in this system; and the limited capacity of this tissue to repair itself is also notorious. As these two aspects of the CNS were identified as distinctive, the hypothesis formed was that raised hydrostatic pressure, to the extent which is seen during secondary injury, directly affects the activities of cells of the central nervous system. The null hypothesis was that raised ICP has no direct effect on CNS cells.

The key cellular activities identified as important for repair, that this study focussed on were:

- The proliferation of stem cells that are required to replace damaged cells
- The migration of these cells to the site where they are required
- The differentiation of stem cells into specialised cells that require replacing.

In this chapter, the design of a model and equipment for studying the effects of raised ICP on cells *in vitro* was developed. The designs incorporated both the application of biomimetic pressure to the cells, as well as enabling their migration in three dimensions (3D) to be studied. The migration model under pressure was developed using the C6 glial cell line. A pressure model was designed based on Lundberg "A" waves. Stem cells were cultured under pressure using media compositions aimed at maintaining pluripotency or inducing differentiation to better understand what the effects of pressure may be *in vivo*. Under three different pressure scenarios, the proliferation of the cells were compared using successive ATPlite and CyQuant assays, the phenotype of the cells were compared using immunostaining and the migration of cells were compared using the developed migration assay.

5.1.1 Aim and Objectives

The aims of this chapter were to develop an appropriate model for raised ICP such as that observed in secondary injury, to develop a 3D migration model that was able to confirm migration of the cells and to assess the viability, phenotype and migration of neural stem cells in a raised pressure environment. An overview of the tasks and the specific objectives they relate to is detailed in Figure 73.

Specific Objectives

1. **To develop an *In Vitro* Model for Secondary Injury**
   Design a pressure model to investigate the effect of pressure at key levels, mimicking Lundberg A waves. Evaluate existing methods of applying pressure, if necessary design an appropriate method for this study, and develop the

apparatus to be used. The system was required to apply pressure to the cells. Evaluate existing migration assays and if necessary design an appropriate method for this study.

2. **To investigate the response of CNS stem cells to raised ICP**
   Study the phenotype, proliferation and migratory response to investigate whether the raised pressure environments during secondary injury had a direct effect on stem cell activities.

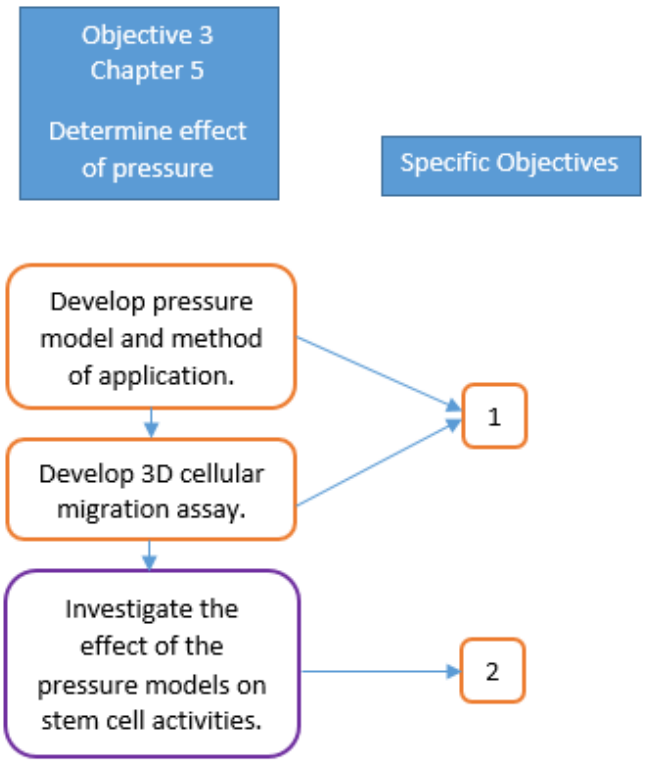

Figure 73: Overview of the tasks of chapter 3 and the specific objectives these relate to.

5.2 Methods

For the initial development of the migration assay, a cellular investigation was performed using C6 glial cells in two dimensions (2D) using a bright field microscope, and in 3D using live/dead staining and a fluorescent microscope. Later, the effects of pressure on the proliferation, migration and differentiation of CB660 stem cells was investigated further, as described in Table 38. The volume of the hydrogel used was determined based on the amount of manipulation required and the application.

Table 38: Samples created for studying cell response to pressure.

Analysis	Hydrogel Volume	Container
2D Migration (Development)	N/A	12WP
3D Migration (Development)	200μl	24WP
ATPlite and CyQuant Assays	100μl	96WP
Live/Dead Migration	200μl	48WP
Immunostaining	N/A	8 well multitest slide

5.2.1 Hydrogel Preparation

The collagen for the hydrogels was harvested from rat tails as described in Section 2.3.1. 1,3-phenylenediacetic acid (Ph) hydrogels were synthesised as described in Section 2.3.3. Ph hydrogels were used in this study as they were the original hydrogel described by Tronci et al. (2013b). This study and the previous study (on the effects of the mechanical and physical properties of the hydrogel on the neural stem cells) were completed simultaneously due to time restraints, and the improved conditions that the tartaric acid (Ta) hydrogel may have provided were unknown at the time.

5.2.2 Cellular Investigation of the Effect of Pressure on Neural Stem Cells

Cell Culture

To investigate the response of cells to the hydrogels, CB660 cells were cultured as described in Section 2.4.4.

Cell Seeding

Hydrogels were sterilised by soaking in ethanol and washed with PBS as described in Section 3.3.1. CB660 cells (*NIBSC*) were seeded onto Ph hydrogels for analysis at day 1 and day 10. Cell seeding in 2D was performed by coating sterilised multitest slides with laminin as described in Section 2.4.4 24 hours before seeding to promote cell attachment.

Determination of Cell Viability

To assess the effect of pressure on the viability of neural stem cells, 100μl Ph hydrogels were synthesised as described in Section 2.3.3 in 96 well plates and were sterilised and pre-soaked with Neurocult proliferation media, prepared as described in Section 13. Cells were seeded at a density of 1x10^{5}cells/ml, based on the findings presented in Section 3.5.4, using proliferation media and incubated overnight at 37°C, in air with 5% (v/v) carbon dioxide (CO_2). At day 1, media was changed to proliferation medium, differentiation medium (prepared as described in Section 13) or 50:50 expansion medium and 70% (v/v) ethanol and plates were transferred into modular incubators as will be described. Three repeats per media type were conducted. Cell survival was investigated by the CyQuant and ATPlite assays successively, as originally described in Sections 2.5.3 and 2.5.2 respectively, using the methodology that was optimised in Section 3.5.5.

Determination of Cell Phenotype

To assess the differentiation and morphology of neural stem cells under pressure, cells were seeded onto laminin-coated multitest slides at a seeding density of 2x10^5 cells/ml using 50 μl per spot in Neurocult proliferation media. At day 1, the medium was changed so that half the cells were cultured in proliferation medium and half were changed to Neurocult differentiation medium, both media types are described in Table 13. Due to low cell numbers, two repeats per pressure level were conducted.

At day 1, the cells were transferred into the modular incubators as will be described. At day 10 the cells were fixed and immunofluorescently labelled as outlined in 2.5.4. Phenotypic proteins CD133 and PSA-NCAM were targeted in the cells, as these were indicated by Sun et al. (2008) to be early indicators (<1 week) of neuronal differentiation, the details of which are described in Table 32, Section 4.2. DAPI was used to counterstain the nuclei blue. The cells were imaged using a fluorescent microscope. Five images were taken per spot.

Two negative controls were used. Cells were labelled with either an isotype primary antibody, or the primary antibody was ommitted and then the secondary antibody was applied as normal. DAPI DNA stain was also used. Images of the cells were captured using a fluorescent confocal microscope. Each experiment had two repeats, and each repeat had five images taken. The x and y positions of the hydrogel were

measured using the confocal microscope and images were taken in the centre, top, bottom, left and right areas of the spot. A summary of this experiment set up is detailed in Table 39, and a schematic diagram of the imaging strategy and fields of view is presented in Figure 74.

Table 39: Experimental set up to measure the phenotypic response.

Experiment	Pressure	Fixing date	Staining
Day 1	N/A	Day 1	Normal
Day 10, 10mmHg	10mmHg	Day 10	Normal
Day 10, 30mmHg	30mmHg	Day 10	Normal
Day 10, 50mmHg	50mmHg	Day 10	Normal
Isotype	10mmHg	Day 10	Isotype primary, normal secondary
No Primary	10mmHg	Day 10	No primary, normal secondary

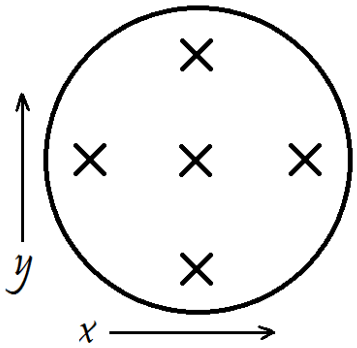

Figure 74: Plan view of the imaging strategy with five fields of view for each cell sample used for determination of phenotype, crosses indicate area where an image was taken.

Phenotype analysis

The phenotype of the cells was assessed using the same image analysis strategy as developed in the Fluorescent Image Analysis in Section 4.3.3. The images for each colour (blue, green, red) were analysed separately, and cell counts were made using the Analyse Particles tool in ImageJ (Schneider et al., 2012).

Projection analysis

Many of the cells that expressed the stem (CD133) protein had dendritic projections. These projections were measured in three ways:

- Proportion of the stem cells that displayed projections.
- Average number of projections per cell.
- Average length of projections.

The number of stem cells with projections, and the number of projections were counted manually. The average length of projections was measured using the NeuronJ plugin (Meijering et al., 2004) for ImageJ (Schneider et al., 2012). The plugin allows the user to manually select the start and end of a projection, and automatically maps the path of this projection. The start of the projection was chosen at the boundary of the nucleus, and the contrast of the image was increased to improve visualisation of the end of the projection. For images with more than ten cells, cells that were not located in close proximity to other cells were chosen preferentially to ensure that accurate measurements were made. In these cases, the same cells were used for measuring both the number of projections per cell and the length of projections.

5.2.3 Statistical Analysis

The statistical test was chosen based on the flow diagram presented in Figure 28 in Section 2.8 and was performed to compare between the three different pressure scenarios (10mmHg, 30mmHg and 50mmHg), using the ANOVA or Kruskal-Wallis tests. For experiments with only two repeats, the variance of the data was assumed to be equal. For the migration studies, there was only one sample and therefore no statistical analysis was performed.

5.3 Results

5.3.1 Development of an *In Vitro* Model for Raised ICP

The model for raised ICP was developed in order to investigate key waveforms or pressure levels that may affect patient outcome predictions. A system to apply raised pressures to cell cultures allowed investigation of whether the raised pressures have

a direct effect on the cells. Identification and subsequent development of an assay to investigate the migration of the cells in 3D was also required to investigate whether their migration in 3D is affected by the raised pressure.

Specific Objectives

1. Evaluation of existing methods for applying pressure *in vitro*, and if necessary design of an appropriate method for this study.
2. Testing and development of apparatus for applying pressure, including the ability to hold the pressure that the model required (initially estimated to be 140mmHg above atmospheric pressure), sterility and cell survival.
3. Evaluation of existing 3D cell migration assays, and if necessary design of an appropriate assay for this study.
4. Testing and development of a 3D migration assay that is appropriate for easily tracking cell migration.
5. Design of a pressure model that adequately mimics key features of interest of raised ICP during secondary injury after traumatic impact to the CNS, particularly Lundberg A waves.

Evaluation of Existing Methods of Applying Presssure

Secondary Injury Model Design Specification

The injury model must meet the following criteria:

- Must be able to support the growth of cell cultures, both in 2D and within a 3D hydrogel, confirmed by viability assays.
- Must be able to be sterilised and maintain aseptic conditions, confirmed by visual assessment.
- Must be able to maintain a constant pressure of up to 140mmHg above atmospheric pressure (10.7kPa).
- Must be able to be used in an incubator or maintain a temperature of 37°C.
- Must require modest resources such as low cost, low time to set up.

Evaluation of Available Methods

Of the published literature on *in vitro* studies into sustained pressure (reviewed in Section 1.4.3), there were two methods identified that were applicable to this study. The first was to culture cells under a column of media, the depth of which can be increased in order to increase the pressure as described by Lei et al. (2011). This was an attractive solution as it ensured a constant pressure at any temperature, however to create an pressure environment of 80mmHg would have required a column over one metre tall which is both impractical in terms of incubation and a waste of resources. The second option was to pressurise the air around the cell culture vessel as described by Yu et al. (2011) and detailed in Figure 75. This required only an air tight vessel capable of creating an increased pressure environment and a supply of compressed air with 5% (v/v) CO_2. The drawback of this method was that it required monitoring for the first few hours because increasing the temperature from room temperature to 37 °C also caused the pressure to increase. Of the two methods, the air pressure method was deemed most appropriate to model the effect of raised ICP on cells as it fit the specification best. Yu et al. (2011) also tested the pH, PCO_2 and PO_2 of the media and found no significant difference between the media used at atmospheric pressure and that used at 120mmHg.

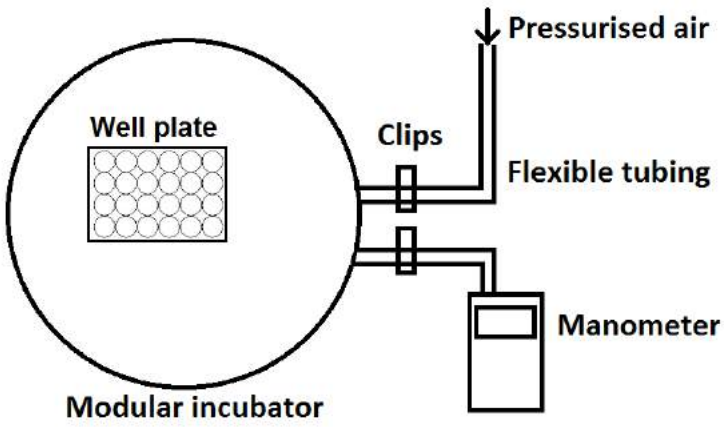

Figure 75: Schematic diagram of the experimental set up to increase the air pressure of the experiment, adapted from Yu et al. (2011)

Development of a Method for Applying Pressure

A pressurised environment was created using a modular incubator with clip closings, a pressurised air source containing 5% (v/v) CO_2 was used to raise the pressure and

a manometer was used to record the pressure of the environment, as shown in Figure 76. The method was adapted from Yu et al. (2011), who used a syringe to inject air directly into a cell culture flask, using an in-line pressure gauge and laboratory film to seal the interfaces. As the modular incubator was larger than the flask, compressed air was used to fill the chamber. As the modular incubator had two openings, the air feed and the manometer were able to be fitted to separate openings, and the clip closings allowed for reliable sealing of the container.

As the experiment was set up at room temperature and sealed before putting into an incubator at 37°C, the initial pressure increased until the entire experiment was at 37°C. This pressure increase was estimated using the ideal gas law noted in Equation 22, where P is pressure, V is volume, n is the number of moles of substance, R is the ideal gas constant and T is the temperature.

$$PV = nRT \tag{22}$$

Assuming V and n to be constant, the equation can be simplified to Equation 23.

$$P_1/T_1 = P_2/T_2 \tag{23}$$

Assuming the temperature will increase from 20°C to 37°C, which is 293K to 310K, it follows that the pressure will rise by approximately 6% of its initial pressure. As this is absolute pressure, for example a 6% rise from atmospheric pressure, at 760mmHg, is 45.6mmHg. This difference *in vivo* would raise the pressure in the CNS from a normal level of 5-15mmHg to approximately 50-60mmHg, which is above the requirement for classification of a Lundberg A wave (i.e. above 40mmHg) and may therefore be of significance to the activity of the cells. For this reason, the pressure was checked again after 1 hour incubation, and altered as necessary.

Figure 76: In the pressure model, a modular incubator is pressurised, using a manometer to monitor the pressure increase.

A 2D scratch assay was performed using C6 glial cells in a 12 well plate to record an initial response of pressure on cell migration. Cells were seeded at a density of $1x10^5$ cells/well into each well and cultured for 24 hours to ensure attachment before a scratch was created by drawing a 1ml pipette tip across the surface of the culture plastic. The cells were cultured for 4 days, either at 0mmHg or 135mmHg. The pressure of 135mmHg was used for this inital 2D test to ensure that if the cells did have a migratory response to increased pressure at levels recorded *in vivo*, it would be evidenced in this test. A standard inverted light microscope was used to record migration of the cells into the scratch over a three day time period. A representative image is presented in Figure 77. There was no discernible difference in migration seen between the pressurised and unpressurised cells, and alignment of the neurites could be seen within the scratch, possibly due to small grooves in the plastic caused by the scratch. However, this test showed that the cells were able to survive at this pressure.

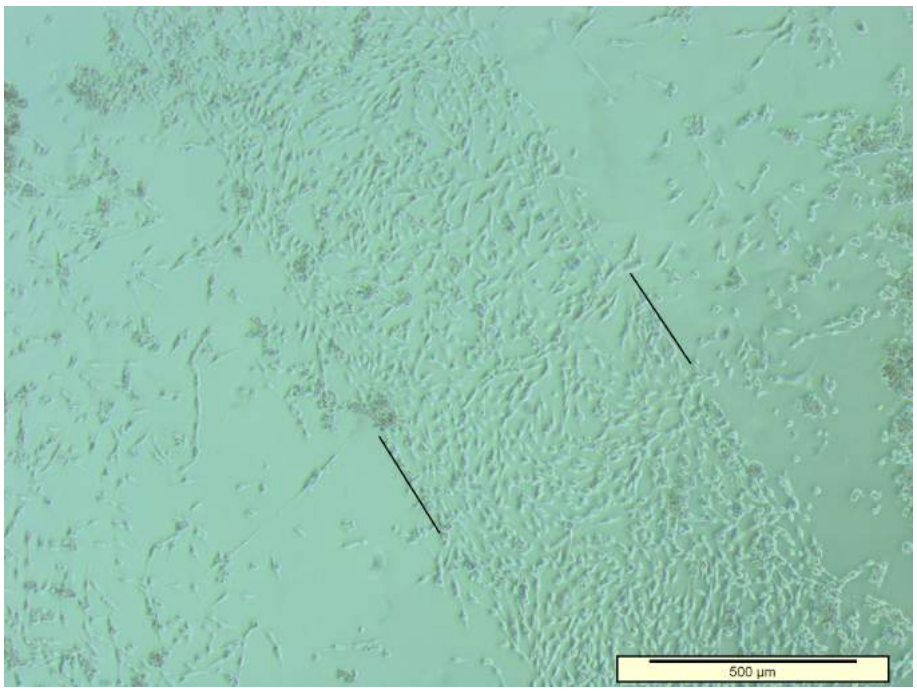

Figure 77: A scratch assay was performed on a 2D culture of C6 glial cells seeded at 1x10^5 cells/well in a 12 well plate. At day 4, the boundaries of where the scratch was performed is indicated by the black lines and is inhabited by cells after culture in a pressurised environment at 135mmHg.

Development of a 3D Migration Assay

Assay Design Specification

The migration assay must meet the following requirements:

- Must be able to maintain cell cultures
- Must allow for 3D migration of cells
- Must not be affected by pressurised environments
- Must replicate a biomimetic migration environment
- Must be able to be sterilised and maintain aseptic conditions

Evaluation of Available Assays

Migration assays describe assays in which the cells move in 2D, while 3D movements are known as invasion assays. The name is due to their popularity among researchers of the migration of cancer cells which are said to "invade" other tissues. Schematic

diagrams of the popular migration assays that were identified are presented in Figure 78.

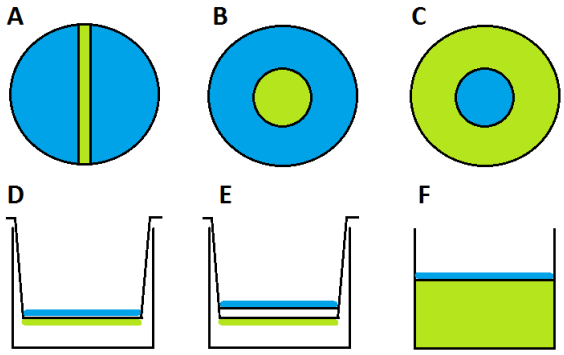

Figure 78: Schematic diagrams of cell migration assays described in the literature. Blue indicates cell seeding area, green indicates area that is investigated for cells. A: plan view of a scratch assay. B: plan view of a cell exclusion zone assay. C: plan view of a fence ring assay. D: side view of a Boyden chamber assay. E: side view of a coated Boyden chamber assay. F: side view of a vertical hydrogel migration assay.

Migration Assays

Scratch Assay

The scratch assay is the simplest and least expensive of the migration assays. A confluent layer of cells was scratched using a pipette tip, which created a stripe devoid of cells. The stripe was then be monitored over time to record the reduction in width as the cells migrated inwards. This was a 2D assay in which the migration could be easily measured. However the width of the stripes were likely to vary from one sample to another due to the hand drawn nature of the stripe, involved damaging the cells proximal to the site and any coatings applied to the tissue culture plastic were likely to be damaged which could inadvertently affect the cells.

Cell Exclusion Zone Assay or Fence Ring Assay

These assays block an area of the well plate (either a central circle of the well or the outer edges, leaving the central circle unblocked) while adherent cells are seeded for a confluent layer. Once the cells are attached, the block is removed and microscopy is used to record the change in size of the central area (i.e. the area devoid of cells or the area only with cells). The results are easily quantifiable by measurement of the central area, and the assay involves no damage of cells or of the well plate surface.

Boyden Chamber Assay

The Boyden chamber assay is the most common migration assay and involves cells seeded on to a porous membrane. A chemoattractant is placed in a well and the membrane is suspended over the well, with media on top. After the elapsed time, the top of the membrane is cleaned and fluorescently labelled, and only cells that have migrated to the underside of the membrane will be stained. The membrane can then be observed through a fluorescent microscope. As this is a popular assay technique, membranes with defined pore sizes for different cell sizes are available, making this assay directly comparable with others.

Invasion Assays

Coated Boyden Chamber Assay

Again, Boyden chambers are the most popular choice for invasion assays. The membrane is coated with a layer of Matrigel (Corning, USA), ontop of which the cells are seeded. Again, the chemoattractant is placed in the well below and the cells are suspended above, and must migrate through both the hydrogel and membrane to be fluorescently tagged on the other side.

Vertical Gel Migration

A thick layer of hydrogel can also be used to study 3D migration, by seeding the cells on top of the hydrogel and tracking their progress through the hydrogel, driven either by chemoattraction or by gravity. This is a much simpler experimental set up as it can be constructed in-house, however fluorescent labelling and confocal microscopy is required to optically section the hydrogel to see cells that have migrated further into the material. The advantage of this assay is that the exact distance of migration can be measured, while the Boyden chamber only give the number of cells that have migrated a set distance. Drawbacks of this method are that media may be unable to reach the centre of thick hydrogels and this could result in the death of migrated cells with no access to nutrients, while hydrogels have to be transferred to glass slides before imaging can take place, potentially disturbing the dimensions of the hydrogel, leading to inaccurate measurements.

Using an invasion assay was identified as the most appropriate assay for this work as it allowed for 3D cell migration. The vertical hydrogel assay was identified as the most suitable as it was the most biomimetic assay. Using an in-house hydrogel

assay was appealing as it was inexpensive and made use of the hydrogels already developed. The main drawback of the vertical hydrogel migration is that it requires both a hydrogel that is transparent enough, and confocal microscopy to be able to examine the cells that have migrated into the hydrogel. As the developed hydrogel is not adequately transparent for this purpose, a novel invasion, or 3D migration assay was developed to negate this problem.

3D Migration Assay Development

A 3D assay was performed using seeded and non-seeded hydrogels. Hydrogels were synthesised using the method described in Section 2.3.3 using phenylenediacetic acid and tartaric acid. Volumes of 200μl hydrogel were cast into the wells of a 24 well plate. C6 glial cells and PC12 neural cell lines were seeded on top of half of the hydrogel samples. After 24 hours incubation, each hydrogel was cut in half vertically, to form two semi-circular samples and then swapped so that a seeded hydrogel half was next to an unseeded half. The hydrogels were cultured in pressurised (135mmHg) and non-pressurised (control) conditions. A pressure of 135mmHg was used for this initial 3D test to ensure that if the cells did have any migratory response to pressure, was more likely to be evidenced in this test rather than one at a lower pressure. After five days culture, hydrogel halves that were previously unseeded were incubated with the live/dead stain, containing calcein AM (green: live cells) and ethidium homodimer (red: dead cells) as described in Section 2.5.1. Images of the fluorescently labelled cells observed in the non-seeded hydrogels are presented in Figure 79. Images of the PC12 cell line in the non-pressurised test within the Ta hydrogel and the pressurised test within the Ph hydrogel are not presented as there were no cells observed. The figures showed that more live C6 glial line cells were present in the unseeded hydrogel that had been cultured under pressure compared to the control, while the difference neuronal cell line is less obvious.

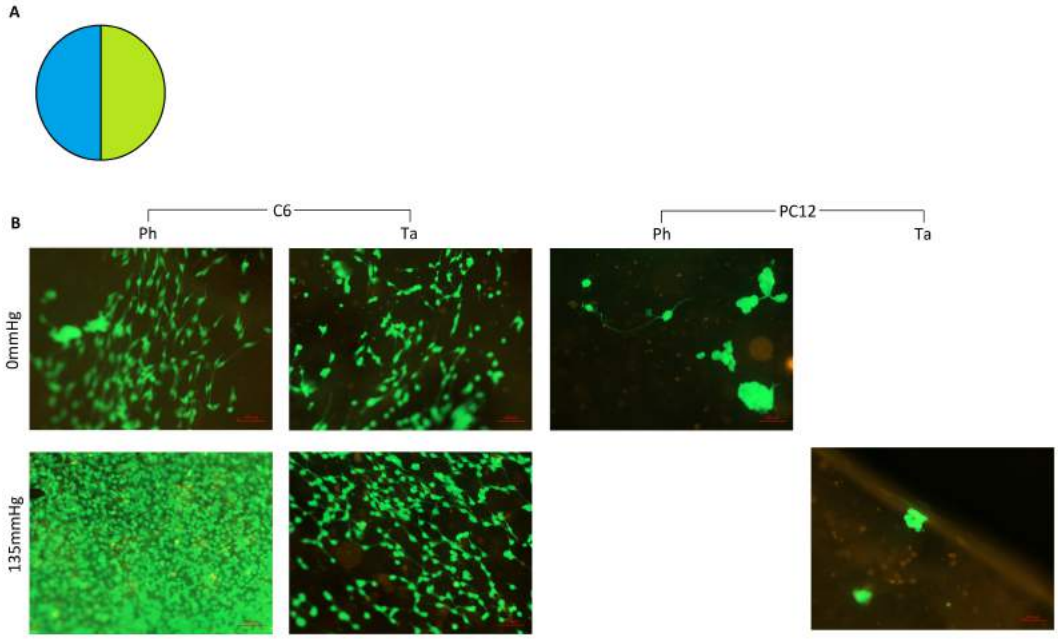

Figure 79: A: Experimental set up of a well (plan view) where a seeded hydrogel (blue) has been placed next to a non-seeded hydrogel (green). B: Live dead staining of unseeded hydrogels at day 5 placed next to hydrogel seeded with cells. Cells stained with calcein AM (green) to identify live cells and ethidium homodimer (red) for dead cells. Image includes hydrogels cultured at atmospheric and 135mmHg pressure, C6 and PC12 cell lines and 1,3-Phenylenediacetic acid (Ph) and Tartaric acid (Ta) hydrogel types as indicated. No cells were found in the non-pressurised PC12 Ta hydrogel or the pressurised PC12 Ph hydrogel, indicating that cell migration had not occurred in these tests. Scale bars represent 100μm.

This test showed a difference in cell number between the two pressure, however this may not have been a true 3D assay, as cells may not have needed to move through the hydrogel to migrate to the unseeded one, it was possible they moved across the surface. A novel 3D migration assay was designed which monitored cell migration through the hydrogel, using layers to physically separate cells that had migrated a larger distance than cells that had not. As each hydrogel layer was relatively thin (approximately 2mm assuming a 24 well plate well area of 0.95cm^2), it also allowed for standard fluorescent microscopy to be used to visualise the cells within the hydrogel, whereas a thicker sample would require confocal microscopy. The stacking of individual hydrogel layers may have also aided media flow to cells in lower layers, as there may be small spaces between the layers, forming channels.

This 3D assay was performed, again using seeded and non-seeded hydrogels synthesised using phenylenediacetic acid and tartaric acid as described in Section 2.3.3. Hydrogels of 200μl volumes were cast into the wells of a 24 well plate. The hydrogels were incubated for 24 hours to allow cell attachment. At day 1 the hydrogels were layered so that a seeded hydrogel was on top of two non-seeded hydrogels. Half of the hydrogels were cultured at a pressure of 135mmHg and half were cultured at atmospheric pressure. At day 5 the top two layers of hydrogel were removed and the bottom layer was stained with live/dead as described in Section 2.5.1. The results are presented in Figure 80 and show the survival of the cells is good, with few dead cells observed in the lowest layer of the hydrogel, even when cultured under an increased pressure. As may be seen, there were increased numbers of live C6 cells observed and lower numbers of live PC12 cells in the pressurised cultures compared to their respective controls. Clumping of the PC12 line cells into discrete areas was also observed.

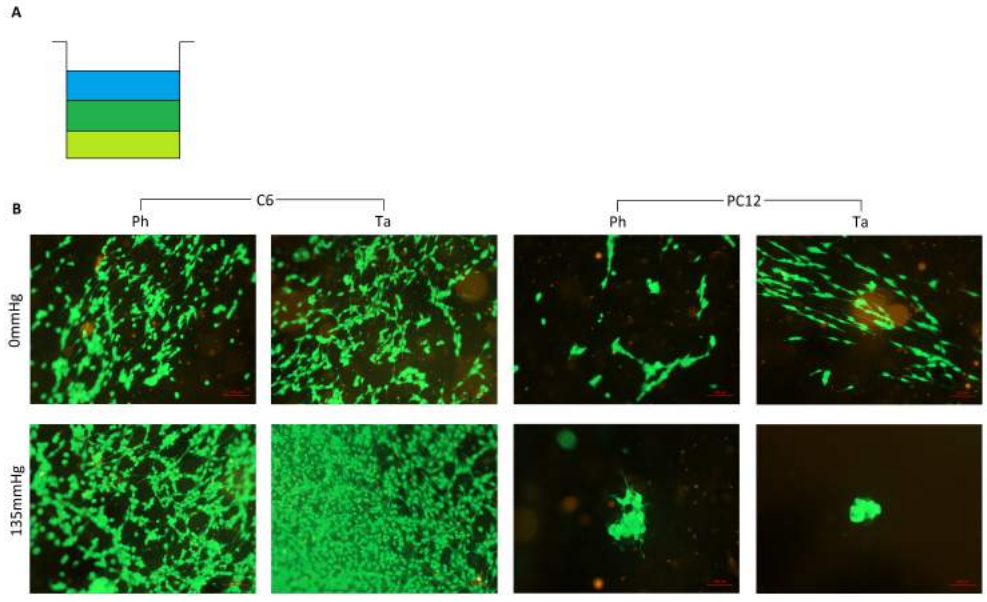

Figure 80: A: Experimental set up of a well (side view) where a seeded hydrogel (blue) has been placed on top of two non-seeded hydrogels (dark and light green). B: Live dead staining of unseeded hydrogels at day 5 placed below a cell seeded hydrogel and a non-seeded hydrogel (i.e. the light green hydrogel depicted in A). Cells stained with calcein AM (green) to identify live cells and ethidium homodimer (red) for dead cells. Image includes hydrogels cultured at atmospheric and 135mmHg pressure, C6 and PC12 cell lines and 1,3-Phenylenediacetic acid (Ph) and Tartaric acid (Ta) hydrogel types as indicated. Scale bars represent 100μm.

The information collected during the development of the migration model showed that the cells were able to migrate in 3D through the hydrogel and further that this migration appeared to be affected by pressure. While 135mmHg pressure has been observed in pathology during the secondary injury phase of a trauma, due to the positive result seen by this test, the effect of Lundberg A waves specifically were chosen for further investigation.

Final Design of 3D Migration Assay

A layered 3D assay was performed using Ph hydrogels synthesised as described in Section 2.3.3. Hydrogels of volumes of 200μl were synthesised in 48 well plate wells and were sterilised by incubation in 70% (v/v) ethanol and washed with PBS as described in Section 3.3.1. Three different pressures were applied: no pressure, 25mmHg and 50mmHg. These pressures were chosen to be above and below the 40mmHg "cut off" that defines Lundberg A waves. After 4 days culture each of the three hydrogel layers were stained live/dead as described in Section 2.5.1. Images of each layer were captured using fluorescent microscopy, presented in Figure 81.

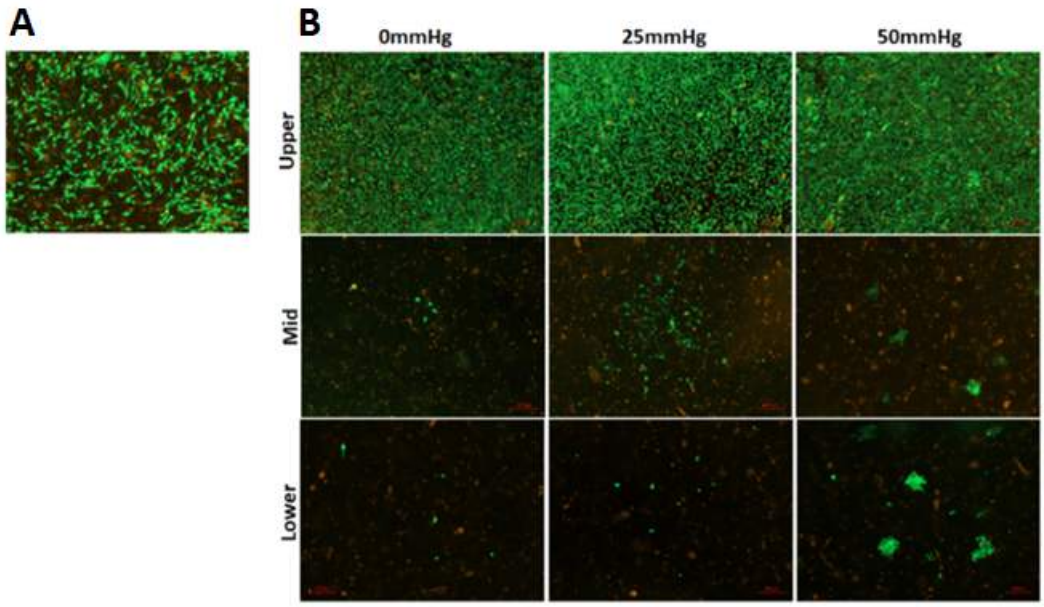

Figure 81: Fluorescent microscopy of representative samples of C6 cells stained with calcein AM (green) to identify live cells and ethidium homodimer (red) for dead cells. A: Cell population of cell-seeded hydrogel on day 1, before pressurisation. B: Upper cell-seeded hydrogels and mid and lower non-seeded hydrogels on day 4 after incubation under 0, 25 and 50mmHg pressure as indicated. Scale bars represent 100μm.

For mid and lower layers, all live cells in the image were counted. The results of this cell count are presented in Figure 82, and the Kruskal-Wallis statistical test (presented in Table 45 in Appendix 1, Section 7.1) suggested that a 50mmHg increase of pressure increased cell migration, but this was not significant.

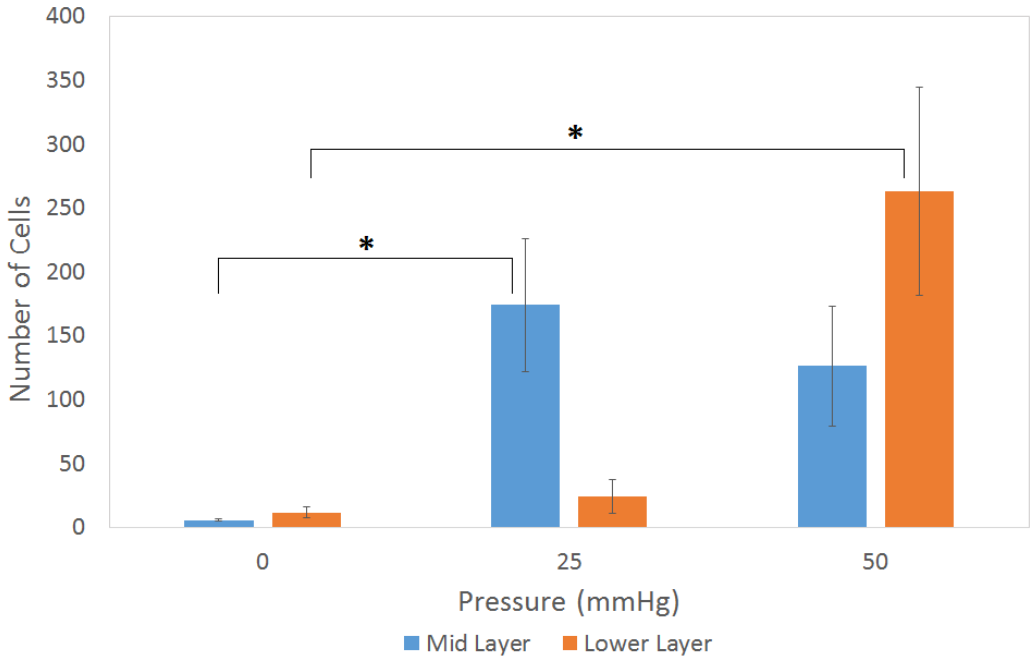

*Figure 82: Average cell numbers of mid and lower hydrogels on day 4 as determined by visual analysis. Error bars represent standard error, N=3. * signifies a significant difference in medians ($p<0.05$).*

The Dunn post-hoc test performed is summarised in Table 46 in Appendix 1, Section 7.1. Comparing the cell counts in the lower layers, the Dunn test indicated that the highest cell count at 50mmHg was significantly different ($p<0.05$) compared to 0mmHg. The cell count in the mid layer was highest when cultured at 25mmHg, and was found to be significantly different ($p<0.05$) to that cultured at 0mmHg. This suggests that increased pressure encouraged cell migration.

Design of Pressure Model

Following successful development and testing of a method to create a pressurised environment, a suitable pressure model to be applied to the cells was determined.

ICP after injury can present several distinct waveforms, as characterised by Lundberg (1960). 'A' waves have been regarded as the most clinically significant wave-

form, the occurrence of these is associated with a better patient survival rate (Cox et al., 2014). 'A' waves are described as a sharp rise in pressure to over 40mmHg which is sustained for over 5 minutes (North and Reilly, 1990), however the pressure can reach as high as 80mmHg and can last up to 30 minutes (Cox et al., 2014). After 30 minutes, cerebral ischaemia can occur and so becomes detrimental to the patient's health. 'B' and 'C' waves are regarded as less clinically significant (North and Reilly, 1990).

Given that the occurrence of 'A' waves have been noted to indicate a reduced chance of patient mortality (Cox et al., 2014), the typical pressures recorded during 'A' waves became the focus of this study and the effect of this on the cells was examined. Three pressures of interest were chosen, 10mmHg - normal ICP as a negative control, 30mmHg - raised ICP but lower than the criteria for 'A' wave classification and 50mmHg - raised ICP, at a level for 'A' wave classification.

While it has been recorded that 'A' waves are a predictor of improved patient outcome only if they last less than 30-40 minutes, this is because the pressure causes blood vessel walls to collapse, cutting off the supply of oxygen to the brain and creating cerebral ischaemia. As this study was to be conducted *in vitro*, the *in vivo* effects of ischaemia were not considered, and so the pressure could be maintained for as long as necessary. A constant pressure model was chosen to allow the direct effects of certain pressure levels to be ascertained.

5.3.2 Response of CNS Cells to the Raised Pressure Model

Atmospheric pressure was measured once per day for the duration of pressure experiments using a barometer. The barometer was placed in the cell culture room containing the pressurised modular incubators. The readings of atmospheric pressure are presented in Figure 83 and show a variation of up to 16.3mmHg (approximately 2%) over the course of the experiment.

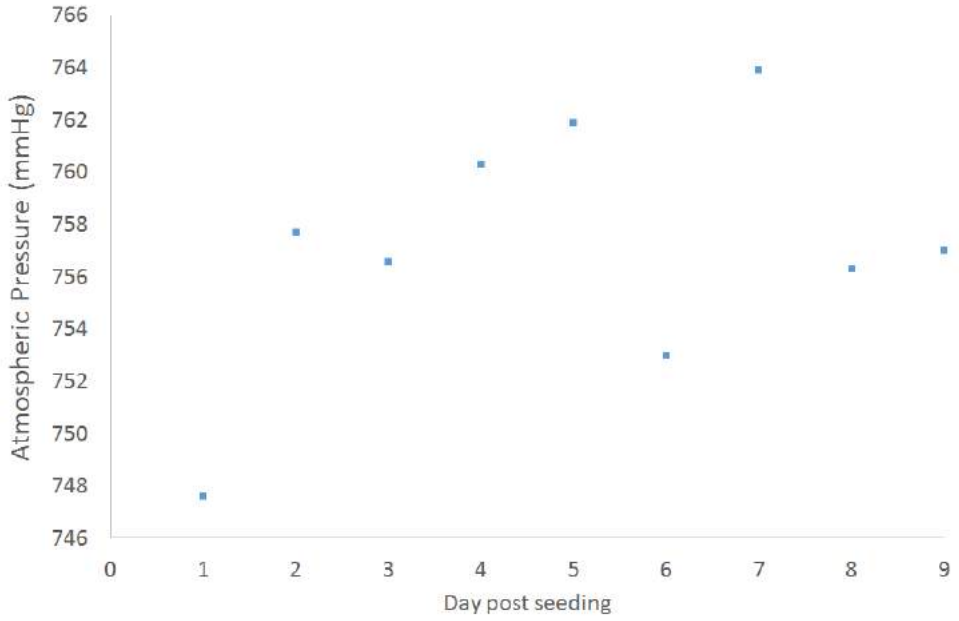

Figure 83: Atmospheric pressure during the course of the experiment as measured by barometer.

The gauge pressure of each modular incubator was measured using a manometer. The pressure was measured in mmHg while the incubator was filled with pressurised air containing 5% (v/v) CO_2, and one hour later after incubation at 37°C. On days where the media was not changed, the pressure was checked once per day and altered as necessary.

Specific Objectives

1. Culture the cells in 2D and in the 3D migration assay under various pressures, using the pressure model design.
2. Examine the proliferation, migration and differentiation of neural stem cells in direct response to raised hydrostatic pressure.

Determination of Cell Viability

To assess the viability of the CB660 neural stem cell line under pressure, each variable had three repeats and the assays were performed at day 1 and 5. Cells were cultured in "stem" Neurocult proliferation medium or "diff" Neurocult differentiation medium, prepared as described in Table 13. A sample of cells "eth" were cultured in Neurocult proliferation medium with 50% (v/v) ethanol. Cells were cultured in 50% (v/v) ethanol for use as controls. The results of the CyQuant and ATPlite assays are presented in Figures 84 and 85. While the "eth" group worked as a control for the ATPlite assay, it produced high readings in the CyQuant assay, and so this assay may be invalid.

Using ANOVA or Welch's statistical analysis, the variance of means between days and pressures for each media condition was compared. The p-values calculated using this analysis are presented in Table 45 in Appendix 1, Section 7.1 while the Games-Howell post-hoc test is presented in Table 46. Statistical analysis of the CyQuant assay indicated no significant difference in readings between the three pressures. The readings for the ATPlite assay were significantly ($p<0.05$) higher for cells cultured in differentiation media at 30mmHg than at 50mmHg.

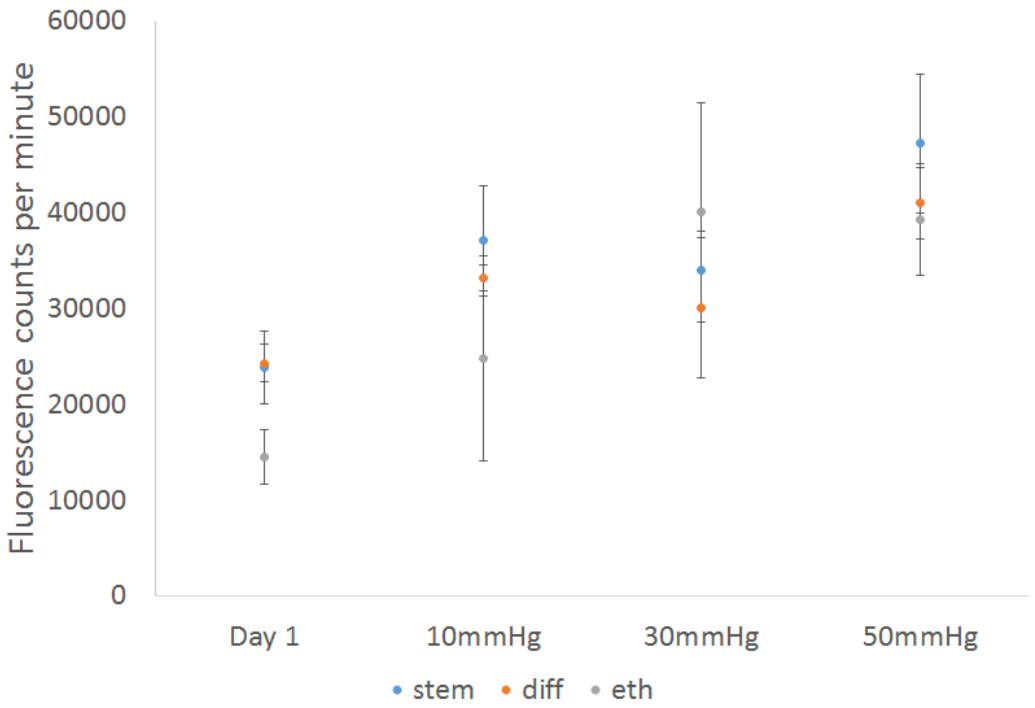

Figure 84: CyQuant fluorescence counts per minute of neural stem cells at days 1 and 5. Cells at day 5 had been cultured for 4 days under 10, 30 or 50mmHg pressure, as indicated. Error bars represent standard error, n=3.

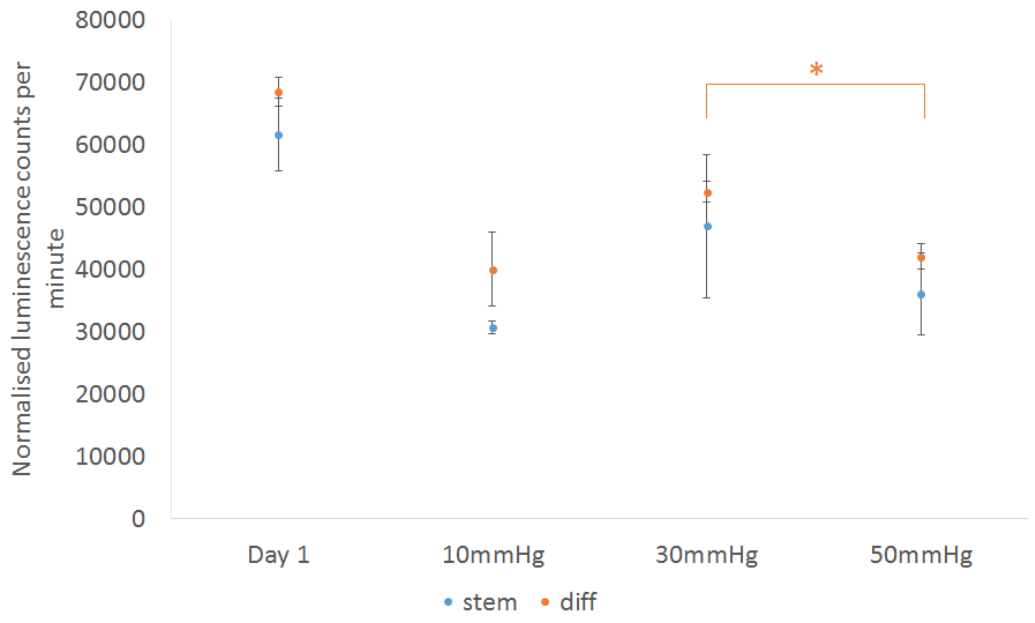

*Figure 85: ATPlite luminescence counts per minute of neural stem cells at days 1 and 5. Cells at day 5 had been cultured for 4 days under 10, 30 or 50mmHg pressure, as indicated. Error bars represent standard error, n=3. * indicates a significant difference in means ($p<0.05$) for cells cultured in differentiation media.*

Determination of 3D Cellular Migration

To assess the migration of neural cells under pressure, 200μl Ph hydrogels were syntheised in 48 well plate wells which were sterilised in ethanol, washed in PBS and pre-soaked in Neurocult proliferation media, prepared as described in Table 13. CB660 cells were seeded using proliferation media in the upper layers at a density of 1x10^5 cells/ml, based on the findings presented in Section 3.5.4. At day 1 the layers were placed on top of each other. The hydrogel layers (upper, mid and lower) were stained at day 5 using calcein AM (green for live cells) and ethidium homodimer (red for dead cells). Three images per hydrogel layer were taken using a fluorescent confocal microscope as described in Figure 86. The thickness of the hydrogel layer was calculated by recording the z-position of the microscope where the cells became out of focus. This information was used to take images of the cells in the centre of each hydrogel. The average thickness of each layer was found to be 116μm $\pm$10.52.

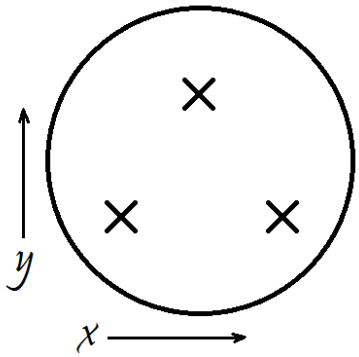

Figure 86: Imaging strategy with three fields of view for each cell-seeded hydrogel sample. Each image was taken at a depth half way between the top and bottom of the hydrogel, as determined by the Z position of the microscope when the cells became out of focus. The x and y positioning of the hydrogel was determined and images were taken in the centre, left and right areas of the hydrogel, as shown.

Live cells were counted using ImageJ software (Schneider et al., 2012). After setting the scale using the scale bar, the smooth tool was used to reduce noise. The image was converted to 8-bit and the auto local threshold tool was used to create a binary image. The particles were then analysed, particles with an area of less than 5μm^2 were assumed to be out of focus and were not counted. An example of a binary and counted cell image is presented in Figure 87.

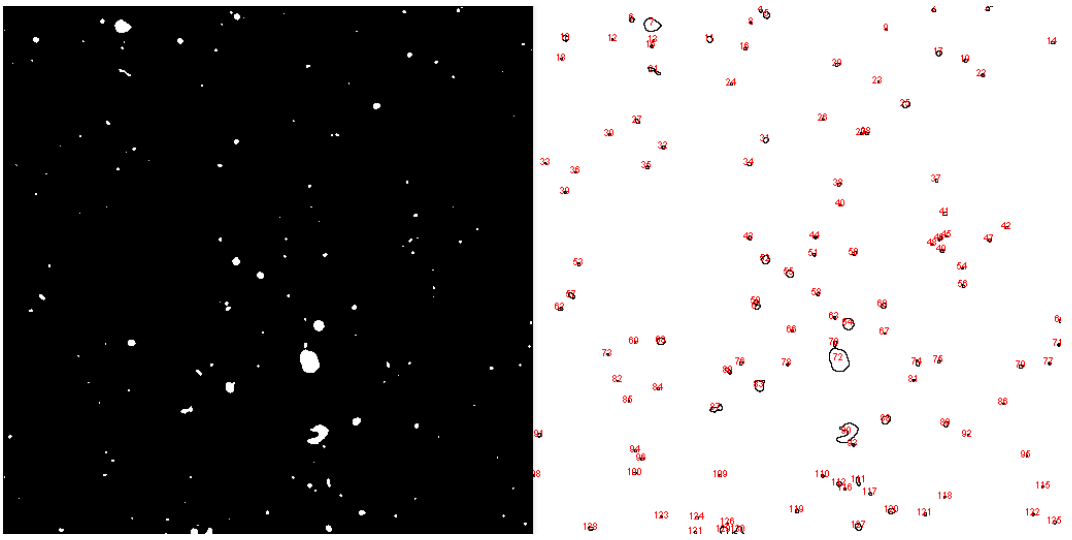

Figure 87: An example of a binary image of cells, and the cell count performed by ImageJ software.

The average counts are displayed in Figure 88. The largest variation in cell counts between pressures was found to be in the lower layer between 10 to 30mmHg, where cell numbers reduced by 61.5%. The decrease in numbers at the lower layer between 10 and 50mmHg was 55.8%.

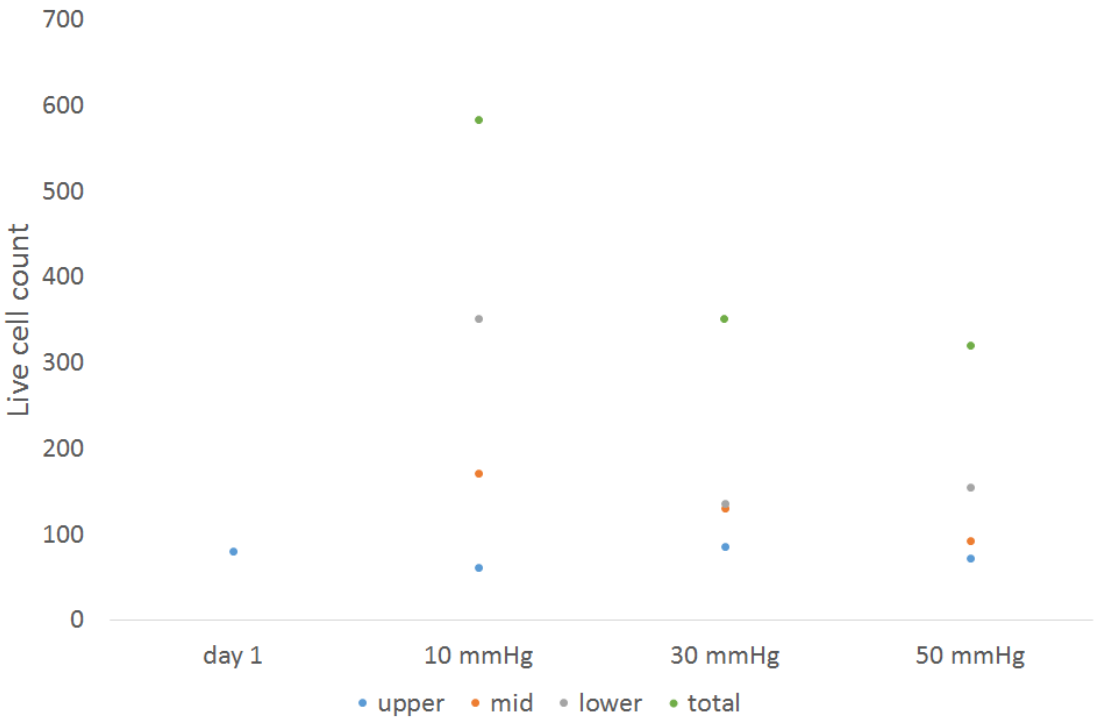

Figure 88: Average counts of live cells for the upper layer for day 1 and upper, mid and lower layers for day 5, after treatment with 10mmHg, 30mmHg or 50mmHg as indicated, n=1. Scale bars removed to prevent the inclusion of these in the analysis.

Determination of Cell Phenotype

Individual cells were identified by a blue nucleus, and the colour staining around each nucleus was recorded. Cells with green staining (CD133) were recorded as stem cells, cells with red staining (PSA-NCAM) were recorded as neuronal progenitors and cells with no staining were recorded as glial progenitors, however these lineages are assumptions based on the protein expressions. A representative image is presented in Figure 89. The cell counts from the five images were then averaged. The proportions of each cell type are presented in Figure 90.

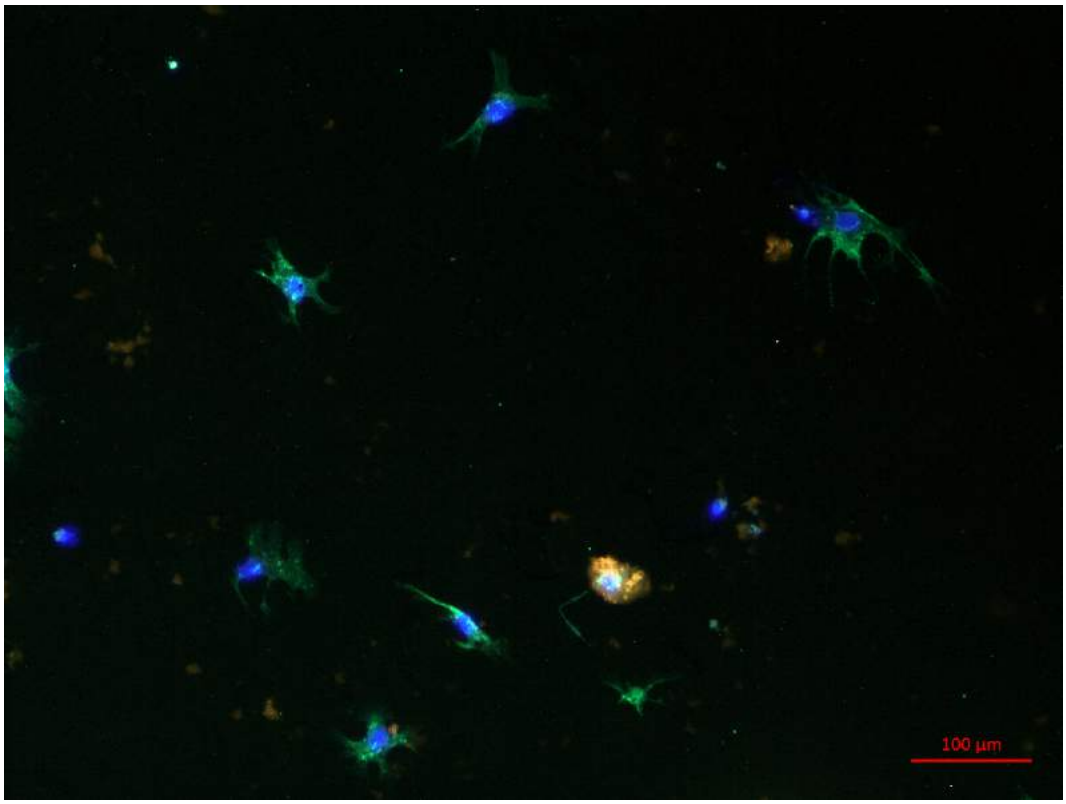

Figure 89: Representative image of cells cultured under 10mmHg at day 10. The nuclei of the cells in blue, CD133 (stem) expression in green and PSA-NCAM (neuronal progenitor) expression in red. Microscope wavelengths used were 595nm (red) 518nm (green) and 421nm (blue).

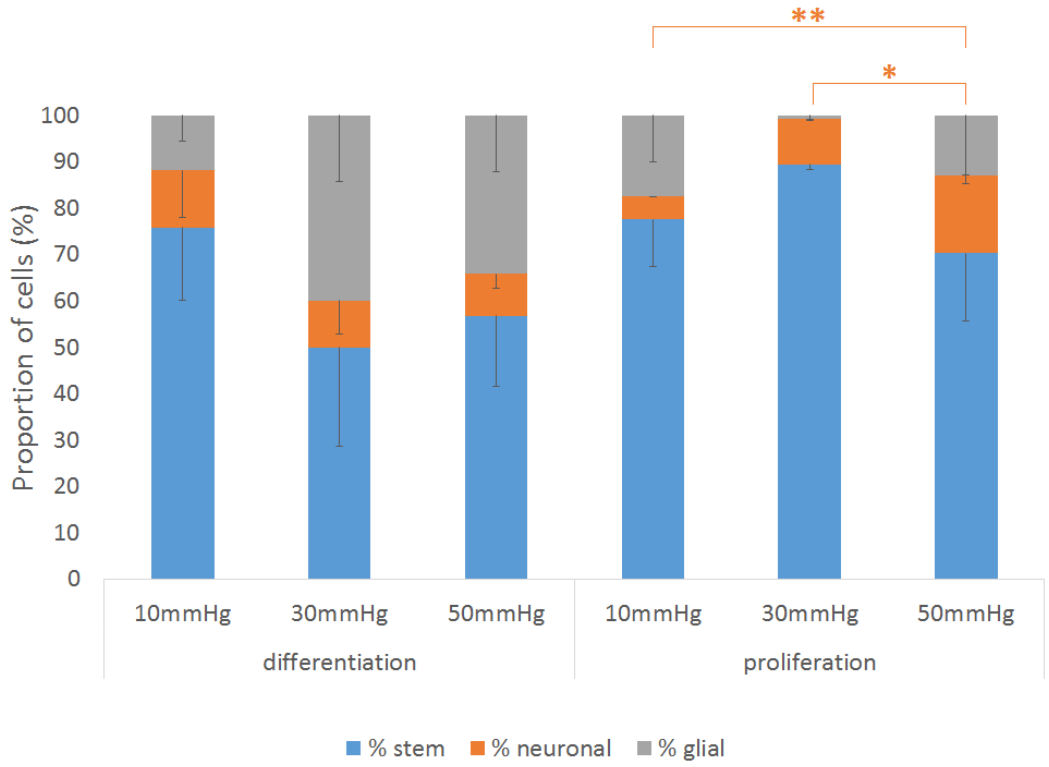

*Figure 90: Average proportions of cells cultured in differentiation or proliferation media and under 10, 30 or 50mmHg pressure. Error bars represent standard error (only negative error displayed for clarity), n=2. * signifies a statistical difference in means ($p<0.05$) and ** signifies a highly significant difference in means ($p<0.01$) of neuronal proportions.*

The proportions of cells cultured in proliferation media that were expressing a neuronal progenitor phenotype were found to be highly statistically different ($p<0.01$). Full results are presented in Table 45 in Appendix 1, Section 7.1. A Tukey's post-hoc analysis of this was conducted, summarised in Table 46, finding that the difference between 10 and 50mmHg was highly different ($p<0.01$), while the difference between 30 and 50mmHg was significantly different ($p<0.05$). There were no significant differences in the proportions of cells cultured in differentiation medium. These findings suggest that an increase in pressure may induce stem cells to differentiate to the neuronal lineage when cultured in proliferation medium.

Characterisation of Projections

Proportions of Stem Cells With Projections

The proportion of cells displaying visible projections was counted manually, the results are presented in Figure 91. The difference between pressures of proportions of cells with projections when cultured in differentiation media was found to be significantly different ($p<0.05$), the results are presented in Table 45 in Appendix 1, Section 7.1. The Tukey post-hoc test, presented in Table 46, found that the proportions of cells was significantly higher at 10mmHg compared with 50mmHg ($p<0.05$). No significant differences were observed in the cells cultured in proliferation media.

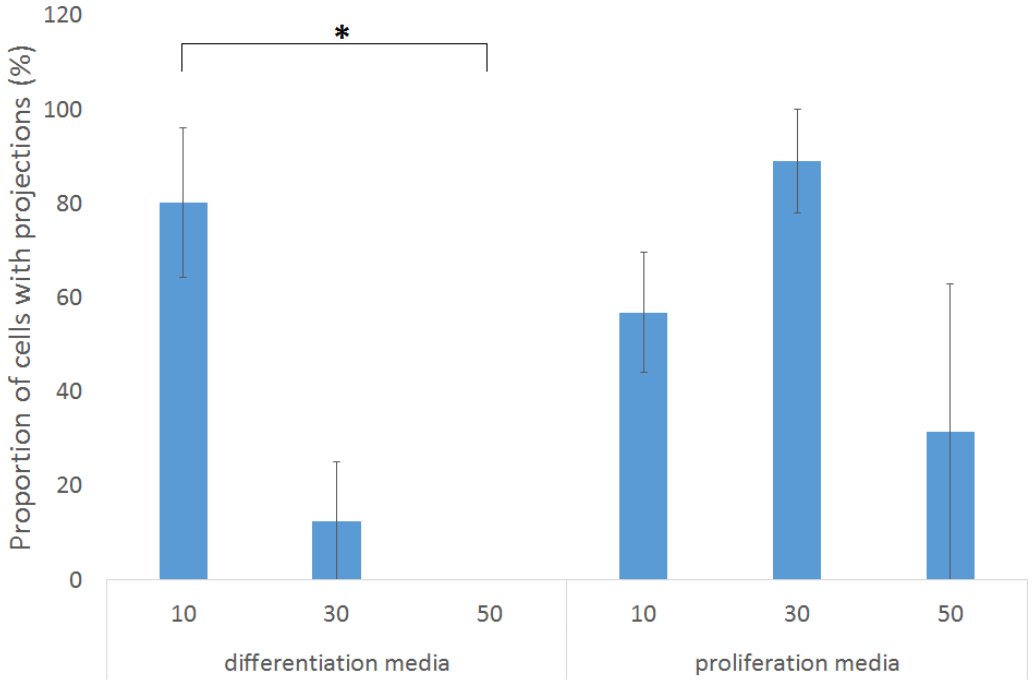

*Figure 91: Average proportions of stem cells with projections cultured in proliferation or differentiation media and under 10, 30 or 50mmHg pressure. Error bars represent standard error, n=2. * signifies a statistical difference in means ($p<0.05$).*

Average Number of Projections Per Cell

For cells with projections, the number of projections per cell were counted and averaged. The results of which are presented in Figure 92. Statistical analysis was performed using a Kruskal-Wallis test, the results are presented in Table 45 in Appendix 1, Section 7.1, finding no significant differences ($p>0.1$) in the number of projections per cell at the different pressures in either the proliferation or differentiation media.

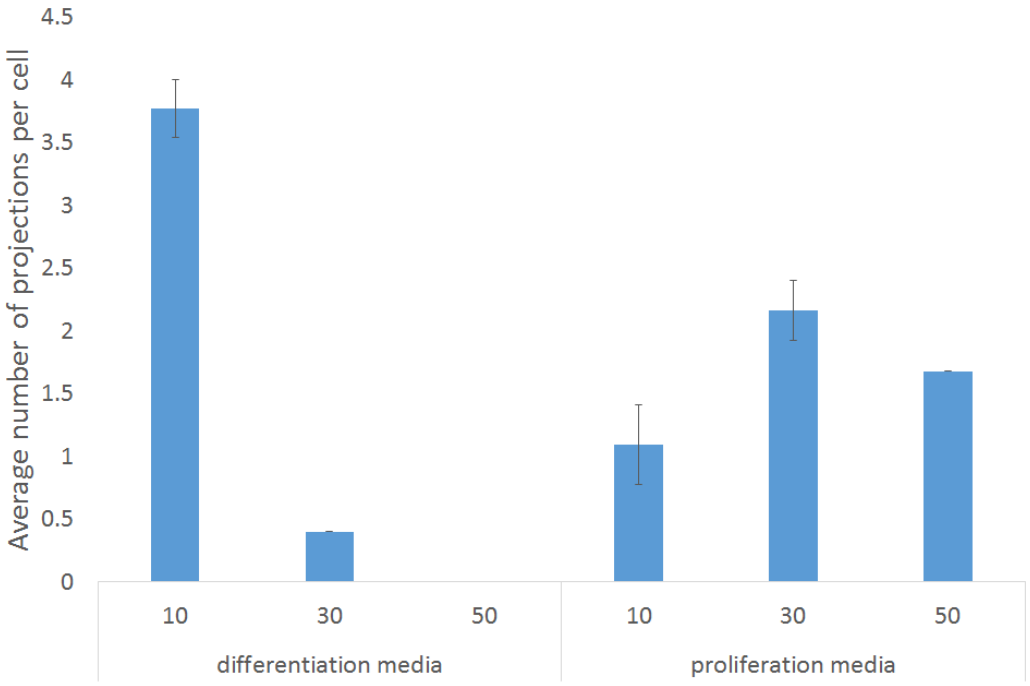

Figure 92: Average number of projections per cell cultured in proliferation or differentiation media and under 10, 30 or 50mmHg pressure. Error bars represent standard error, n=2.

Average Length of Projections

The length of each projection was measured using NeuronJ (Meijering et al., 2004), the average lengths are presented in Figure 93. As no projections were observed for cells cultured in differentiation media, at 50mmHg, this sample was not included in the comparison. Statistical analysis was performed using an ANOVA test. The results are presented in Table 45 in Appendix 1, Section 7.1 and found no significant differences ($p>0.1$) in the average length of projections in either media at any of the pressure values, indicating that the pressure did not affect the length of neurites significantly.

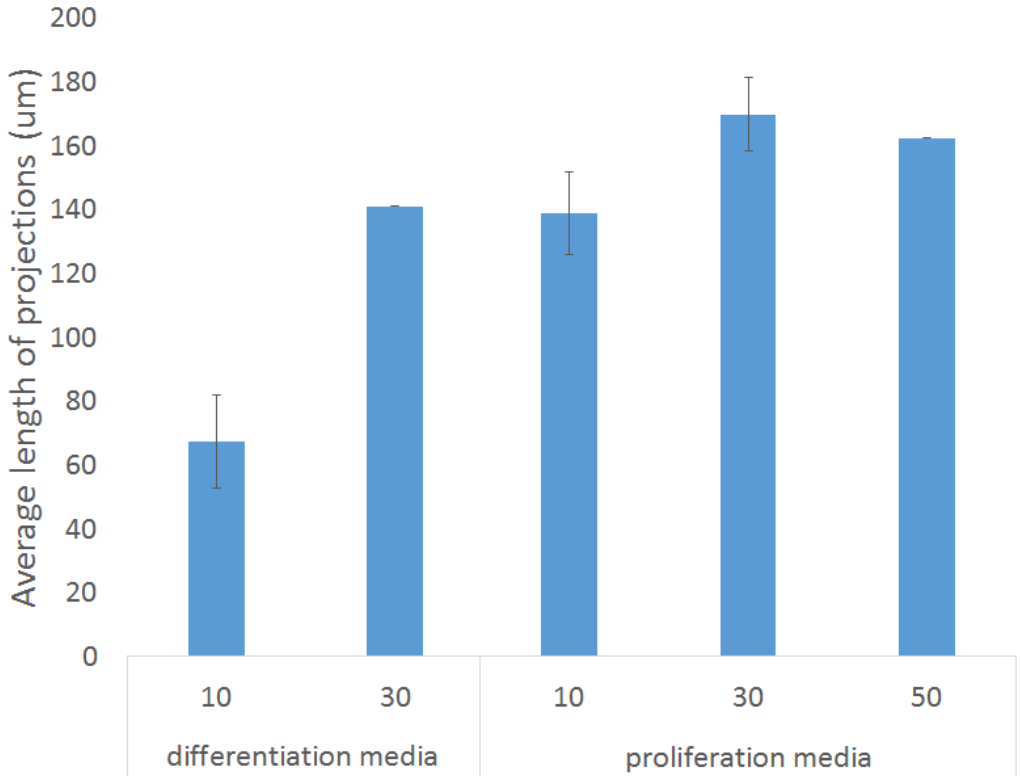

Figure 93: Average length of projections per cell cultured in proliferation or differentiation media and under 10, 30 or 50mmHg pressure. Projection length for cell numbers cultured in differentiation media at 50mmHg not displayed as no cells under these conditions expressed projections. Error bars represent standard error, n=2.

5.4 Discussion

The aims of this chapter were to develop an appropriate model for raised ICP such as that observed in secondary injury after a traumatic event, to develop a 3D migration model that was able to confirm migration of the cells, and to assess the viability, phenotype and migration of neural stem cells in a raised pressure environment.

5.4.1 Development of an *In Vitro* Model for Secondary Injury

A pressure model was designed that examined the difference in cellular activities in three key pressure scenarios: at normal ICP, at raised pressure under the 40mmHg threshold identified for Lundberg "A" waves, and at raised pressure over the threshold. The length of the application of the pressure was not included in the present study, however this may have limited the clinical relevance of the study. *In vivo*, extended periods of high pressure, i.e. over 30 minutes, indicate an increased likelihood of patient mortality, however this is thought to be because long periods of high pressure create cerebral ischaemia (Cox et al., 2014), which is not of consequence *in vitro*.

Published 3D invasion assays were evaluated, including the coated Boyden chamber and the vertical gel migration assay. The vertical gel migration assay was identified as the most appropriate for this work due to its biomimetic qualities, however two main concerns were recognised. Firstly, the hydrogel that had been synthesised as described in previous chapters lacked the level of transparency to allow adequate monitoring of cells cultured within a thicker hydrogel. Secondly, the flow of media within the centre of the hydrogel was assumed to be limited, which could negatively affect cell survival. A novel, layered, 3D invasion assay was developed that both took advantage of the biomimetic environment of a 3D hydrogel, while allowing the migrated cells to be separated into layers. This meant that the cells could more easily be observed and that the media could flow between the layers more readily. The results of the development study suggested that for C6 glial cells, increasing pressure induced cell migration, as significantly more cells ($p<0.05$) migrated to the lower layer when cultured under 50mmHg, compared to the 0mmHg pressure environment.

A recurring characteristic of the cells was identified; the migrated cells tended to be clustered together in "pockets". There are numerous ways in which this could have occurred. For example:

- One cell migrated, and then proliferated once it had reached the lower hydrogel level, causing its descendants to be clustered around it.
- The migration of one cell caused a local fluid flow which induced bleb formation in other neighbouring cells, polarised in the direction of the migrating cell's recently vacated space. As the initial cell continued to migrate, the neighbouring cells followed in its path.
- Inconsistencies in the hydrogel matrix, such as larger pores or a collection of collagen fibrils orientated through the depth of the hydrogel could have meant that the path through the hydrogel happened to be conducive to cell migration at this point compared to other areas.

This effect was also noted by Choi et al. (2014) who found melanocytes that migrated through a 3D Matrigel hydrogel became clustered. Using time lapse footage, noted that the melanocytes had become clustered before migrating. In vivo, Lammermann (2016) noted that neutrophils can move into clusters when migrating through the interstitial tissue.

5.4.2 Effect of Pressure on Stem Cells

To find the effect of raised pressure on the viability of neural stem cells, the proliferation of CB660 stem cells was measured by CyQuant and ATPlite assays, which measure amount of DNA or free ATP present, respectively. A significantly ($p<0.05$) higher reading was found for cells cultured in differentiation media at 30mmHg compared to 50mmHg by the ATPlite assay while no significant difference was observed in the CyQuant assay readings. The ATPlite assay measures adenosine triphosphate (ATP) production which can become increased when cells are stressed, independently of cell number, while the CyQuant assay measures DNA content, which

should always be proportional to cell number. The ATPlite assay is also highly sensitive while it appears the CyQuant assay is less so in 3D. The significant difference in the results of the ATPlite assay may indicate that cell proliferation was higher at 30mmHg compared to at 50mmHg, or alternatively they may indicate that the cells were most stressed at this pressure level, which increased their ATP production. Indeed, the lack of significant difference in the CyQuant readings may indicate the latter. In either case, the overall activity of the cells cultured at 30mmHg was increased compared to at 50mmHg.

It was also noted however that the control sample of cells cultured in 50% (v/v) ethanol did not produce a negative reading for the CyQuant assay, and was indeed higher than the reading for the cells at 30mmHg and therefore the CyQuant assay experiment was invalid. A more suitable control should be therefore established for this assay, however this was unable to be completed within the resource limits for the present study. Migration was found to decrease with increasing pressure, with markedly more cells found in the mid and lower layers cultured at 10mmHg compared to the higher pressures, however statistical analysis was unable to be performed due to the low sample size.

The phenotype of cells was measured at day 10 as Sun et al. (2008) had noted that the expression of the CD133 (neural stem) and PSA-NCAM (neuronal progenitor) markers changed between weeks one and two for differentiating CB660 cells. In the present study, the expression of PSA-NCAM when cultured in proliferation media was found to decrease with increasing pressure. At 10mmHg, there were significantly more cells expressing PSA-NCAM counted compared to at 50mmHg and more compared to at 30mmHg. This is summarised in Table 40. A significantly greater ($p<0.05$) of the cells expressed projections when compared to the number of cells cultured at 50mmHg. The number of projections per cell and the average length of projections was not significantly different at the different pressures or in the different media types.

Table 40: Change in cell type proportions between pressures and significance.

		Mean change			
Media type	Cell type	10-30mmHg	Sig.	30-50mmHg	Sig.
Differentiation	Stem	↓	$p>0.05$	↑	$p>0.05$
	Neuronal	↓	$p>0.05$	↓	$p>0.05$
	Glial	↑	$p>0.05$	↓	$p>0.05$
Proliferation	Stem	↑	$p>0.05$	↓	$p>0.05$
	Neuronal	↑	$p<0.01$	↑	$p<0.05$
	Glial	↓	$p>0.05$	↓	$p>0.05$

These results suggest that increased pressure may inhibit many stem cell activities that are important for tissue repair, as both proliferation, migration and numbers of cells with projections were all observed to be reduced at higher pressures, under certain media conditions. This effect may be due to the formation of these activities being initiated by blebbing, which requires a higher internal pressure compared to external (Driscoll and Danuser, 2015). To postulate an explanation, as the external pressure increases, the cell may find it more difficult to generate an internal pressure high enough for bleb formation, preventing stem cell proliferation, migration and the formation of projections (Charras and Paluch, 2008). The pressure may therefore directly inhibit some stem cell repair activities during the secondary injury, or primary repair phase. PSA-NCAM expression was found to be highly significantly increased with increasing pressure for stem cells cultured in proliferation media, comparing 10 to 50mmHg.

With regards to published literature on the effect of pressure on CNS cells, it appears only glial cells have so far been studied. For example, studies of glaucoma performed by Lei et al. (2011) and Salvador-Silva et al. (2004) investigated the effect of 7.4mmHg on the migration of astrocytes in culture. Lei et al. (2011) found no increase in migration, while Salvador-Silva et al. (2004) found a 38% increase in migration compared to a control group at 1.1mmHg. The functionality of retinal glial cells was found to be improved *in vitro* at 40 and 60mmHg compared to 0mmHg by Yu et al. (2011) who studied their production of glutamine synthase. The findings in the literature of increased migration and activity of glial cells under pressure

therefore correlates well with the findings of the present study using glial C6 cells.

In terms of the effect of pressure on stem cells, Hess et al. (2010) and Zhao et al. (2015) have studied human and rat mesenchymal stem cells (respectively) under pressure, finding that increased pressure (300-375kPa and 90kPa, or 2250-2812mmHg and 675mmHg, respectively) was able to directly stimulate the cells to both proliferate and undergo differentiation to both osteogenic and chondrogenic lineages. Becquart et al. (2016) have studied the effect of cyclic hydrostatic pressure on human mesenchymal stem cells, using 10, 50, 75 or 100kPa pressures (75, 375, 563, 750mmHg respectively) at 2Hz, for 30 minutes. For cells cultured under 50kPa, the upregulation of several genes involved in various aspects of the tissue healing process was observed. While the pressures used in these studies were higher than in the present study, the findings that an application of pressure can directly affect the activities of cells correlates with the observations made in this study of PSA-NCAM upregulation, which may indicate neuronal differentiation is increased with increasing pressure.

5.4.3 Conclusion

A novel 3D invasion assay was developed that had the advantage of allowing for 3D biomimetic migration to occur, while maintaining the opportunity to visualise the cells in thin layers. It also included a larger surface area of hydrogel compared to the vertical gel migration assay, which provided a greater opportunity for the flow of nutrients into and out of the hydrogel. The main limitation of this assay was the potential damage caused to cells when the hydrogel layers were transferred between wells both at the start and end of the experiment.

It was observed that increased pressure generally diminished the activities of the stem cells, including their migration, proliferation and formation of projections. This could potentially be caused by limiting the cell's ability to form blebs which are known to be instrumental in cell division and migration. This indicates that raised intracranial pressure *in vivo* may have a direct effect on the stem cells that line the ventricles as *in vitro* their activities appear to be limited as pressure increases. In contrast, the preliminary studies using a glial cell line found pressure to increase the

migratory abilities, suggesting the pressure induced these cells to be more active.

Again, a major limitation of the studies performed on the CB660 stem cell line was the low sample size, as only 1 or 2 repeats were performed. This was due to the slow proliferation of the stem cells, however means that the results presented in this study should be regarded with caution.

6 Discussion

Damage to the central nervous system (CNS), especially during events such as traumatic brain injury (TBI), is extremely debilitating and therefore can affect not only the patient but the loved ones they come to be reliant on. The tissue is notoriously poor at repairing itself and the role of the stem cells in the repair process is not well documented. It is known that the Lundberg A waveform of intracranial hypertension is a predictor of improved patient outcome. The waveform is characterised by a rise in pressure to over 40mmHg for between 5 and 30 minutes before a return to normal intracranial pressure (ICP) levels or 5-15mmHg. The reason behind this correlation is unknown and it was hypothesised that the pressure directly influences the activities of CNS cells. In addition, the ability to direct the differentiation of stem cells through their mechanosensing abilities was discovered by Engler et al. (2006), however this study and many subsequent studies, particularly the 3D neural studies that the present research focussed on (Banerjee et al., 2009; Her et al., 2013; Bozza et al., 2014), were all noted to change the concentrations of the components of the hydrogels used in the studies, which has been found (when examined) to change other properties of the hydrogels, most notably the pore size (Her et al., 2013). It was hypothesised that the elastic modulus could affect the activities of neural stem cells independently of pore size.

The research that was conducted for this project has included the development of materials, cells, assays and analysis and some insight has been gained into how the activities of neural stem cells can be affected by their physical surroundings. The results have indicated that pore size may be an important factor in the mechanosensitive abilities of stem cells, and that raised intracranial pressure may have a direct effect on the cellular repair process in the CNS. As will be discussed, many of the results presented were extremely limited by low repeat numbers, which was caused by slow proliferation of the CB660 cell line. With extra resources such as time and materials, the future work to be carried out must include repetitions of the experiments carried out here to raise the power of the studies.

6.1 Summary

New materials and methods were developed in this project to contribute to the *in vitro* models of extracellular matrix (ECM) and ICP. Studies of the effects these models had on stem cells were also conducted. Naturally there were limitations to these studies, as with any model.

A hydrogel system was developed for this research that allowed modification of the elastic modulus of the material through changing the crosslinker type. Two suitable and available systems were identified and evaluated using a decision matrix. The decision matrix was effective as it provided the opportunity to weight the important attributes accordingly and allowed the two systems to be more effectively compared. The results of this analysis showed that the chemically crosslinked hydrogels were most suitable for this project as they had an elastic modulus closer to the biomimetic target and were more easily and quickly synthesised than the UV-crosslinked hydrogels.

The main drawback of the hydrogels later became apparent when multiple batches were synthesised and tested mechanically. This showed that the elastic modulus of the hydrogels varied significantly between batches. This variability was compared with the ambient temperature, humidity and pressure at the time of synthesis, however no correlation was found. The variability was suggested to be caused by the purity of the collagen that was harvested from the rat tails, and not the hydrogel synthesis process itself.

A limitation of the hydrogels for use as a CNS model was that they were collagen based, while the natural ECM of the CNS has little collagen, and is mostly comprised of hyaluronic acid (Lau et al., 2013; Li et al., 2012). However, collagen is comparatively inexpensive to acquire, contains cell attachment molecules and is widely used and therefore were able to be compared to other studies. As the focus of the study was on the physical and mechanical nature of the hydrogels and not the chemical composition, it was deemed an acceptable limitation. Another limitation was that the hydrogels did not meet the target biomimetic shear elastic modulus range of 200-600Pa at 1Hz, as identified by (Brands et al., 1999; Shen et al., 2006; Hrapko et al., 2006). This means that the findings of this study may not be rel-

evant to the *in vivo* setting. Indeed, although the elastic moduli of the hydrogels were significantly different, they may not have been different enough to alter the differentiation of the stem cells.

Testing the suitability of the hydrogel with cells initially provided good results as the C6 glial cell line and PC12 neuronal cell line showed good viability, as cell numbers increased from day 0 to 2, as measured by the ATPlite assay. Obtaining a suitable stem cell line for the study proved to be more challenging. Initially the CB660 cell line showed good viability within the hydrogels, determined by staining with live/dead at day 6, however difficulties in culturing and expanding these cells meant that alternative cell sources were sought. The CX cell line showed no problems when expanded in culture, however initial attempts to seed into the hydrogels were unsuccessful, the cells appeared not to attach to the hydrogel. Attachment was achieved through incorporation of laminin into the hydrogel, however the cells remained rounded and did not express any projections into the hydrogel.

The issue with culturing the CB660 cell line proved to be multifaceted including the requirements of a specific laminin type to coat the flask, a different media type for cell culture and a lower passage number. These issues were identified and corrected by the NIBSC, however 12 months of the project were depleted by this issue. The speed of the cell proliferation remained slow but due to their improved viability when seeded in the hydrogels compared to the CX cells shown in Figures 39 and 40 in Section 3.5.1, the CB660 cells were chosen for study during the final experiments.

The low number of cells yielded meant that many of the experiments presented in this work had only two repeats. This meant that the statistical analysis performed had very limited power, and the variance of the data was assumed to be equal for these cases. Aside from the low repeat numbers, the use of a cell line rather than primary cells means that the repeats presented in this study are technically replicates and therefore the statistical methods used to analyse the data are limited in their validity (Vaux et al., 2012).

The CyQuant assay was originally designed for two dimensional (2D) cell cultures where the cell fluorescence is read through the bottom of the plate, negating the need for cell washes. This assay was adapted for use in three dimensions (3D), using

PBS washes to wash away the initial stain, allowing the fluorescence to be detected by a top-reading plate reader, as it was assumed that the majority of cells would be closer to the top of the hydrogel. The original readings showed no significant difference between seeding densities, however rinsing the hydrogels with PBS after the staining was performed provided results that were significantly different. This optimised assay method was used for further work.

Successive cell viability assays were also developed to take advantage of the non-lysing nature of the CyQuant assay. The CyQuant assay was applied and the fluorescence read, followed by the ATPlite assay which was applied and the luminescence read. Although the CyQuant assay did diminish the ATPlite signal, the luminescent signal change between samples with and without a preceding CyQuant assay was found to be not significantly different at day 5.

Scanning electron microscopy (SEM) image analysis to find the diameter of pores was conducted using the BoneJ plugin (Doube et al., 2010). Previous studies using cortical bone have found 2D measurements comparable to 3D measurements (Boutroy et al., 2011) and the SEM images of the hydrogels were noted to be qualitatively similar to that of cortical bone. The BoneJ plugin was originally developed for images of cortical bone, however the SEM images of the hydrogel were visually similar so the plugin was deemed suitable for image analysis. The ability of the plugin to measure pore size was validated by comparison with manual measurements, finding no significant difference between the two methods of measurement. The BoneJ plugin was therefore deemed suitable for SEM image analysis.

Current 3D migration assays, known as invasion assays, all have limitations, for example the coated Boyden chamber only has a short migration distance, while the vertical hydrogel migration assay has capabilities for a longer migration distance but decreased imaging potential, as the transparency of hydrogels can diminish with depth. A novel 3D migration assay was developed that used thin layered hydrogels to provide the benefits of a long migration distance which could also be viewed separately for clearer microscopic imaging. The main disadvantage of this assay was the practicality of transferring the soft hydrogels from one well to another as well as the cellular damage that may have been incurred, however this would be much easier when using hydrogels with higher elastic moduli.

The storage and loss moduli of the Ta hydrogel was found via rheology to be significantly higher than the Ph hydrogel, while the SEM analysis, nuclear magnetic resonance (NMR) T2 logging and the trinitrobenzenesulfonic acid (TNBS) assay found no significant differences in pore diameter or degree of crosslinking. The response of the stem cells to the hydrogel variants was not significantly different in terms of cell number or differentiation, however projections and greater spreading was observed for the neural stem cell line when seeded onto the tartaric acid (Ta) hydrogel compared to the 1,3-phenylenediacetic acid (Ph) hydrogel. These results indicated that differentiation may well be influenced by pore size rather than elastic moduli, and hence it would be wise for further research conducted in this area to include pore size measurement. The porosity of the hydrogels was found by measuring water content of wet and dry hydrogels and indicated a high significant difference between the two hydrogels. Given that the pore size was similar, this may indicate that the fibre thickness of the collagen matrix may be thicker in the Ph hydrogel compared to the Ta hydrogel. (Christopherson et al., 2009) reported that fibre diameter affected the proliferation and differentiation of neural stem cells, so this change may be of significance to the activities of the cells.

Raised pressure generally inhibited the activities of the stem cells, with experiments indicating 3D migration and expression of neurites was reduced in raised pressure environments. In contrast, preliminary studies showed an increased migratory ability of glial cells. *In vitro*, this may mean that intracranial hypertension after injury both limits the regenerative effects of neural stem cells and also mobilises glial cells, contributing to the formation of a glial scar. As well as forming a mechanical barrier to the regrowth of neuronal axons, the glial cells in the scar are known to produce chemicals to further inhibit this growth (Smith-Thomas et al., 1995). This means that it may not be the high pressure of the Lundberg A waves that contributes to improved patient mortality, but the relative short wavelength and infrequency of these waves, combined with the normal pressure levels observed between waves.

The investigations into stem cell responses were limited by low cell number due to the slow expansion of the CB660 cells and the limited time and materials of the project. Only two repeats per experiment were able to be performed, while only one sample was studied in the migration experiment. This means that the results

in this study should be treated with caution, indicating the responses that may be worth investigating further. The phenotype of the stem cells was monitored using immunostaining. With greater cell numbers, an additional phenotype assay, for example polymerase chain reaction (PCR) would have also been conducted.

The assumption was made that cells identified by blue nuclei that were not expressing CD133 or PSA-NCAM were differentiating down a glial lineage, i.e. any neural lineage except neurons. CD133 is described by Sun et al. (2008) to be a marker for neural stem cells, and the expression of which was observed to become diminished between weeks one and two for cells which were differentiating along a neuronal lineage. PSA-NCAM was also observed by Sun et al. (2008) to be upregulated between weeks one and two for the same cell samples, differentiating along a neuronal lineage, finding that 66 $\pm$ 5.8% of PSA-NCAM positive cells at week two would be βIII-tubulin positive at week four, while approximately 82% of the PSA-NCAM negative cells became positive for GFAP, an astrocytic marker at week four. The assumption that cells not expressing CD133 or PSA-NCAM were glial progenitors therefore has limitations in its accuracy.

The loss of CD133 expression without an upregulation of PSA-NCAM may not neccessarily indicate glial differentiation. While Sun et al. (2008) described these proteins as markers for neuronal differentiation, they may not neccessarily be early indicators for glial differentiation as well. Secondly, 34% of PSA-NCAM positive cells at week two had not become βIII-tubulin positive at week four, and therefore the assumption that these cells are all neuronal progenitors may not be valid.

The novel developments made in this work were:

- A method for modifying the elastic modulus of a hydrogel without producing significant change to the microarchitecture.
- The adapatation of the ImageJ application, BoneJ (Doube et al., 2010), to measure the pore size of hydrogels.
- A layered 3D migration assay.
- A successive 3D viability assays.

No significant difference in stem cell differentiation in response to changing elastic modulus, indicating that pore size and not elastic modulus may affect stem cells. This has significant implications to research in this field which has primarily focussed on elastic modulus and not pore size (Engler et al., 2006; Banerjee et al., 2009; Her et al., 2013; Bozza et al., 2014). Increased glial 3D migration was observed in response to increased pressure. This finding correlates with findings in 2D (Salvador-Silva et al., 2004; Yu et al., 2011). The differentiation to neuronal progenitors was significantly upregulated in response to increased pressure, while projection formation, viability and migration were decreased. Increased ICP after injury may directly affect the activities of neural stem cells *in vivo* and thereby affect patient survival (Rose and Johnson, 1996; Cox et al., 2014).

6.2 Conclusion and Context

The findings of the experiments are summarised below in relation to the initial aims of the project. The rationale behind these aims was revisited and the clinical and experimental implications are summarised.

6.2.1 Investigation into the Effects of Matrix Elastic Modulus on Neural Stem Cell Differentiation

The aim of this part of the study was to test the hypothesis that the activities of neural stem cells are affected by the elastic moduli of hydrogels, independently of pore size. The findings indicated that the hypothesis may be rejected for some cellular activities. The two hydrogel variants synthesised showed significant and highly significant differences in their storage and loss moduli respectively, while pore size was found to be not significantly different by SEM, NMR and TNBS assay. Although projections and the spread of the cells were affected, protein expression was found to not be significantly different between cells seeded onto the two hydrogel types. These results indicate that it may be the differences in pore size and not the differences in elastic moduli that produced the changes in neural stem cell differentiation described by Banerjee et al. (2009), Her et al. (2013), and Bozza et al. (2014), and indeed Engler et al. (2006).

The elastic moduli of type I collagen strands isolated from rat tails has been found to vary from 5-11.5GPa by atomic force microscopy Wenger et al. (2007) and so the elastic modulus that each stem cell experiences *in vivo* may vary substantially. The variability of this property casts doubt on whether cells would use this property to discern their environment. If the mechanical properties of the ECM surrounding one stem cell are markedly different from that of another nearby stem cell, how should they discern from this property that they are located within the same tissue type? This evidence may provide an argument that the pore size could have more influence than elastic modulus on stem cell differentiation, however, no research into the pore size of natural CNS ECM could be identified, and it may well vary as much as elastic modulus.

Putting this finding into context with the natural hydrogels found *in vivo* is more complex. Firstly, different polymer types have different elastic moduli (Guthold et al., 2007), and so the protein make up of different tissues will inherently cause differences in the elastic moduli of the tissues as a whole. Secondly, these different proteins may also have variations in the number of binding sites with which cells may form focal adhesions. If pore size does indeed affect stem cell activity, it is likely that it is because smaller pores create an increase in binding sites available to the cells. This means that the protein types that the cell comes into contact with could also affect cellular activities purely due to binding site availability and not due to their varied elastic moduli.

The rationale for the determination of the importance of measuring pore size as well as elastic moduli of hydrogels was to inform future *in vitro* research that explores the relationship between cells and their physical surroundings. Although the power of the research in this present study is limited, if further work into this relationship correlates with these findings, then a case should be made for future research in this area to include pore size measurements.

6.2.2 Investigation into the Effects of Raised ICP on Neural Stem Cell Activities

The aim of this part of the study was to test the hypothesis that the activities of neural stem cells are directly affected by the raised pressure that occurs during secondary injury after TBI. The findings of the development work indicated that raised pressure increased migration of the C6 glial cell line, which correlates with findings of other researchers (Salvador-Silva et al., 2004; Lei et al., 2011). In the mid layer, significantly more cells were counted at 25mmHg compared to at 0mmHg, while in the lower layer significantly more cells were observed at 50mmHg compared to at 0mmHg.

The findings of the work using stem cells indicated that proliferation, phenotype and the proportion of cells that expressed projections were significantly affected by changing pressure, while migration also appeared to be affected. Expression of PSA-NCAM of the neural stem cell line was measured by immunofluoescence and was observed to be increased ($p<0.01$) at higher pressures, comparing 10 to 50mmHg, which may indicate neuronal differentiation (Sun et al., 2008). The proportion of cells that expressed projections were reduced at higher pressures, with $p <0.05$ comparing 10 to 50mmHg. Significantly higher luminescence readings were observed at 30mmHg compared to at 50mmHg by ATPlite assay, however it is unclear if this was due to a high proliferation rate of the cells cultured at 30mmHg, or if each cell was producing more ATP, perhaps due to being aggravated by the pressure level. The migration experiment showed that cell number was reduced at 30mmHg compared to 10mmHg by 61.5% in the lower hydrogel layer.

These results indicated that many stem cell activities may be directly affected by raised ICP. High pressure was observed to inhibit proliferation, migration and the expression of projections, however may also induce neuronal differentiation. No significant difference was observed in the number of projections expressed per cell or the average length of projections, when comparing cells cultured at the different pressure levels.

In context, this may provide new insight into the direct effect that intracranial hypertension has on cellular activities during the secondary injury stage which, as

the conclusion of the literature review argued, is also the stage of primary repair of the tissue due to the reparative processes that are initiated in the same time frame. Neural stem cells are known to be found in the subventricular zone (SVZ) and subgranular zone (SGZ) of the brain (Ricks et al., 2014). As the name suggests, the SVZ is in proximity to the lateral ventricles while the SGZ is also close to the ventricles compared to many other areas of the brain, indicating that stem cells here are not protected from these pressures by ECM as they would be if they were located further away from the ventricles.

The occurrance of Lundberg A waves with high pressure waves (>40mmHg) lasting less than 30 minutes and returning to normal levels (5-15mmHg) between waves have been observed to indicate an improved outcomes for the patient (Cox et al., 2014). The high levels of pressure characteristic of Lundberg A waves may induce neuronal differentiation, which could help to replace damaged or necrotic neurons. The short wavelength of Lundberg A waves, and the normal pressure levels measured between the waves may also be instrumental for repair, allowing the migration of stem cells to the injury site and expression of new projections to take place. Pressure levels that are consistently high without returning to normal levels may also contribute to the formation of the glial scar, as this appears to increase glial cell migration.

The rationale for determining of the stem cell repair processes directly affected by pressure was to inform future clinical practice on treating patients with TBI or SCI. If further work into this relationship correlates with these initial findings, then this may inform further *in vivo* work with the aim of the treatment of these injuries being improved.

6.3 Future Work

Many aspects of the project could have been expanded upon with resources permitting. Two objectives for expansion were identified. Of primary importance, work is required to improve the power of the arguments made in this thesis and secondarily, there are many other areas for further expansion to decrease the limitations of the studies.

6.3.1 Improvements to the Power of the Argument

An obvious route for future work is to increase the sample size of the cellular studies to improve the power of these studies. A sample size of two is not adequate for confidence in these findings and they should therefore be treated with caution. Repetition of these initial studies should be considered of primary importance to benefit the research community. These repetitions should include a larger number of time points as well as further repeats. The use of primary cells, other cell sources and the addition of phenotyping by PCR would also add weight to the findings.

For the studies involving the elastic modulus of the hydrogels, commercially sourced collagen may be of higher quality than the collagen that was harvested in-house from rat tails. A higher purity or quality may reduce the variability of the hydrogels, and therefore increase confidence in the results that were obtained. Further research into other crosslinkers may lead to hydrogels with larger ranges of elastic moduli which would bring further confidence and more biomimetic relevance in the findings of this study.

By performing the pressure studies with the CX cells in a hydrogel that has already been developed for use with these cells, for example the RAFT-stabilised described by Murray-Dunning et al. (2015), the issues with cell numbers and therefore low repetitions performed may be avoided.

6.3.2 Areas for Expansion

Studies examining the effects of the initial impact followed by an increased pressure, for example mimicking a car crash scenario, may also provide valuable insight into the effects of real-world forces on the stem cells. An *in vitro* study including a traumatic impact to cells cultured in hydrogels followed by a period of culture under pressure would increase the clinical relevance of these findings.

The development work for the migration assay was carried out with the C6 glial cell line and the results indicated that this cell line was in fact mobilised instead of impeded by an increase in pressure. Studies examining the effects of pressure on other neural cell types would provide valuable information on how these biomimetic

pressures directly affect their activities, for example how pressure affects glial migration and proliferation may provide further insight into the mechanisms of glial scar formation, while the effects of pressure on neuronal projection growth may also provide further insight into other barriers for functional regeneration. Using partially differentiated cells and examining their phenotype under pressure may be used to explore if pressure can reverse the differentiation process, allowing stem cells to become less committed to a particular lineage.

Molecular studies into the intracellular mechanisms may provide further insight. Although the contractions of cells have been described (Mohammadi et al., 2015), the change in contraction force with respect to changing pore size as well as elastic modulus may allow for further conclusions to be drawn about this topic. In terms of pressure, studying mechanisms such as blebbing in relation to differentiation, projection formation and migration would provide further insight into exactly how pressure is affecting the cellular processes. It is possible that studies into the intracellular mechanisms may conclude that cell response to pressure and to pore size or elastic modulus is governed by the same core mechanism.

References

Aaron, B. B. and Gosline, J. M. (1981). Elastin as a Random-Network Elastomer: A Mechanical and Optical Analysis of Single Elastin Fibers. *Biopolymers* 20.6, pp. 1247–1260.

Abraham, L. C., Zuena, E., Perez-Ramirez, B., and Kaplan, D. L. (2008). Guide to collagen characterization for biomaterial studies. *J. Biomed. Mater. Res. Part B Appl. Biomater.* 87.1, pp. 264–285.

Adigun, O. O. and Bhimji, S. S. (2017). *Anatomy, Cerebrospinal Fluid*. URL: `https://www.ncbi.nlm.nih.gov/books/NBK459286/`.

Ahmed, E. M. (2015). Hydrogel: Preparation, characterization, and applications: A review. *J Adv Res* 6.2, pp. 105–121.

Alperin, N. J., Lee, S. H., Loth, F., Raksin, P. B., and Lichtor, T. (2000). MR-Intracranial pressure (ICP): a method to measure intracranial elastance and pressure noninvasively by means of MR imaging: baboon and human study. *Radiology* 217.3, pp. 877–885.

Altman, G. H., Horan, R. L., Martin, I., Farhadi, J., Stark, P. R., Volloch, V., Richmond, J. C., Vunjak-Novakovic, G., and Kaplan, D. L. (2002). Cell differentiation by mechanical stress. *FASEB J.* 16.2, pp. 270–272.

American Spinal Injury Association Impairment Scale (2013). Accessed: 10th June 2015. URL: `http://www.asia-spinalinjury.org/elearning/ASIA_ISCOS_high.pdf` (visited on 10/06/2016).

Aung, K. Z., Pereira, B. P., Tan, P. H., Han, H. C., and Nathan, S. S. (2012). Interstitial fluid pressure as an alternate regulator of angiogenesis independent of hypoxia driven HIF-1a in solid tumors. *J. Orthop. Res.* 30.12, pp. 2038–2045.

Banerjee, A., Arha, M., Choudhary, S., Ashton, R. S., Bhatia, S. R., Schaffer, D. V., and Kane, R. S. (2009). The influence of hydrogel modulus on the proliferation and differentiation of encapsulated neural stem cells. *Biomaterials* 30.27, pp. 4695–4699.

Becquart, P., Cruel, M., Hoc, T., Sudre, L., Pernelle, K., Bizios, R., Logeart-Avramoglou, D., Petite, H., and Bensidhoum, M. (2016). Human mesenchymal stem cell responses to hydrostatic pressure and shear stress. *Eur Cell Mater* 31, pp. 160–173.

Beduer, A., Vieu, C., Arnauduc, F., Sol, J. C., Loubinoux, I., and Vaysse, L. (2012). Engineering of adult human neural stem cells differentiation through surface micropatterning. *Biomaterials* 33.2, pp. 504–514.

Bellner, J., Romner, B., Reinstrup, P., Kristiansson, K. A., Ryding, E., and Brandt, L. (2004). Transcranial Doppler sonography pulsatility index (PI) reflects intracranial pressure (ICP). *Surg Neurol* 62.1, pp. 45–51.

Bernhardt, M., Hynes, R. A., Blume, H. W., and White, A. A. (1993). Cervical spondylotic myelopathy. *J Bone Joint Surg Am* 75.1, pp. 119–128.

Bershadsky, A. D., Balaban, N. Q., and Geiger, B. (2003). Adhesion-dependent cell mechanosensitivity. *Annu. Rev. Cell Dev. Biol.* 19, pp. 677–695.

Bilston, L. E. and Thibault, L. E. (1996). The mechanical properties of the human cervical spinal cord in vitro. *Ann Biomed Eng* 24.1, pp. 67–74.

Bilston, L. E., Liu, Z., and Phan-Thien, N. (1997). Linear viscoelastic properties of bovine brain tissue in shear. *Biorheology* 34.6, pp. 377–385.

Bodenberger, N., Kubiczek, D., Abrosimova, I., Scharm, A., Kipper, F., Walther, P., and Rosenau, F. (2016). Evaluation of methods for pore generation and their influence on physio-chemical properties of a protein based hydrogel. *Biotechnol Rep (Amst)* 12, pp. 6–12.

Bott, K., Upton, Z., Schrobback, K., Ehrbar, M., Hubbell, J. A., Lutolf, M. P., and Rizzi, S. C. (2010). The effect of matrix characteristics on fibroblast proliferation in 3D gels. *Biomaterials* 31.32, pp. 8454–8464.

Boutroy, S., Vilayphiou, N., Roux, J. P., Delmas, P. D., Blain, H., Chapurlat, R. D., and Chavassieux, P. (2011). Comparison of 2D and 3D bone microarchitecture evaluation at the femoral neck, among postmenopausal women with hip fracture or hip osteoarthritis. *Bone* 49.5, pp. 1055–1061.

Bozza, A., Coates, E. E., Incitti, T., Ferlin, K. M., Messina, A., Menna, E., Bozzi, Y., Fisher, J. P., and Casarosa, S. (2014). Neural differentiation of pluripotent cells in 3D alginate-based cultures. *Biomaterials* 35.16, pp. 4636–4645.

Brammer, K. S., Oh, S., Cobb, C. J., Bjursten, L. M., Heyde, H. van der, and Jin, S. (2009). Improved bone-forming functionality on diameter-controlled TiO(2) nanotube surface. *Acta Biomater* 5.8, pp. 3215–3223.

Brands, D. W. A., Bovendeerd, H. M., and M., P. G. W. (1999). Comparison of the Dynamic Behavior of Brain Tissue and Two Model Materials. *Proceedings of the 43rd Stapp Car Crash Conference*.

Briar, C. and Lasserson, D. (2003). *Nervous system*. English. London: Mosby. ISBN: 9780723432906; 0723432902.

Caiazzo, M., Okawa, Y., Ranga, A., Piersigilli, A., Tabata, Y., and Lutolf, M. P. (2016). Defined three-dimensional microenvironments boost induction of pluripotency. *Nat Mater* 15.3, pp. 344–352.

Cancer Research UK (2014). Accessed: 4th June 2015. URL: http://www.cancerresearchuk.org/health-professional/cancer-statistics/statistics-by-cancer-type/brain-tumours/incidence#heading-Zero (visited on 10/06/2016).

Cannas, A., Spissu, A., Floris, G. L., Congia, S., Saddi, M. V., Melis, M., Mascia, M. M., Pinna, F., Tuveri, A., Solla, P., Milia, A., Giagheddu, M., and Tacconi, P. (2002). Bipolar affective disorder and Parkinson's disease: a rare, insidious and often unrecognized association. *Neurol. Sci.* 23 Suppl 2, S67–68.

Cells, C. *NIBSC*.

Cen, L., Liu, W., Cui, L., Zhang, W., and Cao, Y. (2008). Collagen tissue engineering: development of novel biomaterials and applications. *Pediatr. Res.* 63.5, pp. 492–496.

Charras, G. and Paluch, E. (2008). Blebs lead the way: how to migrate without lamellipodia. *Nat. Rev. Mol. Cell Biol.* 9.9, pp. 730–736.

Charras, G. T., Coughlin, M., Mitchison, T. J., and Mahadevan, L. (2008). Life and times of a cellular bleb. *Biophys. J.* 94.5, pp. 1836–1853.

Chaussy, C., Schmiedt, E., Jocham, D., Brendel, W., Forssmann, B., and Walther, V. (1982). First clinical experience with extracorporeally induced destruction of kidney stones by shock waves. *J. Urol.* 127.3, pp. 417–420.

Cheng, S., Clarke, E. C., and Bilston, L. E. (2008). Rheological properties of the tissues of the central nervous system: A review. *Medical Engineering and Physics* 30.10. Accessed: 6th October 2016, pp. 1318 –1337. ISSN: 1350-4533. DOI: http://dx.doi.org/10.1016/j.medengphy.2008.06.003. URL: http://www.sciencedirect.com/science/article/pii/S1350453308001057 (visited on 10/06/2016).

Chippada, U., Yurke, B., and Langrana, N. (2010). Simultaneous determination of Young's modulus, shear modulus, and Poisson's ratio of soft hydrogels. *JOURNAL OF MATERIALS RESEARCH* 25.3, 545–555. ISSN: 0884-2914. DOI: {10.1557/JMR.2010.0067}.

Choi, H., Jin, S. H., Han, M. H., Lee, J., Ahn, S., Seong, M., Choi, H., Han, J., Cho, E. G., Lee, T. R., and Noh, M. (2014). Human melanocytes form a PAX3-expressing melanocyte cluster on Matrigel by the cell migration process. *J. Dermatol. Sci.* 76.1, pp. 60–66.

Choices, N. (2016). *Meningitis Symptoms*. URL: `https://www.nhs.uk/conditions/meningitis/symptoms/`.

Choices, N. (2017). *Cervical Spondylosis*. URL: `https://www.nhs.uk/conditions/cervical-spondylosis/`.

Christopherson, G. T., Song, H., and Mao, H. Q. (2009). The influence of fiber diameter of electrospun substrates on neural stem cell differentiation and proliferation. *Biomaterials* 30.4, pp. 556–564.

Coates, G. R., Xiao, L., and Prammer, M. G. (1999). *NMR Logging. Principles and Applications*. Houston: Halliburton Energy Services. URL: `http://www.halliburton.com`.

Collins, M. N. and Birkinshaw, C. (2008). Physical properties of crosslinked hyaluronic acid hydrogels. *J Mater Sci Mater Med* 19.11, pp. 3335–3343.

Cooper, G. (2000). *The Cell: A Molecular Approach. 2nd edition*. Sunderland (MA): Sinauer Associates.

Cooper, G. and Hausman, R. (2013). *The Cell: A molecular approach*. 6th. Sinauer Associates.

Cowman, M. K., Lee, H. G., Schwertfeger, K. L., McCarthy, J. B., and Turley, E. A. (2015). The Content and Size of Hyaluronan in Biological Fluids and Tissues. *Front Immunol* 6, p. 261.

Cox, L. A. E., Ramakers, B. P., and Abdo, W. F. (2014). Plateau Waves, Intracranial Hypertension and Prognosis. How Identical Waves can Lead to Different Outcomes in Two Patients with Traumatic Brain Injury. *Journal of Anesthesiology and Critical Care Medicine* 1.1, pp. 1–4.

Dalby, M. J., Gadegaard, N., Tare, R., Andar, A., Riehle, M. O., Herzyk, P., Wilkinson, C. D., and Oreffo, R. O. (2007). The control of human mesenchymal cell differentiation using nanoscale symmetry and disorder. *Nat Mater* 6.12, pp. 997–1003.

De Santis, G., Lennon, A. B., Boschetti, F., Verhegghe, B., Verdonck, P., and Prendergast, P. J. (2011). How can cells sense the elasticity of a substrate? An analysis using a cell tensegrity model. *Eur Cell Mater* 22, pp. 202–213.

Del Mar, N., Buttlar, X. von, Yu, A. S., Guley, N. H., Reiner, A., and Honig, M. G. (2015). A novel closed-body model of spinal cord injury caused by high-pressure air blasts produces extensive axonal injury and motor impairments. *Exp. Neurol.* 271, pp. 53–71.

Diamond, M., Scheibel, A., and Elson, L. (1985). *The Human Brain Coloring Book*. HaarperCollins.

Donato, R., Miljan, E. A., Hines, S. J., Aouabdi, S., Pollock, K., Patel, S., Edwards, F. A., and Sinden, J. D. (2007). Differential development of neuronal physiological responsiveness in two human neural stem cell lines. *BMC Neurosci* 8, p. 36.

Dorkoosh, F., Brussee, J., Verhoef, J. C., Borchard, G., Rafiee-Tehrani, M., and Junginger, H. Preparation and NMR characterisation of superporous Hydrogels (SPH) and SPH composites. *Polymer* 41, pp. 8213–8220.

Doube, M., Kłosowski, M., Arganda-Carreras, I., Cordeliéres, F., Dougherty, R., Jackson, J., Schmid, B., Hutchinson, J., and Shefelbine, S. (2010). BoneJ: free and extensible bone image analysis in ImageJ. *Bone* 47, pp. 1076–9.

Driscoll, M. K. and Danuser, G. (2015). Quantifying Modes of 3D Cell Migration. *Trends Cell Biol.* 25.12, pp. 749–759.

Ellis, E. F., McKinney, J. S., Willoughby, K. A., Liang, S., and Povlishock, J. T. (1995). A new model for rapid stretch-induced injury of cells in culture: characterization of the model using astrocytes. *J. Neurotrauma* 12.3, pp. 325–339.

Elson, K., Ribeiro, R. M., Perelson, A. S., Simmons, A., and Speck, P. (2004). The life span of ganglionic glia in murine sensory ganglia estimated by uptake of bromodeoxyuridine. *Exp. Neurol.* 186.1, pp. 99–103.

Engler, A., Sen, S., and Discher, D. (2006). Matrix elasticity directs stem cell differentiation. *Journal of Biomechanics* 39, Supplement 1.0. World Congress of Biomechanics, S269 –. ISSN: 0021-9290. DOI: `http://dx.doi.org/10.1016/S0021-9290(06)84031-5`. URL: `http://www.sciencedirect.com/science/article/pii/S0021929006840315` (visited on 10/06/2016).

Escher, M. C. (1960). *Circle Limit V*. Woodcut. Accessed: 17th April 2015. URL: `http://www.ma.utexas.edu/users/shirley/Wall-Escher-Main/home.html`.

Evers, S., Verbaan, D., Sanchez, E., and Peerdeman, S. (2015). 3D volumetric measurement of neurofibromatosis type 2-associated meningiomas. Association between tumor location and growth rate. *World Neurosurg.*

Fawcett, J., Rosser, A., and Dunnett, S. (2002). *Brain Damage, Brain Repair*. Oxford: Oxford University Press.

Fee, D., Crumbaugh, A., Jacques, T., Herdrich, B., Sewell, D., Auerbach, D., Piaskowski, S., Hart, M. N, Sandor, M., and Fabry, Z. (2003). Activated/effector CD4+ T cells exacerbate acute damage in the central nervous system following traumatic injury. *Journal of Neuroimmunology* 136.1–2, pp. 54 –66. ISSN: 0165-5728. DOI: http://dx.doi.org/10.1016/S0165-5728(03)00008-0. URL: http://www.sciencedirect.com/science/article/pii/S0165572803000080 (visited on 10/06/2016).

Fleischman, D. and Allingham, R. R. (2013). The role of cerebrospinal fluid pressure in glaucoma and other ophthalmic diseases: A review. *Saudi J Ophthalmol* 27.2, pp. 97–106.

Foisner, R. (2000). Dynamic Connections of Nuclear Envelope Proteins to Chromatin and the Nuclear Matrix. *Madame Curie Bioscience Database [Internet]*. URL: Availablefrom:http://www.ncbi.nlm.nih.gov/books/NBK6125/.

Franze, K., Janmey, P. A., and Guck, J. (2013). Mechanics in neuronal development and repair. *Annu Rev Biomed Eng* 15, pp. 227–251.

Frisen, L. (1982). Swelling of the optic nerve head: a staging scheme. *J. Neurol. Neurosurg. Psychiatr.* 45.1, pp. 13–18.

Gage, F. H. (2000). Mammalian neural stem cells. *Science* 287.5457, pp. 1433–1438.

Garraway, S. M., Woller, S. A., Huie, J. R., Hartman, J. J., Hook, M. A., Miranda, R. C., Huang, Y., Ferguson, A. R., and Grau, J. W. (2014). Peripheral noxious stimulation reduces withdrawal threshold to mechanical stimuli after spinal cord injury: Role of tumor necrosis factor alpha and apoptosis. *PAIN®* 155.11, pp. 2344 –2359. ISSN: 0304-3959. DOI: http://dx.doi.org/10.1016/j.pain.2014.08.034. URL: http://www.sciencedirect.com/science/article/pii/S0304395914004011 (visited on 10/06/2016).

Gefen, A. and Margulies, S. S. (2004). Are in vivo and in situ brain tissues mechanically similar? *J Biomech* 37.9, pp. 1339–1352.

Glasgow Coma Score (2014). Accessed: 10th June 2015. URL: http://www.glasgowcomascale.org/ (visited on 10/06/2016).

Globocan (2012). Accessed: 4th June 2015. URL: http://globocan.iarc.fr/Pages/fact_sheets_population.aspx (visited on 10/06/2016).

Greve, M. W. and Zink, B. J. (2009). Pathophysiology of traumatic brain injury. *Mt. Sinai J. Med.* 76.2, pp. 97–104.

Griffin, M. F., Butler, P. E., Seifalian, A. M., and Kalaskar, D. M. (2015). Control of stem cell fate by engineering their micro and nanoenvironment. *World J Stem Cells* 7.1, pp. 37–50.

Guilak, F., Cohen, D. M., Estes, B. T., Gimble, J. M., Liedtke, W., and Chen, C. S. (2009). Control of stem cell fate by physical interactions with the extracellular matrix. *Cell Stem Cell* 5.1, pp. 17–26.

Guthold, M., Liu, W., Sparks, E. A., Jawerth, L. M., Peng, L., Falvo, M., Superfine, R., Hantgan, R. R., and Lord, S. T. (2007). A comparison of the mechanical and structural properties of fibrin fibers with other protein fibers. *Cell Biochem. Biophys.* 49.3, pp. 165–181.

Hamid, S. and Hayek, R. (2008). Role of electrical stimulation for rehabilitation and regeneration after spinal cord injury: an overview. *Eur Spine J* 17.9, pp. 1256–1269.

Hamou, C., Callaghan, M. J., Thangarajah, H., Chang, E., Chang, E. I., Grogan, R. H., Paterno, J., Vial, I. N., Jazayeri, L., and Gurtner, G. C. (2009). Mesenchymal stem cells can participate in ischemic neovascularization. *Plast. Reconstr. Surg.* 123.2 Suppl, 45S–55S.

Harrington, D. K., Fragomeni, F., and Bonser, R. S. (2007). Cerebral perfusion. *Ann. Thorac. Surg.* 83.2, pp. 799–804.

Haschek, W. M., Rousseaux, C. G., Wallig, M. A., Bolon, B., and Ochoa, R. (2013). *Toxicology Pathology*. Amsterdam: Elsevier.

Hausner, T., Pajer, K., Halat, G., Hopf, R., Schmidhammer, R., Redl, H., and Nogradi, A. (2012). Improved rate of peripheral nerve regeneration induced by extracorporeal shock wave treatment in the rat. *Exp. Neurol.* 236.2, pp. 363–370.

Head, D. A., Tronci, G., Russell, S. J., and Wood, D. J. (2016). In Silico Modeling of the Rheological Properties of Covalently Cross-Linked Collagen Triple Helices. *ACS Biomater. Sci. Eng.* 2.8, pp. 1224–1233.

Headway (2015a). *Acquired Brain Injury*. Accessed: 4th June 2015. URL: `https://www.headway.org.uk/statistics-resources.aspx` (visited on 10/06/2016).

Headway (2015b). *What happens in a TBI?* Accessed: 8th June 2015. URL: `https://www.headway.org.uk/What-happens-in-a-TBI.aspx` (visited on 10/06/2016).

Helmy, A., Simoni, M. D., Guilfoyle, M. R., Carpenter, K. L., and Hutchinson, P. J. (2011). Cytokines and innate inflammation in the pathogenesis of human traumatic brain injury. *Progress in Neurobiology* 95.3, pp. 352 –372. ISSN: 0301-0082. DOI: http://dx.doi.org/10.1016/j.pneurobio.2011.09.003. URL: http://www.sciencedirect.com/science/article/pii/S0301008211001638 (visited on 10/06/2016).

Her, G. J., Wu, H. C., Chen, M. H., Chen, M. Y., Chang, S. C., and Wang, T. W. (2013). Control of three-dimensional substrate stiffness to manipulate mesenchymal stem cell fate toward neuronal or glial lineages. *Acta Biomater* 9.2, pp. 5170–5180.

Hess, R., Douglas, T., Myers, K. A., Rentsch, B., Rentsch, C., Worch, H., Shrive, N. G., Hart, D. A., and Scharnweber, D. (2010). Hydrostatic pressure stimulation of human mesenchymal stem cells seeded on collagen-based artificial extracellular matrices. *J Biomech Eng* 132.2, p. 021001.

Heyeraas, K. J. and Berggreen, E. (1999). Interstitial fluid pressure in normal and inflamed pulp. *Crit. Rev. Oral Biol. Med.* 10.3, pp. 328–336.

Hidalgo-Bastida, L. A. and Cartmell, S. H. (2010). Mesenchymal stem cells, osteoblasts and extracellular matrix proteins: enhancing cell adhesion and differentiation for bone tissue engineering. *Tissue Eng Part B Rev* 16.4, pp. 405–412.

Hoffman-Kim, D., Mitchel, J. A., and Bellamkonda, R. V. (2010). Topography, cell response, and nerve regeneration. *Annu Rev Biomed Eng* 12, pp. 203–231.

Hrapko, M., Dommelen, J. A. van, Peters, G. W., and Wismans, J. S. (2006). The mechanical behaviour of brain tissue: large strain response and constitutive modelling. *Biorheology* 43.5, pp. 623–636.

Hsiong, S. X., Carampin, P., Kong, H. J., Lee, K. Y., and Mooney, D. J. (2008). Differentiation stage alters matrix control of stem cells. *J Biomed Mater Res A* 85.1, pp. 145–156.

Huang, S., Ingber, D. E., and Ingber, D. E. (2000). Shape-dependent control of cell growth, differentiation, and apoptosis: switching between attractors in cell regulatory networks. *Exp. Cell Res.* 261.1, pp. 91–103.

Huebsch, N., Arany, P. R., Mao, A. S., Shvartsman, D., Ali, O. A., Bencherif, S. A., Rivera-Feliciano, J., and Mooney, D. J. (2010). Harnessing traction-mediated manipulation of the cell/matrix interface to control stem-cell fate. *Nat Mater* 9.6, pp. 518–526.

Hughes, C. S., Postovit, L. M., and Lajoie, G. A. (2010). Matrigel: a complex protein mixture required for optimal growth of cell culture. *Proteomics* 10.9, pp. 1886–1890.

Invitrogen (2009). URL: `https://assets.thermofisher.com/TFS-Assets/LSG/manuals/mp35011.pdf`.

Isobe, N., Kimura, S., Wada, M., and Deguchi, S. (2018). Poroelasticity of Cellulose Hydrogel. *Journal of the Taiwan Institute of Chemical Engineers* 84.

Janmey, P. A., McCormick, M. E., Rammensee, S., Leight, J. L., Georges, P. C., and MacKintosh, F. C. (2007). Negative normal stress in semiflexible biopolymer gels. *Nat Mater* 6.1, pp. 48–51.

Janmey, P. A., Wells, R. G., Assoian, R. K., and McCulloch, C. A. (2013). From tissue mechanics to transcription factors. *Differentiation* 86.3, pp. 112–120.

Jehn, M., Appel, L. J., Sacks, F. M., and Miller, E. R. (2002). The effect of ambient temperature and barometric pressure on ambulatory blood pressure variability. *Am. J. Hypertens.* 15.11, pp. 941–945.

Jha, A. K., Hule, R. A., Jiao, T., Teller, S. S., Clifton, R. J., Duncan, R. L., Pochan, D. J., and Jia, X. (2009). Structural Analysis and Mechanical Characterization of Hyaluronic Acid-Based Doubly Cross-Linked Networks. *Macromolecules* 42.2, pp. 537–546.

Johansson, C. B., Momma, S., Clarke, D. L., Risling, M., Lendahl, U., and Frisen, J. (1999). Identification of a neural stem cell in the adult mammalian central nervous system. *Cell* 96.1, pp. 25–34.

Johnson, K. R., Leight, J. L., and Weaver, V. M. (2007). Demystifying the effects of a three-dimensional microenvironment in tissue morphogenesis. *Methods Cell Biol.* 83, pp. 547–583.

Kaivosoja, E., Barreto, G., Levon, K., Virtanen, S., Ainola, M., and Konttinen, Y. T. (2012). Chemical and physical properties of regenerative medicine materials controlling stem cell fate. *Ann. Med.* 44.7, pp. 635–650.

Kang, D. W., Oh, D. A., Fu, G. Y., Anderson, J. M., and Zepeda, M. L. (2013). Porcine model to evaluate local tissue tolerability associated with subcutaneous delivery of protein. *J Pharmacol Toxicol Methods* 67.3, pp. 140–147.

Kannicht, C. (2008). *Post-translational modifications of proteins: tools for functional proteomics*. English. Vol. 446.; 446. Totowa, N.J: Humana Press. ISBN: 9781603270847; 1603270841; 1588297195; 9781588297198.

Katz, M. A. (1978). Validity of interstitial fluid hydrostatic pressure measurement in hollow porous polyethylene capsules. *Microvasc. Res.* 16.3, pp. 316–326.

Kawoos, U., McCarron, R. M., Auker, C. R., and Chavko, M. (2015). Advances in Intracranial Pressure Monitoring and Its Significance in Managing Traumatic Brain Injury. *Int J Mol Sci* 16.12, pp. 28979–28997.

Kepp, O., Galluzzi, L., Lipinski, M., Yuan, J., and Kroemer, G. (2011). Cell death assays for drug discovery. *Nat Rev Drug Discov* 10.3, pp. 221–237.

Kim, S. H., Im, S. K., Oh, S. J., Jeong, S., Yoon, E. S., Lee, C. J., Choi, N., and Hur, E. M. (2017). Anisotropically organized three-dimensional culture platform for reconstruction of a hippocampal neural network. *Nat Commun* 8, p. 14346.

Kornblum, H. I. (2007). Introduction to neural stem cells. *Stroke* 38.2 Suppl, pp. 810–816.

Koser, D. E., Thompson, A. J., Foster, S. K., Dwivedy, A., Pillai, E. K., Sheridan, G. K., Svoboda, H., Viana, M., Costa, L. D., Guck, J., Holt, C. E., and Franze, K. (2016). Mechanosensing is critical for axon growth in the developing brain. *Nat. Neurosci.* 19.12, pp. 1592–1598.

Kosmidis, G., Bellin, M., Ribeiro, M. C., Meer, B. van, Oostwaard, D. Ward-van, Passier, R., Tertoolen, L. G., Mummery, C. L., and Casini, S. (2015). Altered calcium handling and increased contraction force in human embryonic stem cell derived cardiomyocytes following short term dexamethasone exposure. *Biochem. Biophys. Res. Commun.* 467.4, pp. 998–1005.

Kothapalli, C. R. and Kamm, R. D. (2013). 3D matrix microenvironment for targeted differentiation of embryonic stem cells into neural and glial lineages. *Biomaterials* 34.25, pp. 5995–6007.

Kreger, S. T., Bell, B. J., Bailey, J., Stites, E., Kuske, J., Waisner, B., and Voytik-Harbin, S. L. (2010). Polymerization and matrix physical properties as important design considerations for soluble collagen formulations. *Biopolymers* 93.8, pp. 690–707.

Lam, W. A., Chaudhuri, O., Crow, A., Webster, K. D., Li, T. D., Kita, A., Huang, J., and Fletcher, D. A. (2011). Mechanics and contraction dynamics of single platelets and implications for clot stiffening. *Nat Mater* 10.1, pp. 61–66.

Lammermann, T. (2016). In the eye of the neutrophil swarm-navigation signals that bring neutrophils together in inflamed and infected tissues. *J. Leukoc. Biol.* 100.1, pp. 55–63.

Lau, L. W., Cua, R., Keough, M. B., Haylock-Jacobs, S., and Yong, V. W. (2013). Pathophysiology of the brain extracellular matrix: a new target for remyelination. *Nat. Rev. Neurosci.* 14.10, pp. 722–729.

Law, J. and Rennie, R. (2015). *Dictionary of Physics*. Oxford: Oxford University Press.

Lazarus, R. C., Buonora, J. E., Jacobowitz, D. M., and Mueller, G. P. (2015). Protein carbonylation after traumatic brain injury: cell specificity, regional susceptibility, and gender differences. *Free Radical Biology and Medicine* 78.0, pp. 89 –100. ISSN: 0891-5849. DOI: http://dx.doi.org/10.1016/j.freeradbiomed.2014.10.507. URL: http://www.sciencedirect.com/science/article/pii/S0891584914010089 (visited on 10/06/2016).

Lee, B. H., Lee, K. H., Kim, U. J., Yoon, D. H., Sohn, J., Choi, S. S., Yi, I., and Park, Y. G. (2004). Injury in the spinal cord may produce cell death in the brain. *Brain Research* 1020.1–2, pp. 37 –44. ISSN: 0006-8993. DOI: http://dx.doi.org/10.1016/j.brainres.2004.05.113. URL: http://www.sciencedirect.com/science/article/pii/S0006899304008947 (visited on 10/06/2016).

Lee, J. H., Yu, H. S., Lee, G. S., Ji, A., Hyun, J. K., and Kim, H. W. (2011). Collagen gel three-dimensional matrices combined with adhesive proteins stimulate neuronal differentiation of mesenchymal stem cells. *J R Soc Interface* 8.60, pp. 998–1010.

Lei, Y., Rajabi, S., Pedrigi, R. M., Overby, D. R., Read, A. T., and Ethier, C. R. (2011). In vitro models for glaucoma research: effects of hydrostatic pressure. *Invest. Ophthalmol. Vis. Sci.* 52.9, pp. 6329–6339.

Leipzig, N. D. and Shoichet, M. S. (2009). The effect of substrate stiffness on adult neural stem cell behavior. *Biomaterials* 30.36, pp. 6867–6878.

Li, X., Katsanevakis, E., Liu, X., Zhang, N., and Wen, X. (2012). Engineering neural stem cell fates with hydrogel design for central nervous system regeneration. *Progress in Polymer Science* 37.8. Topical Issue on Biorelated polymers, pp. 1105 –1129. ISSN: 0079-6700. DOI: http://dx.doi.org/10.1016/j.progpolymsci.2012.02.004. URL: http://www.sciencedirect.com/science/article/pii/S0079670012000202 (visited on 10/06/2016).

Li, Y., Chen, J., and Chopp, M. (2002). Cell proliferation and differentiation from ependymal, subependymal and choroid plexus cells in response to stroke in rats. *J. Neurol. Sci.* 193.2, pp. 137–146.

Liao, W., Huang, N., Yu, J., Jares, A., Yang, J., Zieve, G., Avila, C., Jiang, X., Zhang, X. B., and Ma, Y. (2015). Direct Conversion of Cord Blood CD34+ Cells Into Neural Stem Cells by OCT4. *Stem Cells Transl Med*.

Lin, Y. H. (2010). *Polymer viscoelasticity: basics, molecular theories, experiments and simulations*. Online: World Scientific Pub Co.

Liu, D. and Bao, F. (2015). Hydrogen peroxide administered into the rat spinal cord at the level elevated by contusion spinal cord injury oxidizes proteins, {DNA} and membrane phospholipids, and induces cell death: Attenuation by a metalloporphyrin. *Neuroscience* 285.0, pp. 81 –96. ISSN: 0306-4522. DOI: http://dx.doi.org/10.1016/j.neuroscience.2014.10.063. URL: http://www.sciencedirect.com/science/article/pii/S030645221400935X (visited on 10/06/2016).

Liu, D., Liu, J., and Wen, J. (1999). Elevation of hydrogen peroxide after spinal cord injury detected by using the Fenton reaction. *Free Radical Biology and Medicine* 27.3–4, pp. 478 –482. ISSN: 0891-5849. DOI: http://dx.doi.org/10.1016/S0891-5849(99)00073-8. URL: http://www.sciencedirect.com/science/article/pii/S0891584999000738 (visited on 10/06/2016).

Long, H., Li, G., Lin, E., Xie, W., Chen, W., Luk, K., and Hu, Y. (2013). Is the speed of chronic compression an important factor for chronic spinal cord injury rat model? *Neuroscience Letters* 545.0, pp. 75 –80. ISSN: 0304-3940. DOI: http://dx.doi.org/10.1016/j.neulet.2013.04.024. URL: http://www.sciencedirect.com/science/article/pii/S030439401300373X (visited on 10/06/2016).

Louveau, A., Smirnov, I., Keyes, T. J., Eccles, J. D., Rouhani, S. J., Peske, J. D., Derecki, N. C., Castle, D., Mandell, J. W., Lee, K. S., Harris, T. H., and Kipnis, J. (2015). Structural and functional features of central nervous system lymphatic vessels. *Nature*.

Lu, Y., Franze, K., Seifert, G., Steinhäuser, C., Kirchhoff, F., Wolburg, H., Guck, J., Janmey, P., Wei, E., Käs, J., and Reichenbach, A. (2006). Viscoelastic properties of individual glial cells and neurons in the CNS. 103.47, pp. 17759–17764. DOI: 10.1073/pnas.0606150103.

Luders, E., Toga, A. W., Lepore, N., and Gaser, C. (2009). The underlying anatomical correlates of long-term meditation: larger hippocampal and frontal volumes of gray matter. *Neuroimage* 45.3, pp. 672–678.

Lundberg, N. (1960). Continuous recording and control of ventricular fluid pressure in neurosurgical practice. *Acta Psychiatr Scand Suppl* 36.149, pp. 1–193.

Maes, M., Vandoolaeghe, E., Degroote, J., Altamura, C., Roels, C., and Hermans, P. (2000). Linear CT-scan measurements in alcohol-dependent patients with and without delirium tremens. *Alcohol* 20.2, pp. 117–123.

Masel, B. E. and DeWitt, D. S. (2010). Traumatic brain injury: a disease process, not an event. *J. Neurotrauma* 27.8, pp. 1529–1540.

McBeath, R., Pirone, D. M., Nelson, C. M., Bhadriraju, K., and Chen, C. S. (2004). Cell shape, cytoskeletal tension, and RhoA regulate stem cell lineage commitment. *Dev. Cell* 6.4, pp. 483–495.

McBride, S. H. and Knothe Tate, M. L. (2008). Modulation of stem cell shape and fate A: the role of density and seeding protocol on nucleus shape and gene expression. *Tissue Eng Part A* 14.9, pp. 1561–1572.

McKeon, R. J., Schreiber, R. C., Rudge, J. S., and Silver, J. (1991). Reduction of neurite outgrowth in a model of glial scarring following CNS injury is correlated with the expression of inhibitory molecules on reactive astrocytes. *J. Neurosci.* 11.11, pp. 3398–3411.

McNamara, L. E., McMurray, R. J., Biggs, M. J., Kantawong, F., Oreffo, R. O., and Dalby, M. J. (2010). Nanotopographical control of stem cell differentiation. *J Tissue Eng* 2010, p. 120623.

Meijering, M., Jacob, M., Sarria, J.-C. F., Steiner, P., Hirling, H., and Unser, M. (2004). Design and Validation of a Tool for Neurite Tracing and Analysis in Fluorescence Microscopy Images. *Cytometry Part A* 58.2, pp. 167–176.

Mezger, T. (2014). *The Rheology Handbook*. English. Hannover: Vincentz Network. ISBN: 9783866308428, 3866308426.

Mikkola, I., Heavey, B., Horcher, M., and Busslinger, M. (2002). Reversion of B cell commitment upon loss of Pax5 expression. *Science* 297.5578, pp. 110–113.

Mittermayr, R., Antonic, V., Hartinger, J., Kaufmann, H., Redl, H., Teot, L., Stojadinovic, A., and Schaden, W. (2012). Extracorporeal shock wave therapy (ESWT) for wound healing: technology, mechanisms, and clinical efficacy. *Wound Repair Regen* 20.4, pp. 456–465.

Mohammadi, H., Arora, P. D., Simmons, C. A., Janmey, P. A., and McCulloch, C. A. (2015). Inelastic behaviour of collagen networks in cell-matrix interactions and mechanosensation. *J R Soc Interface* 12.102, p. 20141074.

Monti, M. M., Schnakers, C., Korb, A. S., Bystritsky, A., and Vespa, P. M. (2016). Non-Invasive Ultrasonic Thalamic Stimulation in Disorders of Consciousness after Severe Brain Injury: A First-in-Man Report. *Brain Stimul* 9.6, pp. 940–941.

Moreno-Arotzena, O., Meier, J. G., Del Amo, C., and Garcia-Aznar, J. M. (2015). Characterization of Fibrin and Collagen Gels for Engineering Wound Healing Models. *Materials (Basel)* 8.4, pp. 1636–1651.

Morykwas, M. J., Argenta, L. C., Shelton-Brown, E. I., and McGuirt, W. (1997). Vacuum-assisted closure: a new method for wound control and treatment: animal studies and basic foundation. *Ann Plast Surg* 38.6, pp. 553–562.

Muiznieks, L. D. and Keeley, F. W. (2013). Molecular assembly and mechanical properties of the extracellular matrix: A fibrous protein perspective. *Biochim. Biophys. Acta* 1832.7, pp. 866–875.

Murad, A., Ghostine, S., and Colohan, A. R. (2012). A case for further investigating the use of controlled lumbar cerebrospinal fluid drainage for the control of intracranial pressure. *World Neurosurg* 77.1, pp. 160–165.

Murray-Dunning, C., Thanabalasundaram, L., Day, A. G. E., Vysokov, N., Sinden, J., Stevenato, L., and Phillips, J. B. (2015). Differentiated CTX human neural stem cells adopt a glial phenotype in RAFT-stabilised collagen hydrogels suitable for nerve tissue engineering. *Tissue and Cell Engineering Society*.

North, B. and Reilly, P. (1990). *Raised Intracranial Pressure*. Oxford: Heinemann Professional Publishing Ltd.

Olesen, J., Gustavsson, A., Svensson, M., Wittchen, H. U., and Jonsson, B. (2012). The economic cost of brain disorders in Europe. *Eur. J. Neurol.* 19.1, pp. 155–162.

Palahniuk, C. (1996). *Fight Club*. New York: W. W. Norton.

Petrie, R. J. and Koo, H. (2014). Direct measurement of intracellular pressure. *Curr Protoc Cell Biol* 63, pp. 1–9.

Petrie, R. J., Koo, H., and Yamada, K. M. (2014). Generation of compartmentalized pressure by a nuclear piston governs cell motility in a 3D matrix. *Science* 345.6200, pp. 1062–1065.

Pollock, C. M. and Shadwick, R. E. (1994). Relationship between body mass and biomechanical properties of limb tendons in adult mammals. *Am. J. Physiol.* 266.3 Pt 2, R1016–1021.

Raboel, P. H., Bartek, J., Andresen, M., Bellander, B. M., and Romner, B. (2012). Intracranial Pressure Monitoring: Invasive versus Non-Invasive Methods-A Review. *Crit Care Res Pract* 2012, p. 950393.

Rao, M., ed. (2010). *Stem Cells and CNS Development*. Humana Press.

Raub, C. B., Putnam, A. J., Tromberg, B. J., and George, S. C. (2010). Predicting bulk mechanical properties of cellularized collagen gels using multiphoton microscopy. *Acta Biomater* 6.12, pp. 4657–4665.

Richards, L. J., Kilpatrick, T. J., and Bartlett, P. F. (1992). De novo generation of neuronal cells from the adult mouse brain. *Proc. Natl. Acad. Sci. U.S.A.* 89.18, pp. 8591–8595.

Ricks, C. B., Shin, S. S., Becker, C., and Grandhi, R. (2014). Extracellular matrices, artificial neural scaffolds and the promise of neural regeneration. *Neural Regen Res* 9.17, pp. 1573–1577.

Rodriguez-Boto, G., Rivero-Garvia, M., Gutierrez-Gonzalez, R., and Marquez-Rivas, J. (2015). Basic concepts about brain pathophysiology and intracranial pressure monitoring. *Neurologia* 30.1, pp. 16–22.

Rohatgi, A. (2017). *WebPlotDigitizer*. Version: 3.12. URL: `http://arohatgi.info/WebPlotDigitizer`.

Rose, F. D. and Johnson, D. A. (1996). *Brain Injury and After*. Chichester: John Wiley and Sons.

Rosner, M. J. and Becker, D. P. (1984). Origin and evolution of plateau waves. Experimental observations and a theoretical model. *J. Neurosurg.* 60.2, pp. 312–324.

Ross, N. and Eynon, C. (2005). Intracranial pressure monitoring. *Current Anaesthesia & Critical Care* 16.4, pp. 255 –261. ISSN: 0953-7112. DOI: `http://dx.doi.org/10.1016/j.cacc.2005.11.013`. URL: `http://www.sciencedirect.com/science/article/pii/S0953711205001043` (visited on 10/06/2016).

Saha, K., Keung, A. J., Irwin, E. F., Li, Y., Little, L., Schaffer, D. V., and Healy, K. E. (2008). Substrate modulus directs neural stem cell behavior. *Biophys. J.* 95.9, pp. 4426–4438.

Salvador-Silva, M., Aoi, S., Parker, A., Yang, P., Pecen, P., and Hernandez, M. R. (2004). Responses and signaling pathways in human optic nerve head astrocytes exposed to hydrostatic pressure in vitro. *Glia* 45.4, pp. 364–377.

Saunders, M. M. (2015). *Mechanical Testing for the Biomechanical Engineer: A Practical Guide*. Online: Morgan and Claypool.

Schneider, C. A., Rasband, W. S., and Eliceiri, K. W. (2012). NIH Image to ImageJ: 25 years of image analysis. *Nat. Methods* 9.7, pp. 671–675.

Schuh, C. M., Heher, P., Weihs, A. M., Banerjee, A., Fuchs, C., Gabriel, C., Wolbank, S., Mittermayr, R., Redl, H., Runzler, D., and Teuschl, A. H. (2014). In vitro extracorporeal shock wave treatment enhances stemness and preserves multipotency of rat and human adipose-derived stem cells. *Cytotherapy* 16.12, pp. 1666–1678.

Shen, F., Tay, T. E., Li, J. Z., Nigen, S., Lee, P. V., and Chan, H. K. (2006). Modified Bilston nonlinear viscoelastic model for finite element head injury studies. *J Biomech Eng* 128.5, pp. 797–801.

Shimada, S., Andou, M., Naito, N., Yamada, N., Osumi, M., and Hayashi, R. (1993). Effects of hydrostatic pressure on the ultrastructure and leakage of internal substances in the yeast Saccharomyces cerevisiae. *Appl Microbiol Biotechnol* 40.1, pp. 123–131.

Shoichet, M. S., Tate, C. C., Baumann, M. D., and LaPlaca, M. C. (2008). "Strategies for Regeneration and Repair in the Injured Central Nervous System". *Indwelling Neural Implants: Strategies for Contending with the In Vivo Environment*. Ed. by R. WM. Boca Raton (FL): CRC Press.

Shoshani, O. and Zipori, D. (2011). Mammalian cell dedifferentiation as a possible outcome of stress. *Stem Cell Rev* 7.3, pp. 488–493.

Skardal, A., Mack, D., Atala, A, and Soker, S. (2012). Substrate Elasticity Controls Cell Proliferation, Surface Marker Expression and Motile Pheontype in Amniotic Fluid-Derived Stem Cells. *J Mech Behav Biomed Mater* 17, pp. 307–316.

Skerry, T. M. (2008). The response of bone to mechanical loading and disuse: fundamental principles and influences on osteoblast/osteocyte homeostasis. *Arch. Biochem. Biophys.* 473.2, pp. 117–123.

Slemmer, J. E., Weber, J. T., and Zeeuw, C. I. D. (2004). Cell death, glial protein alterations and elevated S-100β release in cerebellar cell cultures following mechanically induced trauma. *Neurobiology of Disease* 15.3, pp. 563 –572. ISSN: 0969-9961. DOI: `http://dx.doi.org/10.1016/j.nbd.2003.11.027`. URL: `http://www.sciencedirect.com/science/article/pii/S0969996103002547` (visited on 10/06/2016).

Smith-Thomas, L. C., Stevens, J., Fok-Seang, J., Faissner, A., Rogers, J. H., and Fawcett, J. W. (1995). Increased axon regeneration in astrocytes grown in the presence of proteoglycan synthesis inhibitors. *J. Cell. Sci.* 108 (Pt 3), pp. 1307–1315.

Sofroniew, M. V. and Vinters, H. V. (2010). Astrocytes: biology and pathology. *Acta Neuropathol.* 119.1, pp. 7–35.

Solanki, A., Shah, S., Memoli, K. A., Park, S. Y., Hong, S., and Lee, K. B. (2010). Controlling differentiation of neural stem cells using extracellular matrix protein patterns. *Small* 6.22, pp. 2509–2513.

Spinal Research (2011). Accessed: 4th June 2015. URL: `http://www.spinal-research.org/research-matters/spinal-cord-injury/facts-and-figures/` (visited on 10/06/2016).

Steiner, L. A. and Andrews, P. J. (2006). Monitoring the injured brain: ICP and CBF. *Br J Anaesth* 97.1, pp. 26–38.

Sternberger, L. A. (1986). *Immunocytochemistry*. New York: Wiley.

Stocchetti, N., Colombo, A., Ortolano, F., Videtta, W., Marchesi, R., Longhi, L., and Zanier, E. R. (2007). Time course of intracranial hypertension after traumatic brain injury. *J. Neurotrauma* 24.8, pp. 1339–1346.

Stoddart, M. J. (2011). *Mammalian cell viability: methods and protocols*. English. Vol. 740; 740. New York: Springer. ISBN: 1617791083; 9781617791086.

Sumpio, B. E., Widmann, M. D., Ricotta, J., Awolesi, M. A., and Watase, M. (1994). Increased ambient pressure stimulates proliferation and morphologic changes in cultured endothelial cells. *J. Cell. Physiol.* 158.1, pp. 133–139.

Sun, Y., Pollard, S., Conti, L., Toselli, M., Biella, G., Parkin, G., Willatt, L., Falk, A., Cattaneo, E., and Smith, A. (2008). Long-term tripotent differentiation capacity of human neural stem (NS) cells in adherent culture. *Mol. Cell. Neurosci.* 38.2, pp. 245–258.

Szarko, M., Muldrew, K., and Bertram, J. E. (2010). Freeze-thaw treatment effects on the dynamic mechanical properties of articular cartilage. *BMC Musculoskelet Disord* 11, p. 231.

Tajbakhsh, S. (2009). *Stem cell: what's in a name?* Accessed: 24th February 2016. URL: `http://www.nature.com/stemcells/2009/0906/090625/full/stemcells.2009.90.html` (visited on 10/06/2016).

Tan, J. L., Tien, J., Pirone, D. M., Gray, D. S., Bhadriraju, K., and Chen, C. S. (2003). Cells lying on a bed of microneedles: an approach to isolate mechanical force. *Proc. Natl. Acad. Sci. U.S.A.* 100.4, pp. 1484–1489.

Tata, P. R., Mou, H., Pardo-Saganta, A., Zhao, R., Prabhu, M., Law, B. M., Vinarsky, V., Cho, J. L., Breton, S., Sahay, A., Medoff, B. D., and Rajagopal, J. (2013). Dedifferentiation of committed epithelial cells into stem cells in vivo. *Nature* 503.7475, pp. 218–223.

Temple, S. (1989). Division and differentiation of isolated CNS blast cells in microculture. *Nature* 340.6233, pp. 471–473.

Tronci, G., Russell, S., and Wood, D. (2013a). Photo-active collagen systems with controlled triple helix architecture. *J. Mat. Chem. B* 30.1, pp. 3705–3715.

Tronci, G., Doyle, A., Russell, S. J., and Wood, D. J. (2013b). Triple-helical collagen hydrogels via covalent aromatic functionalization with 1,3-Phenylenediacetic acid. *J Mater Chem B Mater Biol Med* 1.40, pp. 5478–5488.

Varghese, J. S., Chellappa, N., and Fathima, N. N. (2014). Gelatin-carrageenan hydrogels: role of pore size distribution on drug delivery process. *Colloids Surf B Biointerfaces* 113, pp. 346–351.

Vaux, D. L., Fidler, F., and Cumming, G. (2012). Replicates and repeats–what is the difference and is it significant? A brief discussion of statistics and experimental design. *EMBO Rep.* 13.4, pp. 291–296.

Ventura, C. (2013). Tuning stem cell fate with physical energies. *Cytotherapy* 15.12, pp. 1441–1443.

Wall, M. E., Weinhold, P. S., Siu, T., Brown, T. D., and Banes, A. J. (2007). Comparison of cellular strain with applied substrate strain in vitro. *J Biomech* 40.1, pp. 173–181.

Wang, L., Wei, F., Cen, J., Ping, S., Li, Z., Chen, N., Cui, S., Wan, Y., and Liu, S. (2014). Early administration of tumor necrosis factor-alpha antagonist promotes survival of transplanted neural stem cells and axon myelination after spinal cord injury in rats. *Brain Research* 1575.0, pp. 87 –100. ISSN: 0006-8993. DOI: http://dx.doi.org/10.1016/j.brainres.2014.05.038. URL: http://www.sciencedirect.com/science/article/pii/S0006899314007537 (visited on 10/06/2016).

Wang, Q., Tang, X. N., and Yenari, M. A. (2007). The inflammatory response in stroke. *J. Neuroimmunol.* 184.1-2, pp. 53–68.

Waning, B. and Montagne, M. (2001). *Pharmacoepidemiology: Principles and Practice*. New York: McGraw-Hill Education. URL: https://accesspharmacy.mhmedical.com.

Ward, R., Huang, W., Kostusiak, M., Pallier, P., Michael-Titus, A., and Priestley, J. (2014). A characterization of white matter pathology following spinal cord compression injury in the rat. *Neuroscience* 260.0, pp. 227 –239. ISSN: 0306-4522. DOI: http://dx.doi.org/10.1016/j.neuroscience.2013.12.024. URL: http://www.sciencedirect.com/science/article/pii/S0306452213010403 (visited on 10/06/2016).

Weber, J., Rzigalinski, B., Willoughby, K., Moore, S., and Ellis, E. (1999). Alterations in calcium-mediated signal transduction after traumatic injury of cortical neurons. *Cell Calcium* 26.6, pp. 289 –299. ISSN: 0143-4160. DOI: http://dx.doi.org/10.1054/ceca.1999.0082. URL: http://www.sciencedirect.com/science/article/pii/S0143416099900829 (visited on 10/06/2016).

Weightman, A. P., Pickard, M. R., Yang, Y., and Chari, D. M. (2014). An in vitro spinal cord injury model to screen neuroregenerative materials. *Biomaterials* 35.12, pp. 3756–3765.

Weiss, S., Dunne, C., Hewson, J., Wohl, C., Wheatley, M., Peterson, A. C., and Reynolds, B. A. (1996). Multipotent CNS stem cells are present in the adult mammalian spinal cord and ventricular neuroaxis. *J. Neurosci.* 16.23, pp. 7599–7609.

Wen, Q., Basu, A., Janmey, P. A., and Yodh, A. G. (2012). Non-affine deformations in polymer hydrogels. *Soft Matter* 8.31, pp. 8039–8049.

Wenger, M. P., Bozec, L., Horton, M. A., and Mesquida, P. (2007). Mechanical properties of collagen fibrils. *Biophys. J.* 93.4, pp. 1255–1263.

Whitaker, L. R., Degoulet, M., and Morikawa, H. (2013). Social deprivation enhances VTA synaptic plasticity and drug-induced contextual learning. *Neuron* 77.2, pp. 335–345.

Willits, R. K. and Skornia, S. L. (2004). Effect of collagen gel stiffness on neurite extension. *J Biomater Sci Polym Ed* 15.12, pp. 1521–1531.

Wilson, S. L., Ahearne, M., El Haj, A. J., and Yang, Y. (2014). "Chapter 8 Mechanical Characterization of Hydrogels and its Implications for Cellular Activities". *Hydrogels in Cell-Based Therapies*. Accessed: 6th October 2016. The Royal Society of Chemistry, pp. 171–190. ISBN: 978-1-84973-798-2. DOI: 10.1039/9781782622055-

00171. URL: http://dx.doi.org/10.1039/9781782622055-00171 (visited on 10/06/2016).

Winter, B., Pattani, H., and Temple, E. (2014). Spinal Cord Injury. *Anaesthesia & Intensive Care Medicine* 15.9, pp. 424–427.

Wu, T. (2008). *Background Correction Plugin*. Online. Accessed: 28th September 2017. URL: https://imagej.nih.gov/ij/plugins/background.html.

Xie, X., McGregor, M., and Dendukuri, N. (2010). The clinical effectiveness of negative pressure wound therapy: a systematic review. *J Wound Care* 19.11, pp. 490–495.

Yagita, Y., Kitagawa, K., Ohtsuki, T., Takasawa, K, Miyata, T., Okano, H., Hori, M., and Matsumoto, M. (2001). Neurogenesis by Progenitor Cells in the Ischemic Adult Rat Hippocampus. *Stroke* 32, pp. 1890–1896.

Yamashita, T. and Kuwabara, T. (1983). Estimation of rate of growth of malignant brain tumors by computed tomography scanning. *Surg Neurol* 20.6, pp. 464–470.

Yao, S., Liu, X., Wang, X., Merolli, A., Chen, X., and Cui, F. (2013). Directing neural stem cell fate with biomaterial parameters for injured brain regeneration. *Progress in Natural Science: Materials International* 23.2, pp. 103 –112. ISSN: 1002-0071. DOI: http://dx.doi.org/10.1016/j.pnsc.2013.02.009. URL: http://www.sciencedirect.com/science/article/pii/S1002007113000440 (visited on 10/06/2016).

Yoo, H., Jung, E., Nam, B. H., Shin, S. H., Gwak, H. S., Kim, M. S., Zo, J. I., and Lee, S. H. (2011a). Growth rate of newly developed metastatic brain tumors after thoracotomy in patients with non-small cell lung cancer. *Lung Cancer* 71.2, pp. 205–208.

Yoo, S. S., Kim, H., Min, B. K., Franck, E., and Park, S. (2011b). Transcranial focused ultrasound to the thalamus alters anesthesia time in rats. *Neuroreport* 22.15, pp. 783–787.

Yu, J., Zhong, Y., Cheng, Y., Shen, X., Wang, J., and Wei, Y. (2011). Effect of high hydrostatic pressure on the expression of glutamine synthetase in rat retinal Müller cells cultured in vitro. *Exp Ther Med* 2.3, pp. 513–516.

Zhao, Y., Wang, J., Wang, M., Sun, P., Chen, J., Jin, X., and Zhang, H. (2013). Activation of bone marrow-derived mesenchymal stromal cells-a new mechanism of defocused low-energy shock wave in regenerative medicine. *Cytotherapy* 15.12, pp. 1449–1457.

Zhao, Y. H., Lv, X., Liu, Y. L., Zhao, Y., Li, Q., Chen, Y. J., and Zhang, M. (2015). Hydrostatic pressure promotes the proliferation and osteogenic/chondrogenic differentiation of mesenchymal stem cells: The roles of RhoA and Rac1. *Stem Cell Res* 14.3, pp. 283–296.

7 Appendices

7.1 Appendix 1

Table 41: Statistical analyses, Chapter 4

Fig.	Name	Shapiro	Distrib.	Levene	Variances	Statistical Test	p-Value
41	CB660 Original	0.000	Skewed			Kruskal-Wallis	0.584
	CB660 Rinse	0.095	Normal	0.074	Equal	ANOVA	0.000
	CX Original	0.003	Skewed			Kruskal-Wallis	0.779
	CX Rinse	0.002	Skewed			Kruskal-Wallis	0.10
46	ATP 1x10^5	0.044	Skewed	0.034	Unequal	Kolmogorov	0.037
	ATP 2x10^5	0.009	Skewed	0.043	Unequal	Kolmogorov	0.037
	ATP 5x10^5	0.089	Normal	0.039	Unequal	t-test	0.007
	CyQuant 1x10^5	0.898	Normal	0.460	Equal	t-test	0.094
	CyQuant 2x10^5	0.347	Normal	0.127	Equal	t-test	0.122
	CyQuant 5x10^5	0.768	Normal	0.011	Unequal	t-test	0.560
47	ATP 5x10^3				Assumed	Mann-Whitney U	0.021
	ATP 1x10^4				Assumed	Mann-Whitney U	0.021
	ATP 5x10^4				Assumed	Mann-Whitney U	0.021
	CyQuant 5x10^3				Assumed	Mann-Whitney U	0.021
	CyQuant 1x10^4				Assumed	Mann-Whitney U	0.021
	CyQuant 5x10^4				Assumed	Mann-Whitney U	0.021
49	Day 3	0.530	Normal	0.572	Equal	t-test	0.412
	Day 5	0.182	Normal	0.403	Equal	t-test	0.094

Table 42: Post-hoc Analyses that found at least p<0.1, Chapter 4

Figure	Name	Post-Hoc Test	Name	p-Value
41	CB660 Rinse	Tukey	1-2x10^4 seeding density	0.066
			1-5x10^4 seeding density	0.000
			2-5x10^4 seeding density	0.000
	CX Rinse	Dunn's	1-5x10^4 seeding density	0.002
			2-5 x10^4 seeding density	0.096

Table 43: Statistical analyses, Chapter 5

Figure	Name	Shapiro	Distrib.	Levene	Variances	Statistical Test	p-Value
53	Storage	0.318	Normal	0.101	Equal	ANOVA	0.051
Table 35	Ph no control	0.194	Normal	0.090	Equal	ANOVA	0.001
Table 35	Ta no control	0.265	Normal	0.168	Equal	ANOVA	0.000
Table 35	Ph 020816	0.915	Normal	0.374	Equal	t-test	0.071
Table 35	Ta 020816	0.094	Normal	0.130	Equal	t-test	0.000
Table 35	Ph 170816	0.797	Normal	0.647	Equal	t-test	0.313
Table 35	Ta 170816	0.077	Normal	0.348	Equal	t-test	0.000
Table 35	Ph Temp	0.295	Normal	0.521	Equal	t-test	0.000
Table 35	Ta Temp	0.473	Normal	0.474	Equal	t-test	0.001
Table 35	Ph 220916	0.915	Normal	0.892	Equal	t-test	0.013
Table 35	Ta 220916	0.697	Normal	0.577	Equal	t-test	0.035
Table 35	Ph 270916	0.076	Normal	0.095	Equal	t-test	0.053
Table 35	Ta 270916	0.551	Normal	0.662	Equal	t-test	0.029
Table 35	Ph Collagen pH	0.299	Normal	0.060	Equal	t-test	0.002
Table 35	Ta Collagen pH	0.139	Normal	0.064	Equal	t-test	0.000
Table 35	Ph SPB pH	0.754	Normal	0.234	Equal	t-test	0.061
Table 35	Ta SPB pH	0.518	Normal	0.534	Equal	t-test	0.002
Table 36		0.918	Normal			paired t-test	0.712
62	Storage	0.057	Skewed	0.341	Equal	Wilcoxon	0.021
	Loss	0.932	Normal	0.899	Equal	t-test	0.007
64		0.260	Normal	0.170	Equal	t-test	0.212
66	Mean	0.501	Normal	0.245	Equal	t-test	0.083
	Range	0.115	Normal	0.096	Equal	t-test	0.093
	Max	0.041	Skewed	0.044	Unequal	Kolmogorov	0.518
67		0.665	Normal	0.845	Equal	t-test	0.136
68		0.694	Normal	0.220	Equal	t-test	0.002
70	Stem	0.096	Normal		Assumed	t-test	0.328
	Neuronal	0.851	Normal		Assumed	t-test	0.244
	Glial	0.767	Normal		Assumed	t-test	0.144
71		0.553	Normal		Assumed	t-test	0.038

Table 44: Post-hoc Analyses that found at least p<0.1, Chapter 5

Figure	Name	Post-Hoc Test	Name	p-Value
53	Storage	Tukey	Ph-Ad	0.096
			Su-Ad	0.066
Table 35	Ph no control	Tukey	220216-120516	0.001
			220216-060616	0.012
			120516-110716	0.007
	Ta no control	Tukey	220216-120516	0.005
			120516-060616	0.003
			120516-110716	0.000

Table 45: Statistical analyses, Chapter 6

Fig	Name	Shapiro	Distrib.	Levene	Variances	Statistical Test	p-Value
82	Mid layer					Kruskal-Wallis	0.059
	Lower layer					Kruskal-Wallis	0.061
84	Proliferation	0.438	Normal	0.395	Equal	ANOVA	0.313
	Differentiation	0.962	Normal	0.098	Equal	ANOVA	0.320
85	Proliferation	0.244	Normal	0.158	Equal	ANOVA	0.333
	Differentiation	0.333	Normal	0.035	Unequal	Welch's	0.042
90	Differentiation Stem	0.565	Normal		Assumed	ANOVA	0.617
	Differentiation Neuronal	0.482	Normal		Assumed	ANOVA	0.951
	Differentiation Glial	0.637	Normal		Assumed	ANOVA	0.317
	Proliferation Stem	0.070	Normal		Assumed	ANOVA	0.499
	Proliferation Neuronal	0.442	Normal		Assumed	ANOVA	0.009
	Proliferation Glial	0.037	Skewed		Assumed	Kruskal	0.320
91	Differentiation Media	0.079	Normal		Assumed	ANOVA	0.031
	Proliferation Media	0.680	Normal		Assumed	Anova	0.285
92	Differentiation Media				Assumed	Kruskal-Wallis	0.123
	Proliferation Media				Assumed	Kruskal-Wallis	0.180
93	Differentiation Media	0.125	Normal		Assumed	ANOVA	0.489
	Expansion Media	0.017	Skewed			Kruskal-Wallis	0.368

Table 46: Post-hoc Analyses that found at least p<0.1, Chapter 6

Figure	Name	Post-Hoc Test	Name	p-Value
82	Mid layer	Dunn's	0-25mmHg	0.025
			0-50mmHg	0.072
	Lower layer	Dunn's	0-50mmHg	0.025
			25-50mmHg	0.074
85	Differentiation	Games-Howell	30-50mmHg	0.029
90	Proliferation Neuronal	Tukey	10-50mmHg	0.008
			30-50mmHg	0.034
			10-30mmHg	0.095
91	Differentiation Media	Tukey	10-50mmHg	0.033
			10-30mmHg	0.052